LAMINAR AND TURBULENT

FORCED CONVECTION PROCESSES

THROUGH IN - LINE TUBE BANKS

by

Rodney Francis Le Feuvre

Thesis submitted for the degree of
Doctor of Philosophy
in the Faculty of Engineering
University of London
and
for the Diploma of Membership
of Imperial College

Mechanical Engineering Department
Imperial College
London, S.W.7

September, 1973

Abstract

The basis of a general numerical procedure for predicting steady, two-dimensional, incompressible, laminar or turbulent flows in non-rectangular domains is described. The novelties of the procedure include the use of a rectangular grid arrangement for non-rectangular domains (RAND grid), and a 'new - upwind' method of approximating the convection terms in the conservation equations.

The accuracy and convergence properties of the procedure are tested by the prediction of both flows with analytical solutions and laminar flow over a single cylinder. The usefulness of the procedure is demonstrated by new predictions of laminar flow over in - line tube banks.

To permit the prediction of turbulent flows, a version of the Kolmogorov - Prandtl hypothesis of turbulence is employed. Also used is a novel set of wall functions, which specify the variation of the dependent variables next to wall boundaries. The reliability of these models is tested by comparing the predictions of turbulent developing flow through a parallel channel and fully-developed flow through in - line tube banks with appropriate experimental data.

Preface

When I joined the Heat Transfer Section, Mechanical Engineering Department, Imperial College in October 1968, much work had already been done on the development of a procedure for predicting recirculating flows. I was also fortunate to arrive at a time when these developments were being put together in the form of a book, see Gosman et al (1969). The latter contained a systematic presentation of the theory of recirculating flows and the results of a variety of predictions. My understanding of the contents of this book was supplemented by the first course on 'Recirculating Flows', which was run in December 1968.

During most of 1969, I was involved in contributing to the development of the basic 'Elliptic' computer programme, which was designed to solve the elliptic equations for laminar flow. Also I was assigned with my main task of predicting flows through tube banks.

It soon became clear that the main difficulty in embarking on the latter predictions was the difficulty of calculating an orthogonal grid for a typical tube bank domain. Indeed this difficulty is a general one, because there are many practical domains for which orthogonal grids cannot be easily calculated.

Therefore an investigation was conducted along the lines of using a finite - difference grid arrangement which was not necessarily orthogonal with all the boundaries of a particular domain. The basic scheme, which resulted from the preliminary investigation, required much testing to determine its usefulness and prospect of general application. All the initial tests were performed using various laminar flows. Later developments involved the incorporation of turbulence models for predicting turbulent flows. The above is the subject of this thesis.

It is now appropriate that I should acknowledge the assistance I have received throughout the period spent on this work. First and foremost, I wish to express my gratitude to my supervisor, Professor Spalding, for his

guidance, suggestions and encouragement. A number of major steps in this work were inspired by his suggestions, and without his inspiration these steps would probably not have been made. Also the little progress I have made in the matter of technical writing and presentation are due mainly to his encouragement and criticism of my written work. For the benefit of his present and future students, it may be worth putting on record that I have gained most from his supervision by communicating each stage of my work in the form of a short note before discussing it with him.

I wish also to acknowledge the guidance of Drs. A.D. Gosman, W.M. Pun, A.K. Runchal and M. Wolfshtein in helping me to understand the theory of recirculating flows as given in Gosman et al (1969). In particular, Dr Gosman's help and guidance in the initial stages of my use of the Elliptic programme were very welcome. I am also grateful to Dr L.W. Roberts for a number of helpful discussions as we both sought to contribute to the development of the Elliptic programme. I should also like to thank Drs. Lockwood and Singham for their work as members of my thesis committee along with Professor Spalding. Dr Lockwood also read parts of my thesis, and commented on the layout, grammar and phraseology. I am concious that a number of other members of the Heat Transfer Section have in one way or another contributed to this work, and my thanks are due to them. It is appropriate to point out here that I have derived personal benefit by doing research in an atmosphere of a team with a unified objective and direction. Undoubtably the origin and continuation of this beneficial situation is due to the inspiration and organisational ability of Professor Spalding.

Further to the above, I am indebted to Imperial College for employing me as a Research Assistant for four years. Also I am indebted to the Computer Centre at I.C. for a generous allocation of computer time and to the computer advisory staff for helping me to sort out some of the bugs in my programmes. My thanks are due to the Departmental Drawing Office

for their assistance in producing most of the figures in this thesis, and to Miss E. Archer and her colleague for assistance in obtaining a wide range of references. My thanks are also due to Miss M.P. Steele for her patient advice concerning numerous secretarial and administrative problems, and to Miss S. Henshaw for typing this thesis with patience, accuracy and neatness.

Finally my thanks must go to my loving wife for her continuous interest in my work and for encouraging my progress. Also I am grateful to her for putting up with times of loneliness, whilst I pursued the completion of this work and thesis.

Newcastle upon Tyne, R.F. Le Feuvre

September 1973.

CONTENTS

	Page
Abstract	2
Preface	3
1. INTRODUCTION	10
1.1 General objective	10
1.2 Previous knowledge	14
1.3 Outline of thesis	17
1.4 Summary of the present contributions	18
2. THE BASIC EQUATIONS	19
2.1 The differential equations	19
2.1.1 Restrictions	19
2.1.2 The laws of conservation	20
2.2 Auxiliary equations	21
2.3 The vorticity and stream function equations	22
2.4 The differential equations in the form of a single general equation	23
2.5 Boundary equations	24
3. THE NUMERICAL PROCEDURE	28
3.1 The solution technique	28
3.2 The general finite - difference equation	29
3.2.1 The convection terms	31
3.2.2 The complete difference equation	37

		Page
3.3	The treatment of non-rectangular boundaries	39
3.3.1	Review of techniques	40
3.3.2	The present treatment	44
3.3.3	The finite-difference conservation equations for typical F.W.P. and F.N.P. cells	47
3.4	Some properties of the numerical procedure	57
3.4.1	Convergence properties	60
4.	APPLICATION TO PROBLEMS WITH ANALYTICAL SOLUTIONS	64
4.1	The purpose	64
4.2	Inclined - plane Couette flow	67
4.2.1	The problem and the grid arrangement	67
4.2.2	The theory and boundary conditions	67
4.2.3	Tests and results	69
4.3	Cylindrical Couette flow	80
4.3.1	The problem and the grid arrangement	80
4.3.2	The theory and boundary conditions	82
4.3.3	Tests and results	85
4.4	Discussion	90
5.	LAMINAR FLOW PREDICTIONS	93
5.1	Objective	93
5.2	Flow over a single cylinder	94
5.2.1	Previous work and the present contribution	94
5.2.2	Hydrodynamic predictions	97
5.2.3	Heat transfer predictions	120
5.2.4	Discussion	132

Page

5.3 Flow through in - line tube banks 134

5.3.1 Review of available data 134
5.3.2 Boundary conditions 136
5.3.3 Hydrodynamic predictions 141
5.3.4 Heat transfer predictions 155
5.3.5 Discussion 163

6. TURBULENT FLOW PREDICTIONS 164

6.1 Introduction 164

6.2 The flow models 165

6.2.1 The turbulence model 165
6.2.2 The wall functions 169

6.3 Developing flow in a channel 181

6.3.1 Review of available data 181
6.3.2 Boundary conditions 181
6.3.3 The predictions 185

6.4 In - line tube banks 191

6.4.1 Limitations of present turbulence model 191
6.4.2 Review of appropriate data 192
6.4.3 The boundary conditions 199
6.4.4 The predictions 202

6.5 Discussion of results 217

7. DISCUSSION AND CONCLUSIONS 219

7.1 Summary of the main results 219

7.1.1 Introduction to summary 219
7.1.2 The development of the numerical method 219
7.1.3 The application of the turbulence models 222

7.2 Recommendations for future research 223

		Page
APPENDICES		226
A.1	The error due to the standard – upwind scheme for the convection terms	226
A.2	The calculation of parameters associated with the new – upwind method of approximating the convection terms in equation (3.2.1)	229
REFERENCES		232
NOMENCLATURE		237

1. INTRODUCTION

1.1 General objective

(a) The designer's task

Types of machinery and equipment, which involve flowing fluids or materials, are to be found in almost every field of engineering. The design of such machinery has often been based on very slender knowledge of the behaviour of the appropriate materials and fluids. However, in the last two decades or so, some encouraging progress (due to careful research) has been made in furthering our understanding of flowing fluids. In the meantime the designer has also improved his design techniques and made increasing use of the available data. Nevertheless the task of the designer could be made still much easier and less costly if more exact design procedures were available.

As a background to our discussion, we shall consider briefly the nature of the guidelines and tools which the present day designer of a machine or parts of a machine may use. He is first of all given certain specifications, which have to be met. These might be thought of as the boundary conditions of the design problem. These conditions might specify maximum weight and size, range of work output or flow rate, normal running load, etc. From experience, the designer may know (at least roughly) the sort of machine layout which will enable the specifications to be met. Knowing the latter, he may seek to perform the design by:

(i) Rule of thumb. This means that the designer will aim to design something that looks right. Thus the design may be subject very much to the designer's personal opinion and experience.

(ii) Theoretical analysis. This will involve using the available data whichare relevant to the appropriate materials and fluids forming part of the design. The data used will depend on the degree of design

detail. For example when considering flow down a pipe, the designer may require local velocity data in certain circumstances but only mean velocity data in other circumstances.

(iii) A combination of (i) and (ii). Due to the complexities of most pieces of machinery, the designer has, more often than not, to use a combination of personal judgement and theoretical analysis in his work.

After establishing a design, which may meet the specifications, the next stage is usually to build a model or a prototype. The latter is then tested to check that the specifications are met. If the machine does not perform as required, considerable redesign and development work of a hit-and-miss nature may have to be performed. The latter may involve many minor experiments and major model tests.

(b) Methods of reducing design and development costs

The above discussion is a very general one, but it does bring out the point that design procedures to meet certain specifications may be very complex particularly for large machines of the one-off variety. In these circumstances, design and development costs may form a substantial percentage of the total cost. What can be done to assist designers to perform their tasks more efficiently and precisely, i.e. to reduce the costs of design and development?

One method is to continue the task of supplying more experimental test data, which may possibly provide non-dimensional empirical expressions for the behaviour of fluids in a great variety of circumstances. This task is not to be discouraged because for many flow situations there is no other method (at present) of obtaining the required data. However it is obvious that such flow situations are numerous. Also in general the flow parameters involved in each situation may be large, and, if so, many

test runs are required in order to obtain an empirical expression relating all the parameters. The cost of running such a wide range of tests may indeed be prohibitive.

The ideal alternative is to provide designers with quick, accurate, inexpensive and general procedures for guiding their initial designs and for checking that their proposed designs meet the specifications. Such procedures must be based on the ability to produce accurate mathematical models of the behaviour of fluids in any flow situation, and on the ability to solve the relevant equations of motion. An example of such a procedure is given below.

Initially, the preliminary design of a machine involving fluid flow may be performed using the available data of fluid properties and the solutions of simplified equations of motion. Then the next stage is to solve the equations which govern the complete behaviour of the fluids concerned and to check that the predicted behaviour conforms with the specifications. If the latter are not satisfied, the design may then be altered by what is judged to be the required amount and the solution of the appropriate equations repeated. This procedure is continued until a satisfactory design is obtained. If such a design procedure can be produced and shown to be advantageous, then the need for expensive and time consuming model testing and development may be reduced considerably. The general objective behind the present contribution is concerned with the development of analytical design procedures of the type described above. Let us now examine the possibilities of realising this general objective.

(c) Equations of fluid motion

Fluids undergoing some flow process may be classified as behaving according to the laws of laminar or turbulent motion. This simple classification ignores, for the sake of clarity, the fact that flowing

fluids may undergo transition processes between the limiting conditions of predominantly laminar and predominantly turbulent flows.

The differential equations which describe the motion of laminar flows are to be found in many standard texts on fluid mechanics. One particular set of equations for laminar flows is that describing the motion of incompressible constant - viscosity laminar flows. These equations are called the Navier-Stokes equations (see Bird, Stewart and Lightfoot (1960)). For turbulent flows, the main approach is to represent the flow in terms of fluctuating components superimposed on the time - mean flow. Thus by substituting these flow components into the Navier-Stokes equations and time - averaging the resulting terms, the Reynolds equations for steady incompressible turbulent flows are obtained. Similar equations to the latter represent the turbulent transfer of energy and mass.

What are the possibilities of solving such equations? As far as the Navier-Stokes equations are concerned, only a small selection of problems (governed by much simplied versions of the general Navier-Stokes equations) are known to have analytical solutions. However the Reynolds equations are even more complex than the above because they do not represent a closed mathematical system. This is because the introduction of the fluctuating components of flow results in the number of unknowns exceeding the number of equations. The equations can only be made soluble by supplying additional information in the form of physical hypotheses, which seek to model the turbulence quantities in terms of mean flow quantities. Thus the equations governing either laminar or turbulent flows are in general so complex mathematically that analytical solutions are not possible. Indeed for such equations general solution procedures can only be devised by the use of numerical techniques. The latter are used to approximate the differential equations by equivalent numerical equations, which in turn

can be solved by employing numerical techniques in conjuction with the programming facilities of high-speed digital computers.

(d) The objective of this present work

If the present general objective is to be realised then our first aim must be to produce a solution procedure which is generally applicable (i.e. not restricted by types of boundary conditions and flow problems), accurate and economical. The other main aim is to devise and develop physical hypotheses of turbulence, which accurately model the behaviour of turbulent flows in a wide range of flow situations.

It is the particular objective of the present work to forward these aims in relation to one particular set of flows, i.e. two-dimensional flows exhibiting recirculation, and to do so by the development of means of predicting laminar and turbulent flows over in-line tube banks.

1.2 Previous Knowledge

In this section, we summarise some of the previous work concerned with solution procedures and turbulence models, and we focus on some points of the present contribution. The following summary of previous work is deliberately brief because reviews of particular topics are dealt with in the relevant chapters which follow. However it is appropriate to single out some of the stimuli which have influenced in one way or another the development of the present contribution.

One of the pioneers of the application of numerical solution procedures to fluid flow problems is Thom (1933), who predicted low Reynolds number flows over a single cylinder. He simplified the Navier-Stokes equations by using vorticity and steam function as the independent variables. Also he approximated the differential equations by using 'central-differences' and obtained algebraic equations which were solved by an iterative technique. Thom's method, however, was unstable for

Reynolds numbers greater than about 50, and no solution could be obtained for higher Reynolds numbers, (Thom and Apelt (1961)). Many other workers have since predicted flow over a single cylinder using a variety of numerical techniques, and the present contribution includes one further such prediction. The main purpose of the latter is to illustrate the accuracy of the present numerical scheme.

Since the pioneer work of Thom, much progress has been made (particularly in the last decade) in overcoming the numerical instabilities inherent in certain numerical schemes, and in making these schemes more generally applicable. A major contribution in this direction has been made by Gosman et al (1969), who proposed a general scheme for solving heat and mass transfer problems in general two-dimensional flows. The initial developments with regard to this scheme were made primarily by Wolfshtein (1967) and Runchal (1969) under the supervision of Prof. Spalding.

Although generality of application for any scheme is a worthy aim, it may not in certain circumstances lead to ease of application. Indeed this is true of Gosman et al's scheme. One of the main features of their scheme is the use of an integral finite-difference numerical scheme, which is applicable to flows in any domain. However the scheme requires that each domain must be mapped with an orthogonal grid arrangement. Herein lies the point of generality, but not necessarily the ease of application. This is because, for domains with awkward shapes, there are no straightforward methods of calculating orthogonal grids and their required geometric parameters. In this context, awkward domains are classified as those which do not have orthogonal grids governed by analytical solutions or which cannot be mapped by Cartesian, cylindrical or spherical co-ordinate systems. An example of such a domain is the typical area between four tubes within an in - line tube bank. The present contribution

suggests a grid arrangement which does not require that the grid lines should be orthogonal with all the boundaries of the domain. The corresponding numerical scheme is based on that of Gosman et al, but modifications are required at the near-boundary nodes in situations where the grid lines are not orthogonal to the boundaries.

Another main feature of Gosman et al's prediction scheme is that it is applicable to the prediction of both laminar and turbulent flows. This is because turbulent flows are treated like laminar flows, where the turbulent transport properties (such as the so-called 'effective' viscosity) vary from place to place in a flow domain. However further information concerning the behaviour of the turbulent transport properties must be provided. In their work, Gosman et al made use of a model of turbulence which originates from proposals made by Kolmogorov (1942) and Prandtl (1945). This model describes the turbulence as a function of two parameters; a length scale, l, and the kinetic energy of the turbulence, k. Early versions of this model (see Wolfshtein (1967) and Runchal (1969)) used a differential equation for k and an algebraic equation for l. These versions lacked generality because the equations for l depended on the geometry of the problem.

More recently, the work of Launder and Jones (1970, 1971), amongst others, has yielded a more general version, which is expressed in the form of two differential equations, one for k and one for dissipation of turbulence, ε . The latter is directly related to l at high Reynolds numbers by the expression $\varepsilon \propto k^{3/2}/l$. Satisfactory predictions for a range of boundary layer flows have been obtained with this model. However its applicability to the prediction of recirculating flows has not been thoroughly tested. The present work makes a contribution in this direction by applying the model to the prediction of turbulent flows through in - line tube banks.

1.3 Outline of thesis

The thesis is divided into seven chapters. In chapter 2 the differential equations, auxiliary equations and boundary conditions are presented. Then in chapter 3 the differential equations are recast in a finite - difference form. One novelty in chapter 3 is the new - upwind scheme for the convection terms. The latter, which is a development from the standard - upwind scheme used by Gosman et al (1969), is given special prominence. The other important novelty is the grid arrangement, which for the sake of abbreviation is called the RAND (Rectangular Arrangement for Non-rectangular Domain) grid. The latter and the appropriate finite - difference equations are described in detail.

In chapter 4, the procedure is tested for accuracy and convergence by the predictions of two simple flows with analytical solutions. The properties of the new - upwind scheme are demonstrated by these results. Chapter 5 contains two sets of laminar predictions. The first set concerns the detailed predictions of flow over a single cylinder for $Re = 40$, and the comparison of the results with a wide selection of other predictions and measurements. The second set deals with the predictions of flow through a selection of in - line tube banks. The results of the latter are compared with available experimental data. These predictions are unique because no other predictions of this flow are known at the present time.

Chapter 6 contains a description of the turbulence model used here and of the wall functions, which are in effect the boundary conditions for turbulent flows in near - wall regions. The wall functions contain some novelties, which are designed to deal with flows near separation and reattachment regions. The accuracy and validity of the turbulence model and wall functions are tested by the predictions (and comparisons with appropriate experimental data) of developing flow through a channel and

fully - developed flow through in - line tube banks.

Finally, Chapter 7 summarises the main results of this work and makes recommendations for future research.

1.4 Summary of the present contributions

The main contributions of the present work may be summarised as follows:

(i) The new - upwind scheme, which is a novel method of approximating the convection terms in the conservation equations (section 3.2).

(ii) The RAND grid, which is a new finite - difference grid arrangement for domains with awkward boundaries (section 3.3).

(iii) The checks on the properties of the solution procedure, which contains the novelties of (i) and (ii) (Chapter 4 and section 5.2).

(iv) The description of new proposals for turbulent flow wall functions (section 6.2).

(v) The predictions of laminar and turbulent flows through in - line tube banks, which are reported in sections 5.3 and 6.4 respectively.

2. THE BASIC EQUATIONS

This chapter seeks to set the stage for later chapters by listing and rearranging the differential equations which express the laws of conservation of mass, momentum, enthalpy and other convected quantities. Both laminar and turbulent flows are described by the same set of equations by postulating effective exchange coefficients for momentum, enthalpy, etc. The appropriate boundary conditions for these equations are reviewed.

2.1 The differential equations

2.1.1 Restrictions

The differential equations in a generalised form have already been derived in detail by Gosman et al (1969). However here we are concerned to clarify the restrictions under which the equations will be used, and for the sake of clarity to write down these equations in the required simplified form. It should be noted that the following restrictions have been imposed only for this study, and are not necessary for the purpose of solving the generalised equations.

These restrictions are:

(a) Body forces, chemical reaction, mass transfer and thermal radiation are absent.

(b) The molecular (or laminar) viscosity and exchange coefficients are independent of other properties such as temperature and pressure.

(c) The stagnation enthalpy is equal to the fluid temperature times the specific heat, which is independent of temperature and pressure.

(d) The flows are steady, incompressible and either purely laminar or purely turbulent.

(e) All the flows are described by the plane Cartesian co-ordinate system, where x_1 and x_2 represent the Cartesian co-ordinates.

2.1.2 The laws of conservation

With the restrictions of 2.1.1, the laws of conservation of mass, momentum and conserved property ϕ are as follows:

$$\frac{\partial u_i}{\partial x_i} = 0 \qquad (2.1.1)$$

$$\rho u_j \frac{\partial u_i}{\partial x_j} = -\frac{\partial p}{\partial x_i} + \frac{\partial \tau_{ij}}{\partial x_j} \qquad (2.1.2)$$

$$\rho u_j \frac{\partial \phi}{\partial x_j} = -\frac{\partial J_{\phi,j}}{\partial x_j} + S_\phi \qquad (2.1.3)$$

where u_i is the velocity in direction i,

p is the fluid pressure,

τ_{ij} is the component of the shear tensor which operates on the i - plane (the plane normal to the i - direction) in the direction j,

ϕ is any conserved property such an enthalpy,

$J_{\phi,j}$ is the diffusional - flux component of the property ϕ in the direction j , and

S_ϕ is the source term which consists of all terms other than those describing the convection and diffusion of ϕ.

The indexes i and j may take the values 1 and 2, and the summation convention is used. For example $\frac{\partial}{\partial x_j}(a_i b_j) = 0$ represents the following equations:

$$\frac{\partial}{\partial x_1}(a_1 b_1) + \frac{\partial}{\partial x_2}(a_1 b_2) = 0$$

$$\frac{\partial}{\partial x_1}(a_2 b_1) + \frac{\partial}{\partial x_2}(a_2 b_2) = 0$$

2.2 Auxiliary equations

In this section, we proceed to define the components τ_{ij} and $J_{\phi,j}$, which appear in equations (2.1.2) and (2.1.3) respectively.

For laminar Newtonian fluids, the components of the stress tensor τ_{ij} are easily related to the rate - of - strain tensor (velocity gradients) via a generalized form of Newton's law of viscosity, Bird, Stewart and Lightfoot (1960). Similarly, the flux components of enthalpy can be related to the temperature gradients by the generalized form of Fourier's law of heat conduction.

For turbulent flows, we follow an early proposal by Boussinesq (1877) and postulate the existence of effective exchange coefficients to replace the laminar exchange coefficients in the respective stress and flux laws; thus,

$$\tau_{i,j} = -\mu_{eff}\left(\frac{\partial u_j}{\partial x_i} + \frac{\partial u_i}{\partial x_j}\right) \qquad (2.2.1)$$

and

$$J_{\phi,j} = -\Gamma_{\phi,eff}\,\frac{\partial \phi}{\partial x_j} \qquad (2.2.2)$$

where, μ_{eff} and $\Gamma_{\phi,eff}$ are the effective viscosity and diffusivity respectively.

We also postulate that:

$$\Gamma_{\phi,eff} = \mu_{eff}/\sigma_{\phi,eff} \qquad (2.2.3)$$

where, $\sigma_{\phi,eff}$ is the effective Prandtl number for the property ϕ.

Thus we have replaced the two unknowns τ_{ij} and $J_{\phi,j}$ by the unknowns μ_{eff} and $\sigma_{\phi,eff}$. To obtain information about the latter, it is necessary to make use of correlated experimental data for turbulent flows, such as is presented by Hinze (1959). These matters are dealt

with in a summarised form in Chapter 6, so for the time being we proceed on the assumption that μ_{eff} and $\sigma_{\phi,eff}$ can be determined.

2.3 The vorticity and stream function equations

For two - dimensional flows, it is possible to replace the equations (2.1.1) and (2.1.2) with two new equations: one for stream function, ψ, and another for vorticity, ω. These transformed equations, which are derived in detail by Gosman et al (1969), form the basis for the prediction of two - dimensional flows in the present study. The results of these derivations are outlined below.

Stream function is defined by:

$$u_1 = \frac{1}{\rho}\frac{\partial \psi}{\partial x_2} \quad ; \quad u_2 = -\frac{1}{\rho}\frac{\partial \psi}{\partial x_1} \qquad (2.3.1)$$

It is easy to show that the law of conservation of mass, equation (2.1.1), is satisfied by this definition of stream function.

Vorticity is defined by:

$$\omega = \frac{\partial u_2}{\partial x_1} - \frac{\partial u_1}{\partial x_2} \qquad (2.3.2)$$

By substituting (2.3.1) into (2.3.2), the so - called stream function equation is obtained as follows:

$$\frac{\partial}{\partial x_j}\left(\frac{1}{\rho}\frac{\partial \psi}{\partial x_j}\right) + \omega = 0 \qquad (2.3.3)$$

By differentiating the direction - 1 momentum equation with respect to x_2 and the direction - 2 momentum equation with respect to x_1, and subtracting the first from the second, we obtain the conservation equation for vorticity (now called the vorticity equation):

$$\rho u_j \frac{\partial \omega}{\partial x_j} - \frac{\partial^2}{\partial x_j^2}(\mu_{eff}\,\omega) + S_\omega = 0 \qquad (2.3.4)$$

where,

$$S_\omega = 2\left\{\frac{\partial^2}{\partial x_1 \partial x_2}\left[\mu_{eff}\left(\frac{\partial u_2}{\partial x_2} - \frac{\partial u_1}{\partial x_1}\right)\right] + \frac{\partial^2}{\partial x_1^2}\left[\mu_{eff}\frac{\partial u_1}{\partial x_2}\right] - \frac{\partial^2}{\partial x_2^2}\left[\mu_{eff}\frac{\partial u_2}{\partial x_1}\right]\right\} \qquad (2.3.5)$$

Clearly S_ω equals zero in uniform viscosity flow, but even in other types of flow it is not in general very important, and so it is neglected here.

One further modification, that is the elimination of u_j from the vorticity and conserved property equations by using (2.3.1), completes the required reorganization. We proceed in the next section to assemble the equations in a general form.

2.4 The differential equations in the form of a single general equation

The laws of conservation have been redefined in the previous section by equation (2.3.3) for stream function, equation (2.3.4) for vorticity and a modified equation (2.1.3) for conserved property ϕ. All these equations may be represented by a single general equation:

$$a_\phi\left\{\frac{\partial}{\partial x_1}\left(\phi\frac{\partial \psi}{\partial x_2}\right) - \frac{\partial}{\partial x_2}\left(\phi\frac{\partial \psi}{\partial x_1}\right)\right\} - \frac{\partial}{\partial x_1}\left\{b_\phi\frac{\partial}{\partial x_1}(c_\phi\phi)\right\} - \frac{\partial}{\partial x_2}\left\{b_\phi\frac{\partial}{\partial x_2}(c_\phi\phi)\right\} + d_\phi = 0 \qquad (2.4.1)$$

where, ϕ now stands for any of the previous variables ω, ψ or ϕ.

The coefficients a_ϕ, b_ϕ, c_ϕ and d_ϕ are defined in table 2.4.1 for ϕ representing stream function, vorticity and temperature.

ϕ	a_ϕ	b_ϕ	c_ϕ	d_ϕ
ψ	0	$\frac{1}{\rho}$	1	$-\omega$
ω	1	1	μ_{eff}	S_ω
T	1	$\Gamma_{T,eff}$	1	0

Table 2.4.1

2.5 Boundary equations

When applying equation (2.4.1) to a particular problem, the specification of boundary conditions is required to close the equation set. Now equation (2.4.1) is known as an elliptic equation, and for the latter one must prescribe boundary conditions along a closed curve bounding the region of interest. These boundary conditions are usually given by either the value of ϕ or its normal gradient at the boundary. A third possible boundary condition is a combination of the previous two.

Obviously the precise boundary conditions will in general vary from problem to problem. Indeed in later chapters, the boundary conditions for each domain of interest will be clearly stated. However we shall usually encounter boundaries which fall into one of the following categories: (a) inlet planes, (b) outlet planes, (c) planes of symmetry and (d) walls. We proceed to discuss the first three categories (a), (b) and (c) in brief terms and to deal with category (d) in more detail.

(a) Inlet planes

For most problems, the entry conditions of the fluid, such as the temperature and velocity profiles (and hence ω and ψ), are known.

(b) Outlet planes

Outlet conditions are not usually known, and so the simplest practice, that of prescribing a gradient condition, is adopted. Unless more precise information is available, the zero - gradient condition is specified for all the variables.

(c) Planes of symmetry

(i) Stream function: This is a constant value and can be obtained from the data of the problem.

(ii) Vorticity: $\omega = 0$

(iii) Other variables: The symmetry condition demands that the normal gradient is zero.

(d) Walls

We shall illustrate the boundary conditions for this case by considering a simple example, that of an impermeable stationary wall.

(i) Stream function: This is a constant value and can be obtained from the data of the problem.

(ii) Vorticity: As vorticity is composed of gradients of velocity, it can be rarely prespecified. A boundary conditon for vorticity and the gradient of the product of vorticity and viscosity can, however, be obtained from the 'no - slip' condition. This is shown by the following derivation.

In most situations near a wall, the gradients of the dependent variables in the direction parallel to the wall may be neglected in comparision with those in the normal direction. For this case, the vorticity equation (2.3.4) may be written as follows:

$$\frac{d^2}{dx_n^2}(\mu_{eff}\,\omega) = 0 \qquad (2.5.1)$$

where, x_n is the distance normal to the wall.

By integrating (2.5.1) twice, we obtain:

$$\omega = (Ax_n + B)/\mu_{eff} \qquad (2.5.2)$$

where, $A = \left[\frac{d}{dx_n}(\mu_{eff}\,\omega)\right]_s$

$$B = [\mu_{eff}\,\omega]_s$$

and, $\tau_s = -[\mu_{eff}\,\omega]_s$

= wall shear stress

A and B are constants of integration and subscript S refers to the wall.

A second relation for the constants of integration, A and B, may be obtained by writing the stream function equation (2.3.3) as:

$$\frac{d^2\psi}{d^2x_n^2} + \rho(Ax_n + B)/\mu_{eff} = 0 \qquad (2.5.3)$$

By integrating (2.5.3) twice and using the no - slip condition

$$\left[\frac{d\psi}{dx_n}\right]_s = 0,$$

we obtain:

$$\psi - \psi_s = -\rho\int_0^{x_n}\left\{\int_0^{x}(Ax+B)/\mu_{eff}\,dx\right\}dx \qquad (2.5.4)$$

If μ_{eff} is available as a function of x_n, then $\left[\frac{d(\mu_{eff}\,\omega)}{dx_n}\right]_s$ and ω_s

can be obtained from the two simultaneous equations (2.5.2) and (2.5.4) and expressed in terms of ψ and ω values at a short distance from the wall. For example, if μ_{eff} is a constant, which is the case for constant property laminar flows, then:

$$\omega_s = -\frac{\omega_c}{2} - \frac{3(\psi_c - \psi_s)}{\rho\, x_{n,c}^2} \qquad (2.5.5)$$

and,

$$\left[\frac{d(\mu_{eff}\,\omega)}{dx_n}\right]_s = \mu_{eff}\left[\frac{\omega_c - \omega_s}{x_{n,c}}\right]$$

$$= \mu_{eff}\left[\frac{3\omega_c}{2\,x_{n,c}} + \frac{3(\psi_c - \psi_s)}{\rho\, x_{n,c}^3}\right] \qquad (2.5.6)$$

where, subscript C refers to a point within the flow field at a distance of $x_{n,c}$ from the wall.

The practice for determining the vorticity boundary condition in the case of turbulent flows is described in Chapter 6.

(iii) Other variables: The boundary conditions for other variables are usually provided in the form of local values or gradients. For example, the boundary conditions for temperature are given by either temperature or heat flux distributions, where the latter may be either uniform or non - uniform.

3. THE NUMERICAL PROCEDURE

In Chapter 2, the laws of conservation were stated and then altered into the vorticity, stream function and conserved property set. By further manipulation, it was shown that all these equations could be expressed in the form of a general differential equation for conserved property ϕ. In this chapter we outline the numerical procedure, which is used in this work to obtain solutions of the general equation for ϕ and thus for all the properties described by this equation. The novel aspects of the procedure are to be found in section 3.2.1, where a new method of approximating the convection terms is introduced, and in section 3.3, where we present a method of dealing with domains which have non - rectangular boundaries.

3.1 The solution technique

Research into various means of solving the general equation (2.4.1) has been the concern of the Heat Transfer Section since about 1965. At about that time it became clear that the only general method of solving equation (2.4.1), and thus numerous problems in heat and mass transfer, required the use of a finite - difference procedure. Subsequently the work of determining the best available solution procedure resulted in the publication of Gosman et al (1969).

Now in the present work, the procedure of Gosman et al has been used as a basis for further development. The results of this development include two main innovations. The first seeks to improve the accuracy of the finite - difference approximations, and the second to deal with domains which include non - rectangular boundaries, that is boundaries which are not parallel with either the x_1 or x_2 co-ordinate axes.

In the following sections, section 3.2 deals with the formulation of the finite - difference equation for property ϕ. Sub-section 3.2.1 (a), which follows the method of Gosman et al (1969) for approximating the convection terms, may be passed over quickly by the reader who is familiar with this method. Section 3.3 describes the treatment of non - rectangular boundaries and section 3.4 discusses some of the properties of the numerical procedure.

3.2 The general finite - difference equation

Fig. 3.2.1 illustrates a typical section of a finite - difference grid, where the grid lines are positioned at discrete values of the co-ordinates x_1 and x_2, and the spacing between the lines can be either uniform or non-uniform. The intersections of the lines are called nodes and each node is contained within a finite area of unit depth, which is called a cell.

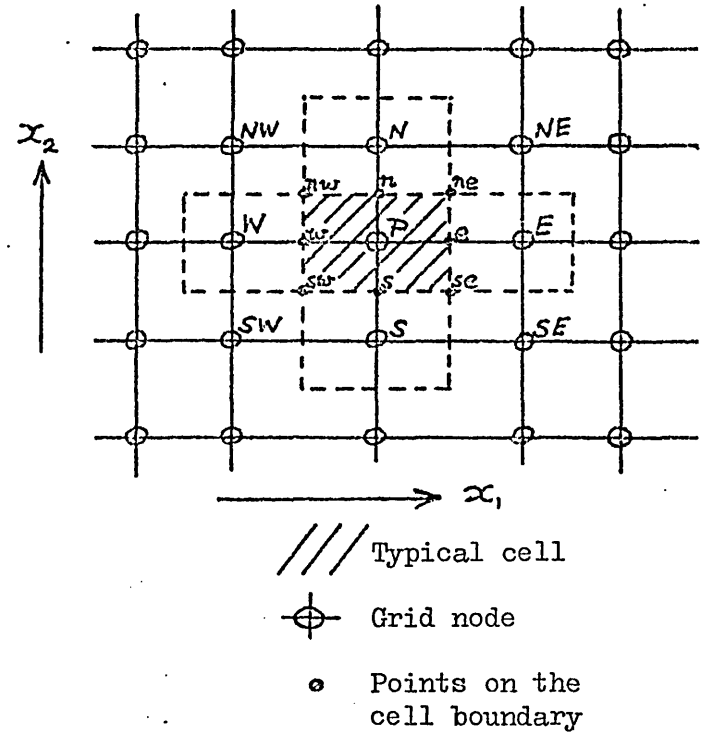


Fig. 3.2.1

Let P denote a typical node of the grid, and nodes N,S,E,W,NE,SE, SW and NW surround it. We shall restrict our attention to the cell, appropriate to node P, which is shaded and denoted by the corner points ne, se, sw and nw. The cell boundaries are arranged so as to lie midway between the neighbouring grid lines.

The first stage of the present finite - difference scheme is to integrate equation (2.4.1) over the typical cell area. Thus equation (2.4.1) becomes:

$$a_{\phi,P}\Bigg[\int_{x_{2,s}}^{x_{2,n}}\left\{\phi_e\left(\frac{\partial\psi}{\partial x_2}\right)_e-\phi_w\left(\frac{\partial\psi}{\partial x_2}\right)_w\right\}dx_2-$$

Convection Terms

$$-\int_{x_{1,w}}^{x_{1,e}}\left\{\phi_n\left(\frac{\partial\psi}{\partial x_1}\right)_n-\phi_s\left(\frac{\partial\psi}{\partial x_1}\right)_s\right\}dx_1\Bigg]-$$

$$-\int_{x_{2,s}}^{x_{2,n}}\left\{(b_\phi)_e\left[\frac{\partial}{\partial x_1}(c_\phi\phi)\right]_e-(b_\phi)_w\left[\frac{\partial}{\partial x_1}(c_\phi\phi)\right]_w\right\}dx_2-$$

Diffusion Terms

$$-\int_{x_{1,w}}^{x_{1,e}}\left\{(b_\phi)_n\left[\frac{\partial}{\partial x_2}(c_\phi\phi)\right]_n-(b_\phi)_s\left[\frac{\partial}{\partial x_2}(c_\phi\phi)\right]_s\right\}dx_1+$$

$$+\int_{x_{2,s}}^{x_{2,n}}\int_{x_{1,w}}^{x_{1,e}}d_\phi\;dx_1\,dx_2 \qquad (3.2.1)$$

Source Term

In sub-section 3.2.1, we shall derive two finite - difference approximations for the convection terms of equation (3.2.1). The first approximation is the same as that derived by Gosman et al (1969), and the second is a modified form of the first. However as the relevant expressions

for the diffusion and source terms are given by Gosman et al (1969), these terms are only quoted as part of the complete difference equation, which is given in sub-section 3.2.2.

3.2.1 The convection terms

(a) Method 1

To demonstrate the approximation of the four convection terms in equation (3.2.1), let us take the first term,

$$I_c = a_{\phi,P} \int_{x_{2,s}}^{x_{2,n}} \phi_e \left(\frac{\partial \psi}{\partial x_2}\right)_e dx_2 \qquad (3.2.2)$$

If both ψ and ϕ are well-behaved functions in x_2, then there exists an average value $\overline{\phi}_e$, such that:

$$\overline{\phi}_e = \int_{x_{2,s}}^{x_{2,n}} \phi_e \left(\frac{\partial \psi}{\partial x_2}\right)_e dx_2 \Big/ \int_{x_{2,s}}^{x_{2,n}} \left(\frac{\partial \psi}{\partial x_2}\right)_e dx_2 \qquad (3.2.3)$$

where the integral in the denominator of (3.2.3) can be written as,

$$\int_{x_{2,s}}^{x_{2,n}} \left(\frac{\partial \psi}{\partial x_2}\right)_e dx_2 = \psi_{ne} - \psi_{se} \qquad (3.2.4)$$

Therefore, from (3.2.2), (3.2.3) and (3.2.4),

$$I_c = a_{\phi,P}\, \overline{\phi}_e\, (\psi_{ne} - \psi_{se}) \qquad (3.2.5)$$

The next tast is to express $\overline{\phi}_e$, ψ_{ne} and ψ_{se} in terms of the values of the variables at the nodes of the grid. We do this for $\overline{\phi}_e$ by making an assumption, which is referred to as the assumption of

upwind differences. For equation (3.2.5), it states that $\bar{\phi}_e$ is equal to that value of ϕ which is representative of the cell lying immediately upstream of the side e.

The implications of this assumption are readily understood if we note that the direction (and magnitude) of the flow across the e - face is given by $\int_{se}^{ne} \rho\, u_1\, dx_2$ and hence from equation (2.3.1) by $(\psi_{ne} - \psi_{se})$. For example, if $(\psi_{ne} - \psi_{se})$ is positive, the direction of flow is from node P towards node E. This implies that $\bar{\phi}_e$ is equal to the representative value of the cell corresponding to node P; we take this value to be ϕ_p. Similarly, if $(\psi_{ne} - \psi_{se})$ is negative $\bar{\phi}_e$ is put equal to ϕ_E.

The above argument can be incorporated into (3.2.5) as follows:

$$I_c = a_{\phi,P}\{\phi_P[(\psi_{ne} - \psi_{se}) + |\psi_{ne} - \psi_{se}|]/2 + \phi_E[(\psi_{ne} - \psi_{se}) - |\psi_{ne} - \psi_{se}|]/2 \qquad (3.2.6)$$

Now we must also express ψ_{ne} and ψ_{se} in terms of the ψ values at the surrounding nodes. This is accomplished by simply assuming that the ψ value at the corner of a cell is given by the arithmetic mean of the ψ values at the four surrounding nodes. Thus,

$$\psi_{se} = (\psi_P + \psi_E + \psi_{SE} + \psi_S)/4 \qquad (3.2.7)$$

Equation (3.2.6) can now be written as:

$$I_c = \phi_P\, A_{E2} - \phi_E\, A_{E1} \qquad (3.2.8)$$

where,

$$A_{E1} = -a_{\phi,P}[(\psi_N + \psi_{NE} - \psi_S - \psi_{SE}) - |\psi_N + \psi_{NE} - \psi_S - \psi_{SE}|]/8$$
$$A_{E2} = a_{\phi,P}[(\psi_N + \psi_{NE} - \psi_S - \psi_{SE}) - |\psi_N + \psi_{NE} - \psi_S - \psi_{SE}|]/8 \qquad (3.2.9)$$

The other convection terms can be expressed in a similar manner, and the sum of the convection terms can be given by:

$$I_{CON} = \phi_P \left[A_{E2} + A_{W1} + A_{N1} + A_{S2} \right] - \\ - \phi_E A_{E1} - \phi_W A_{W2} - \phi_N A_{N2} - \phi_S A_{S1} \qquad (3.2.10)$$

where, in terms of the corner values of ψ ,

$$A_{W1} = -a_{\phi,P}\left[(\psi_{nw} - \psi_{sw}) - |\psi_{nw} - \psi_{sw}|\right]/2$$
$$A_{W2} = a_{\phi,P}\left[(\psi_{nw} - \psi_{sw}) + |\psi_{nw} - \psi_{sw}|\right]/2$$
$$A_{N1} = -a_{\phi,P}\left[(\psi_{ne} - \psi_{nw}) - |\psi_{ne} - \psi_{nw}|\right]/2$$
$$A_{N2} = a_{\phi,P}\left[(\psi_{ne} - \psi_{nw}) + |\psi_{ne} - \psi_{nw}|\right]/2$$
$$A_{S1} = -a_{\phi,P}\left[(\psi_{se} - \psi_{sw}) - |\psi_{se} - \psi_{sw}|\right]/2$$
$$A_{S2} = a_{\phi,P}\left[(\psi_{se} - \psi_{sw}) + |\psi_{se} - \psi_{sw}|\right]/2 \qquad (3.2.11)$$

Although the A's used in equation (3.2.10) are different from those in the corresponding equation (3.23-9) of Gosman et al (1969) the quantity I_{CON} is the same in both cases. The reasons for using different A's in this case will become apparent in the following analysis. It is noted here that the A's can never become negative, but they may fall to zero. This is one of the features which, when using equation (3.2.10), makes the finite - difference formulation for equation (3.2.1) stable and convergent. For the sake of brevity and future reference, the method of approximating the convection terms in equation (3.2.1) by the form given in equation (3.2.10) is called the 'standard - upwind' method.

Unfortunately, although the latter is stable and convergent, it suffers from a truncation error due to the one - sided or upwind difference scheme described above. This error has been investigated in some detail by Wolfshtein (1967), and a summary of his findings are discussed in

Appendix A.1. Wolfshtein concluded that the truncation error, which appears in the form of 'false diffusion', is a function of β, the angle of inclination of the streamlines to the grid lines.

(b) Method 2

We now go on to describe a method of reducing the false diffusion error mentioned above. The new method, which takes into account the angle of inclination β, was first suggested by Spalding (1970). The basis of this method is best described by referring to Fig. 3.2.2, where a node P and its cell are surrounded by its neighbouring nodes N, E, etc. Considering the east wall of cell P, the flow direction through the latter is illustrated by a velocity vector which passes through the point e and is at an angle β_e to the vector for $(u_1)_e > 0$ and $(u_2)_e = 0$.

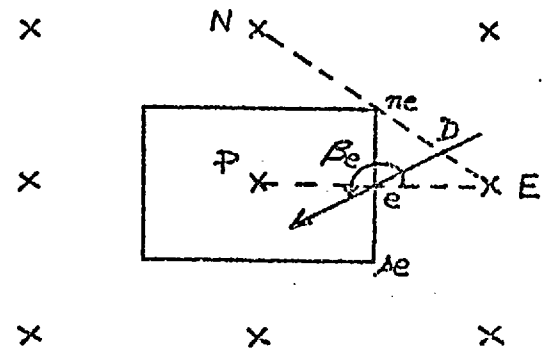


Fig. 3.2.2

As the flow direction is from right to left, the appropriate convection term by the standard - upwind method, equation (3.2.8), is given by:

$$I_c = - \phi_E \, A_{EI} \qquad (3.2.12)$$

However the new method, which takes into account the direction of flow through the east wall, modifies equation (3.2.12) as follows:

$$I_c = - \phi_D \, A_{EI} \qquad (3.2.13)$$

where,

ϕ_D = value of ϕ at point D determined by linear interpolation between ϕ_N and ϕ_E

$$\therefore \quad I_c = - A_{EI} \left[\phi_E (1 - G_{EE}) + \phi_N \, G_{EE} \right] \qquad (3.2.14)$$

where, G_{EE} is a linear interpolation coefficient, which is a function of the angle β_e and the geometrical arrangement of the grid.

Following the above procedure, the complete equation for the east wall convection term can be written as follows:

$$\begin{aligned} I_c &= P_{PE}\left\{A_{E2}\left[\phi_P(1-G_{EP}) + \phi_{SE}\,G_{EP}\right]\right. \\ &\qquad \left. - A_{E1}\left[\phi_E(1-G_{EE}) + \phi_N\,G_{EE}\right]\right\} \\ &+ P_{ME}\left\{A_{E2}\left[\phi_P(1-G_{EP}) + \phi_{NE}\,G_{EP}\right]\right. \\ &\qquad \left. - A_{E1}\left[\phi_E(1-G_{EE}) + \phi_S\,G_{EE}\right]\right\} \end{aligned} \tag{3.2.15}$$

where, $P_{PE} = 1.0$, $P_{ME} = 0$ } $0 < \beta_e < \pi/2$ and, $\pi < \beta_e < 3\pi/2$

$P_{PE} = 0$, $P_{ME} = 1.0$ } $\pi > \beta_e > \pi/2$ and, $2\pi > \beta_e > 3\pi/2$

G_{EE} and G_{EP} are the appropriate interpolation coefficients

β_e = absolute value of the vector angle, $\tan^{-1}\left[(u_2)_e/(u_1)_e\right]$, with respect to the vector for $(u_2)_e = 0$ and $(u_1)_e > 0$

$(u_1)_e$ and $(u_2)_e$ are the velocity components in the x_1 and x_2 directions respectively at point e

It should be noted that in the limits $\beta_e = 0, \frac{\pi}{2}, \pi$ and $3\pi/2$ equation (3.2.15) reduces to the following:

$$\begin{aligned} \beta_e &= 0 \quad ; \quad I_c = A_{E2}\,\phi_P \\ \beta_e &= \pi \quad ; \quad I_c = -A_{E1}\,\phi_E \\ \beta_e &= \frac{\pi}{2} \text{ and } \frac{3\pi}{2} \quad ; \quad I_c = 0 \end{aligned} \tag{3.2.16}$$

Expressions similar to equation (3.2.15) can be derived for the other three convection terms, and the sum of the convection terms can be written as:

$$
\begin{aligned}
I_{CON} = {} & \phi_P \{ A_{N1}(1-G_{NP}) + A_{S2}(1-G_{SP}) + A_{E2}(1-G_{EP}) + A_{W1}(1-G_{WP}) \} \\
& - \phi_N \{ A_{N2}(1-G_{NN}) + P_{PE} A_{E1} G_{EE} + P_{MW} A_{W2} G_{WW} \} \\
& - \phi_S \{ A_{S1}(1-G_{SS}) + P_{ME} A_{E1} G_{EE} + P_{PW} A_{W2} G_{WW} \} \\
& - \phi_E \{ A_{E1}(1-G_{EE}) + P_{MS} A_{S1} G_{SS} + P_{PN} A_{N2} G_{NN} \} \\
& - \phi_W \{ A_{W2}(1-G_{WW}) + P_{PS} A_{S1} G_{SS} + P_{MN} A_{N2} G_{NN} \} \\
& + \phi_{NE} \{ P_{MN} A_{N1} G_{NP} + P_{ME} A_{E2} G_{EP} \} \\
& + \phi_{NW} \{ P_{PN} A_{N1} G_{NP} + P_{PW} A_{W1} G_{WP} \} \\
& + \phi_{SE} \{ P_{PS} A_{S2} G_{SP} + P_{PE} A_{E2} G_{EP} \} \\
& + \phi_{SW} \{ P_{MS} A_{S2} G_{SP} + P_{MW} A_{W1} G_{WP} \} \qquad (3.2.17)
\end{aligned}
$$

where, $P_{PN} = P_{PS} = 1.0$, $P_{MN} = P_{MS} = 0.0$ } $\quad 0 < \beta_{n,s} < \pi/2$ and, $\pi < \beta_{n,s} < 3\pi/2$

$P_{PN} = P_{PS} = 0.0$, $P_{MN} = P_{MS} = 1.0$ } $\quad \pi/2 < \beta_{n,s} < \pi$ and, $3\pi/2 < \beta_{n,s} < 2\pi$

$\beta_{n,s}$ = absolute values of the vector angles $\tan^{-1}[u_1/u_2]$, with respect to the vectors for $u_1 = 0$ and $u_2 > 0$, at points n and s

$$\left.\begin{aligned} P_{PE} &= P_{PW} = 1.0 \\ P_{ME} &= P_{MW} = 0.0 \end{aligned}\right\} \quad 0 < \beta_{e,w} < \pi/2 \text{ and, } \pi < \beta_{e,w} < 3\pi/2$$

$$\left.\begin{aligned} P_{PE} &= P_{PW} = 0.0 \\ P_{ME} &= P_{MW} = 1.0 \end{aligned}\right\} \quad \pi/2 < \beta_{e,w} < \pi \text{ and, } 3\pi/2 < \beta_{e,w} < 2\pi$$

$\beta_{e,w}$ = absolute values of the vector angles $\tan^{-1}[u_2/u_1]$, with respect to the vectors for $u_2 = 0$ and $u_1 > 0$, at points e and w.

Also $G_{NN}, G_{NP}, G_{SS}, G_{SP}, G_{EE}, G_{EP}, G_{WW}$ and G_{WP} are the appropriate interpolation coefficients. u_1 and u_2 are the appropriate velocity components at points n, s, e and w in Fig. 3.2.1.

It is easy to show that when all the G's are put to zero, equation (3.2.17) reduces to equation (3.2.10). Further details about the expressions for the G's and the component velocities u_1 and u_2 are given in Appendix A.2. In order to distinguish the above from the standard - upwind method, it is called the 'new - upwind' method.

3.2.2 The complete difference equation

Before assembling the complete difference equation, which approximates the integrated general differential equation (3.2.1), we need to quote the expressions for the diffusion and source terms from Gosman et al (1969). These are as follows:

$$\begin{aligned} I_{DIFF} = {} & B_N (c_{\phi,N}\phi_N - c_{\phi,P}\phi_P) \\ & + B_S (c_{\phi,S}\phi_S - c_{\phi,P}\phi_P) \\ & + B_E (c_{\phi,E}\phi_E - c_{\phi,P}\phi_P) \\ & + B_W (c_{\phi,W}\phi_W - c_{\phi,P}\phi_P) \end{aligned} \qquad (3.2.18)$$

$$I_{SOR} = \alpha_{\phi,P}\, V_P \tag{3.2.19}$$

$$\begin{aligned}
\text{where, } B_N &= \frac{(b_{\phi,N} + b_{\phi,P})}{4}\left(\frac{x_{1,E} - x_{1,W}}{x_{2,N} - x_{2,P}}\right) \\
B_S &= \frac{(b_{\phi,S} + b_{\phi,P})}{4}\left(\frac{x_{1,E} - x_{1,W}}{x_{2,P} - x_{2,S}}\right) \\
B_E &= \frac{(b_{\phi,E} + b_{\phi,P})}{4}\left(\frac{x_{2,N} - x_{2,S}}{x_{1,E} - x_{1,P}}\right) \\
B_W &= \frac{(b_{\phi,W} + b_{\phi,P})}{4}\left(\frac{x_{2,N} - x_{2,S}}{x_{1,P} - x_{1,W}}\right) \\
V_P &= \frac{1}{4}(x_{2,N} - x_{2,S})(x_{1,E} - x_{1,W})
\end{aligned} \tag{3.2.20}$$

The final equation can now be written as:

$$I_{CON} + I_{DIFF} + I_{SOR} = 0 \tag{3.2.21}$$

where, I_{CON} is given by the new – upwind expression, equation (3.2.17).

Following the numerical method of Gosman et al (1969), we recast equation (3.2.21) into the form of a successive – substitution formula, where the variable ϕ_P is expressed as a function of the ϕ's at the nodes surrounding node P. First equation (3.2.17) is simplified into the form:

$$\begin{aligned}
I_{CON} = {} & \phi_P A_P - \phi_N A_N - \phi_S A_S - \phi_E A_E - \phi_W A_W \\
& + \phi_{NE} A_{NE} + \phi_{NW} A_{NW} + \phi_{SE} A_{SE} + \phi_{SW} A_{SW}
\end{aligned} \tag{3.2.22}$$

where, the A's are easily obtained by equating the coefficients of equations (3.2.17) and (3.2.22). Then by substituting equations (3.2.18), (3.2.19) and (3.2.22) into equation (3.2.21) and rearranging, we obtain the required equation:

$$\phi_P = (N_{CON} + N_{DIFF} + N_{SOR})/D \tag{3.2.23}$$

where,
$$N_{CON} = \phi_N A_N + \phi_S A_S + \phi_E A_E + \phi_W A_W - \phi_{NE} A_{NE} - \phi_{NW} A_{NW} - \phi_{SE} A_{SE} - \phi_{SW} A_{SW}$$

$$N_{DIFF} = \mathcal{B}_N C_{\phi,N} \phi_N + \mathcal{B}_S C_{\phi,S} \phi_S + \mathcal{B}_E C_{\phi,E} \phi_E + \mathcal{B}_W C_{\phi,W} \phi_W$$

$$N_{SOR} = \alpha_{\phi,P} V_P$$

$$\mathcal{D} = A_P + C_{\phi,P}(\mathcal{B}_N + \mathcal{B}_S + \mathcal{B}_E + \mathcal{B}_W)$$

Equation (3.2.23), together with the necessary boundary equations, forms the basis of our present computational iterative procedure.

3.3 The treatment of non - rectangular boundaries

In the previous section, we derived the successive - substitution formula for a general dependent variable ϕ at a general node P. This formula may be applied to a node in any part of a rectangular mesh where the typical node P is surrounded by all its neighbours. The values of the ϕ's at these neighbouring nodes must be either fixed or calculated from the zero - gradient condition or more generally by the same successive - substitution formula. However as shown by Gosman et al (1969) and the work of Roberts (1972), nodes next to wall boundaries require special attention.

In his derivation of formulae for nodes next to rectangular boundaries, Roberts (1972) modified the near - boundary practice of Gosman

et al (1969), which involved the use of half - cells, Fig. 3.3.1, to the practice of using full - cells, Fig. 3.3.2. The latter is particularly advantageous near corners because corner points, such as node C in Fig. 3.3.1, are removed.

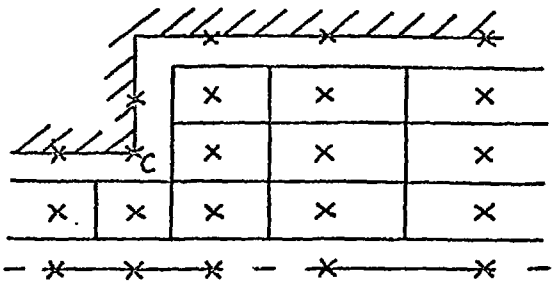


Fig. 3.3.1

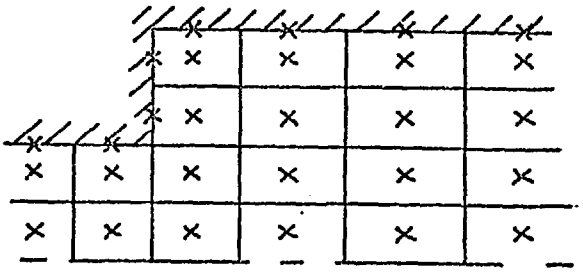


Fig. 3.3.2

This means that the special assumptions, previously required for calculating corner vorticity, are avoided. Successive - substitution formulae for ϕ at near - wall nodes with full - cells are given in some detail by Roberts (1972), so these are not repeated here. Also the formulae for ϕ at near - boundary nodes with half - cells are given by Gosman et al (1969).

However in the present section we are concerned with the description of special forms of the successive - substitution formulae which are relevant to nodes next to non - rectangular wall boundaries, where the latter are matched with a Cartesian co-ordinate grid system. A review of various techniques for treating non - rectangular boundaries is given in section 3.3.1. The present treatment is described in section 3.3.2 and examples of typical finite - difference approximations of equation (2.4.1) as applied to near - wall nodes are given in section 3.3.3.

3.3.1 Review of techniques

The solution of the vorticity - stream function set of equations in a domain of arbitrary shape may be performed using a number of numerical

techniques. The present sub-section is concerned with discussing some of the techniques, which have been applied in particular circumstances, before going on to explain the present procedure in section 3.3.2.

Most of the techniques, which are discussed below, have been applied to the problem of transverse flow over a single cylinder, where the latter is immersed in an infinite expanse of viscous fluid. The earliest work on

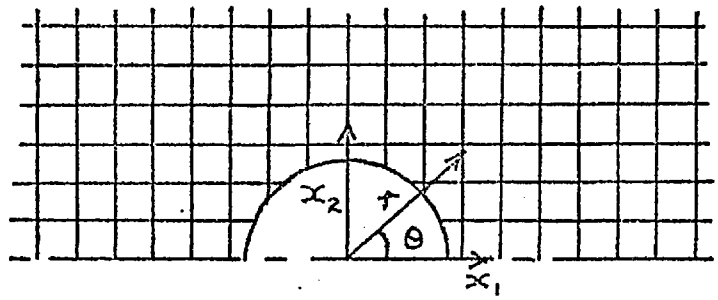


Fig. 3.3.3

this problem was performed by Thom (1933), who used two techniques. In the first, Thom divided the field into a finite - difference grid consisting of square rectangular meshes, Fig. 3.3.3. However at that time the main disadvantage of this method was due to the inherent irregular arm lengths of the finite - difference grid near the curved boundary. The basis of the second technique involved the solution (by graphical or other means) of the equations $\nabla^2\psi = 0$ and $\nabla^2 \phi = 0$ for the given domain. The latter procedure gives an orthogonal network of ψ streamlines and ϕ equipotential lines which are used as the grid for the finite - difference solution procedure. Fortunately this procedure is unnecessary for flow over a single cylinder because the grid network is given by the well - known potential flow solution. Apelt (1958) followed another of Thom (1933)'s suggestions and transformed the equations given in the Cartesian $x_1 - x_2$ plane into equations in the α-β plane, where,

$$\alpha = -k\theta$$

$$\beta = k \log_e r$$

k = constant

r and θ are defined in Fig. 3.3.3

This grid arrangement is particularly advantageous near the cylinder walls where a fine mesh can be used. However special means must be employed to obtain the boundary conditions at some distance from the walls. Kawaguti (1953) used a different set of transformed co-ordinates X and Y, where, $X = 1/r$

$$Y = 2/\pi\ \theta$$

and was therefore able to use boundary conditions relating to $r \to \infty$. A number of other workers have tackled the problem of transient or steady flow over a cylinder and most have used the transformations of either Apelt (1958) or Kawaguti (1953). The work of Thoman and Szewczyk (1969) is however distinct in this field because they used a hybrid mesh cell structure, where the cells are described by an $r - \theta$ system in the region $R \leq r \leq 2R$ (where R = radius of the cylinder) and a rectangular mesh in the outer field. A special calculation procedure is required at the interface between the $r - \theta$ and rectangular cell regions.

In their predictions of flow over a V - shaped notch, Mueller and O'Leary (1970) used a finite - difference procedure with a rectangular mesh. As the V - notch was chosen to be symmetical and formed by a 45°

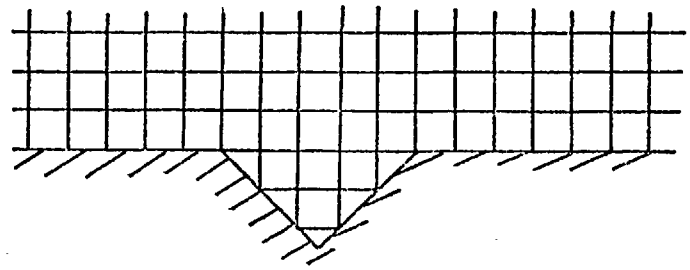


Fig. 3.3.4.

triangle, Fig. 3.3.4, the arms of the finite - difference grid within the notch were regular, and thus no special interpolation procedure was required near the walls.

All the above investigators, except Thoman and Szewczyk (1969) and Mueller and O'Leary (1970), used uniform grid spacings in the transformed

or actual domain and they approximated the differential equations using central - difference formulae. Mueller and O'Leary used linear grid spacings, but unlike the other workers employed upwind differences to approximate the convection terms. Thoman and Szewczyk divided their domain into non - linear cells and positioned the nodes of their grid at the geometric centre of each cell. They also used upwind differences for the convection terms, but because of their cell/node arrangement they were constrained to employ finite - difference approximations for the diffusion terms which are less accurate then the central - difference formulae.

In their general numerical procedure for predicting flow in domains of arbitrary shape, Gosman et al (1969) require the use of orthogonal finite - difference meshes. This means that for a domain of arbitrary shape it is necessary to solve the equations $\nabla^2 \psi = 0$ and $\nabla^2 \phi = 0$ by analytical, graphical or more often by numerical means so as to obtain a network of orthogonal streamlines and equipotential lines and thus a network of orthogonal cells. However for certain restricted but important types of domain an orthogonal grid system can be easily determined. For instance, many domains can be described by the Cartesian, cylindrical or spherical co-ordinate systems, and a much smaller number can be mapped by orthogonal co-ordinates given by analytical transformations. Examples of the latter are the domains for flow over a cylinder, Thom (1933), and flow between rotating eccentric cylinders, Launder and Ying (1971). Nevertheless if we are to use the equations as set up by Gosman et al (1969) for more complicated domains, then it is necessary to determine an orthogonal mesh by numerical or graphical means. Unfortunately, the available numerical methods of calculating orthogonal grids,

Barfield (1970), Apelt and Thom (1961), involve much laborious work before all the required geometrical quantities are obtained. It is obvious that this initial effort should be avoided, if a simpler alternative grid network can be developed. This is the subject of the next section, which shows that a Cartesian co-ordinate system can be used to map a domain with non - rectangular boundaries and that appropriate difference equations can be set up for the near - wall nodes.

3.3.2 The present treatment

The basis of the treatment of non - rectangular boundaries is the use of a RAND (Rectangular Arrangement for Non-rectangular Domains) grid, which is illustrated in Fig. 3.3.5. In this figure a curved surface, which is not orientated in any particular direction, is approximated by a succession of straight lines linking the grid nodes on the surface. The nodes within the domain are arranged in a pattern, which is orthogonal with the x_1 and x_2 co-ordinate axes. The boundaries of each cell lie midway between the grid nodes. This means that the cell adjacent to the wall are triangular in shape, but those in the remainder of the domain are rectangular. Another possible RAND grid arrangement, in which the grid nodes are positioned at the geometric centres of the cells, is described by Le Feuvre (1970). The detailed treatment for this arrangement, which is similar to but less convenient than for the arrangement in

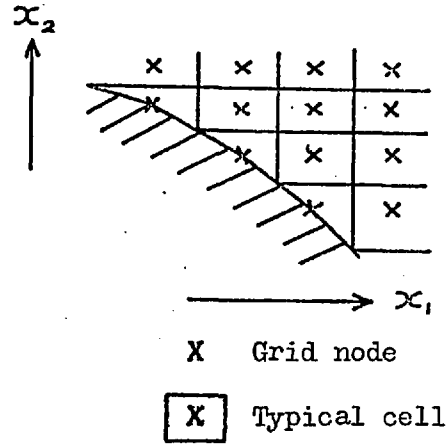
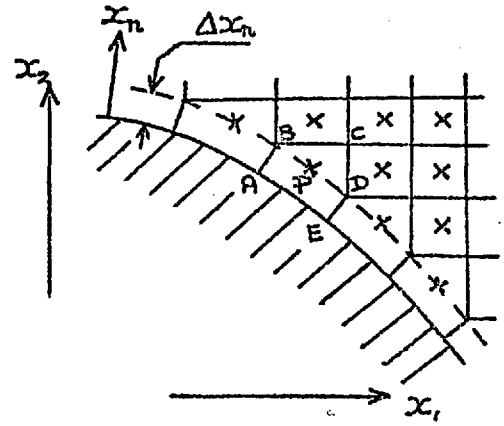


Fig. 3.3.5

Fig. 3.3.5, is also given by Le Feuvre (1970).

If should be pointed out here that the grid in Fig. 3.3.5 is used exclusively for the calculation of low Reynolds number flows. When dealing with the prediction of turbulent flows, the grid in Fig. 3.3.5 is modified to the form given in Fig. 3.3.6, where the wall nodes in Fig. 3.3.5 are moved away from the wall by a small distance Δx_n . The cell walls, AB and DE, of a typical near-wall cell P are normal to the curved surface.



X Grid node

X Cell in field

X Cell near wall

Fig. 3.3.6

So far we have illustrated two cell arrangements for boundaries which are <u>not</u> parallel to the co-ordinate axes. We now illustrate the situation where the curved surface becomes parallel to one of the axes. We do this by considering the near - wall region where the curved surface becomes normal to the x_2 - axis. The appropriate cell arrangements, corresponding to Figs. 3.3.5 and 3.3.6, are shown in Figs. 3.3.7 and 3.3.8 respectively. In Fig. 3.3.7, the curved surface at the top of a cylinder is approximated by a straight line parallel with the x_1 direction. This line forms one side of

the rectangular cell P and the geometrical positions of nodes P, E and SE are inter - related by the requirement that the cell walls lie midway between the nodes. The arrangement in Fig. 3.3.7 is preferred to the use of closely spaced triangular cells up to the top of the cylinder. On the other hand the grid in Fig. 3.3.8 (corresponding to that in Fig. 3.3.6)

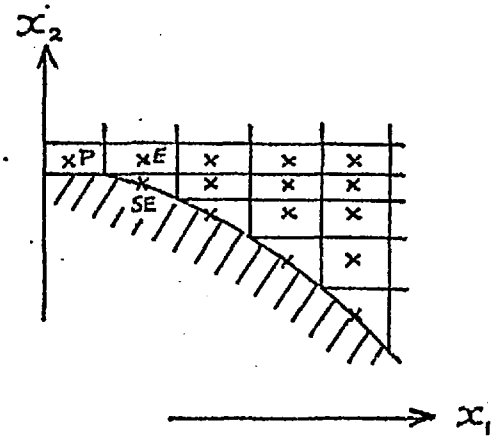


Fig. 3.3.7

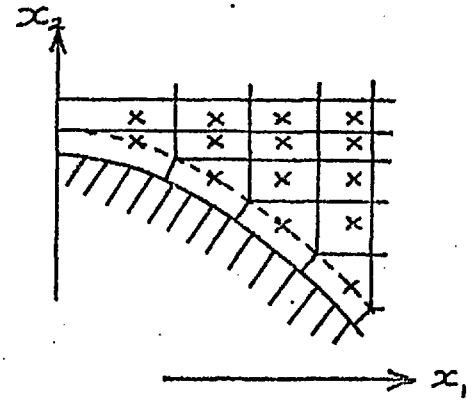


Fig. 3.3.8

shows that the arrangement near the top of a cylinder is essentially unchanged from that lower down.

We should now consider why it is necessary to use two grid arrangements, one for laminar flows and one for turbulent flows. The reason is due to computational difficulties, which became apparent during the process of development. The grid in Fig. 3.3.5 was used in all the Chapter 5 laminar - flow calculations, but when it was applied to the computation of turbulent flows through in - line tube banks divergence problems were encountered. The origin of the divergence was traced to a combination of the use of wall slip values of ϕ (section 3.3.3, equation (3.3.4)) and the instability of the new - upwind terms under certain conditions,

section 3.4.1. This source of divergence was eliminated by rewriting the convection terms so that wall slip values of ϕ were not employed, and to correspond with the latter modification the grid was altered to the form in Fig. 3.3.6.

We now pass on to the next section where we set up the difference equations for the near - wall cells in Figs. 3.3.5 and 3.3.6. For the sake of abbreviation, the grids in Figs. 3.3.5 and 3.3.6 will now be referred to as the F.W.P. (fixed wall point) and F.N.P. (fixed near - wall point) arrangements respectively. The meanings of the abbreviations, F.W.P. and F.N.P. describe appropriately how the corresponding grids are generated.

3.3.3. The finite - difference conservation equations for typical F.W.P. and F.N.P. cells

In this section, we shall first consider the difference equations for the F.W.P. near - wall cells in some detail and then we shall deal more briefly with the equations for the F.N.P. arrangement.

(a) F.W.P. near - wall cell

Referring to Fig. 3.3.9, which illustrates a typical F.W.P. near - wall cell arrangement, we choose cell P as the typical near - wall cell and we assume that the flow through the triangular cells adjacent to the wall is one - dimensional and always parallel to the wall. This assumption means that the flow directions through the west and south boundaries of cell P are fixed by

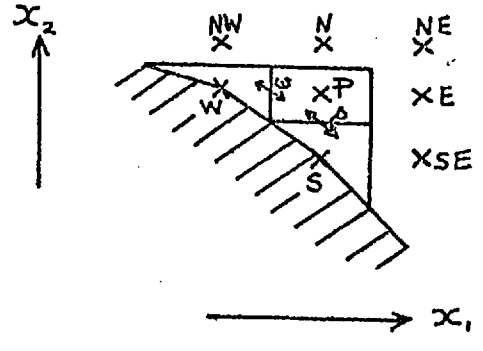


Fig. 3.3.9

the vectors which pass through the cell boundary points w and s and which are parallel to the wall boundary.

We now derive the convection, diffusion and source terms for the ϕ equation appropriate to cell P, and then illustrate the special forms of the near - wall equations for ψ and ω.

(i) Convection terms

The formulation of the convection terms for the near - wall cell boundaries is our first consideration. As an example, we shall derive the expression for the west boundary of cell P. Now we have indicated above that the flow direction through the west boundary is known and therefore the values of P_{PW}, P_{MW}, G_{WW} and G_{WP}, in the new - upwind formulation, section 3.2.1, are known. In this case, P_{PW} is zero and P_{MW} is unity. However it should be noted that when the flow is from right to left, it is not possible to use the new - upwind formulation which indicates that we should interpolate between ϕ_P and ϕ_{SW} because node SW does not exist. Instead we are constrained to interpolate between ϕ_P and ϕ_S. Therefore the convection term for the west boundary is as follows:

$$I_c = A_{w1}\left[\phi_P(1 - G_{WP}) + \phi_S G_{WP}\right] - A_{w2}\left[\phi_w(1 - G_{WW}) + \phi_N G_{WW}\right] \qquad (3.3.1)$$

Similarly the convection term for the south boundary is given by:

$$I_c = A_{s2}\left[\phi_P(1 - G_{SP}) + \phi_W G_{SP}\right] - A_{s1}\left[\phi_S(1 - G_{SS}) + \phi_E G_{SS}\right] \qquad (3.3.2)$$

The complete convection term for cell P, which is obtained by adding equations (3.3.1) and (3.3.2) to the expressions for the north and east cell boundaries, is as follows:

$$
\begin{aligned}
I_{CON} = {} & \phi_P\left[A_{N1}(1-G_{NP}) + A_{S2}(1-G_{SP}) + A_{E2}(1-G_{EP}) + A_{W1}(1-G_{WP})\right] \\
& - \phi_N\left[A_{N2}(1-G_{NN}) + P_{PE}\,A_{E1}\,G_{EE} + A_{W2}\,G_{WW}\right] \\
& - \phi_S\left[A_{S1}(1-G_{SS}) + P_{ME}\,A_{E1}\,G_{EE} - A_{W1}\,G_{WP}\right] \\
& - \phi_E\left[A_{E1}(1-G_{EE}) + P_{PN}\,A_{N2}\,G_{NN} + A_{S1}\,G_{SS}\right] \\
& - \phi_W\left[A_{W2}(1-G_{WW}) + P_{MN}\,A_{N2}\,G_{NN} - A_{S2}\,G_{SP}\right] \\
& + \phi_{NE}\left[P_{MN}\,A_{N1}\,G_{NP} + P_{ME}\,A_{E2}\,G_{EP}\right] \\
& + \phi_{NW}\left[P_{PN}\,A_{N1}\,G_{NP}\right] + \phi_{SE}\left[P_{PE}\,A_{E2}\,G_{EP}\right] \qquad (3.3.3)
\end{aligned}
$$

where, the A's, G's and P's are defined in section 3.2.1.

We should at this stage consider the wall values ϕ_W and ϕ_S, to be assigned to equation (3.3.3). It may seem obvious that the wall values should be given by either the fixed boundary values or, in the case of vorticity, the wall value calculated from the appropriate internal nodes. However if the wall value is assigned in circumstances where the gradient of ϕ at the wall is large, this will lead to grossly inflated convection terms for the near - wall cell boundaries and thus to significant errors in the whole domain. To avoid this possibility, 'wall slip values' are calculated from the values of ϕ at neighbouring nodes and these are assigned to ϕ_W and ϕ_S in equation (3.3.3). The calculation of slip values is performed by assuming that ϕ varies linearly between the wall point and its three neighbours. Referring to Fig. 3.3.9, we assume that ϕ varies linearly between the node W and its neighbours NW, N and P, and between the node S and its neighbours P, E and SE. With this assumption $(\phi_W)_{slip}$ and $(\phi_S)_{slip}$ are given by:

$$
\begin{aligned}
(\phi_W)_{slip} &= \phi_{NW} + \phi_P - \phi_N \\
(\phi_S)_{slip} &= \phi_P + \phi_{SE} - \phi_E \qquad (3.3.4)
\end{aligned}
$$

The latter are close to the actual values only in situations, such as in constant property laminar flows, where ϕ does vary linearly near the wall. In circumstances where the gradient of ϕ is steep at the wall and falls off rapidly away from the wall, the above method gives good approximations for the near - wall convective fluxes.

(ii) Diffusion terms

Now we consider the diffusion terms appropriate to the near - wall cell P in Fig. 3.3.9. As for the convection terms we assume that the flow through the near - wall cell boundaries is one - dimensional, and so the diffusion of ϕ parallel to the wall is negligible compared with the diffusion normal to the wall. Referring to Fig. 3.3.10, this means that the west and south diffusion terms in equation (3.2.1) can be summed and given by either:

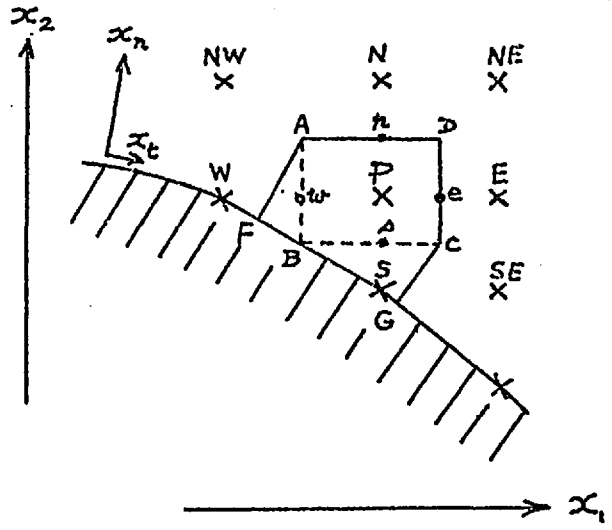


Fig. 3.3.10

$$(I_d)_{west} + (I_d)_{south} = \int_{x_{2,s}}^{x_{2,n}} (v_\phi)_w \left[\frac{\partial}{\partial x_1}(c_\phi \phi)\right]_w \, dx_2 + \int_{x_{1,w}}^{x_{1,e}} (v_\phi)_s \left[\frac{\partial}{\partial x_2}(c_\phi \phi)\right]_s \, dx_1 \qquad (3.3.5)$$

or,

$$(I_d)_{west} + (I_d)_{south} = \int_{x_{t,F}}^{x_{t,G}} (b_\phi)_{wall} \left[\frac{\partial}{\partial x_n}(c_\phi \phi)\right]_{wall} dx_t \qquad (3.3.6)$$

where, x_t and x_n denote the co-ordinates parallel to and normal to the wall respectively.

Equation (3.3.6) can be expressed in the following finite - difference form, if $c_\phi \phi$ varies linearly with x_n, and b_ϕ is independent of x_t:

$$(I_d)_{west} + (I_d)_{south} = (b_\phi)_{wall}\left[\frac{(c_\phi \phi)_P - (c_\phi \phi)_{wall}}{x_{n,P} - x_{n,wall}}\right](x_{t,G} - x_{t,F})$$

$$= B_{wall}\left[(c_\phi \phi)_P - (c_\phi \phi)_{wall}\right] \qquad (3.3.7)$$

where, $B_{wall} = (b_\phi)_{wall}\left[\frac{x_{t,G} - x_{t,F}}{x_{n,P} - x_{n,wall}}\right]$

It should be noted that in general the finite - difference approximations for equation (3.3.6) are much easier to obtain than for the general form of equation (3.3.5). This is particularly true for variables, such as vorticity, which are not usually given fixed wall values and which may vary rapidly in the near - wall region. However where the values of ϕ at the wall nodes are fixed by the boundary conditions, then the use of equation (3.3.5) may be preferred. This is true for the formulation of the stream function equation in the case of constant property laminar flows. In the latter case, equation (3.3.5) for the west and south stream - function - gradient terms is written in the following finite - difference form:

$$(I_d)_{west} + (I_d)_{south} = B_W(\psi_P - \psi_W) + B_S(\psi_P - \psi_S) \qquad (3.3.8)$$

where, B_W and B_S are given by equation (3.2.20), ψ_W and ψ_S are the wall values of stream function.

(iii) Source terms

It is difficult to deal with the derivation of source terms in a general manner. So we shall concentrate our attention on the evaluation of the only source term used in the present predictions of constant property laminar flows. This is the stream function source term which is given by:

$$I_{SOR} = -\int_{x_{2,s}}^{x_{2,n}} \int_{x_{1,w}}^{x_{1,e}} \omega \; dx_1 \, dx_2$$

$$= -\overline{\omega}_P \; V_P \qquad (3.3.9)$$

where, $\overline{\omega}_P$ = space – average vorticity

$$V_P = \tfrac{1}{4}(x_{2,N} - x_{2,S})(x_{1,E} - x_{1,W})$$

As ω varies linearly near the wall then the space – average vorticity, $\overline{\omega}$, can be assumed to be given approximately by the node vorticity, ω_P.

$$\therefore I_{SOR} = -\omega_P \; V_P \qquad (3.3.10)$$

In the above, we have considered typical formulations for the convection, diffusion and source terms for a near – wall node. Now by way of example, we show how the expressions for stream function and vorticity are formed.

(iv) The equation for near – wall stream function

The near – wall stream function equation is formulated by summing equation (3.3.8), equation (3.3.10) and the appropriate north and east gradient terms, and then equating the sum to zero as follows:

$$B_N(\psi_P - \psi_N) + B_S(\psi_P - \psi_S) + B_E(\psi_P - \psi_W) + B_W(\psi_P - \psi_W) - \omega_P V_P = 0$$

Rearranging gives the following equation for ψ_P:

$$\psi_P = \frac{B_N \psi_N + B_S \psi_S + B_E \psi_E + B_W \psi_W + \omega_P V_P}{B_N + B_S + B_E + B_W} \qquad (3.3.11)$$

(v) The equation for near - wall vorticity

After collecting the convection and diffusion terms together, the expression for near - wall vorticity ω_P, based on the nodes in Fig. 3.3.10, is of the following form:

$$\omega_P = \omega_P\{\omega_N, \omega_E, \omega_{NE}, \omega_{NW}, \omega_{SE}, \omega_{wall}\} \qquad (3.3.12)$$

where, $$\omega_{wall} = -\left[\frac{\omega_P}{2} + \frac{3(\psi_P - \psi_{wall})}{\rho x_{n,P}^2}\right] \qquad (3.3.13)$$

Equation (3.3.13) is obtained from equation (2.5.5), where the present subscripts wall and P are substituted for subscripts S and C respectively. Using equation (3.3.13) to eliminate ω_{wall} from equation (3.3.12), then equation (3.3.12) can be written as:

$$\omega_P = \omega_P\{\omega_N, \omega_E, \omega_{NE}, \omega_{NW}, \omega_{SE}, \psi_P, \psi_{wall}\} \qquad (3.3.14)$$

This sort of formulation for near - wall vorticity is called an 'implicit' formulation, Gosman et al (1969), because the wall vorticity no longer appears explicitly in equation (3.3.14). In many circumstances this form of the equation will enable numerical convergence to be obtained. However if the grid point P is very close to the wall, divergence may occur because of the stream function - vorticity interaction. This interaction exists because ψ_P, equation (3.3.11), is a function of ω_P as follows:

$$\psi_P = \psi_P\{\omega_P, \psi_N, \psi_S, \psi_E, \psi_W\} \qquad (3.3.15)$$

Thus ω_P appears on both sides of equation (3.3.14). To enhance convergence in all circumstances, ω_P must be eliminated from the right - hand side of (3.3.14). This is done by rearranging equation (3.3.15) into the following form:

$$\psi_P - \frac{\omega_P}{\Sigma} = f\{\psi_N, \psi_S, \psi_E, \psi_W\}$$
$$\Sigma = (B_N + B_S + B_E + B_W)/V_P \qquad (3.3.16)$$

Then equation (3.3.16) is substituted into equation (3.3.14) to eliminate ω_P completely from the right - hand side. The resulting equation is as follows:

$$\omega_P = \omega_P\{\omega_N, \omega_E, \omega_{NE}, \omega_{NW}, \omega_{SE}, [\psi_P - \frac{\omega_P}{\Sigma}], \psi_{wall}\} \qquad (3.3.17)$$

Equation (3.3.17) is called the 'fully - implicit' formulation for near - wall vorticity. From past experience, this formulation not only enhances convergence but also accelerates the process of convergence.

(b) F.N.P. near - wall cell

We now consider the formulations for the F.N.P. near - wall cells. We shall restrict our attention to the convection and diffusion terms because the source terms for turbulent flows are discussed in Chapter 6. Referring to Fig. 3.3.11, which illustrates a typical F.N.P. near - wall cell we assume that the flow between the parallel curves APC and FD is one - dimensional.

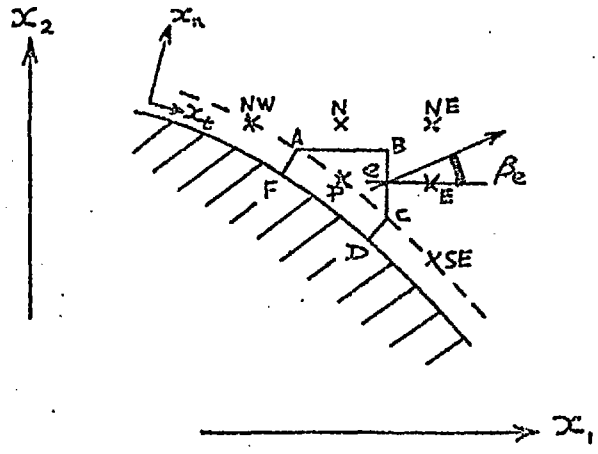


Fig. 3.3.11

(i) Convection terms

For reference purposes, we refer to the cell walls AF and CD in Fig. 3.3.11 as the west and south walls respectively. We are not concerned with the wall FD because it is impermeable. Referring to the west wall and equations (3.2.11), we define A_{W1} and A_{W2} as:

$$A_{W1} = -a_{\phi,P}\left[(\psi_A - \psi_F) - |\psi_A - \psi_F|\right]/2$$

$$A_{W2} = a_{\phi,P}\left[(\psi_A - \psi_F) + |\psi_A - \psi_F|\right]/2 \qquad (3.3.18)$$

where,

$$\psi_A \equiv \psi_{nw}$$

$$\psi_F \equiv \psi_{sw}$$

Similarly A_{S1} and A_{S2} are given by:

$$A_{S1} = -a_{\phi,P}\left[(\psi_C - \psi_D) - |\psi_C - \psi_D|\right]/2$$

$$A_{S2} = a_{\phi,P}\left[(\psi_C - \psi_D) + |\psi_C - \psi_D|\right]/2 \qquad (3.3.19)$$

where,

$$\psi_C \equiv \psi_{se}$$

$$\psi_D \equiv \psi_{sw}$$

Now ψ_D and ψ_F are given by the stream function value on the wall boundary. However ψ_A and ψ_C must be expressed in terms of the surrounding values as follows:

$$\psi_A = \tfrac{1}{2}(\psi_{NW} + \psi_P)$$

$$\psi_C = \tfrac{1}{2}(\psi_P + \psi_{SE}) \qquad (3.3.20)$$

Using the standard - upwind method, the convection terms for the west and south walls are given by:

$$(I_c)_{west} = A_{W1}\,\phi_P - A_{W2}\,\phi_{NW}$$

$$(I_c)_{south} = A_{S2}\,\phi_P - A_{S1}\,\phi_{SE} \qquad (3.3.21)$$

We now provide some explanation of the new - upwind formulations for the north and east walls. Referring to Fig. 3.3.11 and the east boundary of cell P, we consider the possible directions of the mean velocity vector and the corresponding new - upwind interpolations between the ϕ's as follows:

(i) $0 < \beta_e < \pi/2$
$\pi < \beta_e < 3\pi/2$
} as given by $\beta_e = \tan^{-1}[(u_2)_e/(u_1)_e]$

Interpolation between ϕ_P and ϕ_{SE} or between ϕ_N and ϕ_E. The definitions of β_e, $(u_1)_e$, $(u_2)_e$ and the appropriate G's are given in Appendix A.2.

(ii) $\pi/2 < \beta_e < \pi$
$3\pi/2 < \beta_e < 2\pi$
} as given by $\beta_e = \tan^{-1}[(u_2)_e/(u_1)_e]$

Interpolation between ϕ_E and ϕ_{SE} or between ϕ_P and ϕ_{NE}. The G's in this case are calculated by assuming that the velocity vector is parallel with the wall boundary. This latter measure has to be taken so as to obtain converged solutions. Interpolations similar to (i) and (ii) are carried out for the north wall. Collecting all the terms together, the complete convection term for cell P is as follows:

$$
\begin{aligned}
I_{CON} = {} & \phi_P \{A_{N1}(1-G_{NP}) + A_{E2}(1-G_{EP}) + A_{S2} + A_{W1}\} \\
& - \phi_N \{A_{N2}(1-G_{NN}) + P_{PE} A_{E1} G_{EE}\} \\
& - \phi_E \{A_{E1}(1-G_{EE}) + P_{PN} A_{N2} G_{NN}\} \\
& + \phi_{NE} \{P_{MN} A_{N1} G_{NP} + P_{ME} A_{E2} G_{EP}\} \\
& - \phi_{NW} \{P_{MN} A_{N2} G_{NN} + A_{W2} - P_{PN} A_{N1} G_{NP}\} \\
& - \phi_{SE} \{P_{ME} A_{E1} G_{EE} + A_{S1} - P_{PE} A_{E2} G_{EP}\} \qquad (3.3.22)
\end{aligned}
$$

where, the A's, G's and P's are defined in section 3.2.1.

(ii) Diffusion terms

Referring to Fig. 3.3.11, we stated earlier that the flow between the curves APC and FD is assumed to be one - dimensional. Therefore it follows that the diffusion in the direction parallel to the wall through the boundaries AF and CD is negligible compared with the diffusion in the normal direction through boundary FD. The term for the latter is similar to equation (3.3.6) and can be written as follows:

$$(I_d)_{FD} = \int_{x_{t,F}}^{x_{t,D}} (\nu_\phi)_{wall} \left[\frac{\partial}{\partial x_n}(c_\phi \phi)\right]_{wall} dx_t \qquad (3.3.23)$$

One example of equation (3.3.23) is the expression for the total heat flux through FD as follows:

$$(I_d)_{FD} = \int_{x_{t,F}}^{x_{t,D}} \dot{q}''_{wall}/c_p \; dx_t \qquad (3.3.24)$$

where, $\dot{q}''_{wall}$ = heat flux through wall

c_p = specific heat of fluid

The form of $\dot{q}''_{wall}/c_p$ for turbulent flow is given in Chapter 6.

The diffusion terms for the north and east boundaries of cell P are given by the standard form, as shown in equation (3.2.18).

3.4 Some properties of the numerical procedure

The most important properties of a numerical procedure are the factors which affect its convergence, accuracy and economy. These properties as applied to the present procedure have been studied in some detail by Gosman et al (1969), Wolfshtein (1967) and Runchal (1969). It is not the present purpose to reproduce the material discussed by these authors. However we should initially focus our attention on what is meant by the terms convergence, accuracy and economy as applied to a

numerical procedure. Then we shall consider the convergence properties of the new - upwind difference equations in section 3.4.1. Matters, which concern accuracy and economy, are not dealt with here but are discussed in the following chapters with respect to particular problems.

(a) Convergence

It was mentioned in section 3.2.2 that the difference equations are to be solved by an iterative procedure. This means that an initial guess is substituted into the successive - substitution formulae and a new solution is obtained. The latter is then used as a new guess, and so on. It is obvious that this procedure will be useful only if it satisfies the requirement that with each new guess the iterative solution approaches the exact solution of the difference equations. This condition is called the requirement of convergence.

(b) Accuracy and Economy

Assuming that unique solutions exist for the difference and differential equations, then the overall numerical error is the difference between the numerical solution of the difference equations and the exact solution of the differential equations. This difference is a measure of the accuracy with which we are concerned. The economy of a numerical procedure is measured by the computer time required to obtain a numerical solution by interative means.

The overall numerical error consists of three components. Firstly there is the round - off error, which is due to the fact that a computing machine must perform its calculations with a finite number of digits. Experience shows that this error is negligible in machines which use numbers with 8 or more digits.

Secondly there is the iterative error, which is the difference between the iterative numerical solution and the exact solution of the difference equations. This difference may be reduced to a negligible

quantity by allowing the number of iterations to proceed to a very large number. However because the computer time is directly related to the number of iterations one must, for the sake of economy, limit the number of iterations in such a way that the iterative error is below an acceptable level. Such a limit can be determined by the following index of convergence, which can also be regarded as a measure of the iterative error:

$$\underset{\text{(all nodes)}}{\text{Max.}} \left| \frac{\phi^{(N)} - \phi^{(N-1)}}{\phi^{(N)}} \right| \leq \lambda \qquad (3.4.1)$$

where $\phi^{(N)}$ is the value of any dependent variable at the N^{th} iteration. The computations are stopped when λ falls below a prespecified limit λ_{ref}.

However a further test of convergence must be applied to minimise the effect of oscillating small values of $\phi^{(N)}$. For instance, a relatively small value of $\phi^{(N)}$ in the field may oscillate widely from one iteration to another even though the rest of the field is almost settled. This can cause λ to be much greater than λ_{ref} and thus suggest that the field is far from settled. To minimise this effect, λ' is also calculated as follows:

$$\underset{\text{(all nodes)}}{\text{Max.}} \left| \frac{\phi_P^{(N)} - \phi_P^{(N-1)}}{1/4\,(\phi_N^{(N-1)} + \phi_E^{(N-1)} + \phi_W^{(N)} + \phi_S^{(N)})} \right| \leq \lambda'$$

where, subscript P indicates any node surrounded by four neighbouring nodes indicated by subscripts N, E, W and S.

If $\lambda' < \lambda$, then λ' is compared with λ_{ref} instead of λ being compared with λ_{ref}. The experience of Gosman et al (1969) indicates that $\lambda_{ref} = 0.001$ is a sufficient limit for most problems. The above criteria with $\lambda_{ref} = 0.001$ are used in the present computational procedure.

A more rigorous index of convergence, employed by Gosman, Lockwood and Tatchell (1970), is the magnitude of the 'residual source' term in

each ϕ - difference equation at each node. By rearranging the general ϕ - equation in (3.2.23), $R_{\phi,P}$, the residual source term at node P, is defined by:

$$R_{\phi,P} = \phi_P D - (N_{CON} + N_{DIFF} + N_{SOR}) \qquad (3.4.2)$$

An exact solution to equation (3.2.23) requires that $R_{\phi,P}$ is zero, but when the solution is incorrect $R_{\phi,P}$ measures the current error in the solution of (3.2.23). R_ϕ for all ϕ's at all nodes must be reduced to an acceptable level before the computations are stopped. This index is often used in conjunction with equation (3.4.1) but it is not used in the present procedure.

Thirdly, there is the discretization error, which is the difference between the exact solution of the difference equations and that of the differential equations. In other words this error is composed of all the errors due to the approximation of the differential terms in a ϕ - conservation equation by finite - difference terms. This error is the major source of the overall numerical error, because as discussed above the errors from the other sources are reduced to negligible amounts by using sufficient digits and requiring sufficient iterations in the calculation procedure. One obvious way of reducing this error is to use fine grids so that the resulting finite - difference terms give a more exact representation of the differential terms. However the extent to which a grid may be refined (and thus the number of nodes increased) is limited by considerations of economy and computer storage.

3.4.1 Convergence properties

Gosman et al (1969) give a detailed discussion of the convergence properties of the general equation (3.2.23), where the convection terms are approximated by the standard - upwind method. It is the purpose of this section to illustrate the convergence properties of equation

(3.2.23), where in this case the convection terms are given by the new - upwind method.

We must initially consider the following set of equations:

$$x_i = \sum_{j,i\neq j} (a_{ij} x_j + b_i) \qquad (3.4.3)$$

where the x's are the unknowns. It is known that if the equations in (3.4.3) are linear (i.e. the a's and b's are constants) their use as substitution formulae will be convergent if:

$$\sum_{j,i\neq j} |a_{ij}| \leq 1 \qquad (3.4.4)$$

for each i; and for a least one i,

$$\sum_{j,i\neq j} |a_{ij}| < 1 \qquad (3.4.5)$$

Gosman et al (1969) show that equation (3.2.23) with the standard - upwind terms can be written in the form of equation (3.4.3), and that, for this set, equation (3.4.5) is usually satisfied at a boundary. However in general the a's and b's are not linear but vary from one iteration cycle to another. Nevertheless experience has shown that the above criteria are still useful guides, because they are often sufficient but not always necessary conditions for convergence and that they may be mildy contravened without serious effect.

To illustrate the convergence properties of equation (3.2.23) with the new - upwind terms, we shall determine the sum of the coefficients for an optimum flow condition and compare the result with equation (3.4.4). This optimum flow condition is given by the situation where the diffusion terms are negligible, and the difference between the standard - and new - upwind terms is a maximum. A simple example of such a flow is shown in Fig. 3.4.1, where a zero - viscosity uniform - velocity stream is inclined at an angle of 45° to a uniform grid mesh.

The ϕ - equation for the typical cell P is given by:

$$
\begin{aligned}
&-M\left[\phi_N(1-G_{NN}) + \phi_W G_{NN}\right] \\
&-M\left[\phi_W(1-G_{WW}) + \phi_N G_{WW}\right] \\
&+M\left[\phi_P(1-G_{SP}) + \phi_{SW} G_{SP}\right] \\
&+M\left[\phi_P(1-G_{EP}) + \phi_{NE} G_{EP}\right] \qquad (3.4.6)
\end{aligned}
$$

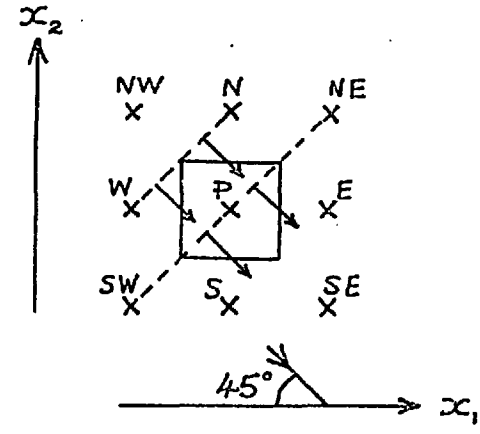


Fig. 3.4.1

where, M = absolute value of flow across any cell wall

and, the G's are defined in section 3.2.1.

For the uniform grid in Fig. 3.4.1, the G's are given by:

$$G_{NN} = G_{WW} = G_{SP} = G_{EP} = 0.25$$

By rearranging equation (3.4.6) we obtain:

$$\phi_P = C_N \phi_N + C_W \phi_W + C_{SW} \phi_{SW} + C_{NE} \phi_{NE} \qquad (3.4.7)$$

where,

$$C_N = \frac{1 - G_{NN} + G_{WW}}{2 - G_{SP} - G_{EP}} = 0.66$$

$$C_W = \frac{1 - G_{WW} + G_{NN}}{2 - G_{SP} - G_{EP}} = 0.66$$

$$C_{SW} = \frac{-G_{SP}}{2 - G_{SP} - G_{EP}} = -0.166$$

$$C_{NE} = \frac{-G_{EP}}{2 - G_{SP} - G_{EP}} = -0.166$$

Now the criteria in equation (3.4.4) indicate that, when using equation (3.4.7) as a successive - substitution equation, convergence is ensured if:

$$\Sigma|C| = |C_N| + |C_W| + |C_{SW}| + |C_{NE}| \leq 1.0$$

However we find that:

$$\Sigma|C| = 1.66$$

Thus this example shows that in the limit the new – upwind equations can seriously contravene the criteria of equation (3.4.4), and indeed computations of this flow situation result in numerical divergence. On the other hand, the stability of the standard – upwind equations is illustrated by the fact that equation (3.4.4) is always satisfied. This can be shown by putting the G's in equation (3.4.7) equal to zero, and thus $\Sigma|C|$ for the standard – upwind equations is given by:

$$\Sigma|C| = 1.0$$

Considering a more general case of Fig. 3.4.1, where the angle between the direction of the stream and the x_1 direction is a variable β, then it can be shown that $\Sigma|C|$ for the new – upwind equations has two limiting values. The upper limit is 1.66 for $\beta = 45^\circ$ and the lower limit is 1.0 for $\beta = 0$. Also it can be shown that the inclusion of diffusion in this example does not alter the lower limit of $\Sigma|C|$ but decreases the upper limit as viscosity increases. This means that $\Sigma|C|$, for the new – upwind formulation, is within the range $1.0 \leq \Sigma|C| \leq 1.66$ for all flows. It is nevertheless encouraging to note that experience with the predictions of an inclined – plane Couette flow, Chapter 4, indicates that $\Sigma|C|$ can be as large as 1.4 without causing divergence or instability. Therefore as we shall see in Chapters 5 and 6, where the laminar viscosity, or in the case of turbulent flow the effective viscosity, is sufficiently large to decrease the upper limit of $\Sigma|C|$ below say 1.4 for all the ϕ equations, then convergence will be obtained. The latter statement applies particularly to the vorticity and temperature equations, which have zero source terms. However as shown by Gosman et al (1969), where a ϕ – equation is strongly dependent on its source term, i.e. the equation for kinetic energy of turbulence, other measures also have to be used to promote convergence.

4. APPLICATION TO PROBLEMS WITH ANALYTICAL SOLUTIONS

In the previous chapter, a general procedure for solving the general conservation equation (2.4.1) was outlined. It was also demonstrated that, by the use of a RAND grid arrangement, the general solution procedure could be applied to the prediction of recirculating flows in domains of arbitrary shape. In this chapter, the properties of the procedure, such as convergence and accuracy, are illustrated by the prediction of flows with analytical solutions and by the comparison of the predicted and theoretical solutions.

4.1 The purpose

In the previous chapter, a general procedure was outlined for predicting flows in domains of arbitrary shape. It is the purpose of this chapter to illustrate the properties of this procedure by:

(a) applying the procedure to flows which have analytical solutions for domains with non - rectangular boundaries.

and, (b) comparing the resulting predictions with the theoretical solutions.

The choice of two - dimensional flows as described in (a) is rather limited. However the latter choice is avoided by making use of two flows with one - dimensional solutions. This is done in such a way that as far as the prediction procedure is concerned the flows are two - dimensional. The details of these flows and the corresponding grid arrangements are given in the following sections.

At this stage in the introduction, it should be mentioned that, for the predictions described in this chapter, the finite - difference grids are arranged so that each grid node is positioned at the geometric centre

of each cell. The appropriate finite - difference equations are described by Le Feuvre (1970). The above grid arrangement is different from that described in Chapter 3, because for the latter the cell boundaries are midway between the grid nodes but for the former this is generally not so. Because of the different grid arrangements, the main difference between the equations in Chapter 3 and those given by Le Feuvre (1970) lies in the approximation of the gradients of ϕ at the cell boundaries. In Chapter 3, the gradients are calculated using a 2 - point approximation, because the cell boundaries are midway between the grid nodes. However for the predictions in this chapter, and those of Le Feuvre (1970) the gradients are calculated using 3 - and 4 - point approximations. The latter are used because in general the cell boundaries are not midway between the grid nodes. Some tests have been performed to determine the relative accuracy of the two sets of finite - difference approximations, and the results show that the differences in accuracy are small. However the computer programme appropriate to the Chapter 3 grid arrangement is much simpler than that for the grid used by Le Feuvre (1970). It was for this reason that the latter was eventually abandoned in favour of the Chapter 3 grid arrangement. Nevertheless the present predictions fulfill the purpose of illustrating the properties of the solution procedure described in Chapter 3.

We now pass on to sections 4.2 and 4.3, which describe the predictions of inclined - plane and cylindrical Couette flows respectively. The final section, 4.4, gives a summary of the main results.

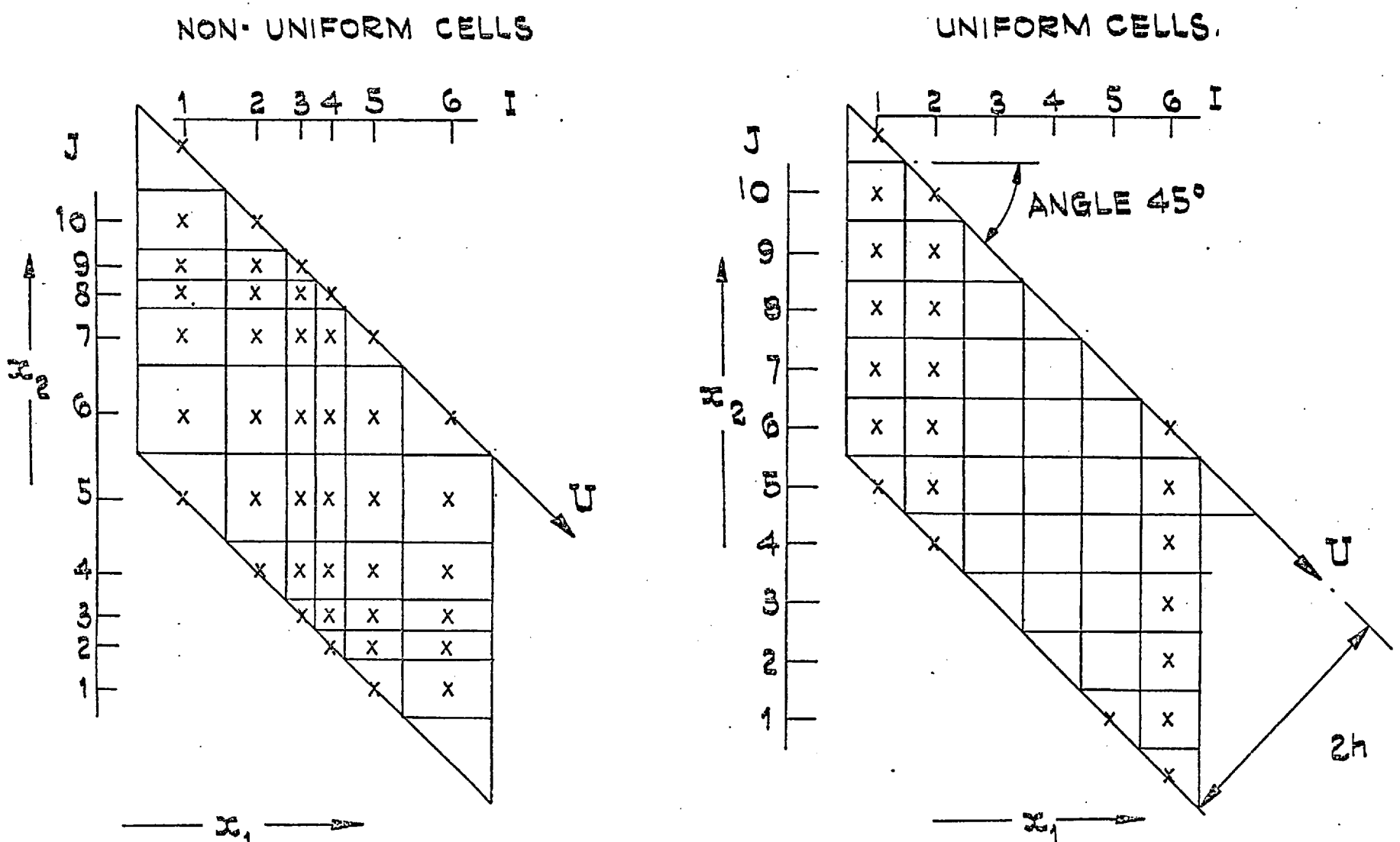


FIG. 4.2.1: INCLINED COUETTE FLOW : NON-UNIFORM AND UNIFORM GRID DISTRIBUTIONS.

4.2 Inclined – plane Couette flow

4.2.1 The problem and the grid arrangement

This section deals with the predictions of inclined – plane Couette flow. The problem of plane Couette flow between two infinite parallel plates, one moving and the other stationary, is one of the simplest flows in fluid mechanics. The problem of inclined – plane Couette flow is the same as the latter, except that the flow geometry is inclined to the finite – difference mesh as shown in Fig. 4.2.1. This means that as far as the solution procedure is concerned the flow is two – dimensional rather than one – dimensional.

In Fig. 4.2.1, two grids which have been used in the present tests are illustrated. One is an arbitrary non – uniform grid and the other is a uniform grid, but both have the same overall dimensions of 6 x 10 and the same angle of inclination of 45° to the flow boundaries. A third grid with a uniform mesh and overall dimensions of 11 x 21 has also been used. The cell size in this case is a quarter of that for the 6 x 10 uniform grid. The main purpose of using three grids is simply to determine the influence of grid non – uniformity and cell size on the accuracy of the solution procedure.

The Couette flow theory and the boundary conditions for the predictions are described in 4.2.2, and the tests and results are summarised in 4.2.3.

4.2.2 The theory and boundary conditions

(a) The theory

The equations describing the vorticity and stream function distributions in a laminar plane Couette flow with a pressure gradient, dp/dX, are as follows:

$$\omega = -\frac{1}{\mu}\frac{dp}{dX}(Y-h) - \frac{U}{2h} \qquad (4.2.1)$$

$$\frac{\psi-\psi_0}{\rho} = \frac{1}{\mu}\frac{dp}{dX}\left(\frac{Y^3}{6} - \frac{hY^2}{2}\right) + \frac{UY^2}{4h} \qquad (4.2.2)$$

where, X = distance parallel to the stationary wall

Y = normal distance from the stationary wall

h = half the normal distance between the parallel walls

U = velocity of the moving wall

ψ_0 = stream function value at the stationary wall

Now plane Couette flows may be described by the parameter $\frac{\rho U h}{\psi_{2h} - \psi_0}$

where, $\psi_{2h} - \psi_0$ = stream function difference between the moving and stationary walls

If U and h are fixed then, from equation (4.2.2), $\psi_{2h} - \psi_0$ is a function only of the pressure gradient divided by the viscosity, $\frac{1}{\mu}\frac{dp}{dX}$.

$$\therefore \frac{\rho U h}{\psi_{2h} - \psi_0} = f\left(\frac{1}{\mu}\frac{dp}{dX}\right),$$

where $f(\ )$ denotes 'a function of'.

In this section two flows, A and B, represented by two values of $\frac{\rho U h}{\psi_{2h} - \psi_0}$ are used as a basis for comparing the predictions with the theoretical solutions. Flows A and B represent two typical wall flows. Due to a positive pressure gradient, flow A has a velocity profile which is characteristic of a separated flow region. On the other hand, flow B has a boundary layer type of velocity profile due to a negative pressure gradient. For $U = h = 1.0$, flows A and B have the following values of the parameter $\frac{\rho U h}{\psi_{2h} - \psi_0}$:

Flow	$\frac{1}{\mu}\frac{dp}{dX}$	$\frac{\rho U h}{\psi_{2h} - \psi_0}$
A	1.0	3.0
B	-1.0	0.6

(b) The boundary conditions

Referring to Fig. 4.2.1, the boundary conditions for the solution procedure are as follows:

(i) The theoretical values of stream function are given on both walls.

(ii) The theoretical profiles of stream function and vorticity are given along the constant I - lines at the left - hand and right - hand sides of the domain.

The boundary conditions are completed by the specification of a Reynolds number parameter, Re. The latter is conveniently defined as follows:

$$Re = \frac{\psi_{2l} - \psi_0}{\mu}$$

This parameter gives a measure of the relative importance of the convection and diffusion terms in the elliptic equation for vorticity. However the value of Re does not influence the theoretical distributions of vorticity and stream function as given by the parameter $\frac{\rho U h}{\psi_{2l} - \psi_0}$.

This is because the chosen values of $\frac{1}{\mu}\frac{dp}{dx}$ are not dependent on Re.

4.2.3 Tests and results

(a) Tests performed

Table 4.2.1 gives a summary of the tests, which were performed using flows A and B. The tests, which converged satisfactorily, are indicated by sets of two numbers separated by a stroke, i.e. 4.2.2/4.2.3. The numbers before and after the stroke represent the numbers of the figures which contain the appropriate plots of stream function and vorticity respectively. For the purpose of comparing different characteristics of the solution procedure, the results of some tests appear on more than one set of figures. It should be noted that the plotted values are those which

Convection Term Method	Grid	Flow A: $\frac{\rho U h}{\psi_{2R} - \psi_0} = 3.0$		Flow B: $\frac{\rho U h}{\psi_{2R} - \psi_0} = 0.6$	
		Re = 0.33	Re = 33.3	Re = 1.66	Re = 166.6
Stand. Upwind	6 x 10 UG	4.2.2/4.2.3	4.2.2/4.2.3 4.2.6/4.2.7 4.2.8/4.2.9	4.2.4/4.2.5	4.2.4/4.2.5
	6 x 10 NUG	4.2.2/4.2.3	4.2.2/4.2.3 4.2.6/4.2.7	4.2.4/4.2.5	4.2.4/4.2.5
	11 x 21 UG	-	4.2.8/4.2.9	-	-
New Upwind	6 x 10 UG	-	4.2.6/4.2.7 4.2.8/4.2.9	-	Diverged
	6 x 10 NUG	-	4.2.6/4.2.7	-	Diverged
	11 x 21 UG	-	4.2.8/4.2.9	-	Diverged

Table 4.2.1

are in the least agreement with the theoretical profiles at a particular value of the x_1 co-ordinate. The blank parts of the table represent tests which have converged solutions but which do not contribute much to the present study and therefore are omitted.

(b) Results

In Figs. 4.2.2 to 4.2.5, the predictions of ψ and ω using the standard - upwind method illustrate the influence of Re and grid non - uniformity. All the predictions for low Re, that is Re = 0.33 (in

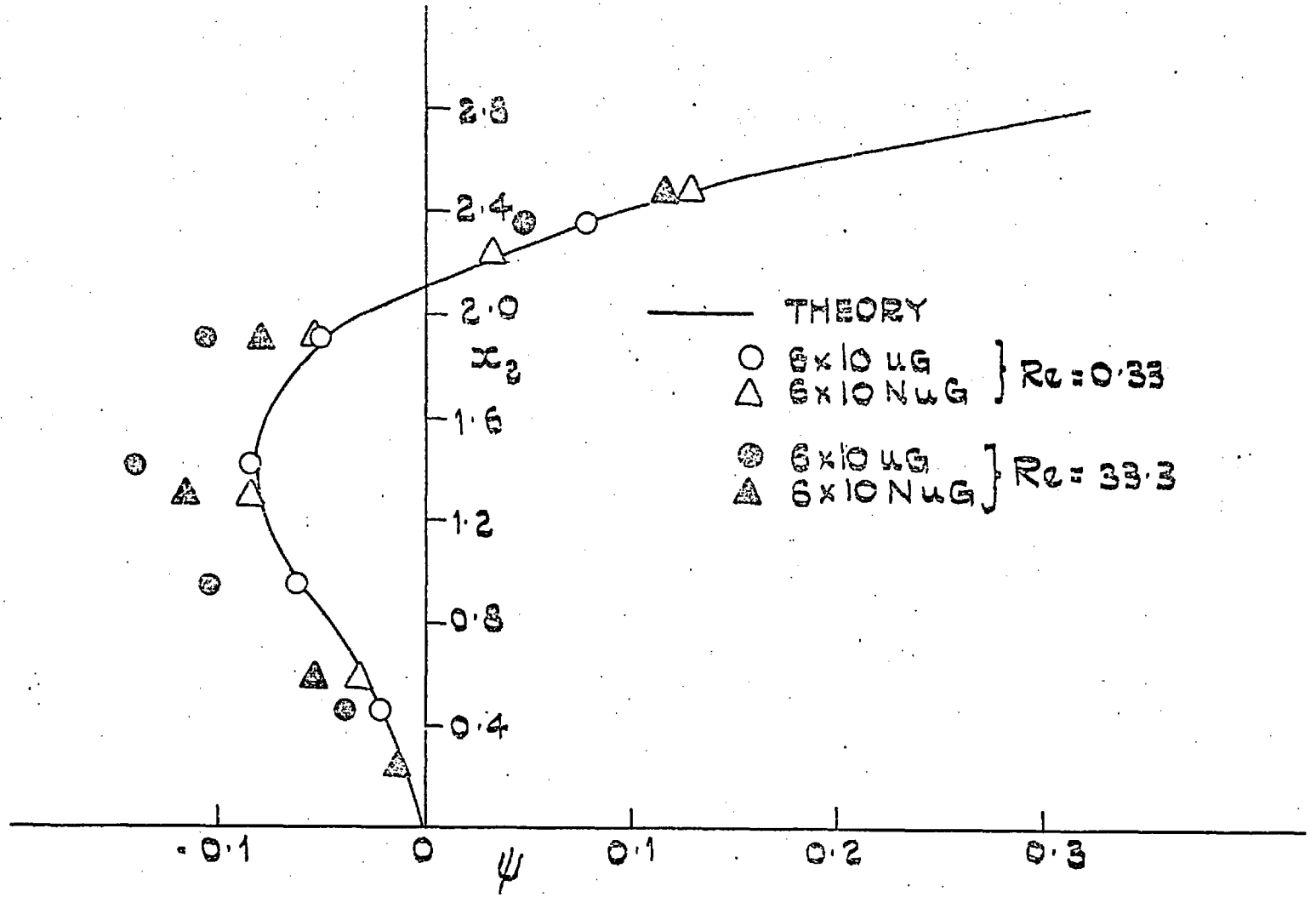


FIG. 4.2.2: INCLINED COUETTE FLOW: INFLUENCE OF Re AND GRID NON-UNIFORMITY ON STREAM FUNCTION PREDICTIONS, STAND. UPWIND, $\rho \bar{U} h / (\psi_{2h} - \psi_0) = 3{\cdot}0$

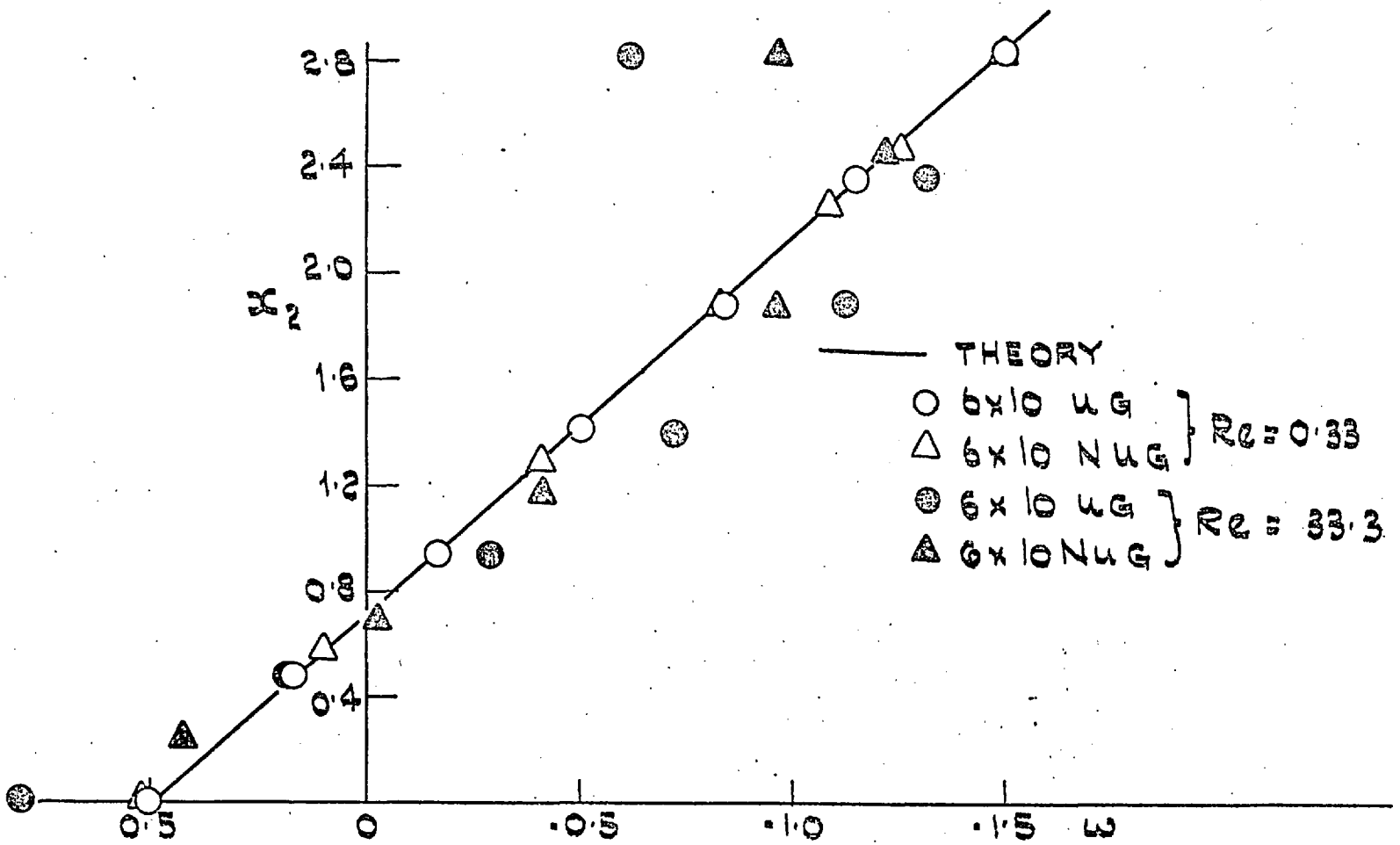


FIG. 4.2.3: INCLINED COUETTE FLOW : INFLUENCE OF Re AND GRID NON-UNIFORMITY ON VORTICITY PREDICTIONS, STAND. UPWIND, $\rho U h / (\Psi_{2h} - \Psi_0) = 3.0$

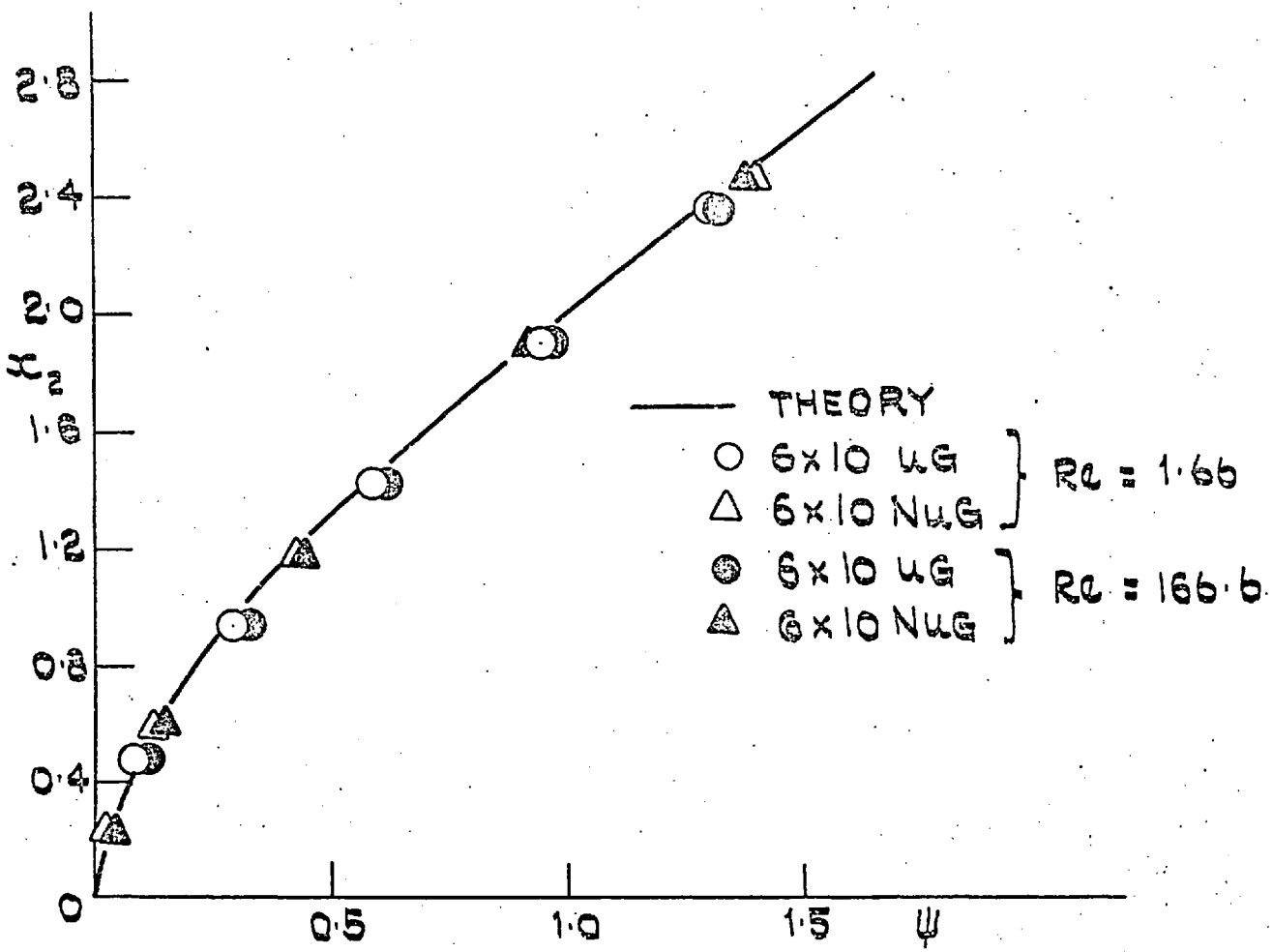


FIG. 4.2.4: INCLINED COUETTE FLOW : INFLUENCE OF Re AND GRID NON-UNIFORMITY ON STREAM FUNCTION PREDICTIONS, STAND. UPWIND, $\rho \bar{U} h / (\psi_{25} - \psi_0) = 0.6$.

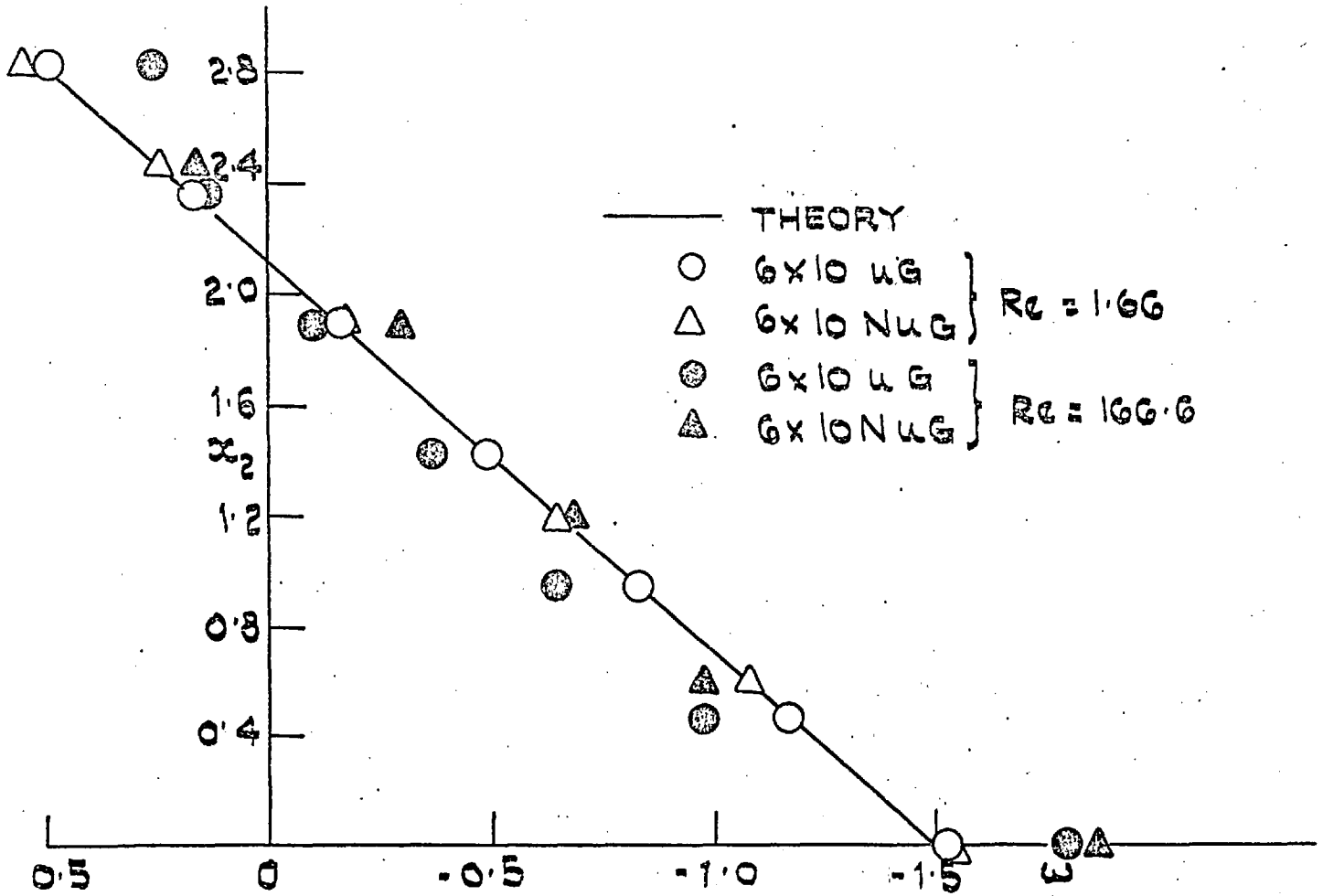


FIG. 4.2.5: INCLINED COUETTE FLOW: INFLUENCE OF Re AND GRID NON-UNIFORMITY ON VORTICITY PREDICTIONS, STAND. UPWIND $\rho U h / (\psi_{2h} - \psi_0) = 0.6$.

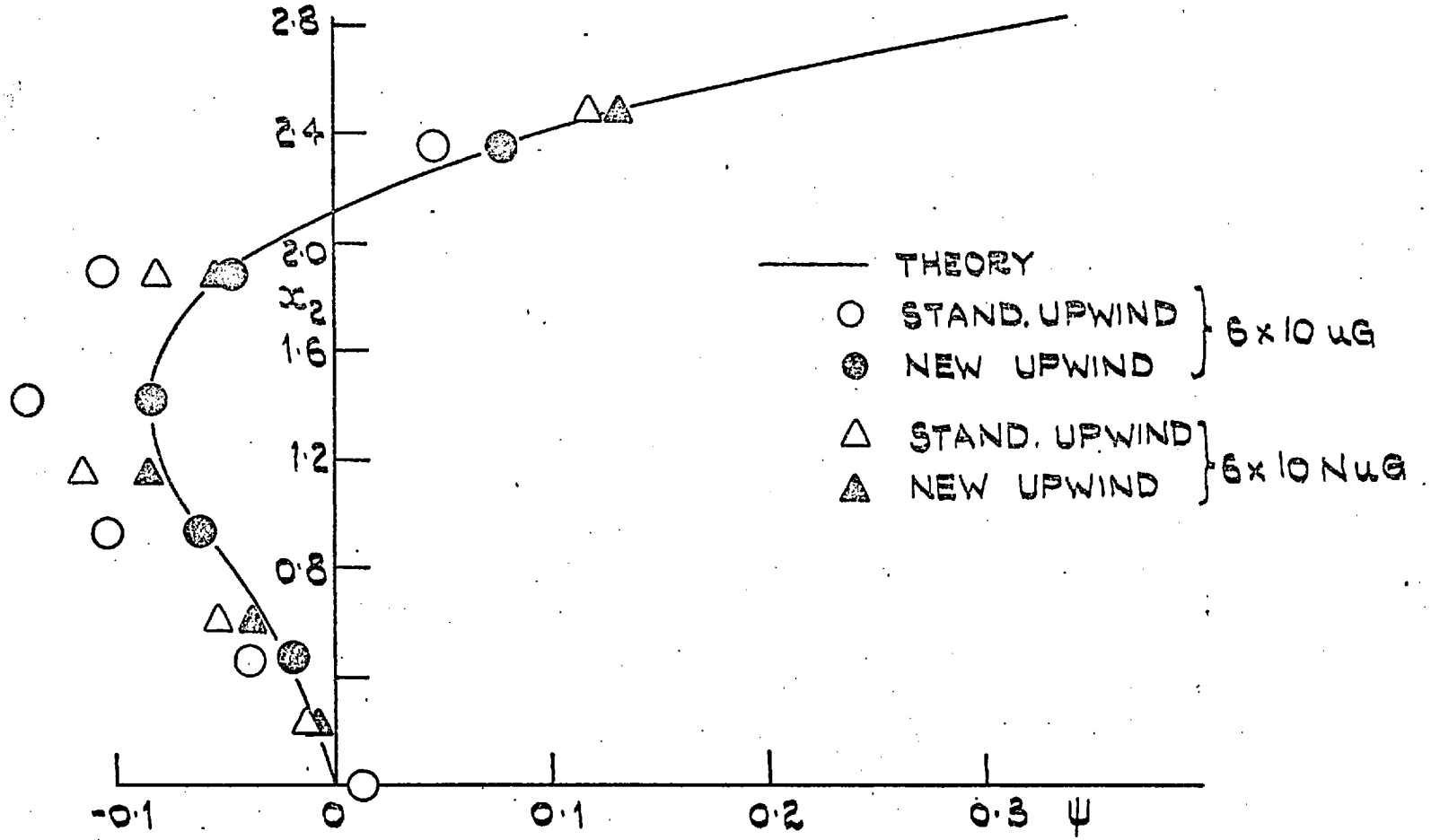


FIG. 4.2.6: INCLINED COUETTE FLOW: INFLUENCE OF CONVECTION TERM METHOD AND GRID NON-UNIFORMITY ON STREAM FUNCTION PREDICTIONS, $Re = 33{\cdot}3$, $\rho U h/(\psi_{2h} - \psi_0) = 3{\cdot}0$.

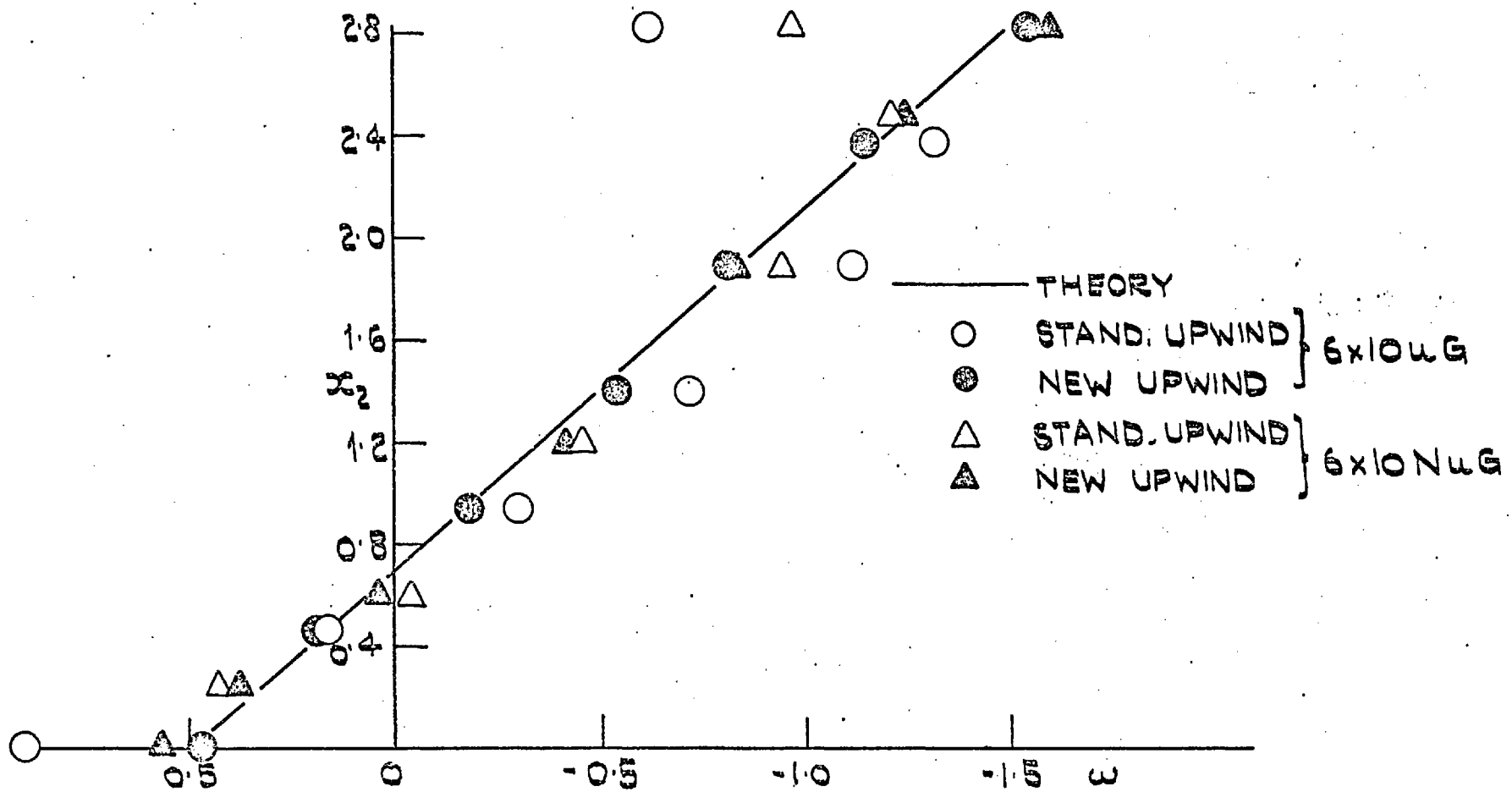


FIG. 4.2.7: INCLINED COUETTE FLOW: INFLUENCE OF CONVECTION TERM METHOD AND GRID NON-UNIFORMITY ON VORTICITY PREDICTIONS, $Re = 33.3$, $\rho U h / (\psi_{2h} - \psi_0) = 3.0$.

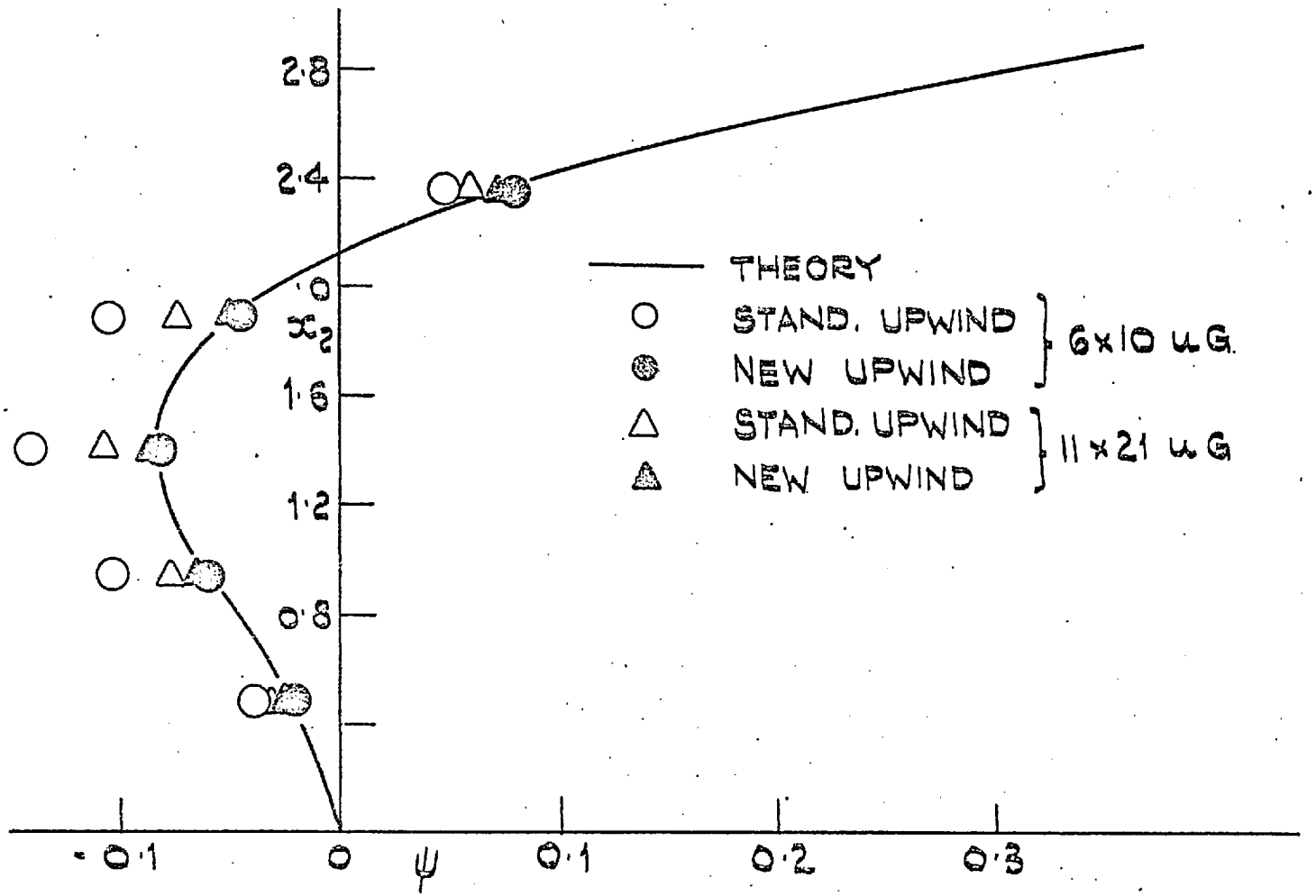


FIG. 4.2.8. INCLINED COUETTE FLOW: INFLUENCE OF CONVECTION TERM METHOD AND GRID REFINEMENT ON STREAM FUNCTION PREDICTIONS, $Re = 33.3$, $\rho \bar{U} h / (\psi_{2h} - \psi_0) = 3.0$.

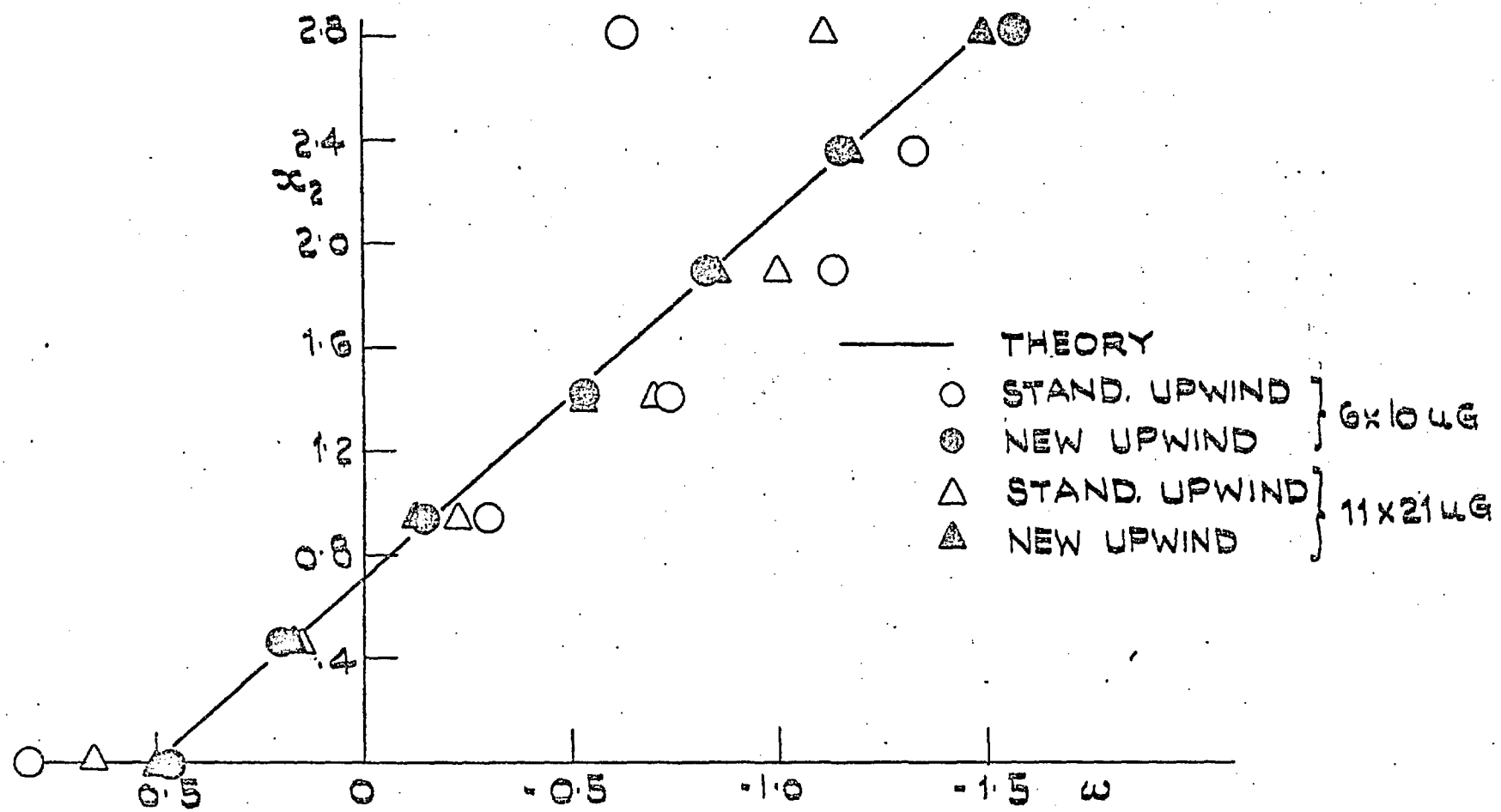


FIG. 4.2.9: INCLINED COUETTE FLOW: INFLUENCE OF CONVECTION TERM METHOD AND GRID REFINEMENT ON VORTICITY PREDICTIONS, $Re = 33.3$, $\rho U h / (\Psi_{2h} - \Psi_0) = 3.0$.

Figs. 4.2.2 and 4.2.3) and Re = 1.66 (in Figs. 4.2.4 and 4.2.5), are in good agreement with the theoretical curves. Now because the values of Re are small, the predicted values of ω and ψ are predominantly controlled by the diffusion fluxes of ω. Thus the above results indicate that the finite - difference approximations for the diffusion (and gradient) terms are satisfactory for these flows.

However the other results in Figs. 4.2.2 to 4.2.5 for high Re (where $Re \geq 33.3$) show that there is on the whole very poor agreement between the theoretical profiles and the predictions for both uniform and non - uniform grids. Now because the values of Re are high, the predicted values of ψ and ω are predominantly controlled by the ω - convection fluxes. The above results therefore show that the errors in the predictions are due to the approximation of the ω - convection terms by the standard - upwind or one - sided difference scheme. The approximations in the latter are responsible for the false - diffusion error, which was investigated in detail by Wolfshtein (1967) and is described briefly in Appendix A.1. The above results confirm one of Wolfshtein's findings that the false - diffusion error increases with Reynolds number.

Some indication of the influence of grid non - uniformity on the false - diffusion error is shown in Figs. 4.2.2 to 4.2.5. The trend of the data indicates that the non - uniform grid results are on the whole in better agreement with the theory than the uniform grid results. However no general rule on the influence of grid non - uniformity can be deduced from this particular trend.

The influence of the new - upwind method of approximating the convection terms is illustrated in Figs. 4.2.6 to 4.2.9. In all cases,

the false – diffusion error is effectively minimised by the use of the new – upwind scheme. However due to the convergence properties of the new – upwind method, section 3.4.1, converged solutions for this flow cannot be obtained for $Re > 100$.

The results in Figs. 4.2.6 and 4.2.7 suggest that the new – upwind predictions for the non – uniform grid are slightly less accurate than the corresponding uniform grid results. Nevertheless this difference in accuracy is small. The new – upwind results in Figs. 4.2.8 and 4.2.9 show that the predictions for the 6 x 10 and 11 x 21 grids are in close agreement, so that there is no advantage in refining the grid. However the false – diffusion error in the standard – upwind predictions is reduced by refining the grid from 6 x 10 to 11 x 21. This result is again in agreement with the findings of Wolfshtein (1967).

4.3 Cylindrical Couette flow

4.3.1 The problem and the grid arrangement

This section is concerned with the predictions of a cylindrical Couette flow. This one – dimensional flow occurs between two concentric cylinders, where the inner one is stationary and in the present case the outer one is rotating in an anti – clockwise direction. A pressure gradient in the circumferential direction is also superimposed on the flow.

The objective of this study is to predict the flow round the inner cylinder and thus to determine the errors due to the Chapter 3 solution procedure for this situation. The results of these tests are important because the flow round the inner cylinder bears some similarity to near – wall flows over single cylinders and through in – line tube banks. Predictions of the latter are discussed in the next chapter.

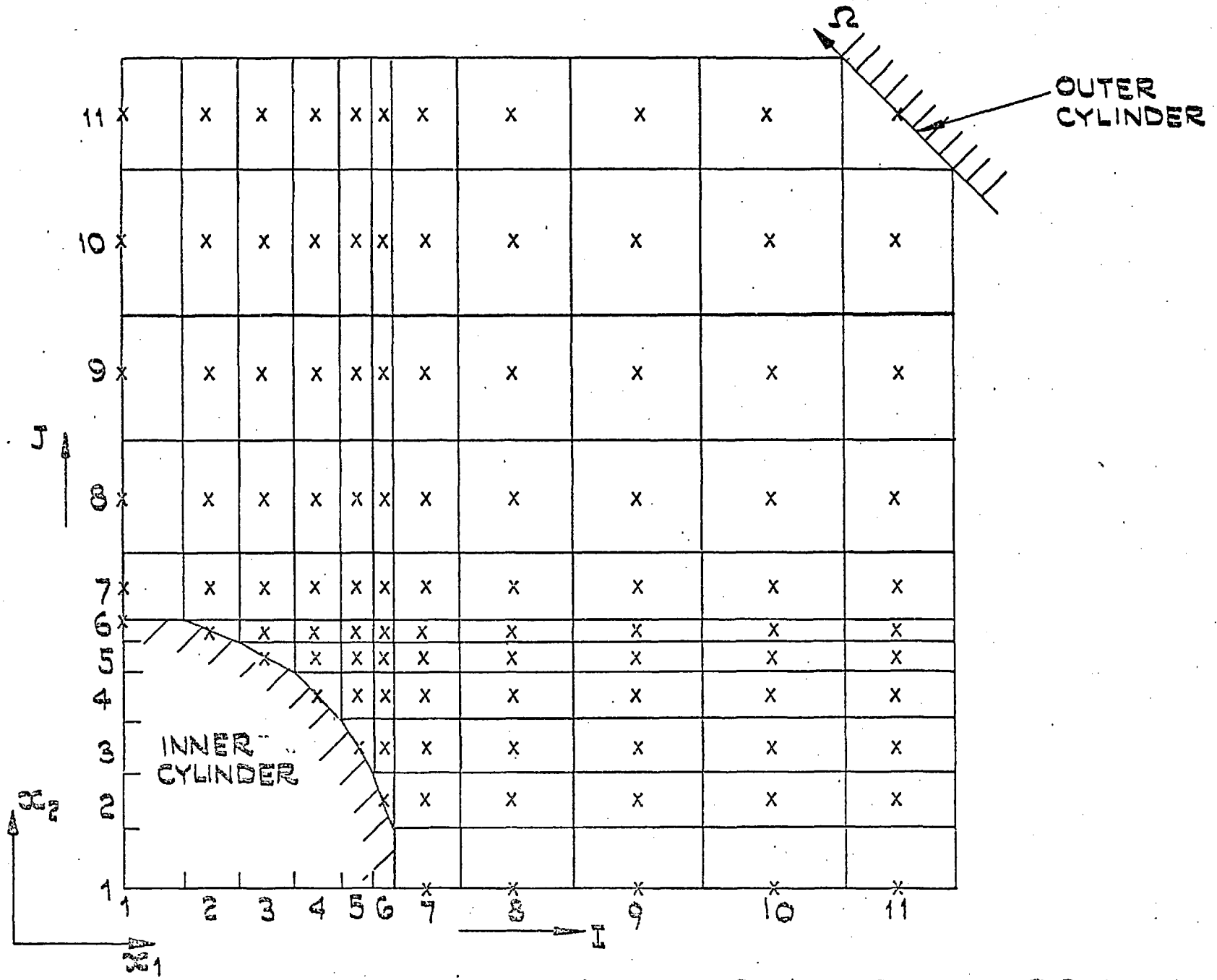


FIG. 4.3.1: CYLINDRICAL COUETTE FLOW: TYPICAL GRID DISTRIBUTION

Fig. 4.3.1 shows the layout of the RAND grid within a quadrant area between the inner and outer cylinders. The domain of grid nodes, which touches the outer cylinder at one corner, is symmetrical about the 45 degree line of the quadrant and completely surrounds the inner cylinder. For most of the tests only one grid of dimensions 11 x 11 was used and this is shown in Fig. 4.3.1.

4.3.2 The theory and boundary conditions

(a) The theory

The equations describing the vorticity and stream function distributions in a laminar cylindrical Couette flow with a circumferential pressure gradient, $dp/d\theta$, are as follows:

$$\omega = A \log_e r + B \tag{4.3.1}$$

$$\frac{\psi_{R_I} - \psi}{\Omega} = \frac{A}{4}\left[r^2 \log_e r - R_I^2 \log_e R_I\right] + \frac{(B-A)}{4}\left[r^2 - R_I^2\right] + C \log_e\left(\frac{r}{R_I}\right) \tag{4.3.2}$$

where, r = radius; where $R_I \leq r \leq R_o$

θ = angle of radial arm with respect to the positive x_1 axis

R_o = outer radius

R_I = inner radius

$x_R = R_I / R_o$

Ω = angular velocity of outer cylinder

ψ_{R_I} = stream function value at $r = R_I$

$A = \frac{1}{\mu}\frac{dp}{d\theta}$

$$B = \frac{2\Omega}{1-x_R^2} - \frac{A}{1-x_R^2}\left\{\left[\log_e R_o - \frac{1}{2}\right] - x_R^2\left[\log_e R_I - \frac{1}{2}\right]\right\}$$

$$C = -\frac{R_I^2}{2}\left\{\frac{2\Omega}{1-x_R^2} + \frac{A}{1-x_R^2}\log_e x_R\right\}$$

The cylindrical Couette flow may be defined by the parameter

$$\frac{\rho \Omega R_o^2}{\psi_{R_I} - \psi_{R_o}} .$$

where,

$\psi_{R_I} - \psi_{R_o}$ = stream function difference between the stationary and moving cylinders

If Ω, R_I and R_o are constant values then, from equation (4.3.2), $\psi_{R_I} - \psi_{R_o}$ is a function only of the circumferential pressure gradient divided by the viscosity, $\frac{1}{\mu}\frac{dp}{d\theta}$.

$$\therefore \frac{\rho \Omega R_o^2}{\psi_{R_I} - \psi_{R_o}} = f\left(\frac{1}{\mu}\frac{dp}{d\theta}\right)$$

Now in this section two flows A and B, represented by two values of $\frac{\rho \Omega R_o^2}{\psi_{R_I} - \psi_{R_o}}$ are used as a basis for comparing the predictions with the theoretical solutions. Flow A has a velocity profile which is characteristic of a separated flow region, and flow B has a boundary layer type of velocity profile. For $\Omega = R_o = 1.0$ and $R_I = 0.25$, flows A and B have the following values of the parameter, $\frac{\rho \Omega R_o^2}{\psi_{R_I} - \psi_{R_o}}$:

Flow	$\frac{1}{\mu}\frac{dp}{d\theta}$	$\frac{\rho \Omega R_o^2}{\psi_{R_I} - \psi_{R_o}}$
A	4.5	6.03
B	-4.5	1.56

(b) The boundary conditions

Referring to Fig. 4.3.1, the boundary conditions for the solution procedure are as follows:

(i) The theoretical values of stream function are given on all the boundaries. This means that stream function is given on:

1. Lines I = 1 and J = 1
2. Lines I = 11 and J = 11
3. The inner cylinder

(ii) The theoretical values of vorticity are given on all the boundaries, except the inner cylinder wall boundary. This means that vorticity is given on:

1. Lines I = 1 and J = 1
2. Lines I = 11 and J = 11

The boundary conditions are completed by the specification of a Reynolds number parameter, Re . The latter, in this case, is specified as follows:

$$Re = \frac{\psi_{R_I} - \psi_{R_o}}{\mu}$$

This parameter gives a measure of the relative importance of the convection and diffusion terms in the elliptic equation for vorticity. This parameter does not, however, influence the theoretical distributions of vorticity and stream function as given by $\frac{\rho \Omega R_o^2}{\psi_{R_I} - \psi_{R_o}}$ for fixed values of Ω , R_I and R_o .

4.3.3 Tests and results

(a) Tests performed

Table 4.3.1 gives a summary of the tests which were performed using flows A and B. In this table, the tests are indicated by sets of two numbers separated by a stroke, i.e. 4.3.2/4.3.3. The numbers before and after the stroke represent the numbers of the figures, which contain the appropriate plots of stream function and vorticity respectively.

Convection Term Method	Grid	Flow A: $\frac{\rho\Omega R_o^2}{\psi_{R_x}-\psi_{R_o}} = 6.03$, Re = 166.0	Flow B: $\frac{\rho\Omega R_o^2}{\psi_{R_x}-\psi_{R_o}} = 1.56$, Re = 644.0
Standard Upwind	11 x 11	4.3.2/4.3.3	4.3.4/4.3.5
	16 x 16	-	- /4.3.5
New Upwind	11 x 11	4.3.2/4.3.3	4.3.4/4.3.5

Table 4.3.1

Referring to Fig. 4.3.1, it should be noted that all the stream function and vorticity results in this section are plotted against the x_2 grid co-ordinate at chosen values of the x_1 co-ordinate. The results are plotted at stations I = 3, 5, 7 and 9 in the x_1 direction for flow A, and at stations I = 3, 5 and 7 for flow B.

(b) Results

The results of tests at low Reynolds numbers, where $Re < 10.0$, are not reproduced here because the agreement between the theory and

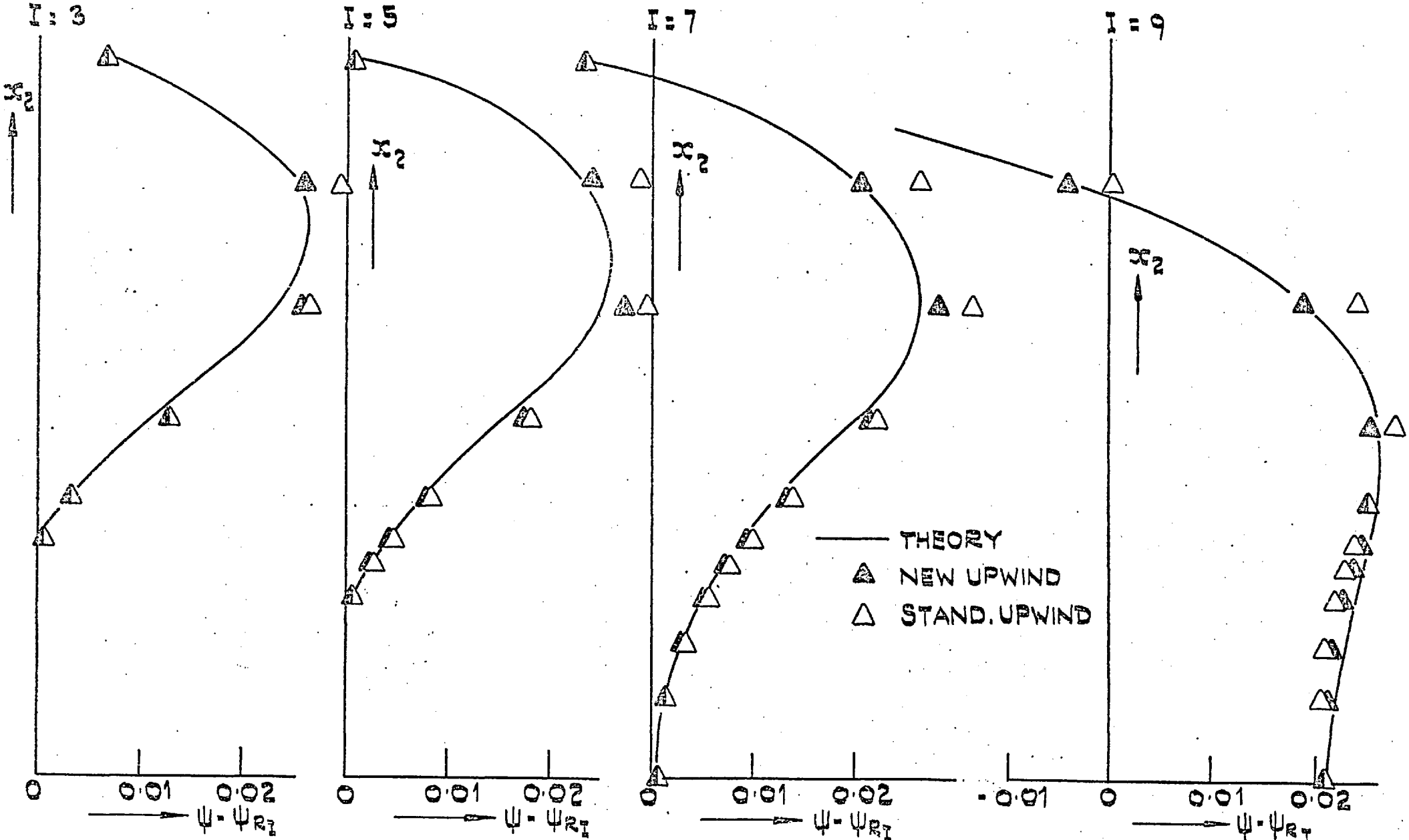


FIG. 4.3.2: CYLINDRICAL COUETTE FLOW: STREAM FUNCTION PREDICTIONS, $\rho \Omega R_0^2/(\psi_{R_I} - \psi_{R_0}) = 6{\cdot}03$, $Re = (\psi_{R_I} - \psi_{R_0})/\mu = 166{\cdot}0$.

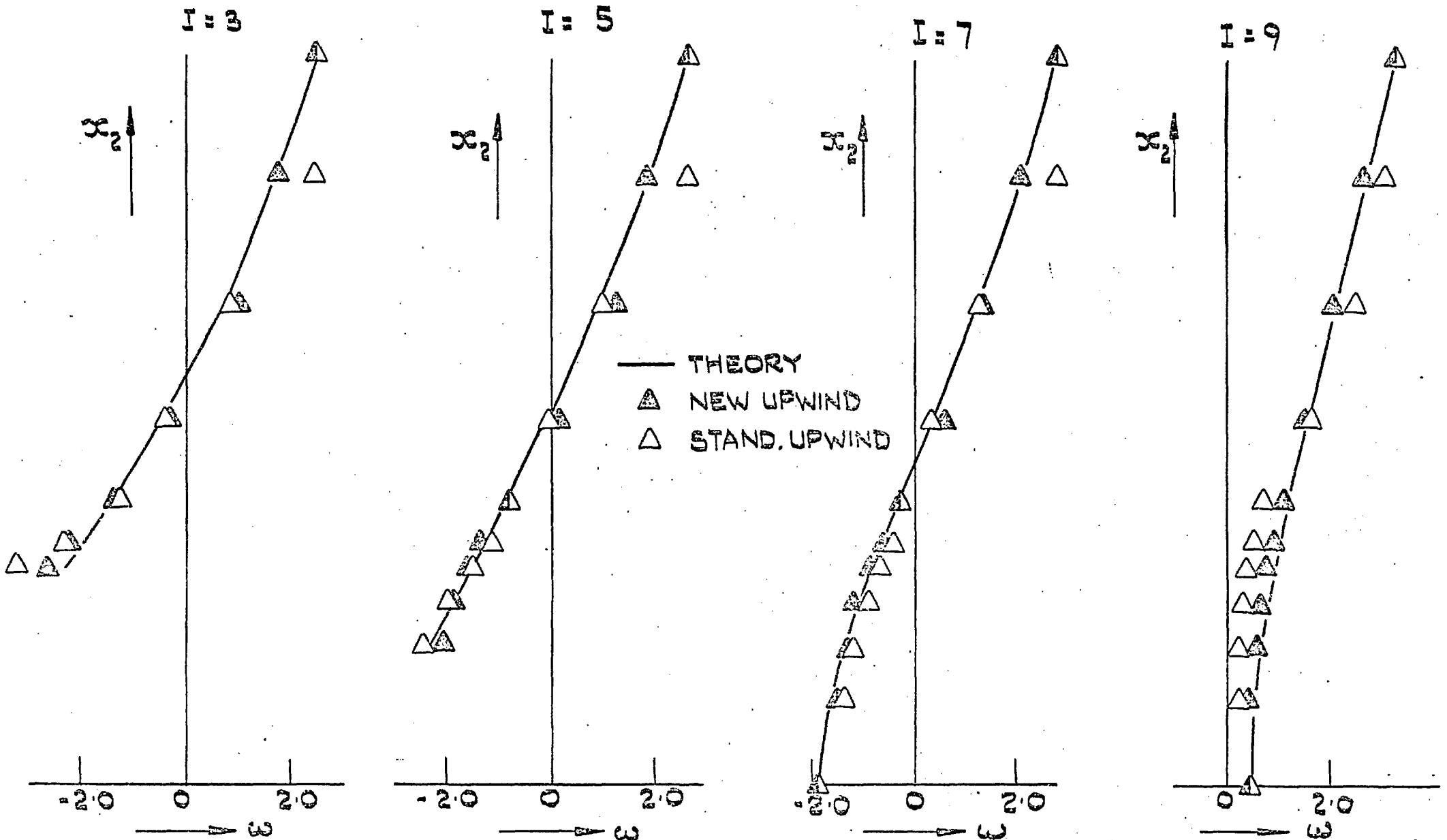


FIG. 4.33: CYLINDRICAL COUETTE FLOW: VORTICITY PREDICTIONS, $\rho \Omega R_0^2 / (\psi_{R_I} - \psi_{R_0}) = 6.03$, $Re = (\psi_{R_I} - \psi_{R_0}) / \mu = 166.0$.

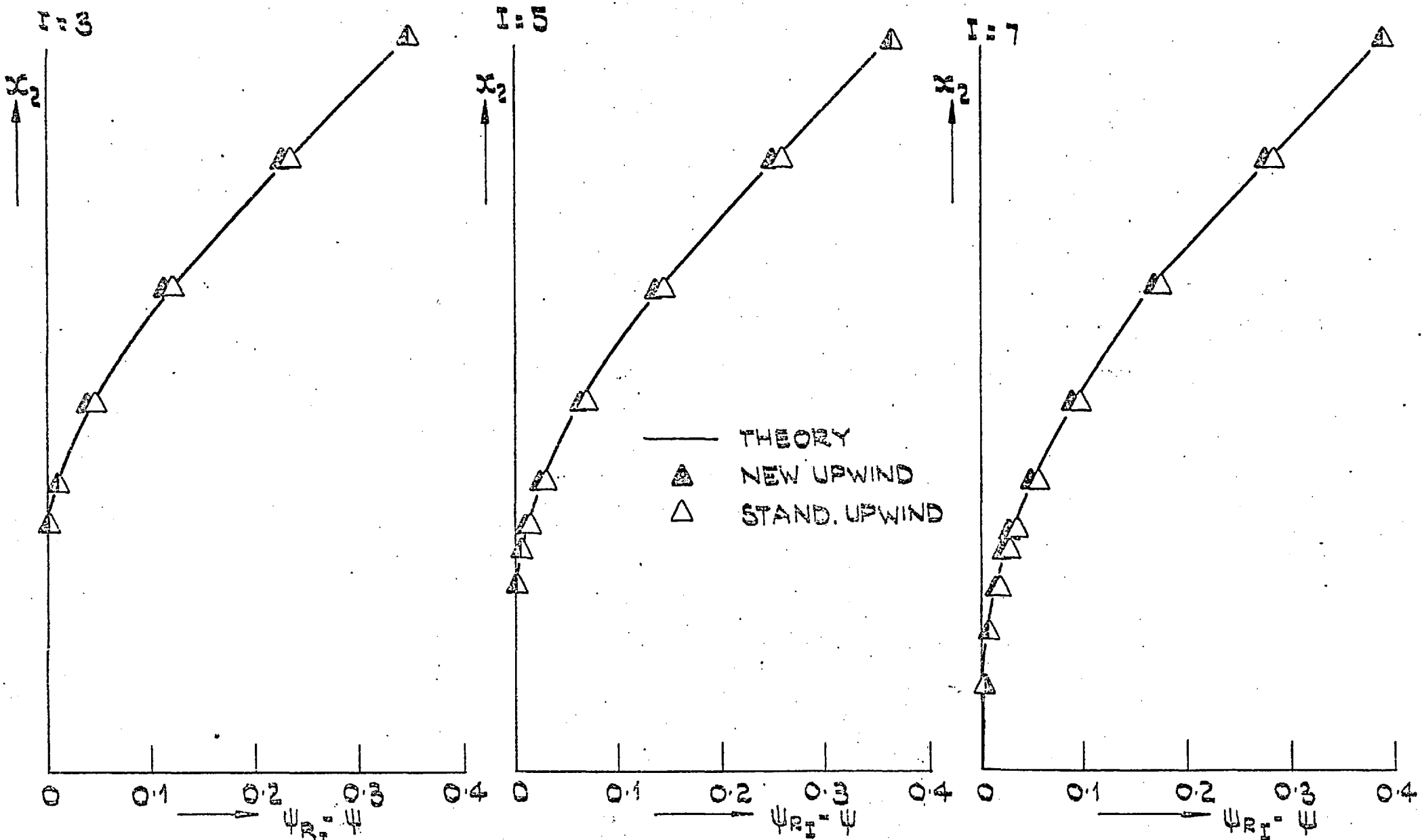


FIG. 4.3.4: CYLINDRICAL COUETTE FLOW: STREAM FUNCTION PREDICTIONS, $\rho \Omega R_0^2 / (\psi_{R_I} - \psi_{R_0}) = 1.56$, $Re = (\psi_{R_I} - \psi_{R_0}) / \mu = 644.0$.

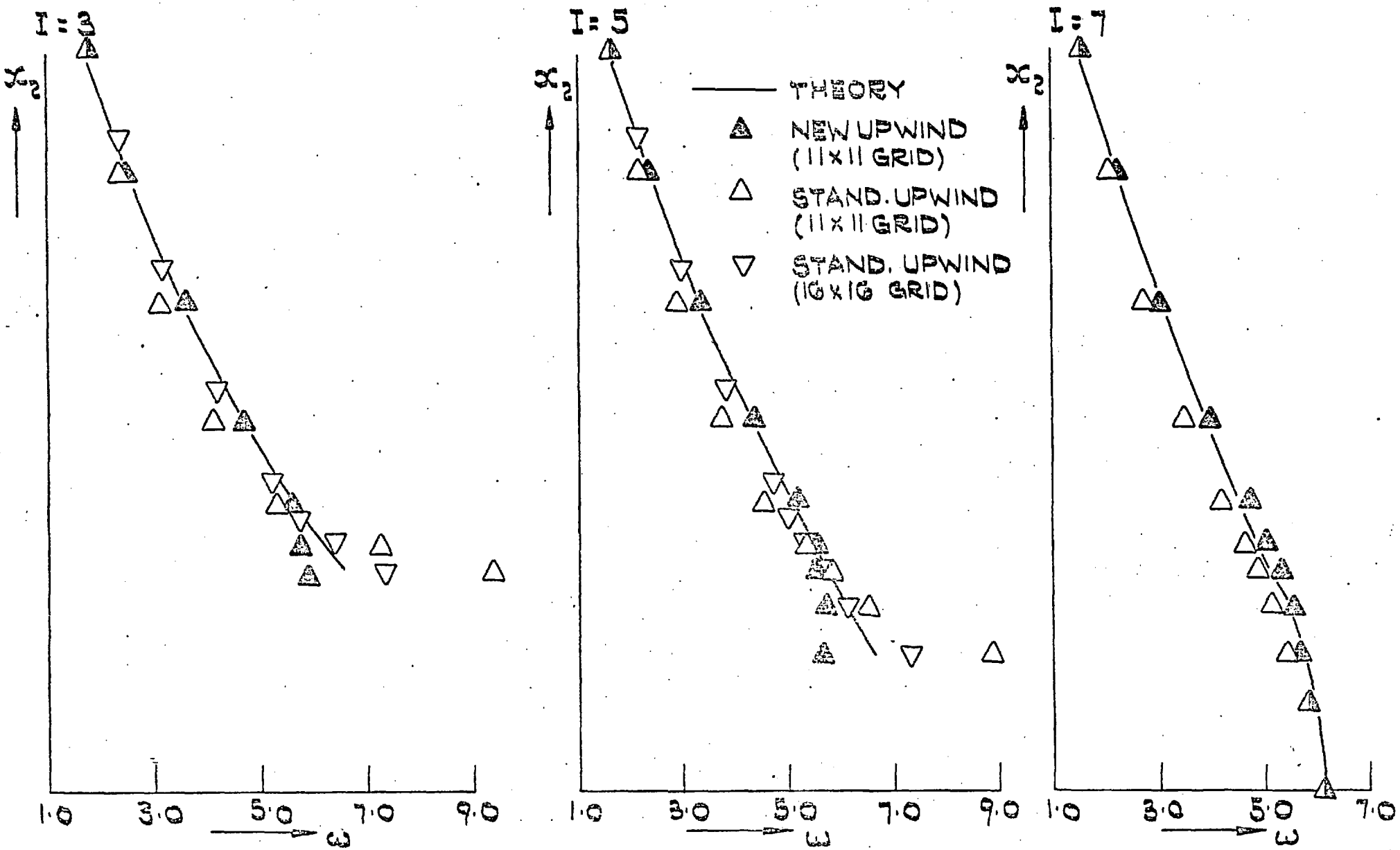


FIG. 4.35: CYLINDRICAL COUETTE FLOW: VORTICITY PREDICTIONS, $\rho \Omega R_0^2 / (\psi_{R_1} - \psi_{R_0}) = 1.56$, $Re = (\psi_{R_1} - \psi_{R_0}) / \mu = 644.0$.

predictions is very good. These results do no more than confirm one of the findings of section 4.2, namely that low Reynolds number flows are accurately predicted by the Chapter 3 solution procedure.

The predictions for flow A in Figs. 4.3.2 and 4.3.3 show the effects of false diffusion at large values of x_2 for all the plots, and at small values of x_2 for the I = 9 plot. On the whole, the new – upwind predictions are more accurate than the standard – upwind predictions.

In Fig. 4.3.4, for flow B, there is only a small difference between the standard – upwind predictions and the theoretical curves for stream function. However in Fig. 4.3.5 for flow B, errors due to false diffusion are apparent in the standard – upwind predictions of vorticity. These errors can be seen in the I = 3 and 5 plots at low values of x_2, where the latter represents points near and on the inner cylinder wall. Nevertheless, as in previous examples, the new – upwind predictions indicate a marked reduction in these errors.

In Fig. 4.3.5, standard – upwind predictions are also given in the I = 3 and 5 plots for a 16 x 16 grid. This grid was produced by refining the coarse 11 x 11 grid for $I \geq 7$ and $J \geq 7$. It is encouraging to note that the false – diffusion error of the 11 x 11 standard – upwind predictions is much reduced by the 16 x 16 grid predictions. Indeed the latter are as accurate as the new – upwind predictions for the 11 x 11 grid.

4.4 Discussion

In this section, we discuss and then finally summarise the main findings of sections 4.2 and 4.3. The predictions are discussed in terms of low and high Reynolds numbers, and in the present context

low Re refer to flows where diffusion is dominant and high Re to flows where convection is dominant.

At low Reynolds numbers, the predictions of both inclined – plane and cylindrical Couette flows are in good agreement with the theoretical solutions. However we know that at low Reynolds numbers, the flow profiles are governed principally by diffusion. Therefore these results give an indiction of the accuracy of the finite – difference approximations for the diffusion (and gradient) terms of the elliptic equations. The results show that these approximations are satisfactory.

At high Reynolds numbers, the effects of false diffusion are evident in the predictions of both inclined – plane and cylindrical Couette flows. The influences of Reynolds number, grid non – uniformity and grid size on the false – diffusion error are illustrated by the standard – upwind predictions for the inclined – plane Couette flows. The results show that the non – uniformity of the grid tends to decrease the error with respect to that for a uniform grid. On the other hand the error is shown to be proportional to Reynolds number and cell size. The latter influences agree with the findings of Wolfshtein (1967), Appendix A.1. However within the limits of convergence, all the new – upwind predictions for the inclined – plane Couette flows reduce the errors to almost negligible amounts. In the case of the cylindrical Couette flow predictions, the false – diffusion error due to the standard – upwind method is substantially reduced by the use of the new – upwind method. Also it is shown that the false – diffusion error is reduced by refining the grid.

It is now appropriate to give a brief summary of the findings of sections 4.2 and 4.3. The above catalogue of results clearly demonstrate that the Chapter 3 solution procedure can be used to predict a large variety of flows in domains with complicated non – rectangular shapes.

Reasonable prediction accuracy can be obtained as long as some measures are taken to minimise the errors due to false diffusion.

5. LAMINAR FLOW PREDICTIONS

In this chapter, we use the solution procedure of Chapter 3 to predict two laminar flows, which are of engineering interest. The first is laminar flow over a single cylinder and the second is laminar flow through in - line tube banks. Wherever possible, the predictions are compared with numerical solutions and experimental data from other sources.

5.1 Objective

In Chapter 3, a solution procedure for predicting flows in awkward non - rectangular domains was outlined; and some of the properties of the procedure, such as accuracy and convergence, were illustrated in Chapter 4. It is now the objective of this chapter to demonstrate that the procedure can be used to predict two - dimensional laminar flows, which are of engineering interest.

In this chapter we are concerned with two flows. The first is transverse laminar flow over a single cylinder. A number of workers have made this flow the object of many flow visualisation, pressure and heat transfer measurements. Also in the last two decades, both mathematicians and engineers have used various numerical techniques to solve the equations of motion for this problem. Thus the capabilities of the present solution procedure may be rigorously tested by comparing the present predictions of laminar flow over a single cylinder with both numerical solutions and experimental data from other sources.

The second flow, with which we are concerned, is laminar flow through in - line tube banks. In contrast to the first flow, this second flow has not attracted a great deal of attention. Experimental data is sparse, and most of the available data deals only with the bulk rather than the local properties of the flow. Also, as far as the author is aware, no analytical or numerical solutions of flow through tube banks have been

published. Therefore, in this case, only a few of the predictions can be compared with the available measurements; and thus the remainder of the predictions must be presented without supporting evidence for the time being. However the unsupported predictions may be discussed on the basis of our knowledge of other flows, and of what is feasible. In the following sections, section 5.2 deals with laminar flow over single cylinders and section 5.3 with laminar flow through in - line tube banks. Both sections contain predictions of hydrodynamic and heat transfer characteristics.

5.2 Flow over a single cylinder

5.2.1 Previous work and the present contribution

(a) Summary

In this sub-section, we first review some measurements of the characteristics of steady - laminar flow over a single cylinder, and then we review selected numerical solutions of this flow. Finally the objectives and the contributions of the present predictions are outlined.

(b) Review of measurements

Thom (1933) was one of the first to perform detailed measurements of the characteristics of laminar flow over a single cylinder. In the range, $0 < Re < 200$, he measured local pressure distributions, drag coefficients and flow patterns. On the other hand, Taneda (1956) and Tritton (1959) concentrated their attention on particular aspects of the flow. Taneda (1956) used a flow visualisation technique to measure details of the wake in the range, $0 < Re < 60$; and Tritton (1959) measured the drag coefficients in the range, $0.5 < Re < 100$. Within the last decade, Grove et al (1964) and Acrivos et al (1965), (1968) performed detailed measurements of the flow both near the cylinder and in the wake for $25 \leq Re \leq 250$. The main objective of these workers was

to extend the understanding of steady - separated flow past bluff bodies at high Reynolds numbers. In the case of flow over a cylinder, this objective was realised by artificially stabilizing the wake for $Re > 40$.

Most of the above workers have been concerned with studying the hydrodynamics of single cylinder flow. Now we consider some corresponding measurements of heat transfer. Both McAdams (1954) and van der Hegge Zijnen (1956) provide comprehensive reviews and correlations of mean Nusselt number measurements for a wide range of Reynolds and Prandtl numbers. However, in the present study, the measurements of Collis and Williams (1959) and Hilpert (1933) for $0 < Re < 45$ and $Pr = 0.7$ are particularly relevant. In contrast to the mean Nusselt number measurements, very few local heat transfer measurements for the laminar flow problem have been published. The notable contributors in this field are Eckert and Soehngen (1952) and Acrivos et al (1965). Eckert and Soehngen (1952) performed measurements in air for the range $20 \leq Re \leq 500$; and Acrivos et al (1965) performed measurements in an oil with $Pr \simeq 1000$ for the range $4.9 \leq Re \leq 225$.

(c) Review of numerical solutions

Solutions of two - dimensional flow over a single cylinder can be divided into two classes. The first class contains the numerical solutions of the equations of steady motion. The second class contains the solutions of the time - dependent equations of motion. In order to focus our attention on the solutions which are relevant to the present work, we shall review only those corresponding to the first class. Thom (1933) was the first to provide hydrodynamic solutions at Re = 10 and 20. Then Kawaguti (1953) and Apelt (1958) both obtained solutions at Re = 40. Subsequently solutions for Reynolds numbers in the range $0 < Re \leq 100$

were obtained by Hamielec and Raal (1969), Takami and Keller (1969) and Dennis and Chang (1970). Most of the above authors illustrated their predictions by providing plots of vorticity distributions, stream function distributions, wake lengths, wake widths, total drag coefficients and local pressure coefficients. Takaisi (1969), on the other hand, restricted his attention to the prediction of the total drag coefficient in the range $0 < Re \leq 100$. However the possibility of predicting laminar forced convection from a single cylinder has not attracted much attention. The only contribution in this field appears to be that of Dennis et al (1968).

(d) Present objectives and contributions

In the above, we have reviewed previous predictions and measurements of steady - state laminar flow over a single cylinder. Now we consider the objectives and contributions of the present predictions. The first objective is to show that the Chapter 3 solution procedure can predict steady - state laminar flow over a single cylinder. The second objective is to evaluate the accuracy of these predictions by the following means:

(i) comparison of the predictions with each other,

and (ii) comparison of the predictions with the results of measurements and predictions from other sources.

For the purpose of looking at the present predictions in some detail, all the predictions have been performed at only one Reynolds number. The latter was chosen as 40, so that the hydrodynamic predictions could be compared with the detailed predictions of Kawaguti (1953) and Apelt (1958) and with the measurements of Grove et al (1964) and Acrivos et al (1968).

It may be thought that the predictions could have been compared with any set of comprehensive measurements. However it should be remembered that valid comparisons can only be made if the main features of the experimental flow correspond with those of the predicted flow. Thus it

was important to check that the experimental flow was both steady in the wake and not much influenced by the presence of remote walls. At $Re = 40$, the experiments of both Grove et al (1964) and Acrivos et al (1968) fulfilled the above conditions. However besides the predictions of flow over a single cylinder immersed in an infinite medium, the present predictions include one important contribution. The latter is the prediction of flow over a cylinder contained within a channel. These predictions are compared with the measurements of Grove et al (1964).

Another important contribution is the predictions of mean and local values of heat transfer for a cylinder immersed in an infinite medium. The only other set of predictions for this problem is that of Dennis et al (1968) for $0.1 \leq Re \leq 40$. Although there are no published measurements of local heat transfer distributions at $Re = 40$, comparisons with the measurements of Eckert and Soehngen (1952) for $Re = 23$ and with those of Acrivos et al (1965) for $Re = 49$ are made on appropriate non - dimensional bases.

We now pass on to describe the hydrodynamic and heat transfer predictions, which are in sub - sections 5.2.2 and 5.2.3 respectively. The main results of the predictions are discussed in 5.2.4.

5.2.2 Hydrodynamic predictions

(a) Outline of sub - section

This sub - section is divided into three parts. The first part, (b), is concerned with the predictions of flow over a cylinder, which is immersed in an infinite medium. For the sake of abbreviation, this flow will be referred to as the free - flow problem. The second part, (c), deals with predictions of flow over a cylinder which is positioned on the centre - line of a channel. This flow will be referred to as the channel - flow problem. The third part, (d), compares the present predictions of drag coefficient with some measurements and predictions

from other sources.

(b) Free flow over a cylinder

(i) Boundary conditions and some definitions

The boundary conditions for the symmetrical free - flow problem, Fig. 5.2.1, are as follows:

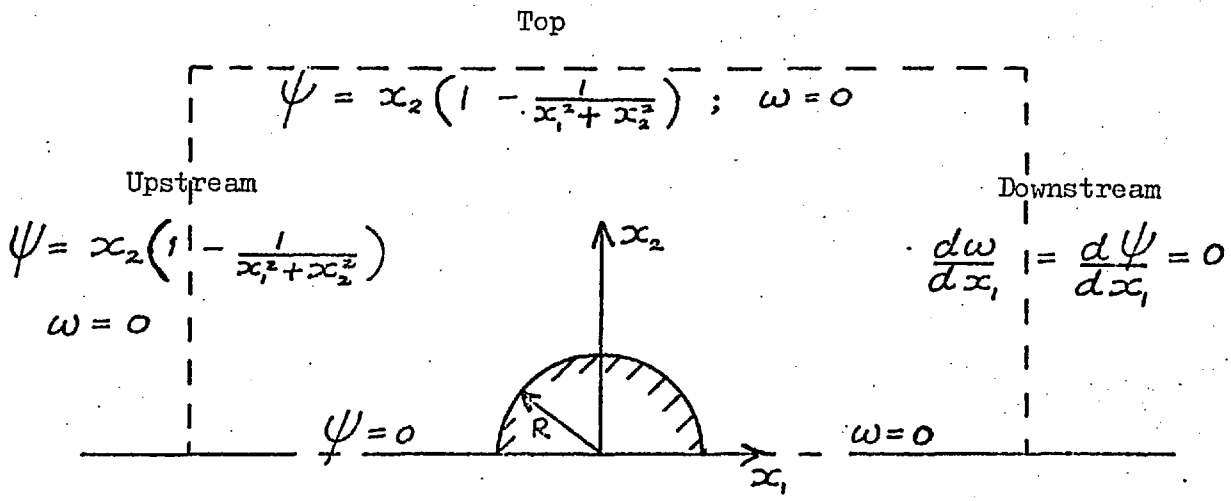


Fig. 5.2.1 Hydrodynamic boundary conditions for laminar free flow over a cylinder

1. Top and upstream boundaries

The potential - flow solution values for ω and ψ are assumed, that is:

$$\omega = 0 \; ; \quad \psi = x_2\left(1 - \frac{1}{x_1^2 + x_2^2}\right)$$

2. Downstream boundary

$$\frac{d\omega}{dx_1} = \frac{d\psi}{dx_1} = 0$$

3. Plane of symmetry

$$\omega = \psi = 0$$

4. Surface of cylinder

$$\psi = 0$$

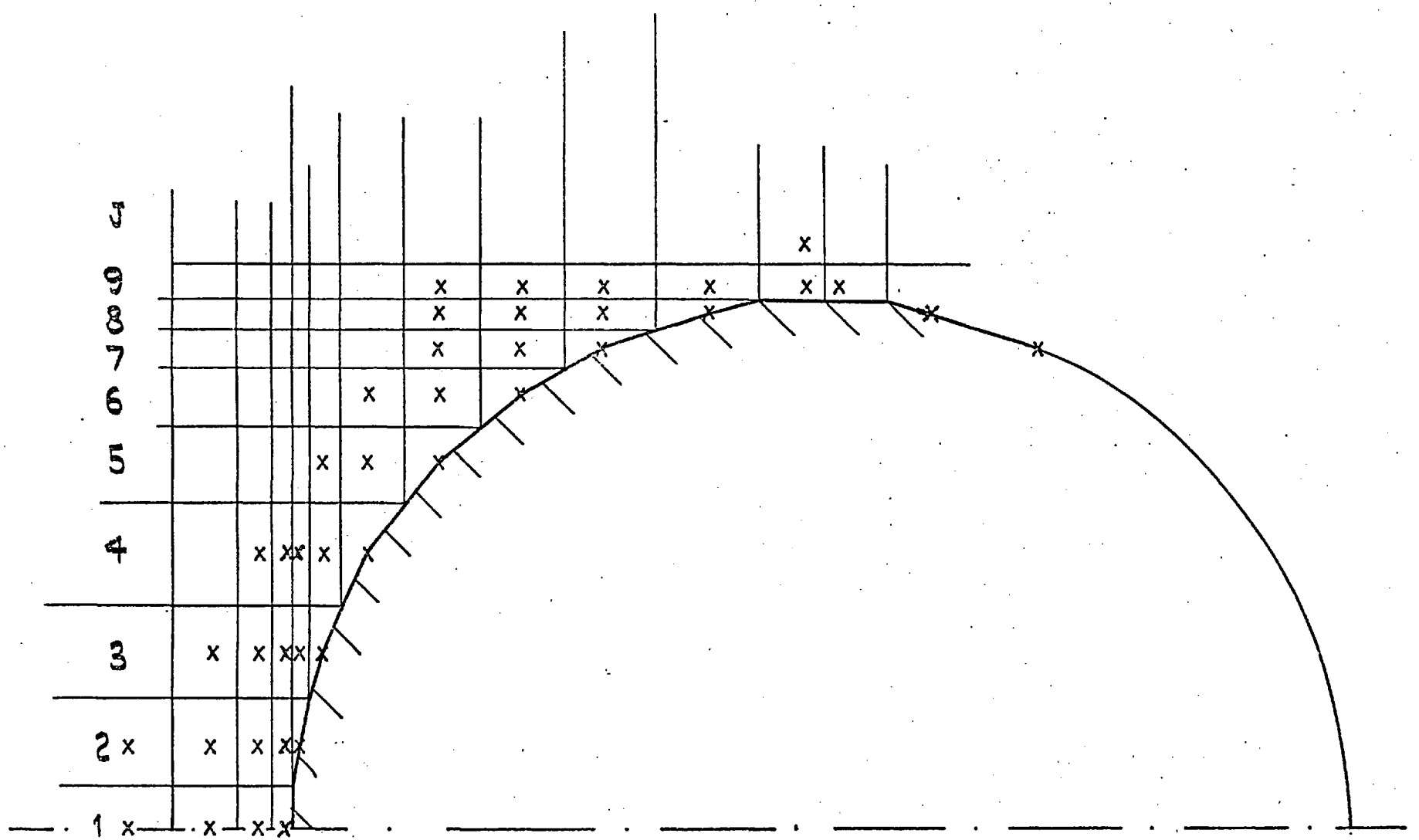


FIG. 5.2.2: AN EXAMPLE OF THE F.W.P. GRID ARRANGEMENT NEAR A CYLINDER WALL.

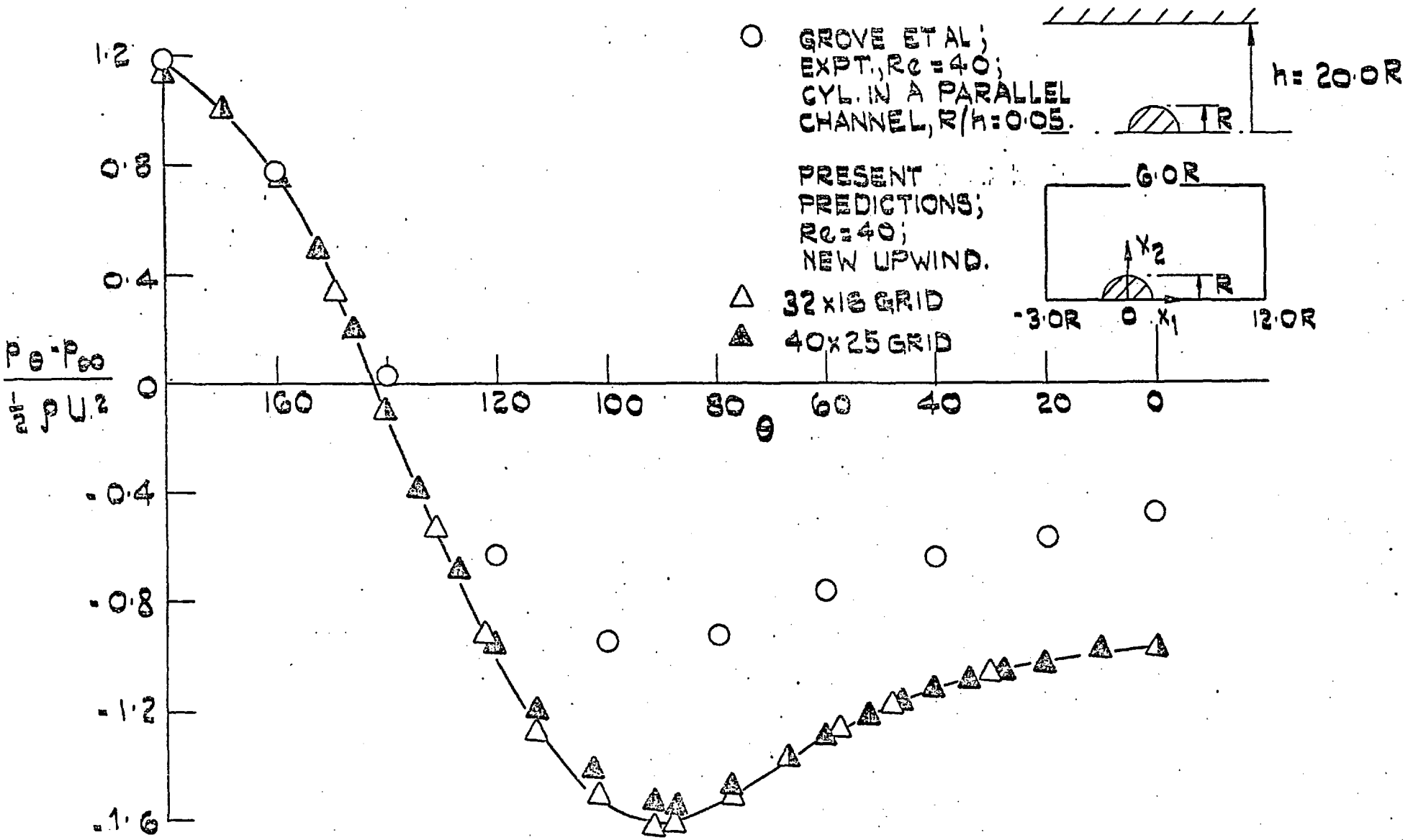


FIG. 5.2.3: FREE FLOW OVER A CYLINDER: INITIAL PREDICTIONS OF PRESSURE DISTRIBUTION.

The Reynolds number and the pressure coefficient are defined as follows:

Reynolds number, $$Re = \frac{U d}{\nu}$$

Pressure coefficient = $$\frac{p_\theta - p_\infty}{\frac{1}{2}\rho U^2}$$

where, U = free - stream velocity

d = diameter of the cylinder

p_θ = static pressure on the cylinder at angle θ

p_∞ = reference static pressure upstream of the cylinder

An example of the F.W.P. finite - difference grid arrangement for a region near a cylinder wall is shown in Fig. 5.2.2.

(ii) Pressure distribution:

1. Initial investigation

Initial predictions of pressure distribution for free flow over a single cylinder are summarised in Fig. 5.2.3. For these predictions, properties of the flow, such as the vorticity distribution round the cylinder wall and the size of the recirculation bubble, seemed to compare favourably with the predictions of Apelt (1958) and Kawaguti (1953) and the experimental data of Taneda (1956), Thom (1933) and Grove et al (1964). Nevertheless, as shown in Fig. 5.2.3, a significant discrepancy was found between the predictions and measurements of pressure distribution round the cylinder circumference. The refinement of the grid from 32 x 16 to 40 x 25 had a negligible effect on this result.

It eventually became clear that the chosen boundary conditions in conjunction with the size of the domain had an important effect on the flow pattern and pressure distribution. In this case, it was found that the

most influential boundary conditons were those for the top boundary. This is because the latter are strictly only applicable as x_2 becomes very large. However with the present finite - difference scheme it is necessary to use finite values of x_2 for the top boundary. The value of the latter corresponding to the results in Fig. 5.2.3 was only $6.0\,R$; and it appears that this small value caused a 'blockage effect' to be exerted on the predicted flow. This blockage effect was responsible for the inaccurate predictions of pressure distribution.

To minimise this undesirable influence, the overall dimensions of the domain in Fig. 5.2.3 were increased to the following dimensions:

$$-8.4R \leq x_1 \leq 88.3R$$

$$0 \leq x_2 \leq 26.6R$$

These dimensions were used for all subsequent free - flow predictions.

In the following comparisons of pressure distribution, the measurements of Grove et al (1964) for a blockage ratio of $\frac{R}{h} = 0.05$, where R = radius of cylinder and h = half - width of test section, are used as the standard for comparison. The reason for this decision is not due to the claim of high accuracy by Grove et al (indeed the accuracy in $(p_\theta - p_\infty)/\frac{1}{2}\rho U^2$ is only about $\mp$ 12% and the accuracy in U or Re is about $\mp$ 5%); but because it can be shown by comparison with the results of Thom (1933) for $R/h = 0.07$ at $Re = 45$ and 36 and the results of Homann (1936) for $R/h = 0.05$ at $Re = 30$ that the measured pressure coefficient distribution is not very sensitive to Re in the range $30 \leq Re \leq 45$ or blockage ratio in the range $0.05 \leq R/h \leq 0.07$.

2. Effect of grid refinement

In Fig. 5.2.4, the new - upwind predictions for three grid dimensions

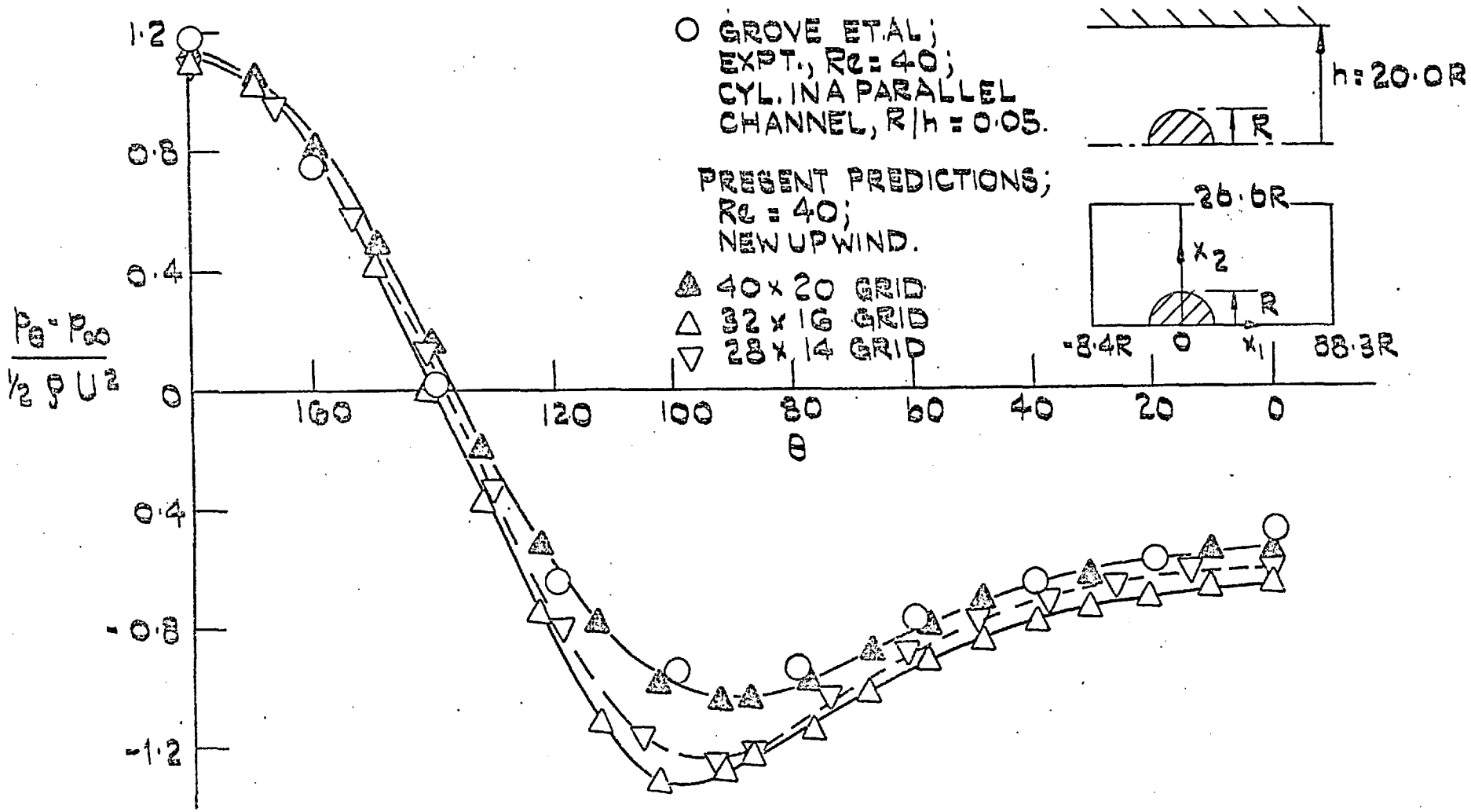


FIG. 5.24: FREE FLOW OVER A CYLINDER: INFLUENCE OF GRID REFINEMENT ON THE PREDICTIONS OF PRESSURE DISTRIBUTION.

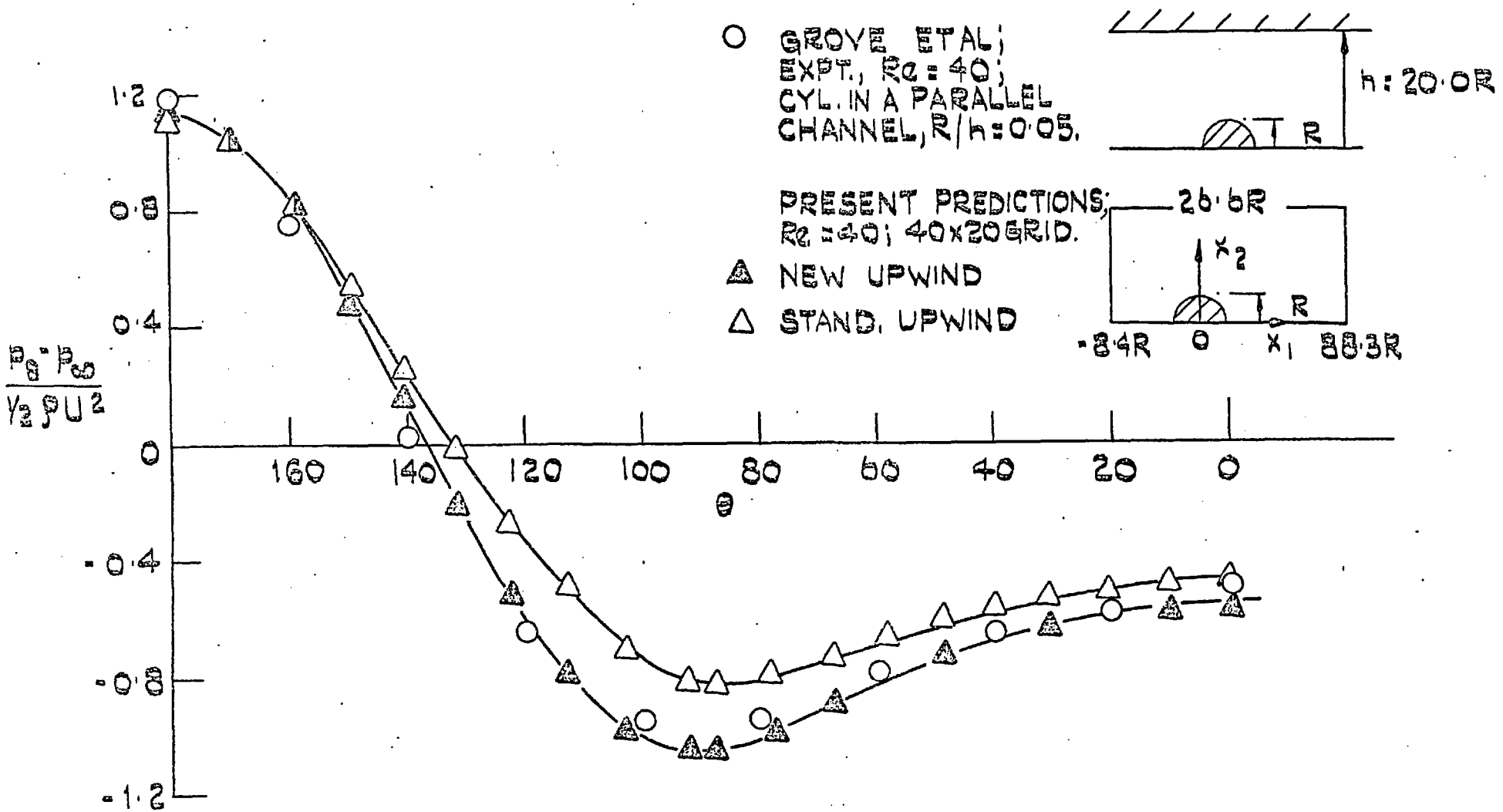


FIG. 5.2.5: FREE FLOW OVER A CYLINDER: INFLUENCE OF CONVECTION TERM METHOD ON THE PREDICTIONS OF PRESSURE DISTRIBUTION.

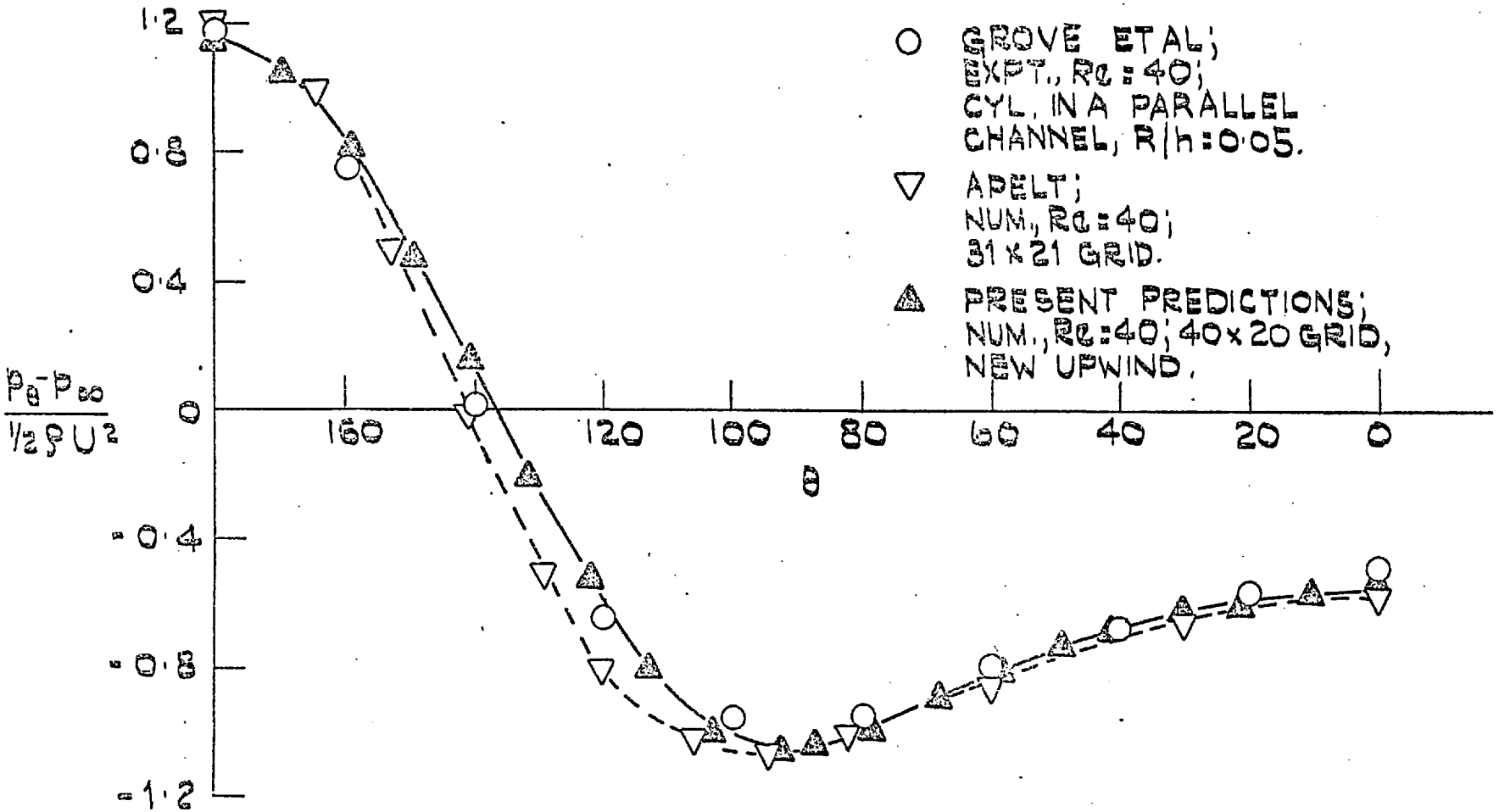


FIG. 5.2.6: FREE FLOW OVER A CYLINDER: COMPARISON OF THE PRESENT PRESSURE DISTRIBUTION PREDICTIONS WITH OTHER PREDICTIONS.

are compared with the measurements of Grove et al. First of all it should be noted that the 32 x 16 grid is obtained from the original 28 x 14 grid by refining the grid round the cylinder, and the 40 x 20 grid is obtained by refining the 32 x 16 grid in parts of the domain beyond the cylinder. It is clear that the 40 x 20 predictions are in much closer agreement with the experimental results than the predictions for the other two dimensions. Therefore the 40 x 20 new - upwind predictions, which are also within the bounds of experimental accuracy, are to be regarded as the most accurate for this set of predictions of free flow over a cylinder. The 28 x 14 predictions appear to be more accurate than the 32 x 16. This effect is probably due to the fact that the 28 x14 grid is more evenly distributed than the 32 x 16 grid.

3. Effect of convection term method

In Fig. 5.2.5, the new - and standard - upwind predictions for the 40 x 20 grid are compared with the measurements of Grove et al. The discrepancy between the new and standard - upwind results is due to false diffusion, the effect of which was demonstrated in the previous chapter. Further proof of the inaccuracy of the standard - upwind predictions is shown in the range $0 \leq \theta \leq 140$, where these predictions are on the whole outside the limits of the experimental accuracy of the measurements.

4. Comparison with other predictions

In Fig. 5.2.6, the 40 x 20 new - upwind predictions are compared with the free - flow predictions of Apelt (1958) and the measurements of Grove et al. Apelt used the parameters $\alpha = -\frac{20}{\pi}\theta$ and $\beta = \frac{20}{\pi}\log_e r$ to transform the ψ and ω equations in the $x_1 - x_2$ plane to

equations in the $\alpha-\beta$ plane. The size of Apelt's domain in terms of θ and τ is as follows:

$$0 \geq \theta \geq -\pi$$

$$R \leq \tau \leq 23.0R \quad \text{for most of the flow}$$

$$R \leq \tau \leq 111.0R \quad \text{for the wake region}$$

The above size corresponds roughly to the size of the present domain. Also the maximum dimensions used by Apelt, 31 x 21, are the same order of magnitude as the maximum dimensions, 40 x 20, used in the present predictions.

An indication of the accuracy of Apelt's computations is given by the maximum vorticity residual, $|(\omega_{new}-\omega_{old})/\omega_{old}|$, which is 0.01 on the surface of the cylinder. The above check suggests that Apelt's predictions should be of the same order of accuracy as the 40 x 20 new - upwind predictions. This is confirmed in Fig. 5.2.6 by the reasonable agreement between the new - upwind and Apelt's predictions. Also Apelt's predictions are within the limits of the experimental accuracy of the measurements.

Kawaguti (1953)'s calculated pressure distribution, which for the sake of clarity is not plotted in Fig. 5.2.6, can be shown to lie only a little above the new - upwind predictions. Thus Kawaguti's predictions also indicate good agreement with the new - upwind predictions, Apelt's predictions and the measurements of Grove et al.

Unlike Apelt, Kawaguti used the parameters $X = 1/\tau$ and $Y = 2/\pi\,\theta$ to transform the ψ and ω equations in the x_1 - x_2 to equations in the $X-Y$ plane. The size of domain, employed by Kawaguti, is as

follows: $\infty \geq r \geq R$

$\pi \geq \theta \geq 0$

Also Kawaguti used a transformed stream function variable, ψ', such that the ψ' values at $r = \infty$ are of the same order of magnitude as values at $r = R$. He employed, however, only two grid points to span the distance between $r = 5R$ and $r = \infty$ and used grid dimensions of only 11 x 21. The coarseness of this grid does not appreciably influence the calculated pressure distribution, but as shown below the size of the recirculation bubble is underestimated.

(iii) Streamline pattern

The accuracy and reliability of the present predictions can be illustrated by comparing the predicted stream - line pattern with the measurements and predictions of other investigators. Now the most easily measured part of the flow is the recirculation bubble on the downstream side of the cylinder. Therefore the following comparisions are based on the overall dimensions of the bubble shown in Fig. 5.2.7.

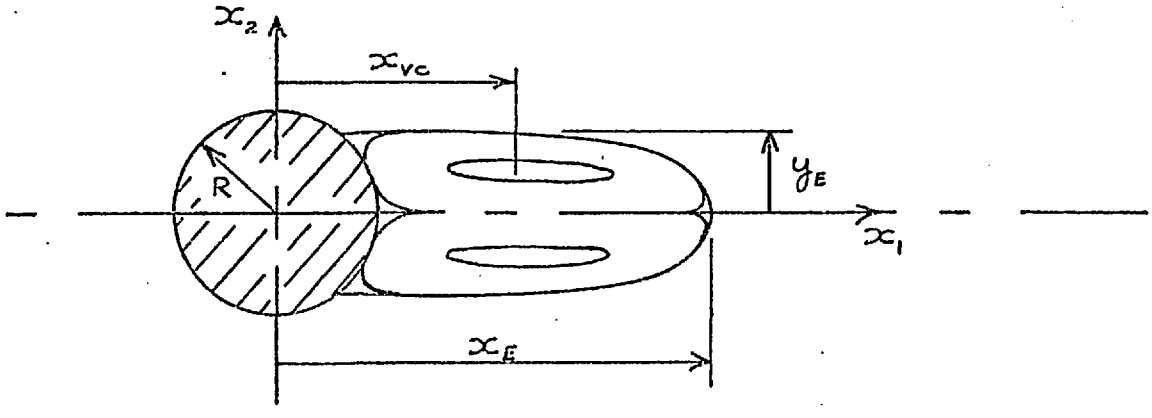


Fig. 5.2.7 Main dimensions of the recirculating bubble due to transverse flow over a cylinder.

It is useful, first of all, to compare all the present predictions against the results of the 40 x 20 new – upwind predictions. The comparison is made in Table 5.2.1. The comparison of the new – upwind predictions shows that the 28 x 14 and 32 x 16 results are larger than

Description of prediction run	x_E/R	y_E/R	x_{Vc}/R
New upwind; 28 x 14 grid	6.23	1.09	$\approx$ 2.6
New upwind; 32 x 16 grid	6.29	1.08	$\approx$ 2.6
New upwind; 40 x 20 grid	5.70	1.05	$\approx$ 2.2
Standard upwind; 40 x 20 grid	5.16	1.00	$\approx$ 2.2

Table 5.2.1

the 40 x 20. This is because the 40 x 20 grid is more refined than the 32 x 16 and 28 x 14 grids in the wake region of the cylinder. The standard – upwind values, on the other hand, are smaller than the corresponding new – upwind results. This disparity is due only to the false – diffusion effect.

In Table 5.2.2, the bubble dimensions for the 40 x 20 predictions are compared with the corresponding measurements and predictions of other investigators. The first three entries in Table 5.2.2 summarise the experimental measurements of Acrivos et al (1968) and Taneda (1956) for different values of the blockage ratio R/h . The trend of these results suggest that as the blockage ratio diminishes, the recirculation

bubble grows and would eventually attain the size corresponding to free - flow conditions. The next two entries summarise the numerical results of Apelt (1958) and Kawaguti (1953). Apelt's predictions fall within the range of the experimental results, but Kawaguti's results underestimate the bubble size. As mentioned earlier, Kawaguti used only two grid points to span the distance between $r = 5R$ and the boundary

Source of results for Re = 40	x_E/R	y_E/R	x_{VC}/R
Acrivos et al (1968); expt; R/ℓ = 0.025	5.60	1.05	-
Taneda (1956); expt; $R/\ell \leq$ 0.03	5.35	1.0	$\approx$2.4
Acrivos et al (1968); expt; R/ℓ = 0.05	5.10	1.0	$\approx$2.4
Apelt (1958); num; free flow	5.30	1.0	$\approx$2.2
Kawguti (1953); num; free flow	4.50	0.94	-
Present, new upwind; num; free flow	5.70	1.05	$\approx$2.2
Present, standard upwind; num; free flow	5.16	1.0	$\approx$2.2

Table 5.2.2

conditions at $r = \infty$. Therefore the low values of x_E/R and y_E/R , which he obtained, may be due to the coarseness of the grid particularly in the part of the wake region which is just downstream

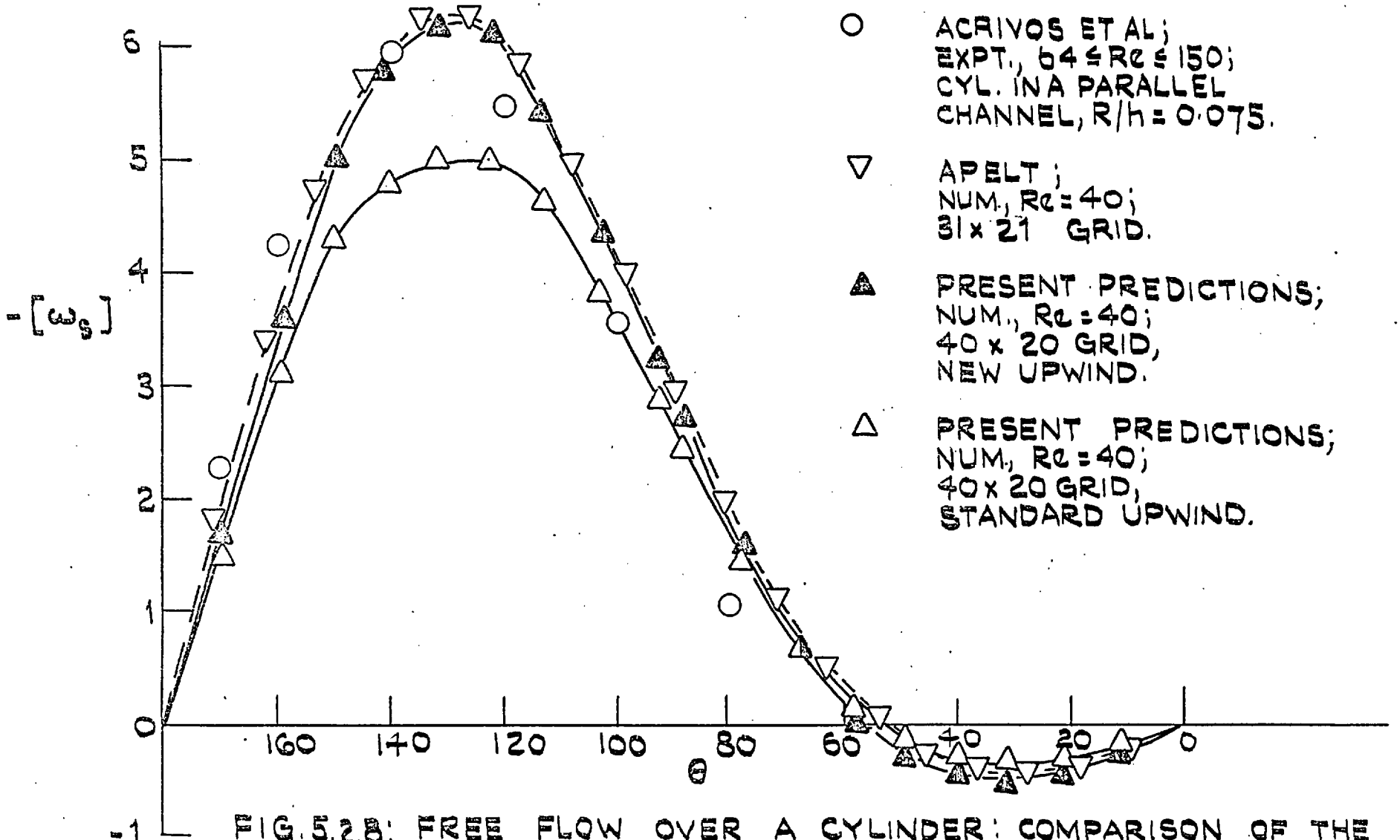


FIG. 5.2.8: FREE FLOW OVER A CYLINDER: COMPARISON OF THE PRESENT WALL VORTICITY PREDICTIONS WITH OTHER PREDICTIONS AND MEASUREMENTS.

of the bubble.

From the last but one entry, it is encouraging to note that the new – upwind result is in agreement with the tendency displayed by the experimental results when these are extrapolated to an R/h of zero. Also the comparison of the last entry and the fourth entry shows that the standard – upwind and Apelt's predictions are in good agreement. Neither of the latter predictions attempt to reduce the false – diffusion effect, so the agreement is not surprising. These favourable comparisons give a further measure of the reliability of the 40 x 20 new – and standard – upwind predictions.

(iv) Vorticity distribution on the cylinder

In Fig. 5.2.8, the vorticity distributions on the cylinder calculated from the new – and standard – upwind predictions are compared with the measurements of Acrivos et al (1968) and the predictions of Apelt (1958). A large discrepancy is evident between the new – upwind and the standard – upwind predictions in the range $160 \geq \theta \geq 90$. The influence of convection is high in this region of the cylinder, and so the discrepancy must be due to false diffusion. On the other hand, there is close agreement between the new – upwind predictions and those of Apelt. This is because the direction of flow next to the upstream side of the cylinder is nearly orthogonal with Apelt's $r - \theta$ grid, and thus the false – diffusion error is effectively minimised in this case.

In order to measure the velocity gradient (or vorticity) at the cylinder wall, Acrivos et al (1968) used an instrument for measuring the cylinder wall shear stress. The measurements were performed for the Reynolds number range, $64 \leq Re \leq 150$. In this Re range the wall velocity gradient $\left(\frac{du_\theta}{dr}\right)_s$ for all θ given by $180 \leq \theta \leq 80$ is shown to be proportional to $\sqrt{Re}$, where u_θ is the velocity in the circumferential direction. Therefore the plots in Fig. 5.2.8 are a result of assuming

that Acrivos et al's plot of $\beta^* = \left(\frac{du_\theta}{d\tau}\right)_s \Big/ \sqrt{Re}$ against Θ for $64 \leq Re \leq 150$ also applies at $Re = 40$. This assumption is justified because the flow properties on the cylinder wall for $80 \leq \Theta \leq 180$ are not greatly affected by the instability in the wake. The agreement between the experimental points and the new - upwind and Apelt's predictions is reasonable. However the small discrepancy between the experiments and the predictions may be partly due to the blockage effect of the channel, which in this case is $R/h = 0.075$.

(c) Flow over a single cylinder in a channel

(i) Geometry and boundary conditions

This section describes the prediction of flow over a single cylinder in a parallel channel with $R/h = 0.05$ and $Re = 40$. The boundary conditions, Fig. 5.2.9, are as follows:

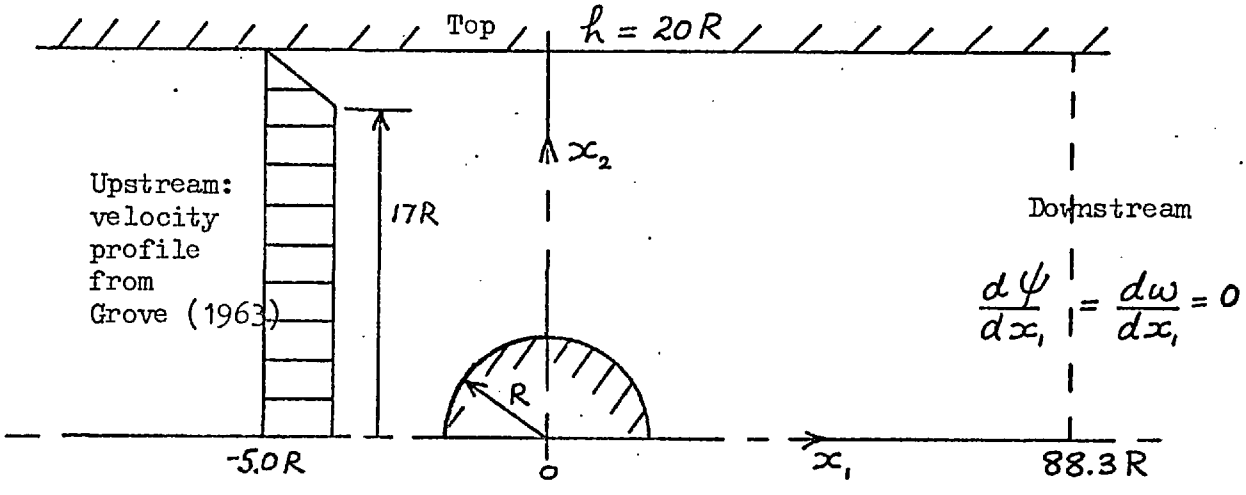


Fig. 5.2.9 Hydrodynamic boundary conditions for laminar channel flow over a single cylinder

1. Upstream boundary

ψ and ω profiles are deduced from an approximate velocity profile measured in Grove (1963)'s test section, and which corresponds to $Re = 40$.

where, $Re = \frac{U_c d}{\nu}$

U_c = velocity at the cylinder position in the absence of the cylinder

d = diameter of cylinder

2. Top boundary

ψ = constant

3. Downstream boundary

$\frac{d\psi}{dx_1} = \frac{d\omega}{dx_1} = 0$

4. Plane of symmetry

$\psi = \omega = 0$

5. Surface of cylinder

$\psi = 0$

(ii) Pressure distribution

For the measurements of Grove (1963), which are also reported in Grove et al (1964), the pressure coefficient $\frac{p_\theta - p_\infty}{\frac{1}{2}\rho U^2}$ is expressed as:

$$\frac{p_\theta - p_\infty}{\frac{1}{2}\rho U^2} = \frac{p_\theta - p_s}{\frac{1}{2}\rho U_c^2}$$

where, U_c is defined above in (i)

p_θ = static pressure on the cylinder at angle θ

p_s = static pressure on the channel wall below the cylinder

In the predictions p_{IN}, the upstream pressure on the plane of symmetry, was chosen as the reference pressure and conveniently set to zero. The predicted values of $\frac{p_\theta - p_s}{\frac{1}{2}\rho U_c^2}$ are therefore given by

$$\left[\frac{(p_\theta - p_{IN}) - (p_s - p_{IN})}{\frac{1}{2}\rho U_c^2}\right]$$

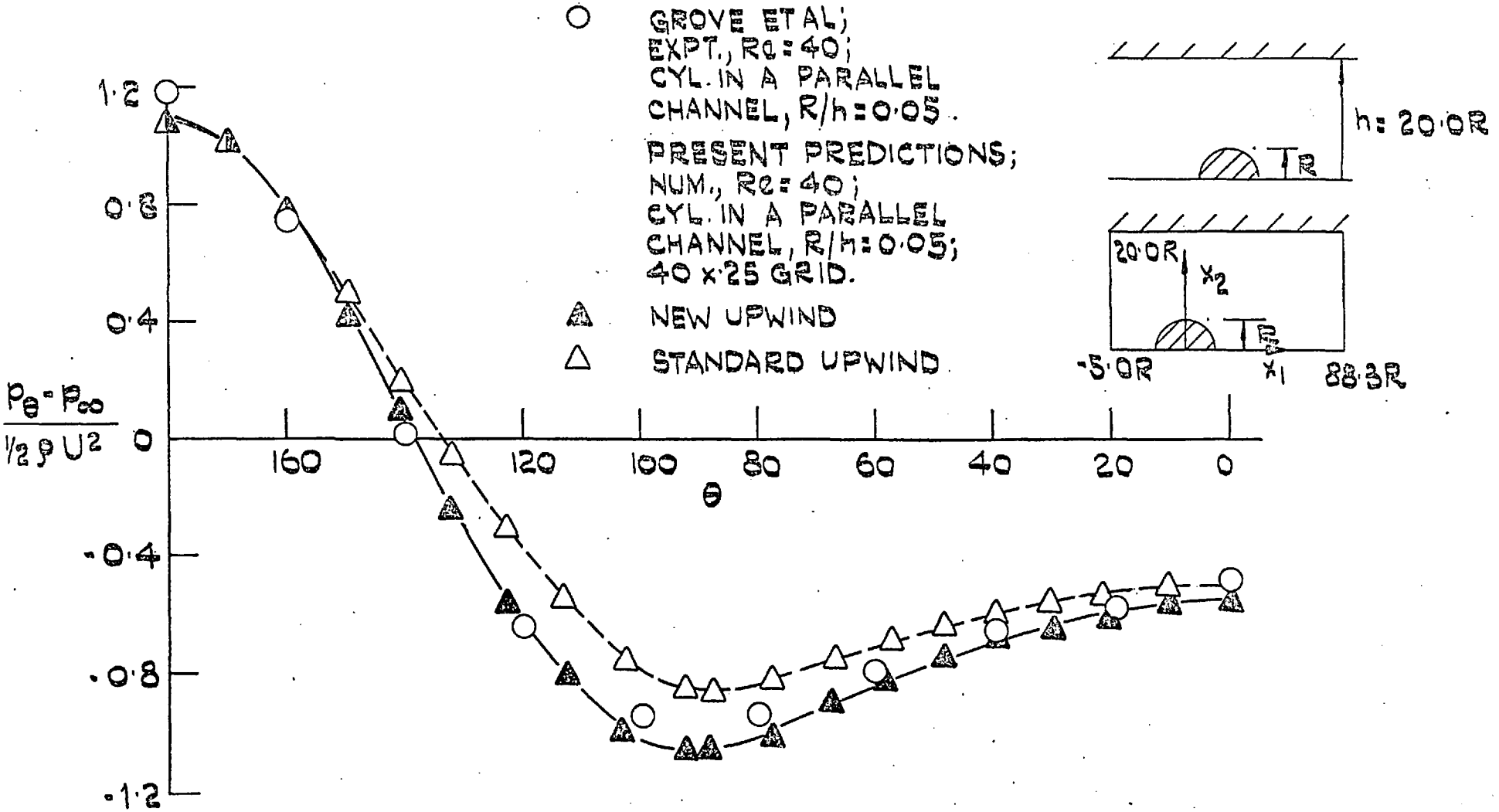


FIG. 5.2.10: CHANNEL FLOW OVER A CYLINDER: INFLUENCE OF CONVECTION TERM METHOD ON THE PREDICTIONS OF PRESSURE DISTRIBUTION.

Fig. 5.2.10 indicates that there is reasonable agreement between the new - upwind predictions and the experimental results. Also the close agreement between the channel- flow pressure predictions in Fig. 5.2.10 and those for free flow in Fig. 5.2.5 confirm that the influence of the blockage effect, $R/h = 0.05$, is small.

(iii) Streamline pattern

The comparison of the predicted and experimental streamline patterns is made in terms of the overall dimensions of the recirculation bubble, x_E/R and y_E/R, which are defined in Fig. 5.2.7.. The results are given in Table 5.2.3.

Source of results for $Re = 40$	x_E/R	y_E/R
Grove et al (1964); $R/h = 0.05$	5.10	1.0
Present; new upwind; 40 x 25 grid	6.10	1.08
Present; standard upwind; 40 x 25 grid	5.20	1.02

Table 5.2.3.

The comparison in Table 5.2.3 tends to suggest that the size of the experimental recirculation bubble is predicted more accurately by the standard - upwind method than by the new - upwind method. But we know that the new -upwind predictions are more accurate than the standard-upwind predictions. One reason for this anomaly is that the

actual flow does not obey the equations of two - dimensional laminar motion in the whole domain. This is probably because of three - dimensional effects which produce components of velocity in the x_3 direction. These effects may be significant in the recirculation bubble where the x_1 and x_2 components of velocity are small. Thus the magnitude of the x_3 velocity components may be sufficient to influence the bubble size.

(d) Drag coefficients

(i) Definitions

The coefficient of drag, C_D, for the flow over a cylinder can be expressed as:

$$C_D = \frac{-2}{\rho U^2}\left[\int_0^{\pi} p_\theta \cos\theta \, d\theta + \mu \int_0^{\pi} \omega_s \sin\theta \, d\theta\right]$$

and, $$C_D = C_{DP} + C_{DF}$$

C_{DP} and C_{DF} are called the pressure drag and the friction drag coefficients respectively, where,

$$C_{DP} = \frac{-2}{\rho U^2}\int_0^{\pi} p_\theta \cos\theta \, d\theta$$

$$C_{DF} = \frac{-2\mu}{\rho U^2}\int_0^{\pi} \omega_s \sin\theta \, d\theta$$

U = characteristic velocity

p_θ = static pressure on cylinder wall

ω_s = vorticity on cylinder wall

(ii) Results

Before comparing the present predictions of C_D, C_{DP} and C_{DF} with the measurements and predictions of other investigators, it is useful to compare the present results for free flow with those for channel flow.

These results are given in Table 5.2.4.

Description of prediction run	C_{DP}	C_{DF}	C_D
Free flow; new upwind, 40 x 20	1.011	0.545	1.557
Free flow; standard upwind, 40 x 20	1.004	0.471	1.475
Channel flow, R/h = 0.05; new upwind, 40 x 25	0.983	0.536	1.519
Channel flow, R/h = 0.05; standard upwind, 40 x 25	0.989	0.466	1.455

Table 5.2.4

It is interesting to note that both channel – flow values agree closely with the corresponding free – flow values. This implies that the blockage effect for the channel, R/h = 0.05, does not have an appreciable influence on these overall coefficients.

In Table 5.2.5, the new – upwind predictions for both free flow and channel flow are compared with the measurements and predictions of other investigators. The first five entries in Table 5.2.5 give a comparison of the predictions and measurements for free flow. Amongst the latter, the results of Relf (1913) and Tritton (1959) were obtained for fine wires and fibres in wind – tunnels, where the diameters of the test pieces

Source of results for $Re = 40$	C_{DP}	C_{DF}	C_D
Apelt (1958); num., free flow	0.928	0.568	1.496
Kawaguti (1953); num., free flow	1.053	0.565	1.618
Relf (1913); expt., free flow	-	-	1.61
Tritton (1959); expt., free flow	-	-	1.46 - 1.62
Present predictions; free flow	1.011	0.545	1.557
Grove et al (1964); expt., channel flow	0.940	0.460	1.400
Present predictions; channel flow	0.983	0.536	1.519

Table 5.2.5

were small compared with the wind - tunnel cross - sectional height. The new - upwind values fall half - way between the values determined by Apelt and Kawaguti, and all the predictions fall within Tritton's scatter of experimental results.

The last two entries give a comparison between the results of Grove et al (1964) for channel - flow and the new - upwind predictions for the same flow geometry. The values of C_{DP} compare reasonably well, but there seems to be some discrepancy between the experimental and predicted values of

C_{DF}. However it should be noted that Grove et al's value of C_{DF} was estimated by means of what they call 'a standard laminar boundary - layer analysis using the measured pressure profile'. It is possible that the use of this analysis has caused the experimental value of C_{DF} to be underestimated.

5.2.3 Heat transfer predictions

(a) Outline of sub - section and boundary conditions

This sub - section is concerned with the predictions of average and local Nusselt numbers for free flow over a cylinder at Re = 40 and Pr = 0.7. The boundary conditions, Fig. 5.2.11, are as follows:

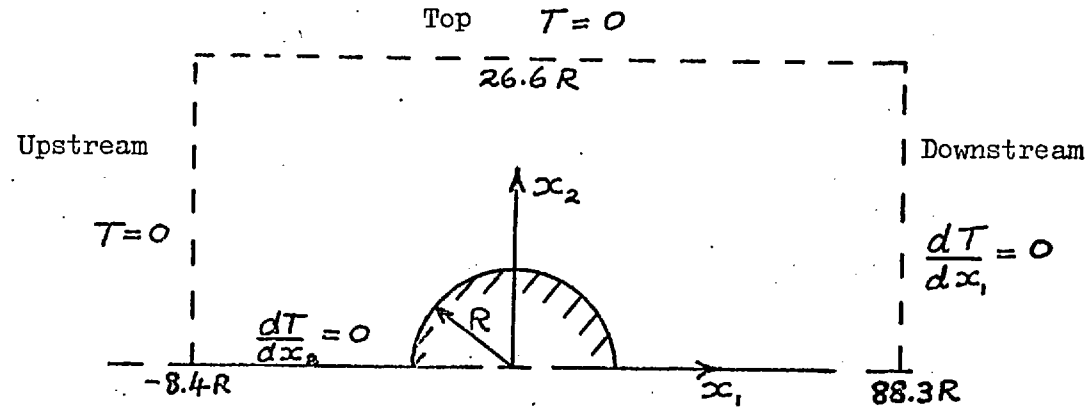


Fig. 5.2.11 Thermal boundary conditions for laminar free flow over a cylinder

1. Upstream and top boundaries: $T = 0$
2. Downstream boundary: $\frac{dT}{dx_1} = 0$
3. Plane of symmetry: $\frac{dT}{dx_2} = 0$
4. Cylinder wall: T_s = constant or $\dot{q}''_s$ = constant
5. Stream - function distributions:

   The ψ distributions are obtained from the free - flow predictions in sub - section 5.2.2 (b).

Source of Results	Equation for mean Nusselt number	Value of $\overline{Nu}$ at Re = 40
McAdams (1954)	$\overline{Nu} = 0.32 + 0.43 Re^{0.52}$ $0.1 \leq Re \leq 1000$	3.25
Hilpert (1933)	$\overline{Nu} = 0.821 \left[Re \left(\frac{T_s}{T_\infty} \right)^{1/4} \right]^{0.385}$ $4 \leq Re \leq 40$	3.35
Collis and Williams (1959)	$\overline{Nu} \left[T_m / T_\infty \right]^{-0.17}$ $= 0.24 + 0.56 Re^{0.45}$ $0.02 \leq Re \leq 44$	3.19
van der Hegge Zijnen (1957)	$\overline{Nu} = 0.35 +$ $0.5 Re^{0.5} + 0.001 Re$ $0.01 \leq Re \leq 500,000$	3.55
Present predictions; new upwind, 40 x 20; T_s = constant	———	3.38
Present predictions; standard upwind, 40 x 20; T_s = constant	———	3.49
Present predictions; new upwind, 28 x 14; T_s = constant	———	3.64
Dennis, Hudson and Smith (1968); numerical, T_s = constant	———	3.48

Table 5.2.6

(b) Average Nusselt numbers

The heat transfer characteristics of flow over transverse cylinders has been the concern of a great number of experimenters, who have performed measurements over a wide range of Reynolds and Prandtl numbers. Those who have concentrated their efforts in the very low Reynolds number range have measured the characteristics of very fine hot - wire probes ($d < 0.005$ cm) which are used extensively in the measurement of the turbulent properties of fluids and in particular air. The size of these wires is such that free - flow conditions can be assumed to exist round the wire. Therefore, in this sub - section, the predictions of average Nusselt numbers at $Re = 40$ under free - flow conditions are compared with available hot - wire correlations.

Table 5.2.6 gives the $\overline{Nu} - Re$ correlations produced by a selected number of investigators for air flow over cylinders. The values of $\overline{Nu}$ at $Re = 40$, calculated from each correlation, are given along with values obtained from the present predictions and the predictions of Dennis, Hudson and Smith (1968). It is gratifying that the 40 x 20 predictions are within 6% of the mean of all the experimental values, and within 3% of the value predicted by Dennis et al. The effect of using a coarse grid is illustrated by the 28 x 14 result, which is greater than the 40 x 20 predictions but within 10% of the mean experimental value.

In the course of their measurements, Collis and Williams (1959) have shown that the effect of natural convection on heat transfer from a wire of $d \leq 0.005$ cm is negligible for Reynolds numbers of the order of 40. Therefore it is particularly valid to compare the predictions with the values of Hilpert (1933) and Collis and Williams (1959), because in both cases the measurements were performed with wires of $d \leq 0.005$ cm and $Re \approx 40$.

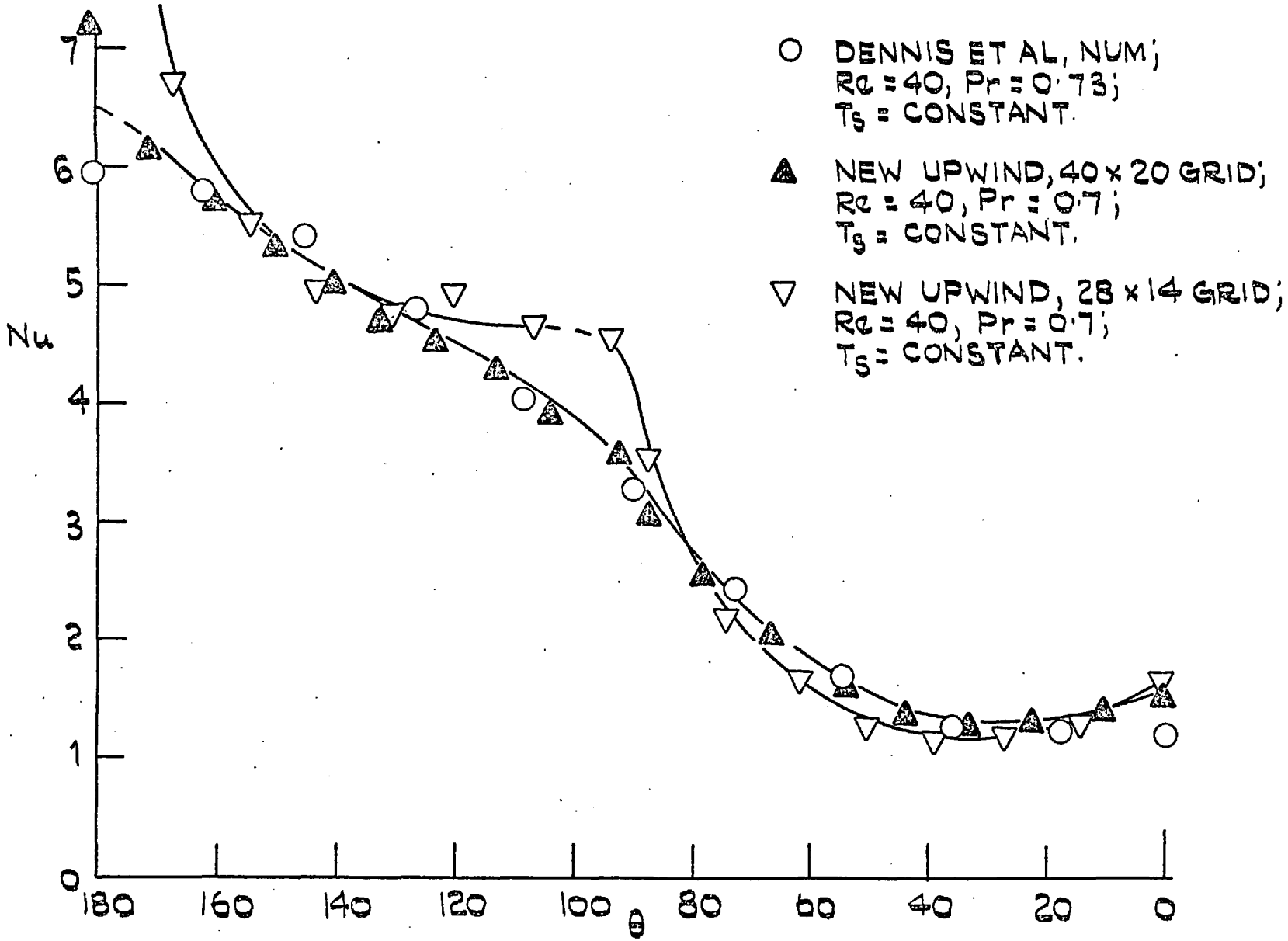


FIG. 5.2.12: HEAT TRANSFER FROM A SINGLE CYLINDER, T_S = CONSTANT: INFLUENCE OF GRID REFINEMENT ON Nu PREDICTIONS.

(c) Local Nusselt numbers

(i) The predictions for T_S = constant

Fig. 5.2.12 illustrates the new - upwind predictions for Re = 40, Pr = 0.7 and grid sizes 28 x 14 and 40 x 20. These predictions are compared with those of Dennis et al for Re = 40 and Pr = 0.73. The latter investigators used the velocity field calculated by Apelt (1958) as a basis for the numerical solution of the elliptic equation for enthalpy. In their finite - difference procedure, Dennis et al (1968) used a polar co-ordinate grid system with the additional change of variable $\xi = \log_e\left(\frac{r}{R}\right)$, where R is the radius of the cylinder. This co-ordinate system is the same as that used by Apelt (1958).

It was shown earlier in sub - section 5.2.2 (b) that Apelt's predictions of wall pressure and vorticity distributions compare closely with the corresponding 40 x 20 new - upwind predictions. It was also concluded that Apelt's predictions are accurate because the near - wall flow is very nearly orthogonal with the grid, and so the effects of false diffusion are minimised in this region. The same argument applies to Dennis et al's predictions of local Nusselt number, which are shown in Fig. 5.2.12.

It is encouraging to note that, except for the values of Nu at the front and rear stagnation points, the 40 x 20 new - upwind predictions compare closely with those of Dennis et al. From this comparison, one can deduce that the new - upwind profiles at the front and rear stagnation points are inaccurate. Now the local Nusselt number can be written as follows:

$$Nu = -\left(\frac{dT^*}{dr^*}\right)_S$$

$$\approx -\left(\frac{T^*_{NP} - T^*_S}{r^*_{NP} - r^*_S}\right)$$

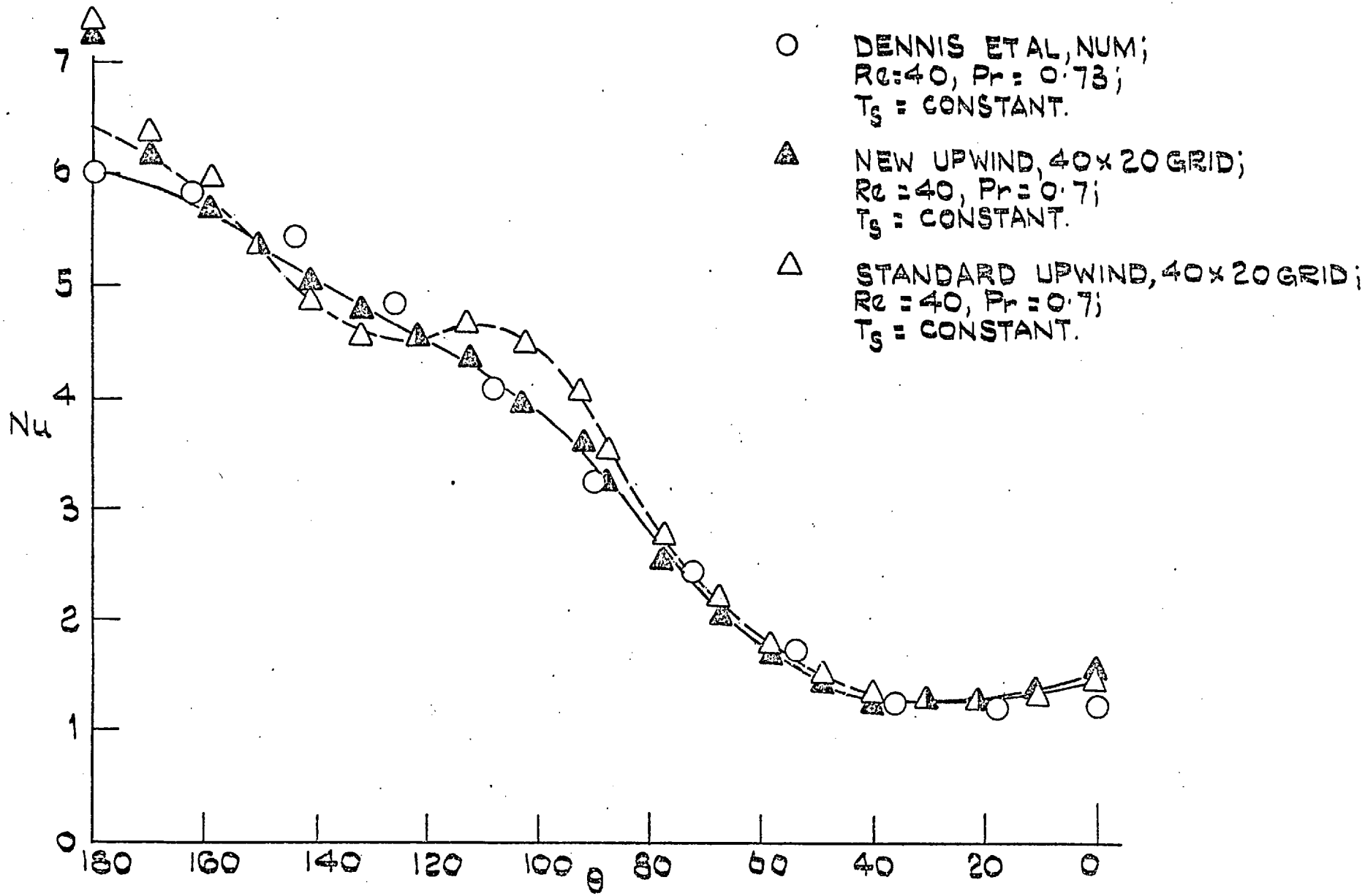


FIG. 5.2.13: HEAT TRANSFER FROM A SINGLE CYLINDER, T_S = CONSTANT: INFLUENCE OF CONVECTION TERM METHOD ON Nu PREDICTIONS

where, $T^* = T/(T_s - T_\infty)$

$r^* = r/d$

T_s = cylinder wall temperature

T_∞ = reference temperature

r = radial distance from axis of cylinder

d = diameter of cylinder

and, subscript NP refers to values at grid nodes next to the cylinder wall and subscript S to values at the cylinder wall.

Referring to Fig. 5.2.2, the grid distribution is such that the values of $r^*_{NP} - r^*_S$ for the grid nodes next to the front and rear stagnation points are very small. Also it follows that $T^*_{NP} - T^*_S$ will be small for these nodes. Therefore a small error in T^*_{NP} can produce a large error in Nu. One cannot therefore place too much confidence in the local values of Nu at these positions on the cylinder wall. Fig. 5.2.12 also shows that by refining the grid from 28 x 14 to 40 x 20, the errors near the front stagnation point and in the region $85 \leq \theta \leq 120$ are reduced.

Fig. 5.2.13 shows that the new - and standard - upwind predictions agree with the predictions of Dennis et al to within $\pm$ 10% in the range $120 \leq \theta \leq 170$. The uncharacteristic shape of the standard - upwind curve for $90 \leq \theta \leq 180$ is attributed to false diffusion, and it is clear that the effect of this error is largely removed by the new - upwind calculation. The false - diffusion error is not so apparent for the downstream side of the cylinder, $90 \geq \theta \geq 0$, because the convection terms in this region are small compared with the diffusion terms.

(ii) Comparison with experiment, T_S = constant

Fig. 5.2.14 compares the new - upwind and Dennis et al's predictions

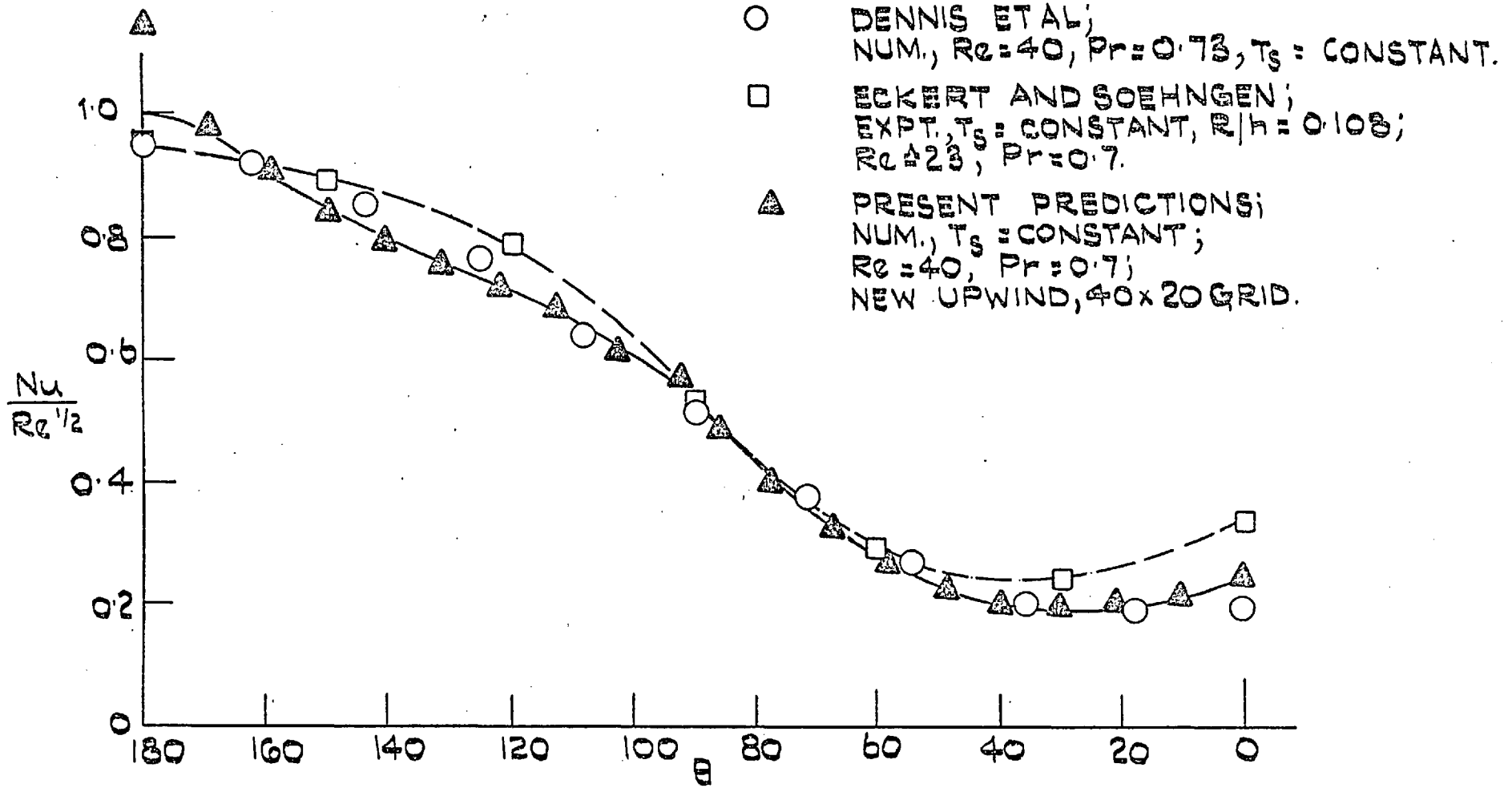


FIG. 5.2.14: HEAT TRANSFER FROM A SINGLE CYLINDER, T_s = CONSTANT: COMPARISON OF THE PRESENT PREDICTIONS WITH OTHER PREDICTIONS AND MEASUREMENTS.

at Re = 40 with the measurements of Eckert and Soehngen (1952) at Re = 23 on the basis of $Nu/Re^{1/2}$ against Θ . A stagnation point analysis for flow over a cylinder, Schlichting (1968) shows that Nu at the front stagnation point is proportional to $Re^{1/2}$ for the case of Pr = 0.7. Therefore the comparison between the predictions and the measurements on the basis of $Nu/Re^{1/2}$ is particularly valid near the front stagnation point.

Before discussing the comparisons we should estimate the validity of comparing the predictions with the measurements of Eckert and Soehngen. The experimental conditions for the latter were as follows:

1. The blockage ratio of the test section, R/h was 0.108.

2. The cylinder wall temperature gradients at the centre plane of the test section were measured using a Zehnder Mach interferometer. Because of the light – ray refraction in the heated boundary layer, temperature corrections were made and amounted to a maximum of 10% of the temperature difference across the boundary layer.

3. The test – section flow velocities could not be measured because no instrument was available for measuring low air velocities of some inches per second. The Reynolds numbers were therefore determined from the measurement of the average Nusselt numbers and the use of a correlation similar to McAdam's formula in Table 5.2.6.

4. The interference photograph for Re = 23 shows a definite asymmetry in the interference lines (or isotherms) on the downstream side of the cylinder. This effect must be due to natural convection.

As indicated by point 2, the local Nusselt number should be accurate to within $\mp$ 5%. However the method used for estimating the Reynolds number (point 3) effectively minimises the influence of the blockage effect (point 1) on the values of $Nu/Re^{1/2}$. This is because $\overline{Nu}$ is assumed to

obey a formula for free flow where $\frac{\overline{Nu}}{Re^{1/2}} \approx$ constant in the range $20 \leq Re \leq 40$; and as most of the heat transfer occurs on the front face of the cylinder this means that the local values of Nu are also made proportional to $Re^{1/2}$. The latter agrees with the theory of the stagnation point analysis for free flow over a cylinder, and thus the effect of blockage is minimised.

The influence of natural convection (point 4) is significant only on the downstream side of the cylinder, $0 \leq \theta \leq 80$, where the local velocities are small. However the heat transfer for this region is only about 20% of the total. Therefore if the error due to natural convection is say 40% in this region, then the error in the total heat transfer is only 8%. But as for the blockage effect, the influence of natural convection on the values of $Nu/Re^{1/2}$ for the upstream face of the cylinder is minimised by the above method of calculating Re.

Thus it is not surprising that there is reasonable agreement between the two sets of predictions and the experimental data in the range $170 \leq \theta \leq 40$. However the error in the new – upwind predictions at the front stagnation point is again clearly evident. Another obvious discrepancy is between the predictions and experimental data in the range $40 \leq \theta \leq 0$. This must be mainly due to the influence of natural convection.

(iii) Comparison with experiment, $\dot{q}''_s$ = constant

Some predictions for $\dot{q}''_s$ = constant are illustrated in Fig. 5.2.15. In the latter, new – upwind predictions for Re = 40 and Pr = 0.7 are compared with the measurements of Acrivos et al (1965) for Re = 49 and Pr = 1200 on the basis of $Nu/\overline{Nu}$ against θ. This basis for comparison is chosen for two reasons. Firstly, the functional relationship between $\overline{Nu}$, Re and Pr is not known for $\dot{q}''_s$ = constant. Secondly, the use of the ratio $Nu/\overline{Nu}$ reduces the importance of the

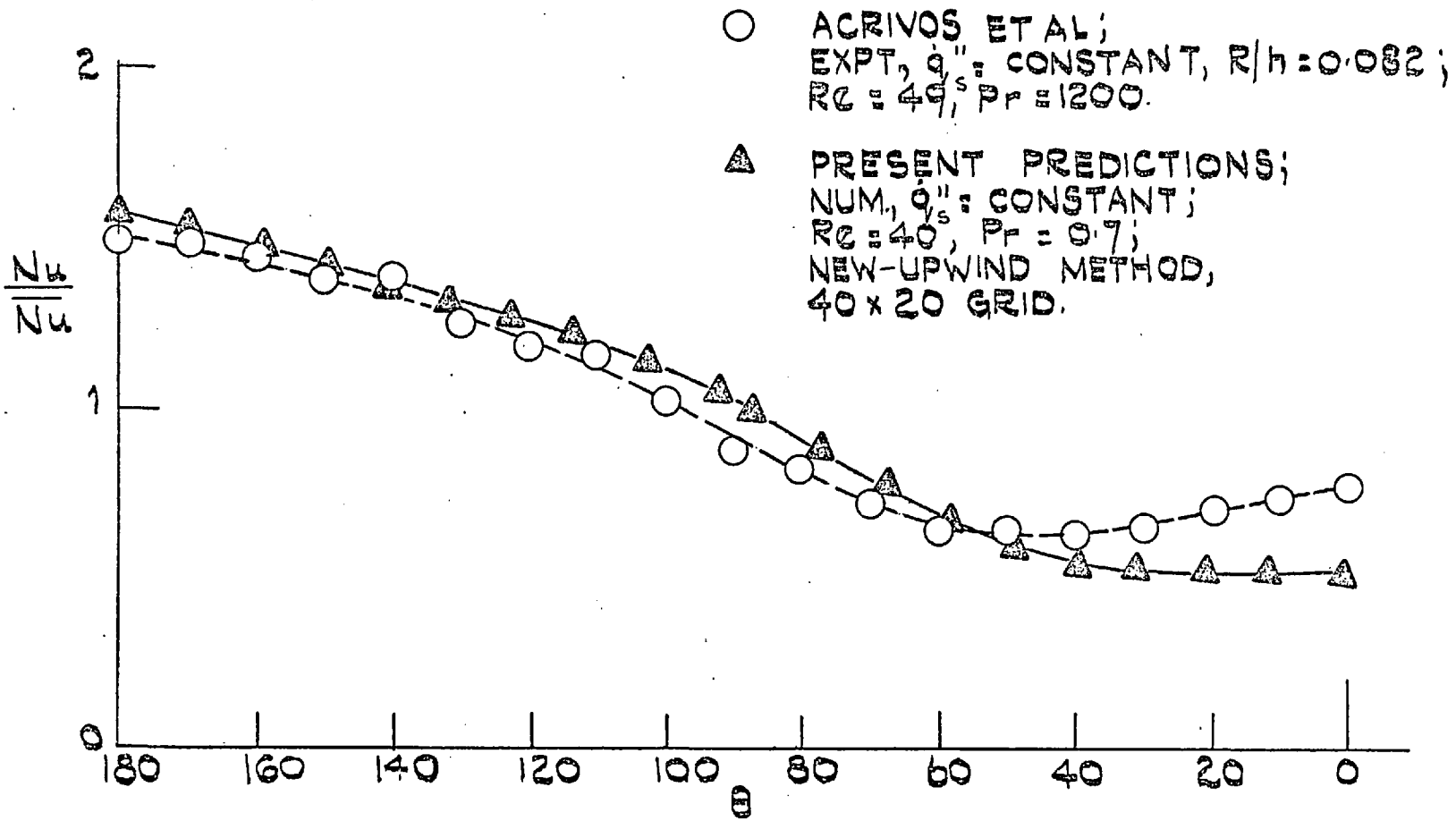


FIG. 5.2.15 : HEAT TRANSFER FROM A SINGLE CYLINDER, $\dot{q}''_s$ = CONSTANT: COMPARISON OF THE PRESENT PREDICTIONS WITH OTHER MEASUREMENTS.

blockage effect, R/h = 0.082, which according to Acrivos et al increases the heat transfer near the front stagnation point by about 10 – 20%.

It will be noted that, unlike the new – upwind predictions for T_S = constant in Fig. 5.2.14, the predictions for $\dot{q}''_{rs}$ = constant do not indicate any uncharacteristic trends near the front stagnation point. This is because the local Nusselt number is defined by:

$$Nu = \frac{\dot{q}''_s \, d/k}{(T_{s,\theta} - T_\infty)}$$

where, $\frac{\dot{q}''_{rs} \, d}{k}$ = constant

k = thermal conductivity of the fluid

$T_{s,\theta}$ = wall temperature at angle θ

Therefore the error in Nu is inversely proportional to the error in $(T_{s,\theta} - T_\infty)$, or $T_{s,\theta}$ if the reference temperature T_∞ is zero. This error is much less than that for the corresponding predictions with T_S = constant, because for the latter the error in Nu is proportional to the error in $T_S - T_{NP}$, where T_{NP} is the temperature at the near – wall node. The agreement between the trend of the experimental and predicted curves near the front – stagnation point suggests that the error in $T_{s,\theta}$ must be small in this region. If this is so, then the error in Nu is small for the whole cylinder, because the error must decrease as $T_{s,\theta}$ increases, that is as Nu decreases.

The agreement between the predictions and the measurements for $50 \leq \theta \leq 180$ is within 12%, which is less than the maximum error due to the blockage effect near the front – stagnation point. The large discrepancy in the range $0 \leq \theta \leq 50$ is probably due to the combination of the blockage effect and natural convection.

5.2.4 Discussion

(a) The matter of accuracy

The previous sub - sections, 5.2.2 and 5.2.3, contain a number of comparisons between the present predictions of flow over a single cylinder and the predictions and measurements of other workers. These comparisons demonstrate that the Chapter 3 solution procedure can be used to give accurate predictions of laminar recirculating flows. However the accuracy of such predictions is dependent on two main factors.

Firstly, the accuracy depends on the method used to calculate the convection terms. For example the present predictions (in agreement with those of Chapter 4) show that the predictions due to the new - upwind method are more accurate than those due to the standard - upwind method. Thus the more accurate new - upwind method should be used for all problems, where its properties do not prevent convergence.

Secondly, the overall accuracy often depends on the accuracy of the near - wall calculations or, in other words, on the grid distribution in the near - wall region. For instance in the case of flow over a cylinder (and other similar flows with stagnation points) the boundary layer thickness on the upstream face is inversely proportional to the square root of the Reynolds number. This means that if we wish to obtain accurate predictions of flow over a cylinder for $Re > 40$, it is necessary to progressively refine the grid so that the near - wall nodes are always within the boundary layer. This could be done with the present grid arrangement. However the required number of grid nodes may cause a prohibitive increase in computer time. Alternatively, the grid in the near - wall region could be refined more efficiently by using a hybrid grid arrangement similar to that of Thoman and Szewczyk (1969). In the work of the latter, the nodes were described by an $r - \theta$ system in the region

$R \leq r \leq 2R$, where R = radius of the cylinder, and a rectangular mesh in the outer field. This arrangement has the disadvantage that the required iteration scheme is more complicated than that for a single grid arrangement. However this disadvantage is outweighed by the important advantage that the details of the flow very close to the wall boundary can be accurately calculated.

(b) Summary of results

The results of using the Chapter 3 solution procedure for predicting flow over a cylinder at Re = 40 are summarised below in two parts. The first part is concerned with free flow over a cylinder and the second is concerned with channel flow. The present predictions are discussed in terms of the results which correspond to the 40 x 20 new - upwind predictions.

For free flow over a cylinder the results show that:

(i) The predictions of pressure and wall vorticity distributions are in good agreement with the measurements and predictions of other investigators. Also the prediction of streamline pattern is in good agreement with the trend of the available measurements.

(ii) The prediction of the coefficient of drag falls midway between the limits of the experimental scatter of results and midway between the values of other predictions.

(iii) The prediction of average Nusselt number for Pr = 0.7 and T_S = constant agrees to within 3% of the value predicted by Dennis et al (1968) and to within 2% of the mean of the available experimental values. Also the predicted local values of Nusselt number are in reasonable agreement with those of Dennis et al (1968). However agreement is poor at the front and rear stagnation point, where the present predictions are inaccurate.

(iv) For both T_S = constant and $\dot{q}''_{rs}$ = constant, the trends of the local Nusselt curves are on the whole in agreement with the available measurements. Exact comparison, however, cannot be expected because the measurements are influenced by a combination of blockage and natural convection effects.

For flow over a cylinder in a channel ($R/H = 0.05$) the results show that:

(i) The predictions and measurements of pressure distribution are in good agreement.

(ii) The streamline pattern is not accurately predicted because three - dimensional effects may influence the experimental bubble size.

5.3 Flow through in - line tube banks

5.3.1 Review of available data

Flow through tube banks has been the subject of many experimental studies, but very little work has been performed in the low Reynolds number range where viscous effects predominate. The most prominent studies in this flow regime are the measurements of Omohundro et al (1949), Bergelin et al (1949), (1950), (1952) and Zhukauskas et al (1968). All three groups used medium - viscosity oils, so that very low Reynolds numbers could be achieved at flow rates within the range of available flow meters. The work of Bergelin et al is particularly comprehensive as it deals with:

(a) a wide range of Reynolds numbers within the laminar regime.

(b) various in - line and staggered arrangements for the non - dimensional spacings 1.25 x 1.25 and 1.50 x 1.50.

(c) the measurement of pressure drop and heat transfer data under isothermal, cooling and heating conditions.

However Bergelin et al chose the restrictions of using 14 tube rows for the staggered geometries and 10 tube rows for the in - line geometry,

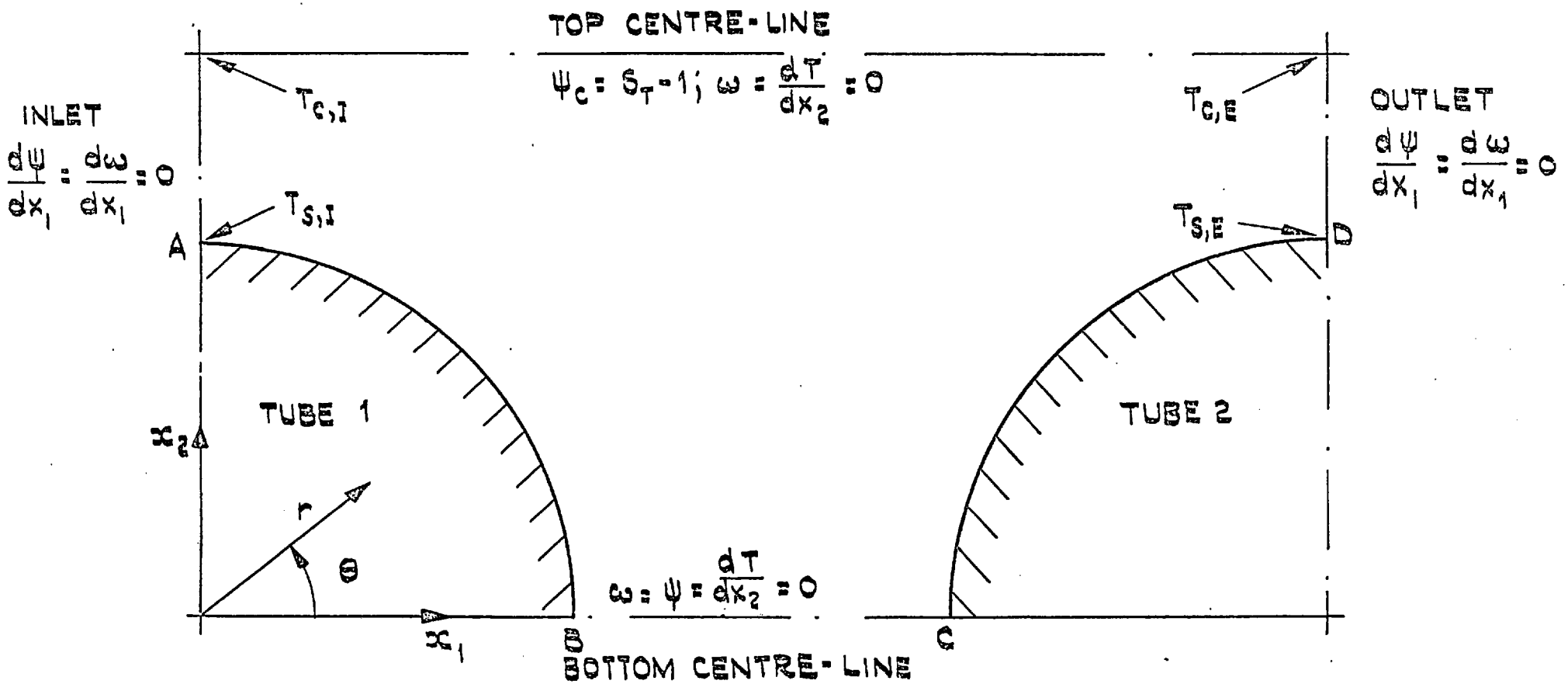


FIG. 5.3.1: BOUNDARY CONDITIONS FOR LAMINAR FLOW THROUGH IN-LINE TUBE BANKS.

and the boundary condition of a constant - temperature tube wall. The work of Zhukauskas et al is not as comprehensive as the above, but it does include measurements of local heat transfer coefficients for the constant - heat - flux boundary condition.

In this section, we are concerned only with in - line tube banks; and most of the predictions are performed for the 1.25 x 1.25 and 1.50 x 1.50 banks so that comparisons can be made with the bulk measurements of Bergelin et al. These comparisons are supplemented by plots of various local characteristics such as flow, pressure, shear stress and Nusselt number distributions.

The following sub - sections 5.3.2, 5.3.3, 5.3.4 and 5.3.5 are concerned with the boundary conditions, hydrodynamic predictions, heat transfer predictions and discussion respectively.

5.3.2 Boundary conditions

The boundary conditions with reference to Fig. 5.3.1 are as follows:

(a) Hydrodynamic

(i) Reynolds number: $$Re = \frac{\rho \bar{u} D_t}{\mu} = \frac{2 \rho \bar{u} R}{\mu}$$

where, $\rho = \bar{u} = R = 1$: $Re = 2/\mu$

$\bar{u}$ = mean velocity through minimum cross - section between the tubes

D_t = diameter of tube

(ii) Inlet and outlet: $$d\psi/dx_1 = d\omega/dx_1 = 0$$

(iii) Tube walls: $$\psi_s = 0$$

(iv) Top centre - line: $$\psi_c = S_T - 1, \quad \omega = 0$$

(v) Bottom centre - line: $$\psi = \omega = 0$$

(vi) Wall shear stress: $$\tau_s = \mu \left[\frac{du_\theta}{dr}\right]_{r=R}$$

$$\therefore \frac{2\tau_s}{\rho \bar{u}^2} = -\frac{2\mu[\omega]_{r=R}}{\rho \bar{u}^2}$$

(vii) Wall presssure gradient and distribution:

$$\frac{1}{R}\frac{dp}{d\theta} = \left[\frac{d\tau}{dr}\right]_{r=R} = -\mu\left[\frac{d\omega}{dr}\right]_{r=R}$$

Integrating w.r.t. θ, $\int_{p_o}^{p_\theta} dp = \int_0^\theta -R\mu\left[\frac{d\omega}{dr}\right]_{r=R} d\theta$

$$\therefore \frac{2(p_\theta - p_o)}{\rho\bar{u}^2} = \frac{2}{\rho\bar{u}^2}\int_0^\theta -R\mu\left[\frac{d\omega}{dr}\right]_{r=R} d\theta$$

Similarly, $\frac{2(p_\pi - p_\theta)}{\rho\bar{u}^2} = \frac{2}{\rho\bar{u}^2}\int_\theta^\pi -R\mu\left[\frac{d\omega}{dr}\right]_{r=R} d\theta$

(viii) Total pressure drop coefficient (Euler number):

$$Eu = (p_A - p_D)/(\rho\bar{u}^2)$$

The Euler number is calculated as follows:

$$Eu = \frac{1}{\rho\bar{u}^2}\left[(p_A - p_B) + (p_B - p_C) + (p_C - p_D)\right]$$

Using the equations in (vii) above, the pressure differences $(p_A - p_B)$ and $(p_C - p_D)$ are calculated via the pressure distribution equations for tubes 1 and 2 respectively. However the pressure difference $(p_B - p_C)$ is calculated from the integration of the x_1 - momentum equation between points B and C. The latter equation may be written as follows:

$$\frac{\partial p}{\partial x_1} = \frac{\partial}{\partial x_1}\left\{2\mu\frac{\partial u_1}{\partial x_1} - \rho u_1^2\right\} + \frac{\partial}{\partial x_2}\left\{\mu\left[\frac{\partial u_1}{\partial x_2} + \frac{\partial u_2}{\partial x_1}\right] - \rho u_1 u_2\right\}$$

By integrating the above equation between points B and C and by using the boundary conditions, $(u_1)_B = (u_1)_C = (u_2)_{x_2=0} = 0$,

and the continuity equation, $\frac{\partial u_1}{\partial x_1} + \frac{\partial u_2}{\partial x_2} = 0$

we obtain:

$$p_B - p_C = \mu\int_B^C \left[\frac{d\omega}{dx_2}\right]_{x_2=0} dx_1$$

or, $$\frac{p_B - p_C}{\rho\bar{u}^2} = \frac{\mu}{\rho\bar{u}^2}\int_B^C \left[\frac{d\omega}{dx_2}\right]_{x_2=0} dx_1$$

(b) Heat transfer

For convenience the boundary conditions for temperature are tabulated in Table 5.3.1 in terms of $\frac{\dot{q}''_s}{C_p}$ = constant and T_S = constant.

Parameters	$\dot{q}''_s / C_p$ = constant	T_s = constant
$T_{c,I}$	$T_{c,I}$	
$T_{c,E}$ (Note 1)	$T_{c,I} + \frac{\dot{q}''_s}{C_p}\left[\frac{\pi R}{\psi_c - \psi_s}\right]$	From $\frac{dT}{dx_1} = 0$
$T_{s,I}$ (Note 1)	$T_{s,E} - \frac{\dot{q}''_s}{C_p}\left[\frac{\pi R}{\psi_c - \psi_s}\right]$	T_s
$T_{s,E}$, T_s (Note 2)	$T_{NP} + \frac{\dot{q}''_s}{C_p}\left[\frac{r_{NP} - R}{\mu/P_r}\right]$	T_s
T_E	From $dT/dx_1 = 0$	
T_I	$T_I - T_{c,I} = (T_{s,I} - T_{c,I})\left[(T_E - T_{c,E})/(T_{s,E} - T_{c,E})\right]$	
$T_{B,I}$, $T_{B,E}$	$\int_R^{S'_T/2} \rho u_1 T\, dx_2 \Big/ \int_R^{S'_T/2} \rho u_1\, dx_2$	
T_{AB}	$(T_{B,I} + T_{B,E})/2$	
T_{LM}	$\frac{(T_{s,E} - T_{B,E}) - (T_{s,I} - T_{B,I})}{\log_e\left[(T_{s,E} - T_{B,E})/(T_{s,I} - T_{B,I})\right]}$	
$(Nu)_{B,I}$ (Note 3)	$\frac{(\dot{q}''_s/C_p)\, D_t}{\mu/P_r \lvert T_s - T_{B,I}\rvert}$	$\left[\frac{T_s - T_{NP}}{T_s - T_{B,I}}\right]\frac{D_t}{(r_{NP} - R)}$
$(Nu)_{B,E}$ (Note 3)	$\frac{(\dot{q}''_s/C_p)\, D_t}{\mu/P_r \lvert T_s - T_{B,E}\rvert}$	$\left[\frac{T_s - T_{NP}}{T_s - T_{B,E}}\right]\frac{D_t}{(r_{NP} - R)}$
$(Nu)_{AB}$ (Note 3)	$\frac{(\dot{q}''_s/C_p)\, D_t}{\mu/P_r \lvert T_s - T_{AB}\rvert}$	$\left[\frac{T_s - T_{NP}}{T_s - T_{AB}}\right]\frac{D_t}{(r_{NP} - R)}$
$(Nu)_{LM}$ (Note 3)	$\frac{(\dot{q}''_s/C_p)\, D_t}{(\mu/P_r)\, T_{LM}}$	$\frac{\lvert T_s - T_{NP}\rvert}{T_{LM}}\frac{D_t}{(r_{NP} - R)}$
$\overline{Nu}$	$\frac{1}{\pi}\int_0^{\pi} Nu\, d\theta$	

Table 5.3.1

Note 1: Equations for $T_{c,E}$ and $T_{s,I}$, $\frac{\dot{q}''_s}{c_p}$ = constant

The local Nusselt numbers at $\theta = \frac{\pi}{2}$ can be given as follows:

$$\left[(Nu)_{B,I}\right]_{\theta=\pi/2} = \frac{\dot{q}''_s \, D_t}{k\,(T_{s,I} - T_{B,I})} \quad \text{and} \quad \left[(Nu)_{B,E}\right]_{\theta=\pi/2} = \frac{\dot{q}''_s \, D_t}{k\,(T_{s,E} - T_{B,E})}$$

For fully - developed conditions:

$$\left[(Nu)_{B,I}\right]_{\theta=\pi/2} = \left[(Nu)_{B,E}\right]_{\theta=\pi/2}$$

$$\therefore \quad T_{s,I} - T_{B,I} = T_{s,E} - T_{B,E}$$

$$\therefore \quad T_{s,E} - T_{s,I} = T_{B,E} - T_{B,I}$$

The heat balance equation for the tube bank section is given by:

$$\dot{q}''_s \, \pi \, R = c_p \, m \, (T_{B,E} - T_{B,I})$$

where, $$m = m_I = \left[\int_R^{S_T/2} \rho \, u_1 \, dx_2\right]_I = \psi_c - \psi_s$$

$$\therefore \quad T_{B,E} - T_{B,I} = \frac{\dot{q}''_s}{c_p} \frac{\pi R}{(\psi_c - \psi_s)}$$

$\therefore$ From above, $T_{s,E} - T_{s,I} = \frac{\dot{q}''_s}{c_p} \frac{\pi R}{(\psi_c - \psi_s)}$

For fully - developed conditions:

$$\frac{T_{s,I} - T_{c,I}}{T_{s,I} - T_{B,I}} = \frac{T_{s,E} - T_{c,E}}{T_{s,E} - T_{B,E}}$$

but $$T_{s,I} - T_{B,I} = T_{s,E} - T_{B,E}$$

$$\therefore \quad T_{s,I} - T_{c,I} = T_{s,E} - T_{c,E}$$

$$\therefore \quad T_{c,E} - T_{c,I} = T_{s,E} - T_{s,I} = \frac{\dot{q}''_s}{c_p} \frac{\pi R}{\psi_c - \psi_s}$$

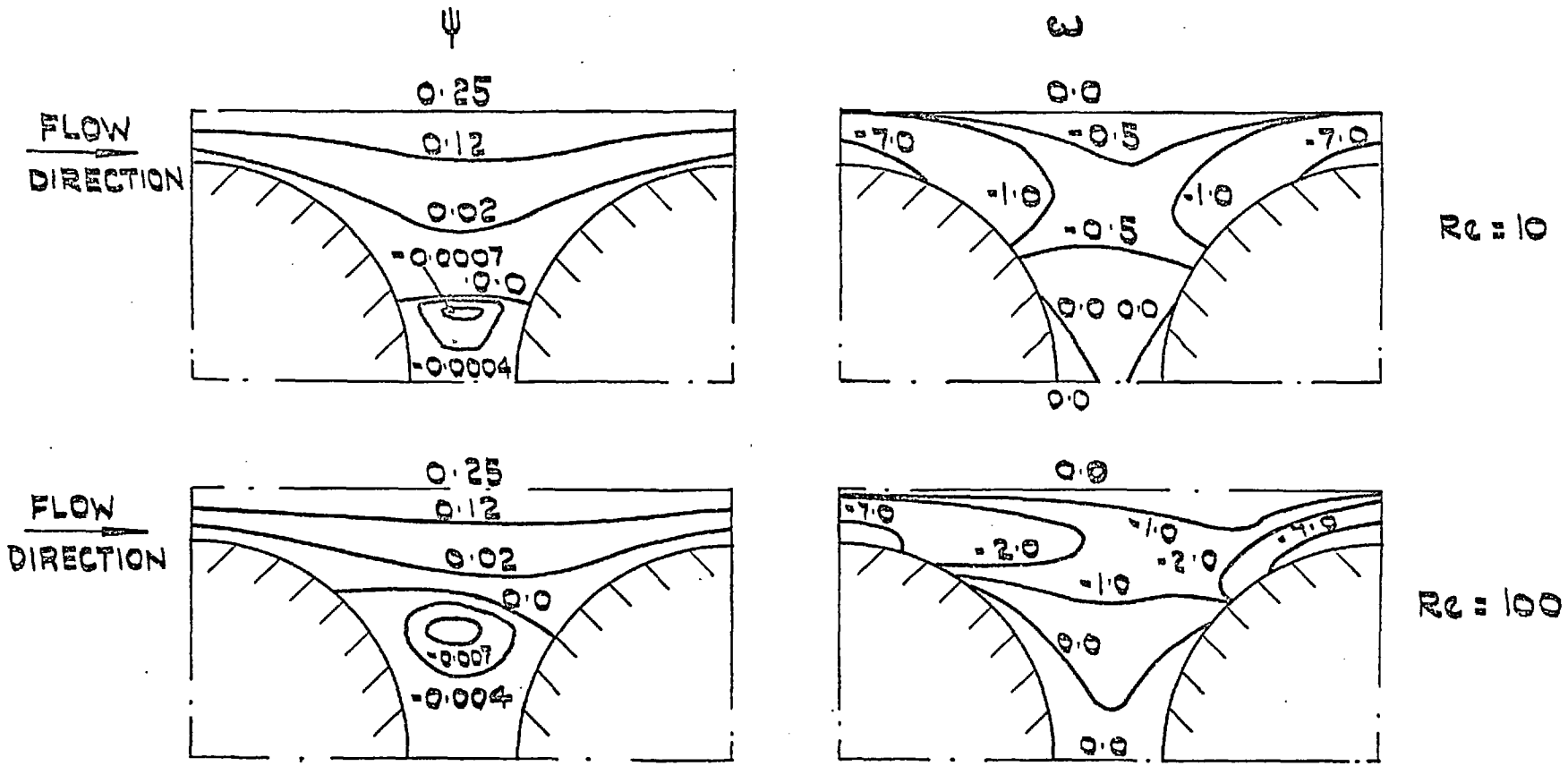


FIG. 5.3.2: THE INFLUENCE OF REYNOLDS NUMBER ON THE FLOW PATTERNS AND VORTICITY CONTOURS: $S_T = S_L = 1{\cdot}25$.

Note 2: Equation for T_s ; $\frac{\dot{q}''_s}{C_p}$ = constant

$$\dot{q}''_s = -k\left[\frac{dT}{dr}\right]_{r=R} = -C_p \frac{\mu}{P_r}\left[\frac{dT}{dr}\right]_{r=R}$$

Applying the appropriate finite - difference approximation assuming that T varies linearly near the wall then,

$$\frac{\dot{q}''_s}{C_p} = -\frac{\mu}{P_r}\left[\frac{T_{NP} - T_s}{r_{NP} - R}\right]$$

Rearranging gives :

$$T_s = \frac{\dot{q}''_s}{C_p}\left(\frac{r_{NP} - R}{\mu/P_r}\right) + T_{NP}$$

Note 3: Nusselt numbers; $\frac{\dot{q}''_s}{C_p}$ = constant and T_s = constant

For $\frac{\dot{q}''_s}{C_p}$ = constant:

$$Nu = \frac{\dot{q}''_s D_t}{\Delta T\, k} = \frac{(\dot{q}''_s/C_p) D_t}{(\mu/P_r)\,\Delta T}$$

For T_s = constant:

$$Nu = \frac{-k\left[\frac{dT}{dr}\right]_{r=R} D_t}{\Delta T\ \ k} = \left(\frac{T_s - T_{NP}}{\Delta T}\right)\left(\frac{D_t}{r_{NP} - R}\right)$$

where, ΔT = characteristic temperature difference

5.3.3 Hydrodynamic predictions

(a) Flow profiles

Typical stream function and vorticity contours are illustrated in Fig. 5.3.2 for $S_T = S_L = 1.25$. The streamlines for $Re = 10$ are almost symmetrical with a small recirculation eddy between the tubes. This flow is associated with a vorticity distribution which is almost symmetrical due to the predominent influence of the diffusive fluxes. The effect of increasing the Reynolds number by a factor of ten is illustrated by the contours for $Re = 100$. In this case the streamline pattern is no longer symmetrical, but the enlarged recirculation region sags towards the downstream tube. The corresponding asymmetry in the vorticity contours

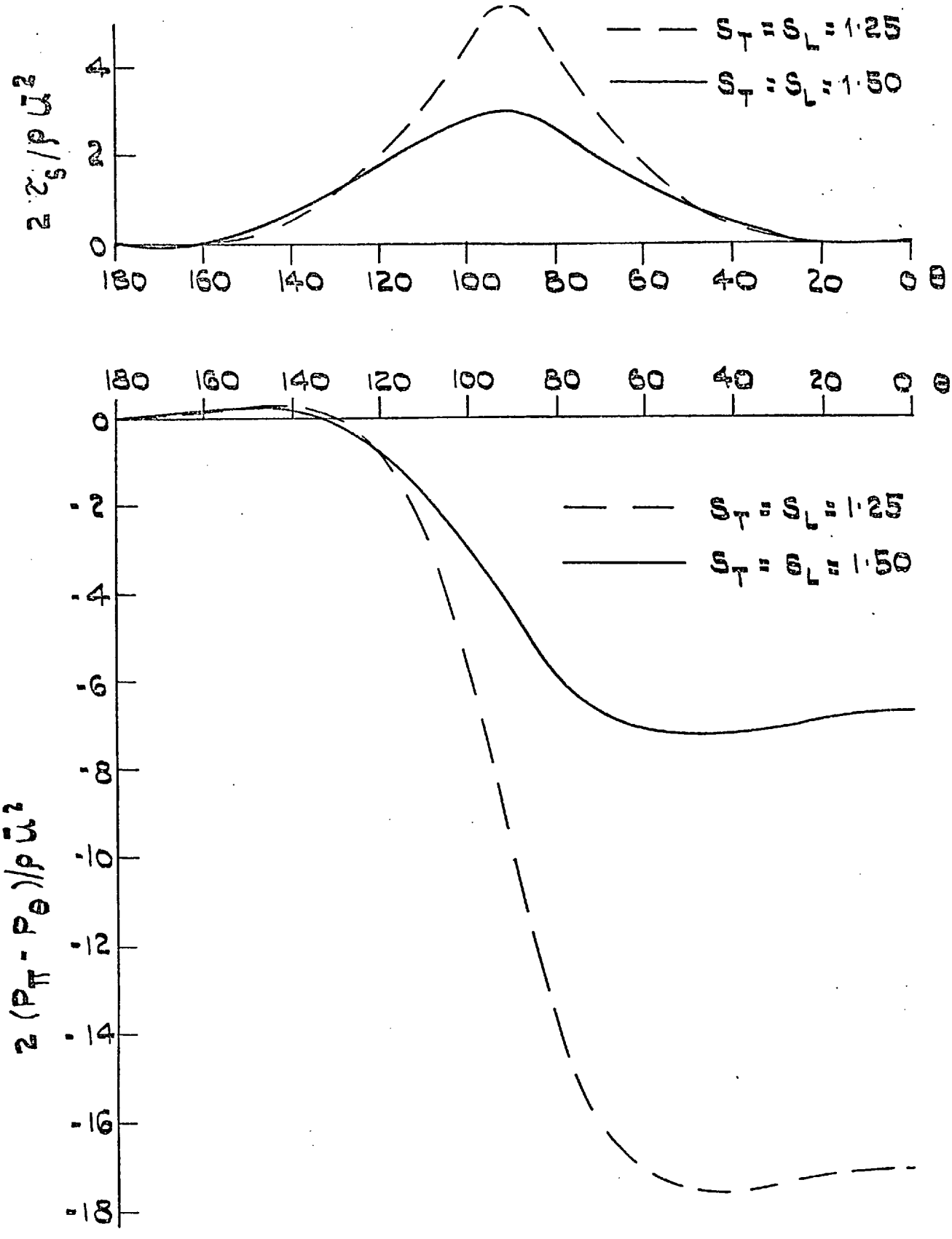


FIG. 5·3·3 : SHEAR STRESS AND PRESSURE DISTRIBUTIONS : Re = 10.

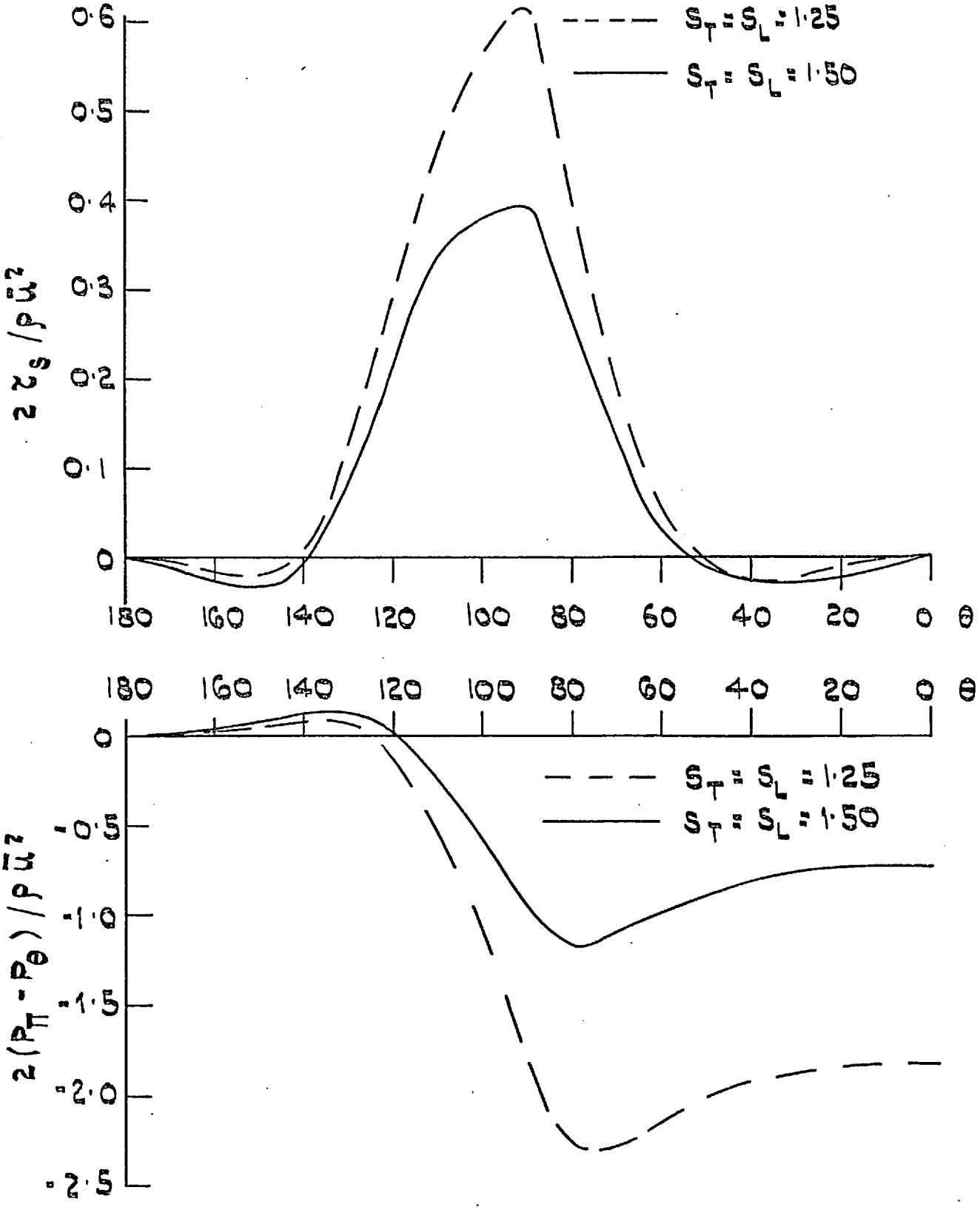


FIG. 5.3.4: SHEAR STRESS AND PRESSURE DISTRIBUTIONS; Re = 100.

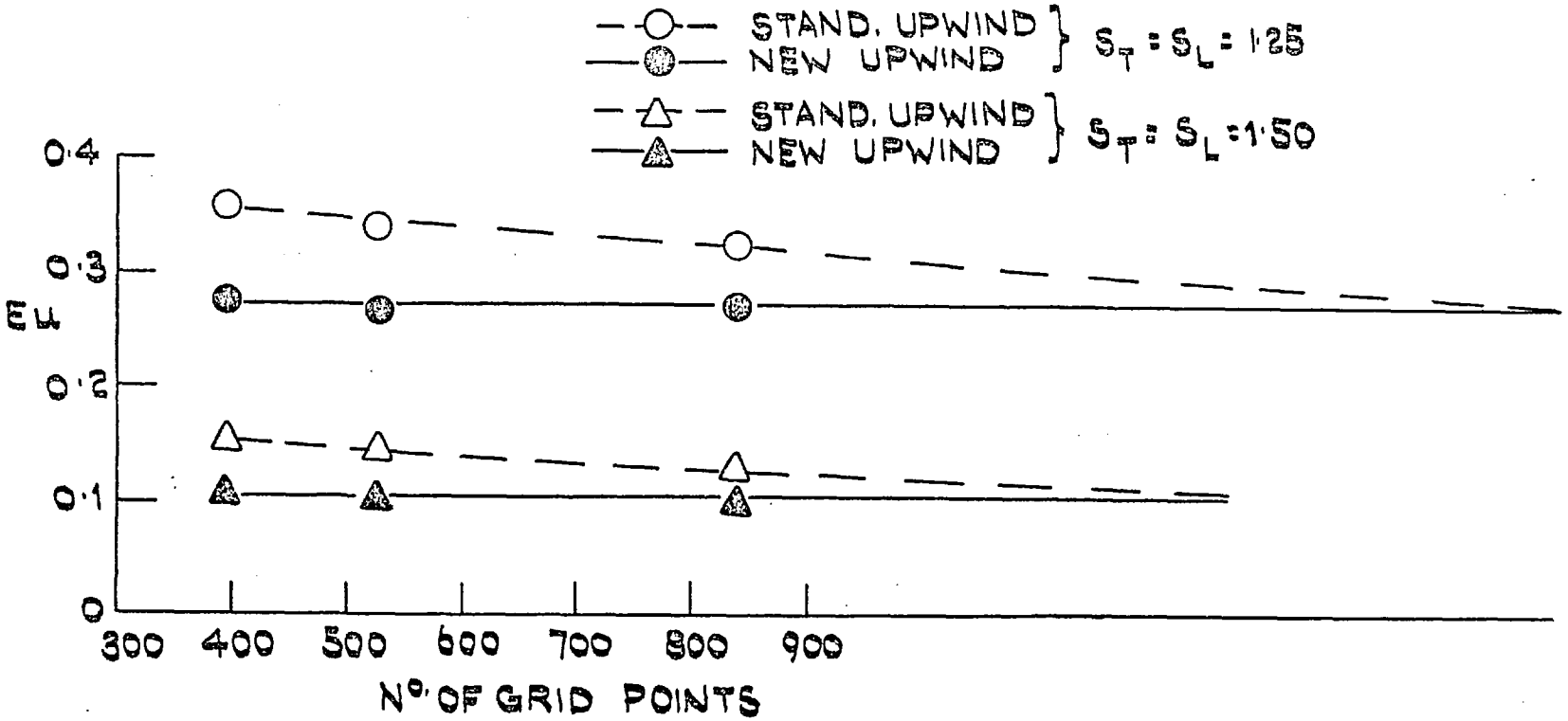


FIG. 5.3.5 : INFLUENCE OF GRID SIZE ON THE PREDICTED PRESSURE DROP USING THE STANDARD- AND NEW-UPWIND METHODS : Re = 400.

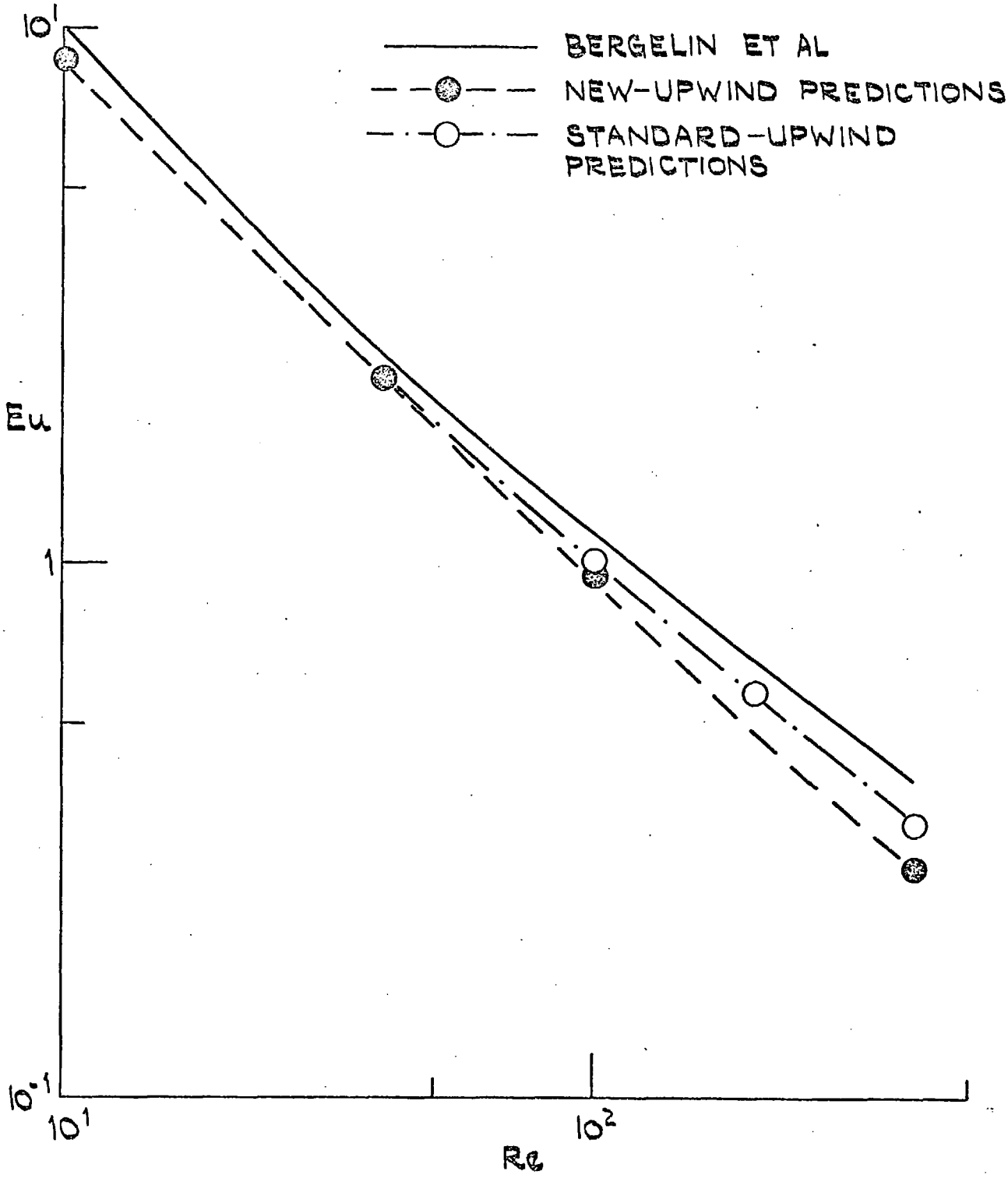


FIG. 5.3.6: PRESSURE DROP CHARACTERISTICS.
$S_T = S_L = 1.25$.

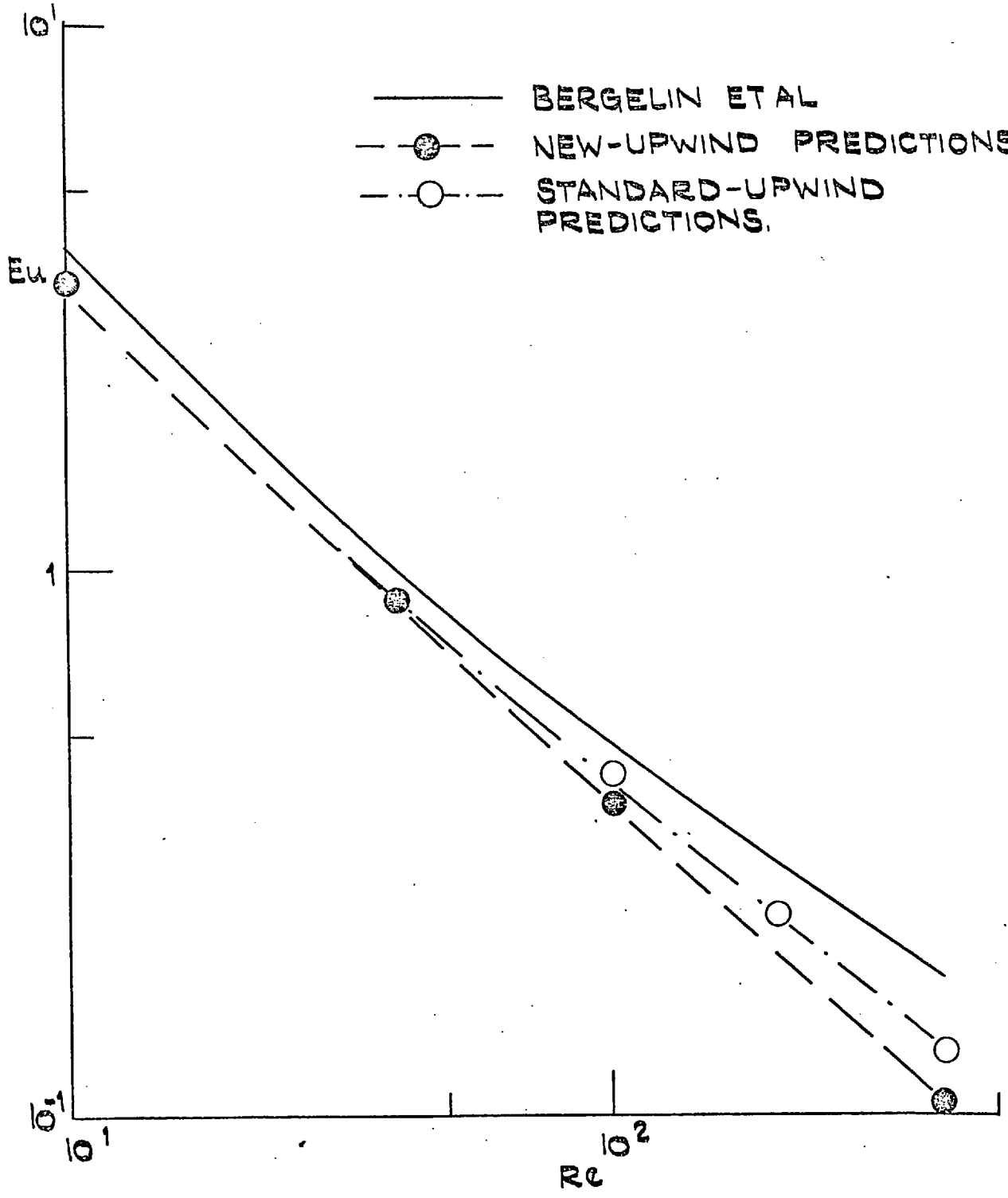


FIG. 5.3.7: PRESSURE DROP CHARACTERISTICS: $S_T = S_L = 1.50$

illustrates the predominent influence of the convective fluxes.

(b) Shear stress and pressure distributions

Figs. 5.3.3 and 5.3.4 illustrate local distributions of non - dimensional shear stress and pressure for Re = 10 and Re = 100 respectively. As one would expect the shear stress distributions for Re = 10, Fig. 5.3.3, are almost symmetrical with a small negative shear stress region corresponding to the recirculation eddy region. The results for Re = 100, Fig. 5.3.4, show a definite asymmetry in the shear stress profiles and a growth in the negative shear stress region. The pressure distributions for Re = 10 and 100, Figs. 5.3.3 and 5.3.4 respectively, are similar because in both cases most of the pressure drop occurs in the range $80 \leq \theta \leq 130$. However the pressure recovery for Re = 100 in the region $0 \leq \theta \leq 80$ is greater than for Re = 10. Another significant trend is that the maximum values of shear stress and pressure drop for $S_T = S_L$ = 1.25 are always greater than the maximum values for $S_T = S_L$ = 1.50.

(c) Pressure drop characteristics

Fig. 5.3.5 shows the effect of grid size on the prediction of overall Euler number at a Reynolds number of 400. For both $S_T = S_L$ = 1.25 and 1.50 the new - upwind predictions are almost independent of grid size, but the standard - upwind predictions tend to converge towards the mean new - upwind value with increasing grid size. These results provide further confirmation that new - upwind predictions are more accurate than corresponding standard - upwind predictions.

Figs. 5.3.6 and 5.3.7 compare the predictions of Euler number with the measurements of Bergelin et al for $S_T = S_L$ = 1.25 and 1.50 respectively. The results of Bergelin et al correspond to average measurements for 10 tube rows whereas the predictions are relevant only to fully - developed flow conditions. Therefore it is not surprising that there is a systematic discrepancy between the measurements and predictions. The fact that the

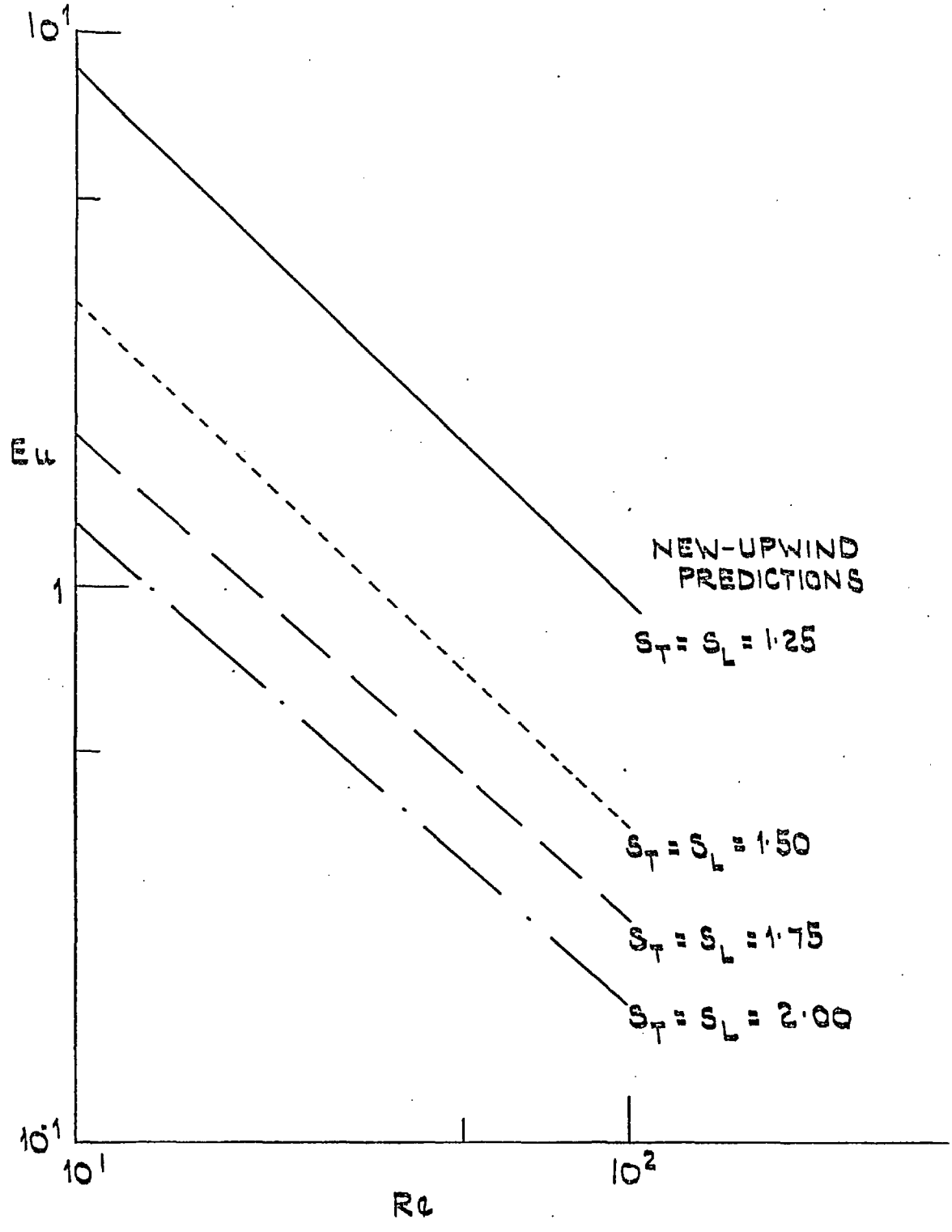


FIG. 5.3.8: PRESSURE DROP PREDICTIONS: $S_T = S_L = 1.25, 1.50, 1.75, 2.00$.

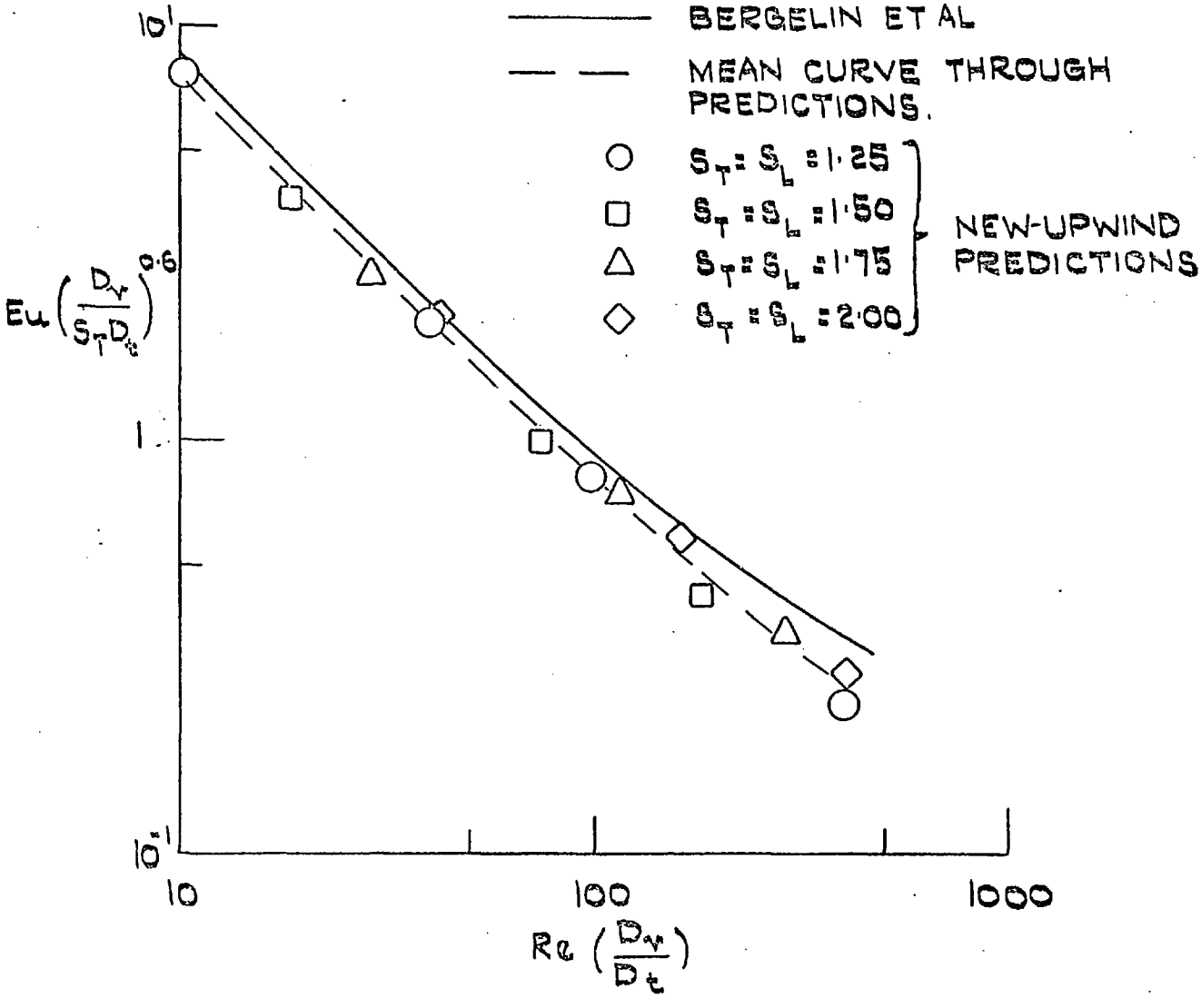


FIG. 5.3.9: PRESSURE DROP CORRELATIONS.

discrepancy is small and almost constant for $Re < 100$ indicates that the flow develops rapidly after the first tube. However for $Re > 100$ the descrepancy increases markedly and this is due to the onset of transition between the fully laminar and fully turbulent flow regimes. The heat transfer results of Bergelin et al (1949), (1950) provide further evidence that the onset of the transition region occurs in the range $40 \leq Re \leq 100$ for both banks.

For the sake of comparison, the predictions for both the new – and standard – upwind methods are shown in Figs. 5.3.6 and 5.3.7. Reasonable agreement between the two methods is obtained for $Re < 100$, but due to the effect of false diffusion the discrepency between the two sets increases for $Re > 100$. Now the results of Fig. 5.3.5 confirm previous conclusions that the new – upwind predictions are superior to the standard – upwind. Therefore in later figures comparison is made only between the measurements and the new – upwind predictions.

Fig. 5.3.8 compares the predicted Euler number characteristics for $S_T = S_L = 1.25$ and 1.50 with further predictions for $S_T = S_L = 1.75$ and 2.00. An attempt to correlate these four sets of predictions is illustrated in Fig. 5.3.9. The latter shows the effect of using a correlation, similar to that suggested by Bergelin et al (1950), that is

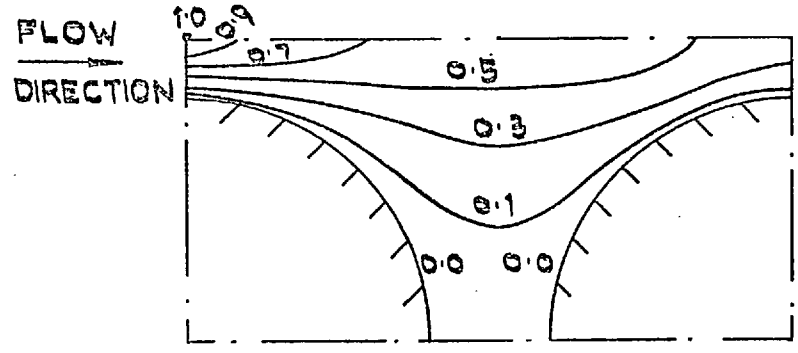
$$Eu \left(\frac{D_v}{S_T D_t}\right)^{0.6} \quad \text{against} \quad Re\left(\frac{D_v}{D_t}\right) \quad \text{where,}$$

$$D_v = \frac{4 \times \text{free volume}}{\text{exposed area of tubes}}$$

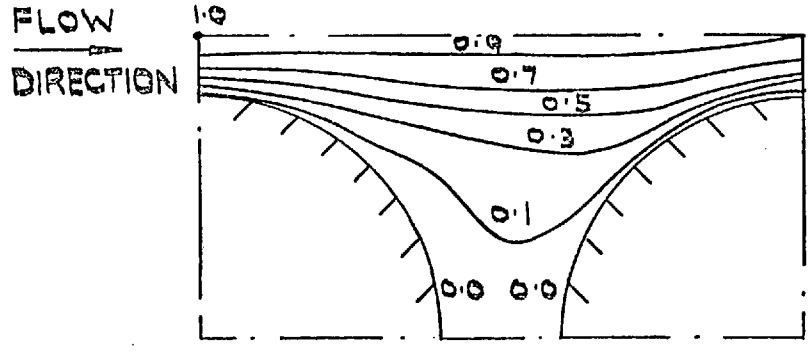
$$\therefore \quad D_v = \frac{2 D_t (2 S_T S_L - \pi/2)}{\pi}$$

and $S_T = S_L$.

The full line represents the mean correlation produced by the results of Bergelin et al for $S_T = S_L = 1.25$ and 1.50. The dashed line



Pr = 1·0



Pr = 10·0

FIG. 5.3.10: THE INFLUENCE OF PRANDTL NUMBER ON THE TEMPERATURE CONTOURS: $S_T = S_L = 1.25$, Re = 100.

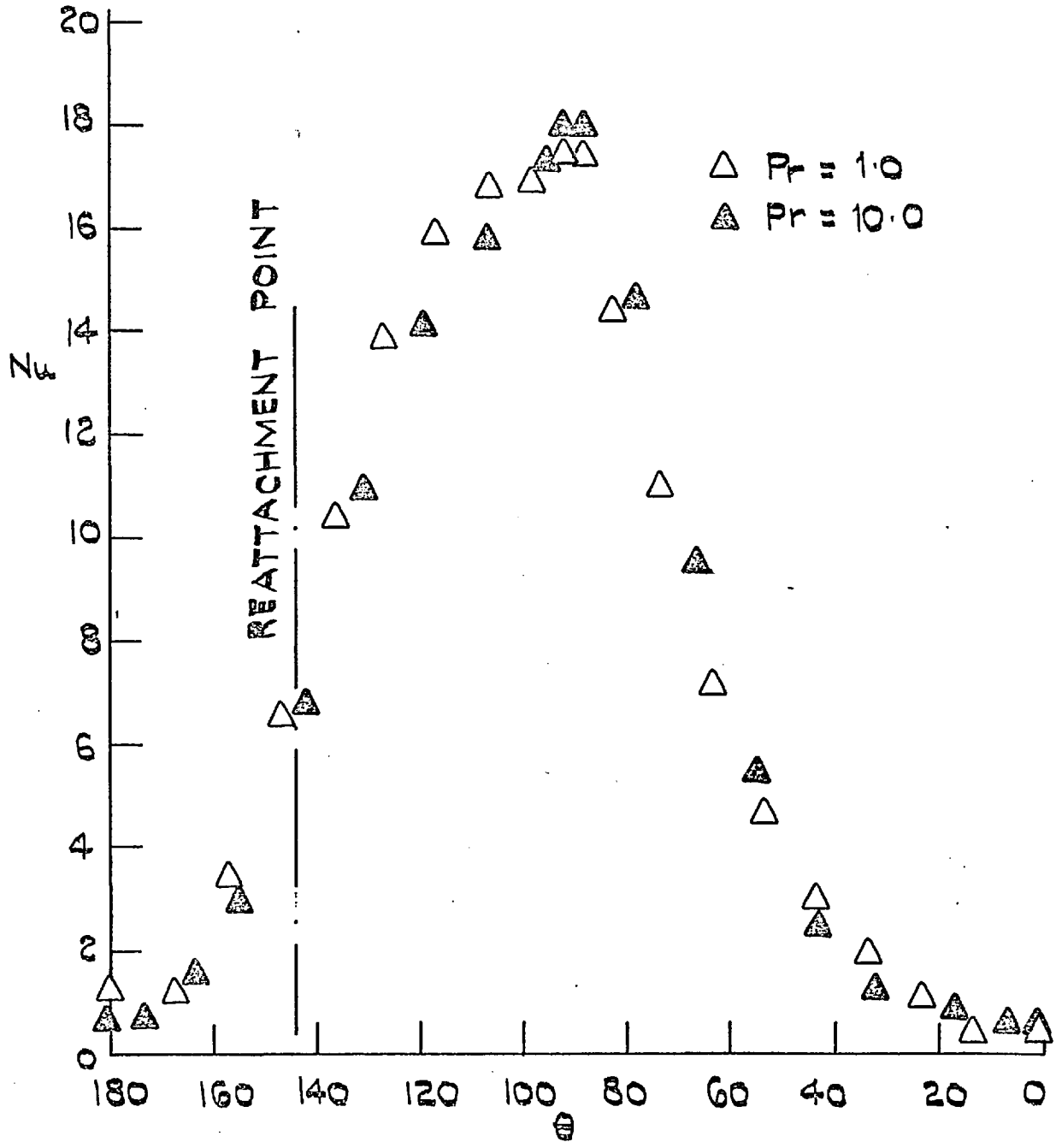


FIG. 5.3.11: LOCAL NUSSELT NUMBER DISTRIBUTION : $S_T = S_L = 1.25$, $Ra = 100$, T_S : CONSTANT.

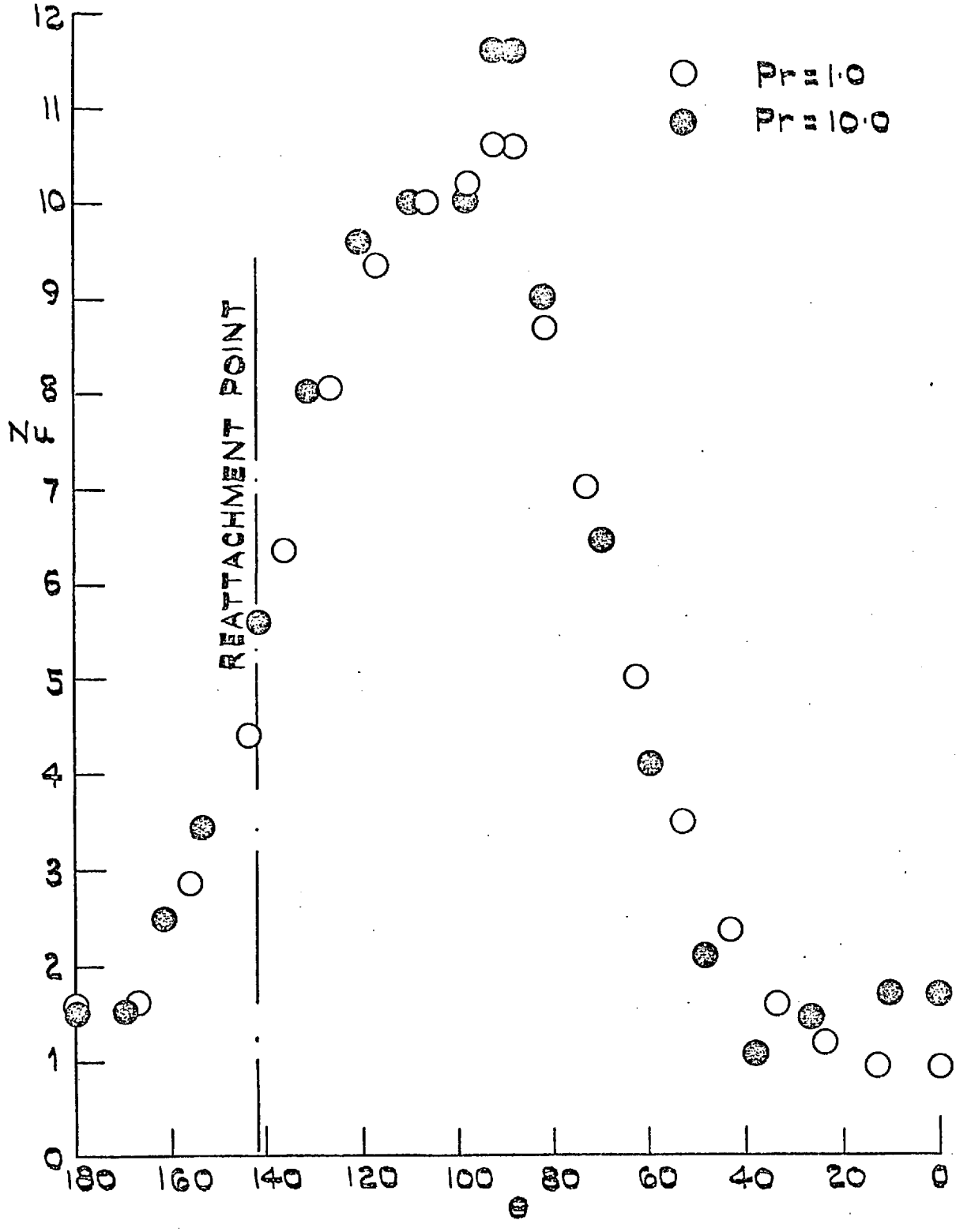


FIG. 5.3.12: LOCAL NUSSELT NUMBER DISTRIBUTION: $S_T = S_L = 1{\cdot}50$, $Re = 100$, T_S = CONSTANT.

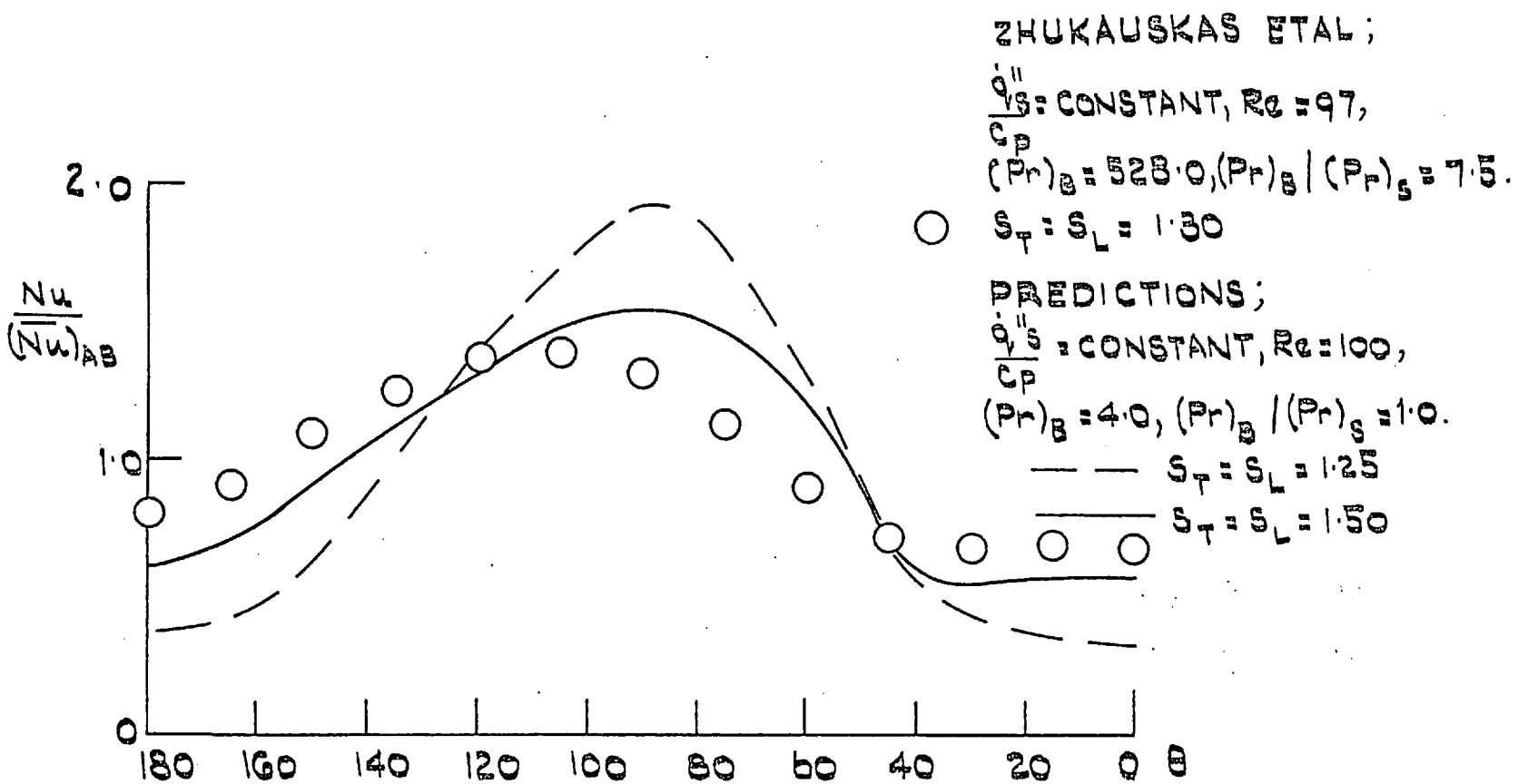


FIG. 5.3.13: COMPARISON OF PREDICTED AND EXPERIMENTAL LOCAL NUSSELT NUMBERS FOR LAMINAR FLOWS THROUGH IN-LINE TUBE BANKS.

indicates that the suggested correlation also gives good agreement between all the predictions for $Re\left(D_v/D_t\right) \leq 100$ and fair agreement for $Re\left(D_v/D_t\right) > 100$.

5.3.4 Heat transfer predictions

(a) Temperature contours

Fig. 5.3.10 illustrates the influence of Prandtl number on the temperature contours for $S_T = S_L = 1.25$ and $Re = 100$. The corresponding flow profile is given in Fig. 5.3.2. The contours are plotted in terms of a non - dimensional temperature T^*, which is given by:

$$T^* = \frac{T - T_s}{T_{c,I} - T_s}$$

The contours for $Pr = 1.0$ indicate a significant temperature drop along the flow centre - line but the corresponding drop for $Pr = 10.0$ is small. In the region between the tubes, the $T^* = 0.1$ contour is nearly symmetrical for $Pr = 1.0$, but is biased towards the downstream tube for $Pr = 10.0$. These characteristics indicate that in the first case, $Pr = 1.0$, the temperature contours are strongly influenced by the effects of heat conduction; and in the second case, $Pr = 10.0$, the influence of heat convection is dominant.

(b) Local Nusselt numbers

Plots of local Nusselt number are given in Figs. 5.3.11, 5.3.12 and 5.3.13. In the first two figures, 5.3.11 and 5.3.12, which correspond to the results for $S_T = S_L = 1.25$ and 1.50 respectively, the predictions for $Pr = 1.0$ are compared with those for $Pr = 10.0$ at $Re = 100$. In the third figure, 5.3.13, the measurements of Zhukauskas et al (1968) for $S_T = S_L = 1.30$ at $Re = 97$ are compared with the predictions for $S_T = S_L = 1.25$ and 1.50 at $Re = 100$. In all three cases, the local Nusselt numbers are calculated so that $\left[(Nu)_{B,I}\right]_{\theta=90} = \left[(Nu)_{B,E}\right]_{\theta=90}$.

This means that for $0 \leq \theta \leq 90$ (upstream tube), Nu is calculated on the basis of $T_{B,I}$, the bulk temperature at inlet; and for $90 \leq \theta \leq 180$ (downstream tube), Nu is calculated on the basis of $T_{B,E}$, the bulk temperature at outlet. Therefore the Nu equations for $0 \leq \theta \leq 90$ and $90 \leq \theta \leq 180$ are given by the equations for $(Nu)_{B,I}$ and $(Nu)_{B,E}$ respectively.

It is obvious from Figs. 5.3.11 and 5.3.12, that as near as doesn't matter the characteristics of Nu are independent of Pr for both $S_T = S_L = 1.25$ and 1.50. It is also clear that the characteristics are not symmetrical about $\theta = 90$. This is because of the strong influence of convection, which causes the temperature gradients on the downstream tube to be greater than those on the upstream tube. Proof of this is evident in Fig. 5.3.10 where, for $Pr = 10$, the temperature contours are bunched up towards the top half of the downstream tube. In this case Nu is dependent only on the local temperature gradients because $T_{B,I} \approx T_{B,E}$.

In turbulent recirculating flow situations, it is usual to suppose that maximum values of heat transfer coefficient occur at the reattachment points. However as illustrated in Figs. 5.3.11 and 5.3.12, this is not necessarily true for laminar recirculating flows. It should be recalled that in turbulent flows, the heat transfer coefficient at a reattachment point is largely controlled by local parameters of turbulence, such as kinetic energy of turbulence (k.e.t.). For instance in such a flow, the near - wall level of k.e.t. attains a maximum value in the region of the reattachment point and this maximum value is associated with a maximum heat transfer coefficient. However for constant - property laminar flows, the heat transfer coefficient is simply a function of the local temperature gradient, which is influenced only by local diffusive and convective fluxes of enthalpy. The two situations are obviously different, and therefore

maximum heat transfer coefficients do not necessarily occur at reattachment points in laminar recirculating flows. Indeed for the in - line tube bank situation, the maximum heat transfer coefficients or Nusselt numbers occur at the top of the tubes, where due to the influence of geometry the thermal boundary layer is thin and the temperature gradients are a maximum.

In Fig. 5.3.13, measurements of local Nusselt number for a medium - viscosity oil, $(Pr)_B = 528.0$, are compared with predictions for a constant property fluid, $(Pr)_B = 4.0$, on the basis of $Nu/(\overline{Nu})_{AB}$. The latter basis effectively removes the importance of the difference in Pr. For reasons of geometrical similarity one would expect close agreement between the predictions for $S_T = S_L = 1.25$ and the measurements for $S_T = S_L = 1.30$. However the two curves are completely different and this is probably due to the following factors:

(i) The predictions correspond to fully - developed flow conditions and the measurements to developing - flow conditions.

(ii) The predictions assume the existence of purely laminar flow, but the measurements probably correspond to flow in a state of transition.

The latter point is illustrated by the local Nusselt number curves in Fig. 5.3.13, where the maximum predicted value occurs at $\Theta = 90$ but the maximum experimental value is at $\Theta = 110$. Because of the probable influence of turbulence effects, the experimental maximum appears to be moving towards the reattachment point, $\Theta \approx 140$. The predictions for $S_T = S_L = 1.50$ are included in order to demonstrate the difference between the two sets of predictions, and thus show the influence of the geometry on the local values. These predictions also illustrate, perhaps fortuitously, close similarity with the measurements. Nevertheless the difference between the positions of predicted and measured maximum Nusselt numbers still remains.

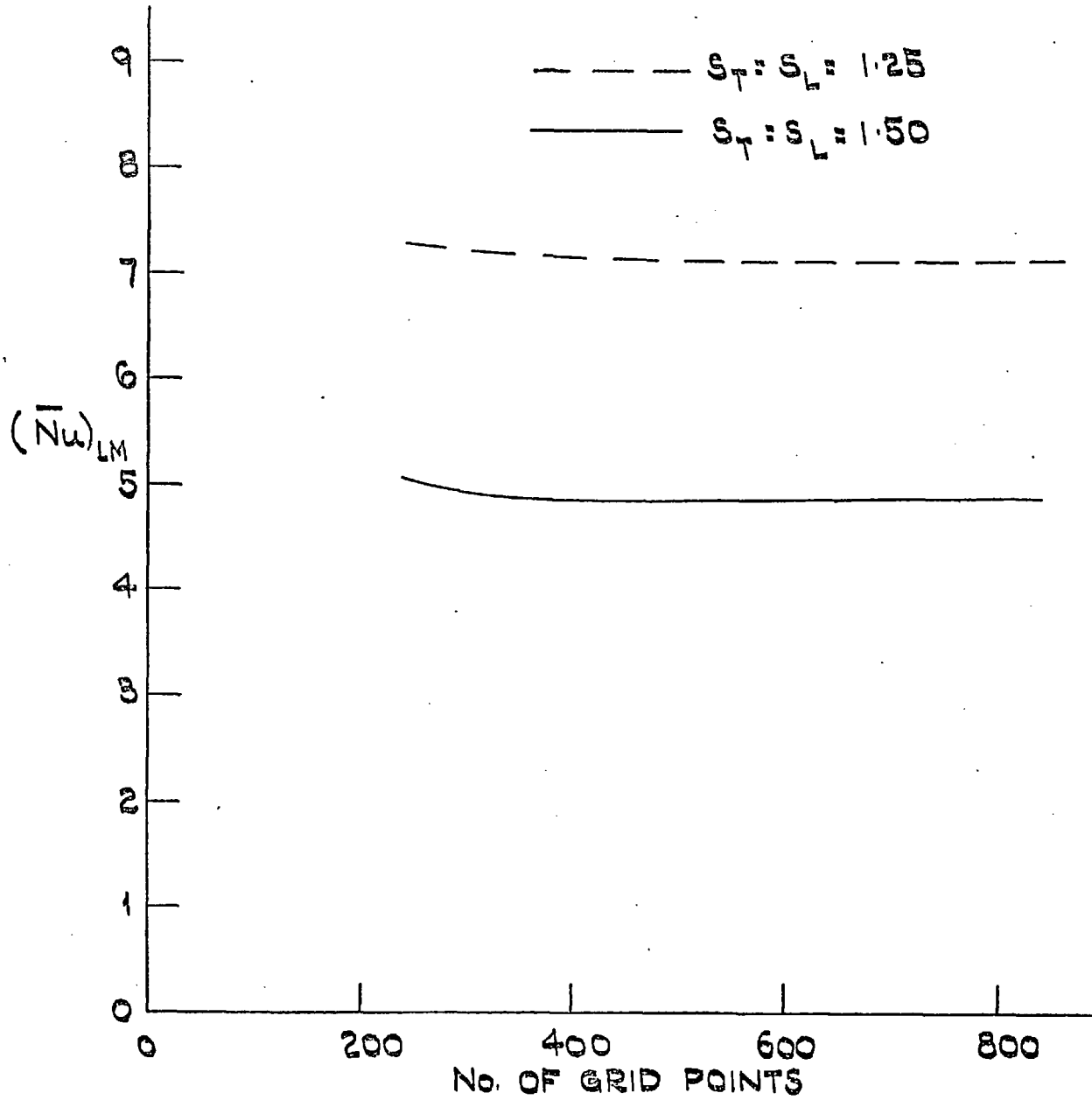


FIG. 5.3.14: EFFECT OF GRID SIZE ON MEAN NUSSELT NUMBER: Re = 100, Pr = 1.0, T_S = CONSTANT.

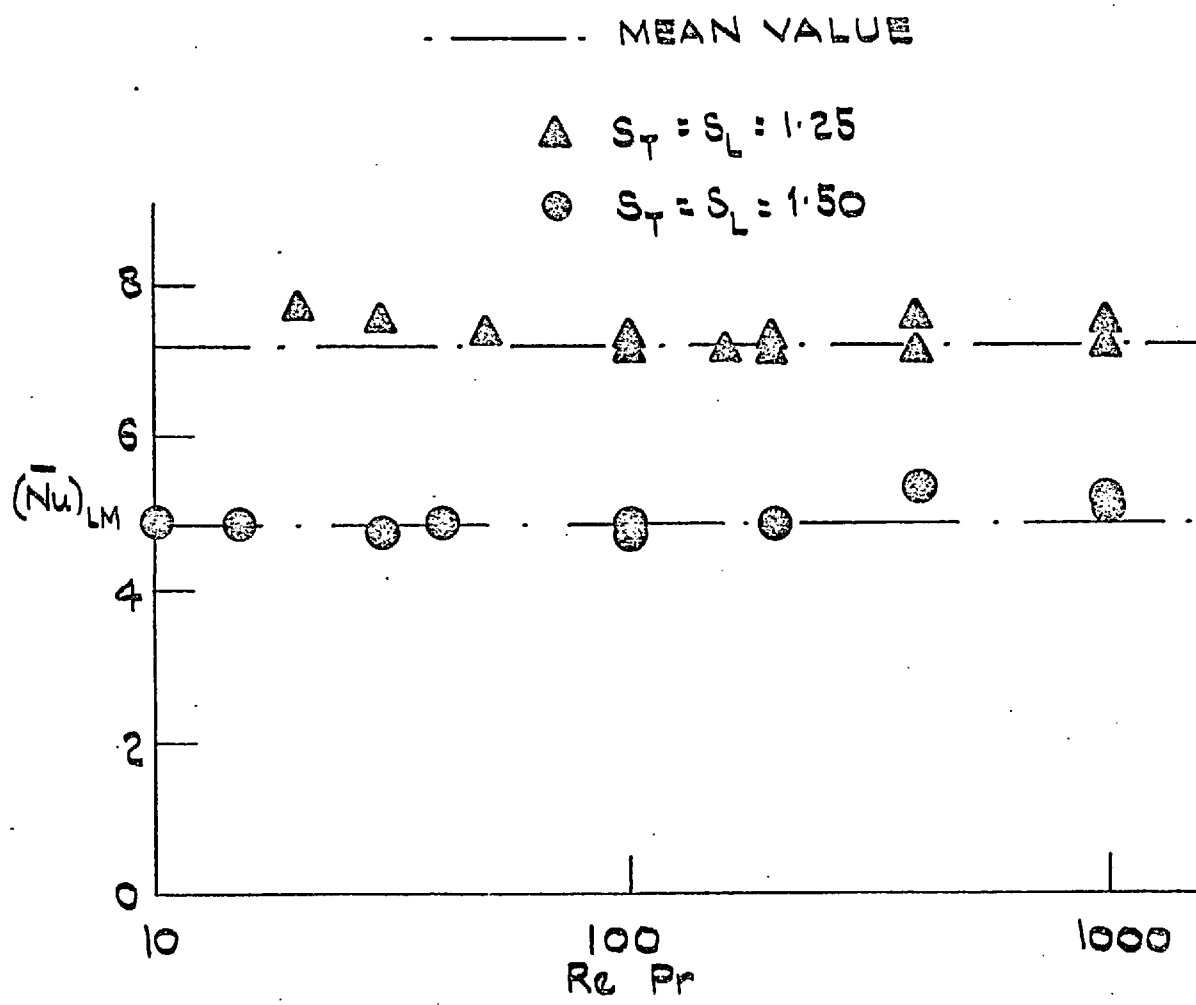


FIG. 5.3.15 : MEAN NUSSELT NUMBER BASED ON THE LOG-MEAN TEMPERATURE DIFFERENCE : T_S = CONSTANT.

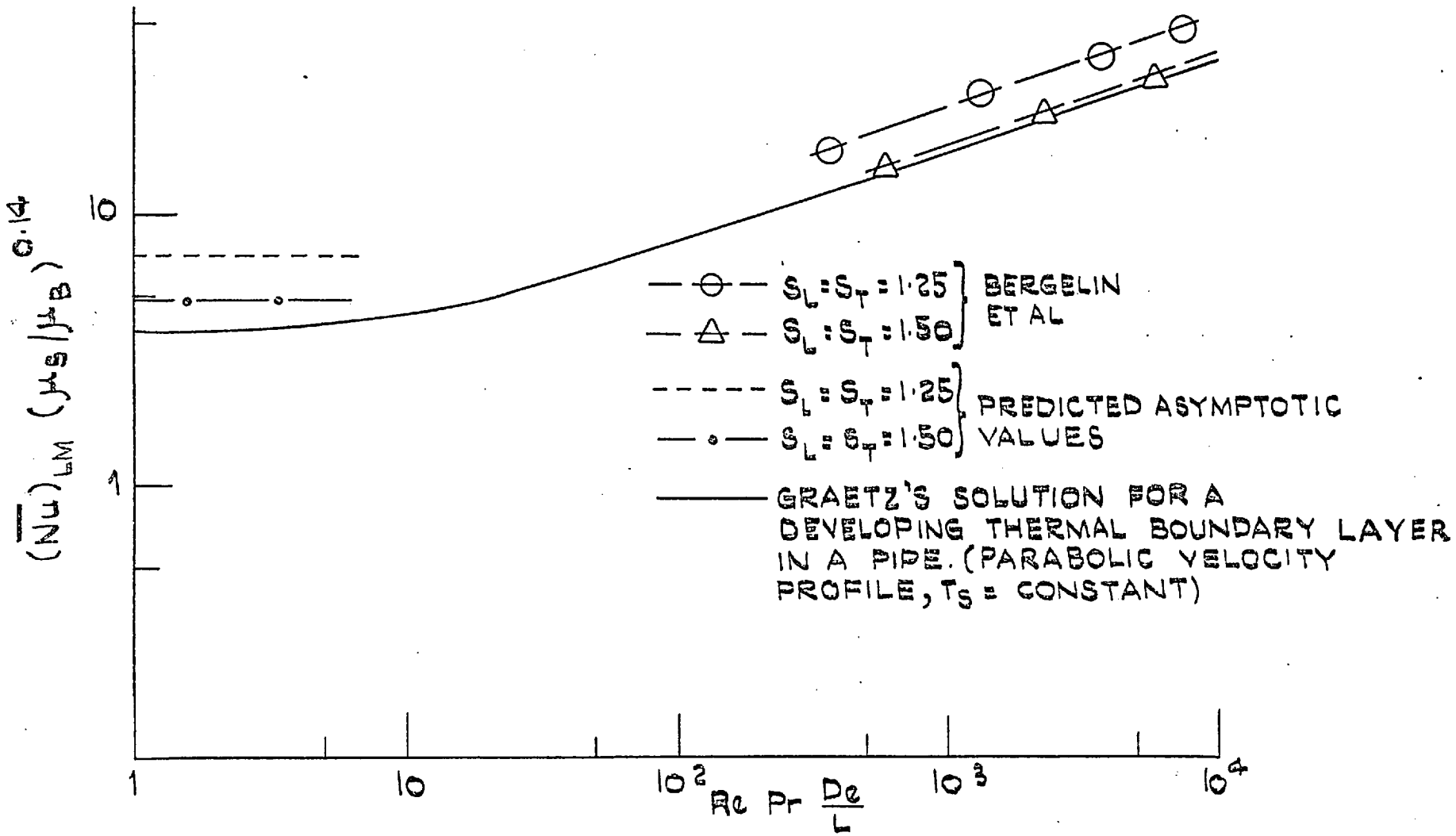


FIG. 5.3.16: COMPARISON OF PREDICTIONS AND DATA FOR IN-LINE TUBE BANKS WITH THE GRAETZ SOLUTION FOR DEVELOPING FLOW IN A PIPE.

(c) Mean Nusselt numbers

Fig. 5.3.14 shows that the predicted mean Nusselt numbers $(\overline{Nu})_{LM}$, based on the log - mean temperature difference, are almost independent of grid size for both $S_T = S_L = 1.25$ and 1.50. This is a clear indication of the accuracy of the predictions. In Fig. 5.3.15, $(\overline{Nu})_{LM}$ is plotted against the Peclet number $(= Re\,Pr)$, which embodies various combinations of Re and Pr. Perhaps contrary to expectation $(\overline{Nu})_{LM}$ is shown to be independent of Peclet number for both $S_T = S_L = 1.25$ and 1.50. Some explanation for this characteristic is illustrated in Fig. 5.3.16, where on a plot of $(\overline{Nu})_{LM}\left(\frac{\mu_s}{\mu_B}\right)^{0.14}$ against $Re\,Pr\,D_e/L$ the predicted values of $(\overline{Nu})_{LM}$ are compared with the measurements of Bergelin et al and the curve of Graetz's solution for a developing thermal boundary layer in a pipe (see Knudsen and Katz (1958)). The parameter D_e/L expresses the ratio between the equivalent diameter and the length of the heated section, which for a round pipe is given by the ratio of the diameter and the length. In the case of an in - line tube bank with $S_T = S_L$ and N tube rows of diameter D_t, D_e/L must be calculated using a somewhat arbitrary expression. The following expressions for D_e and L were chosen:

$$D_e = \frac{4 \text{ x Free volume}}{\text{Exposed area of tubes}}$$

$$= \frac{2D_t(2S_TS_L - \pi/2)}{\pi}$$

and, L = distance between leading edge of first tube and trailing edge of last tube.

$$= (N-1)S_L D_t + D_t$$

For the $S_T = S_L =$ 1.25 and 1.50 banks used by Bergelin et al, the values of D_e/L are as follows:

$S_T = S_L$	N	D_e/L
1.25	10	0.0808
1.50	10	0.1280

This arbitrary designation of D_e/L does not however alter the fact that the results of Bergelin et al obey the following relationship:

$$(\overline{Nu})_{LM} \left(\frac{\mu_s}{\mu_B}\right)^{0.14} \propto (Re\, Pr)^{1/3}$$

The slope of 1/3 is in exact agreement with the solution of Graetz for $Re\, Pr\, D_e/L > 30$ and D_e/L = constant. The Graetz solution indicates that the thermal boundary layer in the pipe is still developing for $Re\, Pr\, D_e/L > 10$. Similarly the results of Bergelin et al suggest that the thermal conditions in the tube banks are not fully developed. Even if fully - developed conditions were attained in the last few rows, the results show that the mean Nusselt numbers are still largely controlled by the values in the inlet region. The Graetz solution gives an asymptotic solution of $(\overline{Nu})_{LM} = 3.66$, and it is obvious that as $L/D_e \to \infty$ this value is independent of $Re\, Pr < \infty$. Under these conditions the thermal boundary layer in most of the pipe is fully - developed. Similarly the predictions for $S_T = S_L =$ 1.25 and 1.50, which correspond to fully - developed thermal conditions, must be independent of $Re\, Pr$ as shown in Fig. 5.3.15. It is interesting to note that for given values of $Re\, Pr\, D_e/L$ both the predicted and measured values of $(\overline{Nu})_{LM}$ for $S_T = S_L =$ 1.25 are greater than the corresponding values for $S_T = S_L =$ 1.50. On the basis of this observation, one could, with some confidence, perform extrapolations between the results of Bergelin et al and the corresponding predicted asymptotic values in order to give curves similar to that for the Graetz solution.

5.3.5 Discussion

The hydrodynamic predictions of flow, shear stress and pressure drop for in - line tube banks display expected trends. The accuracy of the predictions is demonstrated by the plots of Euler number against grid size at $Re = 400$. In the latter, the new - upwind predictions are independent of grid size. The slopes of the predicted pressure drop curves, plotted in the form of Eu against Re, are in good agreement with the slopes of the measured characteristics. However because the measured values of overall pressure drop include the developing - flow region and the predicted values correspond only to fully - developed flow, the predictions underestimate the measurements by about 10 - 20% for $Re < 100$. The growing discrepancy between the measurements and predictions in the range of $Re > 100$ is due to the onset of flow transition in the experimental situation. The pressure drop predictions for $S_T = S_L$ (in the range $S_T = S_L = 1.25$ to $S_T = S_L = 2.00$) and $Re \leq 100$ are given by a single characteristic curve when plotted in the form of $Eu \left(\frac{D_r}{S_T D_t}\right)^{0.6}$ against $Re \left(D_r/D_t\right)$.

The heat transfer predictions produce temperature contours and local Nusselt number curves which display valid trends. Plots of mean Nusselt number against various grid sizes demonstrate that the predictions are almost independent of grid size. Somewhat unexpectedly, the mean Nusselt number is found to be independent of Peclet number for a wide range of Reynolds and Prandtl numbers. This result is clarified by plotting the predictions and the measurements of Bergelin et al in the form of $(\overline{Nu})_{LM} (\mu_s/\mu_B)^{0.14}$ against $Re\, Pr\, D_e/L$ and by making a comparison with the trends of the Graetz solution. It is shown that the measurements correspond to temperature conditions which are not fully - developed, and that the predictions correspond to asymptotic fully - developed conditions where the predicted values of $(\overline{Nu})_{LM}$ are independent of $Re\, Pr$.

6. TURBULENT FLOW PREDICTIONS

So far the capabilities of the Chapter 3 solution procedure have been tested in two ways. The first involved the prediction of flows with analytical solutions, and the second involved the prediction of two laminar recirculating flows. In this chapter, the solution procedure is tested by applying it to the prediction of two turbulent flows, one without recirculation and the other with recirculation. The former is developing flow in a parallel channel and the latter is fully - developed flow through in - line tube banks.

6.1 Introduction

The two previous chapters were concerned with the predictions of laminar flows with constant properties. The latter were used as a basis for testing the numerical accuracy of the Chapter 3 solution procedure. The results of these tests showed that accurate predictions could be achieved by minimising the error due to false diffusion.

In this chapter, we illustrate the results of applying the solution procedure to the prediction of two turbulent flows. The accuracy of predicting such flows depends on two distinct aspects of the procedure. Firstly, there is the numerical accuracy, which has been investigated in previous chapters. Secondly, there is the accuracy of the turbulence models, which seek to model the augmented diffusion due to the turbulent motion. We have already some measure of the numerical accuracy of the Chapter 3 solution procedure. We now need to establish the accuracy of the chosen models of turbulence before we can with some confidence predict a wide range of turbulent recirculating flows.

The accuracy of the chosen models of turbulence are tested initially by their application to a relatively simple flow, that of developing flow in a parallel channel. This flow provides a fundamental test for any

turbulence model because no recirculation is present. Also because the flow is almost parallel to the grid lines in the x_1 direction the numerical error due to false diffusion is very small.

The turbulence models are then subjected to more demanding tests by their application to the prediction of fully - developed turbulent flow through in - line tube banks. The results of both the above sets of predictions are compared with a variety of data. The turbulence (or flow) models are described in 6.2; and the predictions of developing flow in a channel and fully - developed flow through in - line tube banks are illustrated in 6.3 and 6.4 respectively. Finally the results are summarised in section 6.5.

6.2 The flow models

6.2.1 The turbulence model

(a) Introduction

Turbulent motions in any fluid may be represented by the full time - dependent Navier - Stokes equations. However the numerical solution of these equations is neither practical nor desirable as far as the engineer is concerned. It is not practical because very fine grids and very large computer storage facilities would be required to study the detailed behaviour of even the simplest turbulent flows. It is not desirable because the engineer is not in general so much concerned with the detailed behaviour of a fluid at a point in space and time, as with the time - averaged behaviour. This means that the engineer wishes in general to measure or predict the time - averaged properties of a flow such as velocity, temperature and pressure. Thus in order to model the behaviour of turbulent flows in a practical way, we must start from the time - averaged Navier - Stokes equations for turbulent flow, Hinze (1959). The modelling then has to be directed at the turbulence stress (or Reynolds stress) components in

the momentum equations and the turbulence flux components in the energy and other conservation equations.

The modelling of turbulence quantities may be performed using a variety of methods. Three of these methods are listed below in decreasing order of complexity:

(i) Modelling the transport equations for the Reynolds stresses, e.g. Hanjalic and Launder (1971).

(ii) Using an algebraic scheme for modelling the Reynolds stresses, e.g. Launder (1971).

(iii) Using one of the many effective viscosity models.

It is method (iii) that is adopted here. This choice is governed by the reasons that method (iii) is the simplest of the above modelling techniques and that the required solution procedure is the same as that for laminar flows. The latter is due to the fact that the conservation equations for turbulent flow, using the effective viscosity technique, and those for laminar flow are of the same form, see Chapter 2.

However one of the major limitations of effective viscosity models is that the transport of Reynolds stresses cannot be taken into account. For example in a wall jet flow, the diffusive transport of shear stress results in the non - coincidence of positions of maximum velocity and zero shear stress. This situation cannot be modelled by the effective viscosity concept. Nevertheless despite this limitation, we can often expect (depending on the order of complexity of such a model) to predict the correct behaviour of a wide range of flows.

(b) The choice of effective viscosity model

Launder and Spalding (1972) have already provided a comprehensive review of effective viscosity models, so that such a review is not required here. In their conclusions, Launder and Spalding indicate that the most widely applicable effective viscosity models use two conservation equations

one for kinetic energy of turbulence, k , and the other for length scale, ℓ , or another appropriate parameter. The effective viscosity is then linked to k and ℓ via the Prandtl - Kolmogorov formula, where:

$$\mu_{eff} = C_{\mu} \rho k^{\frac{1}{2}} \ell \qquad (6.2.1)$$

It turns out that the length scale ℓ itself is not a particularly well - conditioned variable to employ as the dependent variable of the second equation. Instead workers have selected variables of the form $k^a \ell^b$ where a and b are constants. For example, Ng and Spalding (1969) and Rodi and Spalding (1970) have chosen the product $k\ell$, while Harlow and Nakayama (1968) and Jones and Launder (1970), (1972) have chosen an equation for the turbulence energy dissipation rate, ε , which for high turbulence Reynolds numbers may be interpreted as proportional to $k^{3/2}/\ell$. With the latter variable, equation (6.2.1) may be recast as follows:

$$\mu_{eff} = C_{\mu} \rho k^2/\varepsilon \qquad (6.2.2)$$

Two versions of the k-ε model have been used to predict a wide range of boundary layer flows, Jones and Launder (1970), (1972). The high Reynolds number version is suitable for the prediction of flows where the effective viscosity is much greater than the molecular viscosity; and the low Reynolds number version is applicable to situations near walls where the viscous sublayer exerts an appreciable influence on the flow. It is the high Reynolds number version, which is used here.

(c) Description of the model

The boundary layer or parabolic forms of the high Reynolds number version of the k and ε equations, Launder and Jones (1970), are as follows:

$$\rho u_1 \frac{\partial k}{\partial x_1} + \rho u_2 \frac{\partial k}{\partial x_2} = \frac{\partial}{\partial x_2}\left[\frac{\mu_{eff}}{\sigma_k}\frac{\partial k}{\partial x_2}\right] + \mu_{eff}\left(\frac{\partial u_1}{\partial x_2}\right)^2 - \rho\varepsilon \qquad (6.2.3)$$

$$\rho u_1 \frac{\partial \varepsilon}{\partial x_1} + \rho u_2 \frac{\partial \varepsilon}{\partial x_2} = \frac{\partial}{\partial x_2}\left[\frac{\mu_{eff}}{\sigma_\varepsilon}\frac{\partial \varepsilon}{\partial x_2}\right] + C_1\frac{\varepsilon}{k}\mu_{eff}\left(\frac{\partial u_1}{\partial x_2}\right)^2 - C_2\rho\frac{\varepsilon^2}{k} \qquad (6.2.4)$$

The elliptic forms of equations (6.2.3) and (6.2.4), with ρu_1 and ρu_2 replaced by derivatives of ψ, are as follows:

$$\frac{\partial}{\partial x_1}\left(k\frac{\partial \psi}{\partial x_2}\right) - \frac{\partial}{\partial x_2}\left(k\frac{\partial \psi}{\partial x_1}\right) = \frac{\partial}{\partial x_1}\left(\frac{\mu_{eff}}{\sigma_k}\frac{\partial k}{\partial x_1}\right) + \frac{\partial}{\partial x_2}\left(\frac{\mu_{eff}}{\sigma_k}\frac{\partial k}{\partial x_2}\right) + P_k - \rho\varepsilon \qquad (6.2.5)$$

$$\frac{\partial}{\partial x_1}\left(\varepsilon\frac{\partial \psi}{\partial x_2}\right) - \frac{\partial}{\partial x_2}\left(\varepsilon\frac{\partial \psi}{\partial x_1}\right) = \frac{\partial}{\partial x_1}\left(\frac{\mu_{eff}}{\sigma_\varepsilon}\frac{\partial \varepsilon}{\partial x_1}\right) + \frac{\partial}{\partial x_2}\left(\frac{\mu_{eff}}{\sigma_\varepsilon}\frac{\partial \varepsilon}{\partial x_2}\right) + C_1\frac{\varepsilon}{k}P_k - C_2\rho\frac{\varepsilon^2}{k} \qquad (6.2.6)$$

where,

$$P_k = \mu_{eff}\left\{2\left[\left(\frac{\partial u_1}{\partial x_1}\right)^2 + \left(\frac{\partial u_2}{\partial x_2}\right)^2\right] + \left[\frac{\partial u_1}{\partial x_2} + \frac{\partial u_2}{\partial x_1}\right]^2\right\} \qquad (6.2.7)$$

Equations (6.2.5) and (6.2.6) are in the form of the general equation (2.4.1) for a variable ϕ. The appropriate forms of a_ϕ b_ϕ, c_ϕ and d_ϕ for $\phi = k$ and $\phi = \varepsilon$ are given in Table 6.2.1.

ϕ	a_ϕ	b_ϕ	c_ϕ	d_ϕ
k	1	$\frac{\mu_{eff}}{\sigma_k}$	1	$-P_k + \rho\varepsilon$
ε	1	$\frac{\mu_{eff}}{\sigma_\varepsilon}$	1	$-C_1\frac{\varepsilon}{k}P_k + C_2\rho\frac{\varepsilon^2}{k}$

Table 6.2.1

At high Reynolds numbers, the quantities C_μ, C_1, C_2, σ_k and σ_ε which appear in equations (6.2.2), (6.2.3), (6.2.4), (6.2.5) and (6.2.6) are supposed to take on the constant values given in Table 6.2.2.

C_μ	C_1	C_2	σ_k	σ_ε
0.09	1.45	2.0	1.0	1.3

Table 6.2.2

6.2.2 The wall functions

(a) The purpose

Very often the dependent variables in a turbulent flow change very steeply in the region next to a wall. To obtain reasonable accuracy using the Chapter 3 solution procedure in these circumstances, it is necessary to employ a very fine grid in the near - wall region. This apparent necessity can be avoided by the use of what are called 'wall functions'. The latter involve a number of assumptions concerning the nature of the flow in the near - wall region. Of these assumptions, the main one is that the flow in any near - wall region is one - dimensional.

Following the latter, other assumptions enable us to determine boundary conditions for all the main variables at the near - wall grid nodes.

In this sub - section, the wall functions are described in three stages. The first in (b) is concerned with the Simple Power Law (S.P.L.) wall functions, which are derived on the basis of a constant shear - stress near - wall region. The second in (c) outlines the Modified Power Law (M.P.L.) wall functions, which are a modified form of the S.P.L. wall functions and are designed to deal with stagnation point regions. However the equations in both (b) and (c), which were originally suggested by Spalding (1971), are given in terms of Cartesian co-ordinates only. Therefore a third stage, given in (d), is necessary to describe the special equations appropriate to the F.N.P. cell arrangement, which is illustrated in section 3.3.2.

(b) The Simple Power Law (S.P.L.) wall functions

For the constant shear - stress layer we have the following relationships:

$$\frac{\mu_{eff}}{\mu} = f\left(\frac{y\sqrt{\tau\rho}}{\mu}\right) = f(y_+)$$

$$u = \tau \int_0^y \mu_{eff}^{-1}\, dy$$

where, u = velocity parallel to the wall

y = normal distance from wall

$$u = (\tau/\rho)^{1/2} \int_0^{y_+} \mu_+^{-1}\, dy_+$$

$$u_+ = \int_0^{y_+} \mu_+^{-1}\, dy_+ \qquad (6.2.8)$$

Integrating (6.2.8) gives:

$$u_+ = \frac{1}{K} \log_e (E\, y_+) \qquad (6.2.9)$$

for any point in the fully - turbulent section of a constant shear - stress layer.

Equation (6.2.9) can be approximated by the power law:

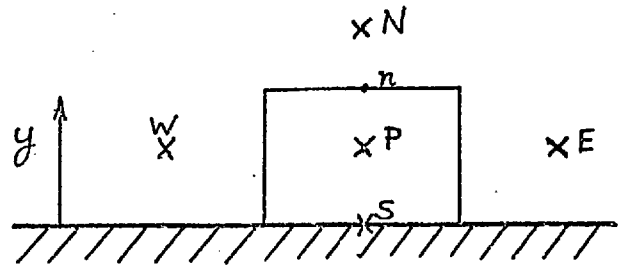


Fig. 6.2.1

$$u_+ = a\, y_+^b \qquad (6.2.10)$$

When using the ω, ψ set of dependent variables, we require a relationship between u and $\psi - \psi_s$ to close the equation set at the near-wall node. Thus from $u = \frac{1}{\rho}\frac{d\psi}{dy}$ and $u_+ = a\, y_+^b$, u is given by:

$$u = \frac{(1+b)}{\rho y}(\psi - \psi_s)$$

or referring to Fig. 6.2.1,

$$u_P = \frac{(1+b)}{\rho y_P}(\psi_P - \psi_s) \qquad (6.2.11)$$

We note that it is much simpler to derive $u = u(\psi)$ by using $u_+ = a\, y_+^b$ than by using $u_+ = \frac{1}{\kappa}\log_e(E\, y_+)$.

We also need to obtain ω_P and $\bar{\omega}_P$, the point and space-average vorticities respectively. These are derived from the power law, $u_+ = a\, y_+^b$, as follows:

$$\omega_P = -\left.\frac{du}{dy}\right|_{y_P} = -b\frac{u_P}{y_P} \qquad (6.2.12)$$

$$\bar{\omega}_P = \frac{1}{y_n}\int_0^{y_n}\left(\frac{du}{dy}\right)dy = -\frac{u_n}{y_n} = \bar{\omega}_P(u_P)$$

In a constant shear - stress region, the production of k = dissipation of k. Therefore the equation for k at the near - wall node is given by:

$$k_P = \frac{\tau}{\rho}\Big/\sqrt{C\mu} = \frac{u_\tau^2}{\sqrt{C\mu}} \qquad (6.2.13)$$

where, u_τ^2 is obtained by a rearrangement of $u_+ = a\, y_+^b$ as follows:

$$u_\tau^2 = \left[\frac{u_P}{a\,(y_P/\nu)^b}\right]^{2/1+b} \qquad (6.2.14)$$

The dissipation ε_P is given by:

$$\varepsilon_P = u_\tau^2 \left|\frac{du}{dy}\right|_P \qquad (6.2.15)$$

Using $u_+ = \frac{1}{K}\log_e(Ey_+)$, equation (6.2.15) becomes:

$$\varepsilon_P = \frac{u_\tau^3}{K\, y_P} \qquad (6.2.16)$$

The flux of ϕ at the wall can be expressed as:

$$\dot{\phi}'' = \frac{\mu_{eff}}{\sigma_{eff}}\frac{d\phi}{dy} = \frac{\mu_+}{\sigma_{eff}}\frac{d\phi}{dy_+}(\tau\rho)^{1/2} \qquad (6.2.17)$$

where, $\mu_+ = \frac{\mu_{eff}}{\mu}$, $\quad y_+ = \frac{y(\tau\rho)^{1/2}}{\mu}$

$$\therefore\ d\phi\,(\tau\rho)^{1/2} = \dot{\phi}''\frac{\sigma_{eff}}{\mu_+}\,dy_+ \qquad (6.2.18)$$

Following the practice of Spalding and Jayatillaka (1965), we may integrate equation (6.2.18) as follows:

$$\left(\frac{\phi - \phi_s}{\dot{\phi}''}\right) \rho u_\tau = \int_0^{y_+} \frac{\sigma_{eff}}{\mu_+} \, dy_+$$

$$= \sigma_0 \left[\int_0^{y_+} \frac{1}{\mu_+} \, dy_+ + \int_0^{y_+} \frac{(\sigma_{eff} - \sigma_0)}{\sigma_0} \frac{dy_+}{\mu_+} \right]$$

$$= \sigma_0 \left[\frac{u}{u_\tau} + P\{\sigma\} \right]$$

where, $\sigma_0 = 0.9$

$$P = 9.24 \left[\left(\frac{\sigma}{\sigma_0} \right)^{0.75} - 1 \right] \left[1 + 0.28 \exp\left(-0.07 \frac{\sigma}{\sigma_0} \right) \right]$$

$$\therefore \quad \dot{\phi}'' = \frac{\rho u_\tau}{\sigma_0 \left[u/u_\tau + P\{\sigma\} \right]} (\phi - \phi_s) \qquad (6.2.19)$$

For example, the expression for heat flux at the wall is:

$$\frac{\dot{q}''_s}{c_p} = \frac{\rho u_\tau}{\sigma_0 \left[\frac{u_P}{u_\tau} + P \right]} (T_P - T_s)$$

or,

$$\frac{\dot{q}''_s}{c_p} = \frac{\rho u_\tau}{\sigma_0 \left[\frac{1}{\kappa} \log_e \{ E(y_+)_P \} + P \right]} (T_P - T_s) \qquad (6.2.20)$$

Equation (6.2.20) provides the boundary condition for calculating the temperature at the near - wall node.

(c) The Modified Power Law (M.P.L.)

The M.P.L. wall functions are obtained as follows:

(i) The first modification to the S.P.L. wall functions involves a modification to the log - law expression and thus to the equation for shear stress. The proposal is that in the argument of

$\mu_+ = \mu_{eff}/\mu = \mu_+\left(\frac{y\sqrt{\tau\rho}}{\mu}\right)$, $(\tau\rho)^{1/2}$ should be replaced by $\rho\, C_\mu^{1/4} k_p^{1/2}$.

$$\therefore \quad y_+ = \frac{y\,\rho\, C_\mu^{1/4} k_p^{1/2}}{\mu}$$

Now in a constant shear - stress region,

$$u = \tau \int_0^y \mu_{eff}^{-1}\, dy$$

$$\therefore \quad u = \frac{\tau}{\rho\, C_\mu^{1/4} k_p^{1/2}} \int_0^{y_+} \frac{dy_+}{\mu_+}$$

and $$u = \frac{\tau}{\rho\, C_\mu^{1/4} k_p^{1/2}} \; \frac{1}{K} \; \log_e (E\, y_+)$$

At node P, $$u_p = \frac{\tau_p}{\rho\, C_\mu^{1/4} k_p^{1/2}} \; \frac{1}{K} \; \log_e\left(\frac{E\,\rho\, y_p\, C_\mu^{1/4} k_p^{1/2}}{\mu}\right)$$

Thus τ, which is given the symbol τ_p, may be written as:

$$\tau_p = \frac{\rho\, K\, C_\mu^{1/4} k_p^{1/2}\, u_p}{\log_e\left(\frac{E\,\rho\, y_p\, C_\mu^{1/4} k_p^{1/2}}{\mu}\right)} \qquad (6.2.21)$$

(ii) The velocity u_p is determined via the equation (6.2.11).

(iii) The point and space - average vorticities are determined using equations (6.2.12).

(iv) By using the above proposal, that $(\tau\rho)^{1/2}$ should be replaced by $\rho C_\mu^{1/4} k_p^{1/2}$, equation (6.2.16) for dissipation and equation (6.2.20) for heat flux are modified as follows:

$$\varepsilon_p = \frac{(\sqrt{C_\mu}\, k_p)^{3/2}}{K\, y_p} \qquad (6.2.22)$$

$$\frac{\dot{q}''_s}{c_p} = \frac{\rho\, C_\mu^{1/4} k_p^{1/2}}{\sigma_o \left[\frac{1}{K} \log_e\left(\frac{E\, y_p\, C_\mu^{1/4} k_p^{1/2}}{\nu}\right) + P\right]} (T_p - T_s) \qquad (6.2.23)$$

(v) Instead of using equation (6.2.13) to obtain the value of k_p, the latter is calculated from the complete conservation equation. The expressions for the generation and dissipation terms and the wall boundary condition are outlined below.

From equation (6.2.7):

The generation term

$$= \left[\mu_{eff}\left\{\left(\frac{\partial u_1}{\partial x_2} + \frac{\partial u_2}{\partial x_1}\right)^2 + 2\left[\left(\frac{\partial u_1}{\partial x_1}\right)^2 + \left(\frac{\partial u_2}{\partial x_2}\right)^2\right]\right\}\right]_p \qquad (6.2.24)$$

where, in this case, x_1 and x_2 are the co - ordinates parallel to and normal to the wall respectively.

In equation (6.2.24), all the velocity gradients and μ_{eff} are calculated at the near - wall node P. The gradients $(\partial u_1/\partial x_1)_p$ and $(\partial u_2/\partial x_1)_p$ are obtained by using the standard 3-point formula. The gradient $(\partial u_2/\partial x_2)_p$ is obtained by assuming that u_2 varies linearly between the wall and the near - wall point. The fourth gradient $(\partial u_1/\partial x_2)_p$ is derived from the log law. Thus, from the S.P.L.

wall functions,

$$\frac{\partial u_1}{\partial x_2} = \frac{u_\tau}{\kappa y}$$

then,

$$\left(\frac{\partial u_1}{\partial x_2}\right)_P = \frac{\sqrt{\tau_P/\rho}}{\kappa y_P} \qquad (6.2.25)$$

From equation (6.2.22):

The dissipation term = $$\frac{\rho (\sqrt{c_\mu}\, k_P)^{3/2}}{\kappa y_P} \qquad (6.2.26)$$

The wall boundary condition is given by:

$$\left[\frac{\mu_{eff}}{\sigma_k} \frac{dk}{dx_2} \right]_S = 0 \qquad (6.2.27)$$

(d) Special equations for the F.N.P. grid arrangement

With the exception of the equation for the near – wall cell space – average vorticity, $\overline{\omega}_P$, the wall functions for the F.N.P. grid arrangement are the same as those given in (c). Now because of the link between ψ_P and $\overline{\omega}_P$ and because the equation for ψ_P (appropriate to the F.N.P. grid) is non – standard *, we are concerned here with the detailed derivation of the equations for both ψ_P and $\overline{\omega}_P$. Referring to Fig. 6.2.2, we start first by deriving the equation for ψ_P. This is done by making use of the circulation equation for the near – wall cell P. The latter may be written as follows:

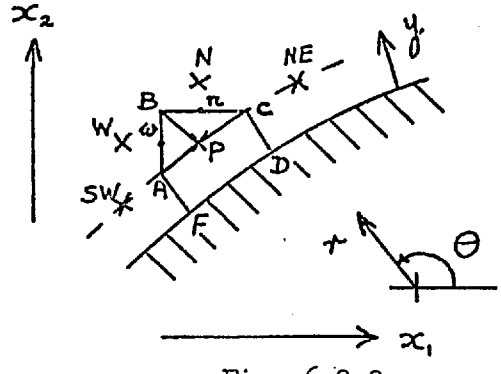


Fig. 6.2.2

* The equation for ψ_P, appropriate to the wall functions in (b) and (c), has been derived in detail by Roberts (1972).

$$-\overline{\omega}_P A_P = \overline{v}_{FA} \ell_{FA} + \overline{v}_{AB} \ell_{AB} + \overline{v}_{BC} \ell_{BC} + \overline{v}_{CD} \ell_{CD} + \overline{v}_{DF} \ell_{DF} \qquad (6.2.28)$$

where, $\overline{\omega}_P$ = space - average vorticity for cell P

A_P = area of cell area A B C D F

$\overline{v}_{nm}$ = mean velocity between points n and m in the direction from n to m

ℓ_{nm} = distance along curve or straight line joining points n and m

Now from the no - slip condition, we know that $\overline{v}_{DF} = 0$. Also we choose to approximate $\overline{v}_{FA}$ and $\overline{v}_{CD}$ by:

$$\overline{v}_{FA} = \frac{1}{2}(v_F + v_A) = \frac{1}{2} v_A$$

$$\overline{v}_{CD} = \frac{1}{2}(v_C + v_D) = \frac{1}{2} v_C$$

where, v_F, v_A, v_C and v_D are velocity components normal to the wall. Therefore equation (6.2.28) reduces to:

$$-\overline{\omega}_P A_P = v_A \frac{\ell_{FA}}{2} + \overline{v}_{AB} \ell_{AB} + \overline{v}_{BC} \ell_{BC} + v_C \frac{\ell_{CD}}{2} \qquad (6.2.29)$$

We approximate v_A , v_C , $\overline{v}_{AB}$ and $\overline{v}_{BC}$ as follows:

$$v_A = \frac{1}{\rho} \frac{(\psi_{SW} - \psi_P)}{r_P(\theta_{SW} - \theta_P)}$$

$$v_C = \frac{1}{\rho} \frac{(\psi_{NE} - \psi_P)}{r_P(\theta_P - \theta_{NE})}$$

$$\overline{v}_{AB} = \frac{1}{\rho} \frac{(\psi_W - \psi_P)}{(x_{1,P} - x_{1,W})} \qquad (6.2.30)$$

$$\overline{v}_{BC} = \frac{1}{\rho} \frac{(\psi_N - \psi_P)}{(x_{2,N} - x_{2,P})}$$

and introduce,

$$A_R = (x_{1,C} - x_{1,B})(x_{2,B} - x_{2,A})$$

$$\ell_{FA} = \ell_{CD} = y_P$$

$$\ell_{AB} = x_{2,B} - x_{2,A}$$

$$\ell_{BC} = x_{1,C} - x_{1,B}$$

Substituting equations (6.2.30) into equation (6.2.29) and making use of the definitions of A_R, ℓ_{FA}, ℓ_{AB} and ℓ_{BC}, we obtain the following equation for ψ_P :

$$\psi_P = \frac{B_N \psi_N + B_W \psi_W + B_{SW} \psi_{SW} + B_{NE} \psi_{NE} + \rho \frac{A_P}{A_R} \bar{\omega}_P}{B_N + B_W + B_{SW} + B_{NE}} \qquad (6.2.31)$$

where,

$$B_N = \frac{1}{(x_{2,N} - x_{2,P})(x_{2,B} - x_{2,A})}$$

$$B_W = \frac{1}{(x_{1,P} - x_{1,W})(x_{1,C} - x_{1,B})}$$

$$B_{SW} = \frac{y_P/2}{r_P A_R} \frac{1}{(\theta_{SW} - \theta_P)}$$

$$B_{NE} = \frac{y_P/2}{r_P A_R} \frac{1}{(\theta_P - \theta_{NE})}$$

Now the equation for $\bar{\omega}_P$ is calculated as follows:

$$\bar{\omega}_P = \bar{\omega}_{ABP} R_{P1} + \bar{\omega}_{BPC} R_{P2} + \bar{\omega}_{APCDF} R_{PS} \qquad (6.2.32)$$

where, R_{P1} = (Area ABP)/A_P

R_{P2} = (Area BPC)/A_P

R_{PS} = (Area APCDF)/A_P

$\overline{\omega}_{ABP}$ = Space - average vorticity for triangle ABP

$\overline{\omega}_{BPC}$ = " " " " " BPC

$\overline{\omega}_{APCDF}$ = " " " " area APCDF

We then determine $\overline{\omega}_{APCDF}$, $\overline{\omega}_{ABP}$ and $\overline{\omega}_{BPC}$ as follows:

1. $\overline{\omega}_{APCDF}$

As one - dimensional flow between node P and the wall is assumed, then,

$$\overline{\omega}_{APCDF} = \frac{1}{y_P}\int_0^{y_P} -\left(\frac{du}{dy}\right) dy = -\frac{u_P}{y_P}$$

Now u_P is obtained from equation (6.2.11)

$$\therefore \quad \overline{\omega}_{APCDF} = -\frac{(1+b)}{\rho\, y_P^2}(\psi_P - \psi_S)$$

$$\therefore \quad \overline{\omega}_{APCDF} = -C_{PS}(\psi_P - \psi_S) \qquad (6.2.33)$$

where, $C_{PS} = \dfrac{(1+b)}{\rho\, y_P^2}$

Also from equation (6.2.12),

$$\omega_P = -b\, C_{PS}(\psi_P - \psi_S) \qquad (6.2.34)$$

2. $\overline{\omega}_{ABP}$ and $\overline{\omega}_{BPC}$

In the determination of $\overline{\omega}_{ABP}$ and $\overline{\omega}_{BPC}$, we first assume that the vorticity varies linearly between nodes N and P and between nodes W and P. Then considering triangle ABP as an example, we assume that $\overline{\omega}_{ABP}$

is given by the point value of vorticity at $x_2 = x_{2,P}$ and $x_1 = x_{1,w} + \frac{1}{3}(x_{1,P} - x_{1,w})$. This point is on a line, which is parallel to AB and which passes through the centroid of the triangle ABP. From the above,

$$\overline{\omega}_{ABP} = \frac{2}{3}\omega_P + \frac{1}{3}\omega_W$$

$$\therefore \quad \overline{\omega}_{ABP} = -\frac{2}{3} b C_{PS}(\psi_P - \psi_S) + \frac{1}{3}\omega_W \qquad (6.2.35)$$

Similarly,

$$\overline{\omega}_{BPC} = -\frac{2}{3} b C_{PS}(\psi_P - \psi_S) + \frac{1}{3}\omega_N \qquad (6.2.36)$$

Substituting equations (6.2.33), (6.2.35) and (6.2.36) into (6.2.32) gives:

$$\overline{\omega}_P = -(\psi_P - \psi_S) C_{PS}\left[\frac{2}{3} b (R_{P1} + R_{P2}) + R_{PS}\right] + \frac{1}{3}(R_{P1}\omega_W + R_{P2}\omega_N) \qquad (6.2.37)$$

Finally, substituting equation (6.2.37) into equation (6.2.31) gives:

$$\psi_P = \frac{B_N \psi_N + B_W \psi_W + B_{SW} \psi_{SW} + B_{NE} \psi_{NE} + N}{B_N + B_W + B_{SW} + B_{NE} + D} \qquad (6.2.38)$$

where, $$N = \frac{\rho A_P}{A_R}\left\{\frac{1}{3}\left[R_{P1}\omega_W + R_{P2}\omega_N\right] + \psi_S C_{PS}\left[\frac{2}{3} b (R_{P1} + R_{P2}) + R_{PS}\right]\right\}$$

$$D = \frac{\rho A_P}{A_R} C_{PS}\left[\frac{2}{3} b (R_{P1} + R_{P2}) + R_{PS}\right]$$

6.3 Developing flow in a channel

6.3.1 Review of available data

The data for fully - developed flow in a channel are more plentiful than for developing flow, so we shall consider the former first of all. As far as mean data are concerned, Knudsen and Katz (1958) have collected both friction factor and heat transfer data from a number of sources. They provide the data in the form of correlations, where the friction factor is given as a function of Reynolds number, and the bulk Nusselt and/or Stanton numbers are given as functions of Reynolds and Prandtl numbers. Clark (1968), on the other hand, provides local data of the hydrodynamics of fully - developed channel flow. His measurements of fully - developed velocity and turbulence profiles compare closely with the previous results of Comte - Bellot (1965) and Laufer (1951).

It appears that the only available data on developing flow in a channel are those of Byrne et al (1969). The interesting data, in this case, are the local plots of Stanton number.

6.3.2 Boundary conditions

Referring to Fig. 6.3.1, the boundary conditions for the problem of developing flow in a channel may be summarised as follows:

(a) Reynolds and Prandtl numbers

The Reynolds number based on equivalent diameter is given by:

$$(Re)_{de} = \frac{4\rho \bar{U} h}{\mu}$$

where, h = channel half - width

$\bar{U}$ = mean velocity

The value of Prandtl number, appropriate to air, is:

$$Pr = 0.7$$

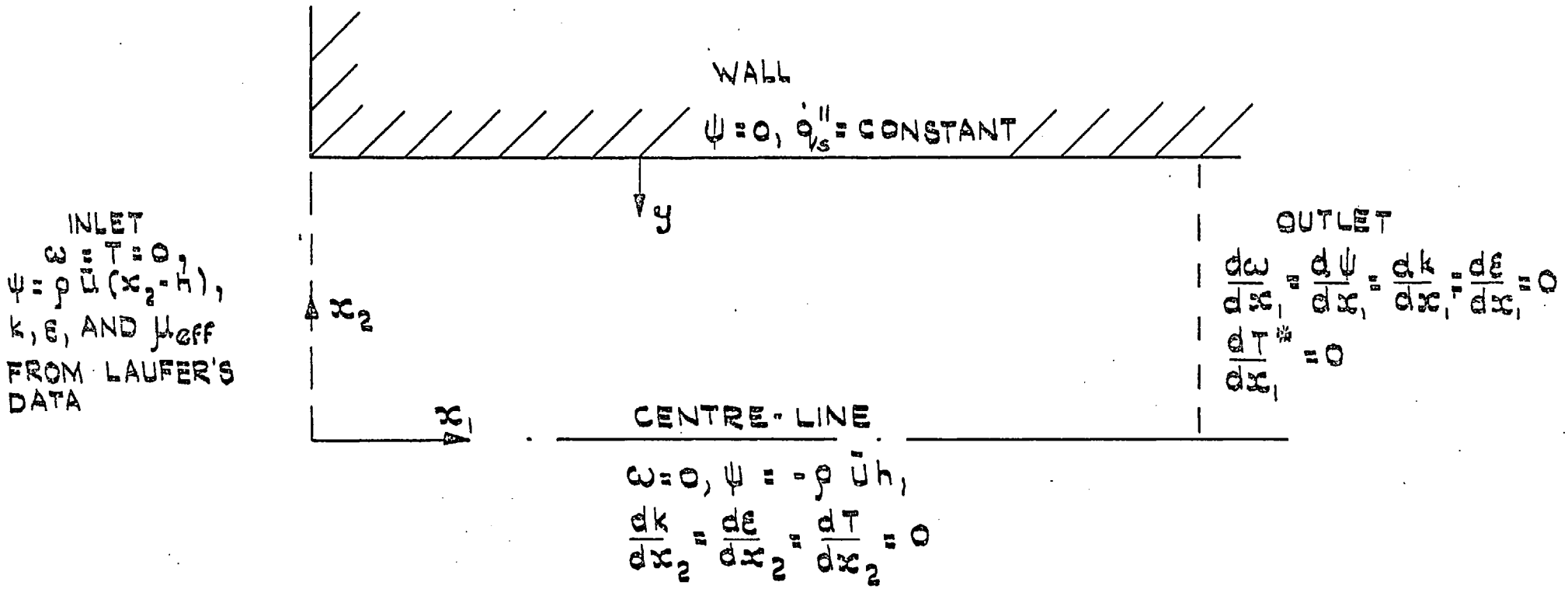


FIG. 6.3.1 : BOUNDARY CONDITIONS FOR DEVELOPING FLOW IN A CHANNEL.

(b) Inlet

$$\omega = 0 ; \quad \psi = \rho \bar{u} (x_2 - h); \quad T = 0$$

Distributions of k and μ_{eff} are obtained from Laufer's measurements in fully - developed pipe flow. These measurements, which are reported in Hinze (1959), were performed at a Reynolds number, based on the maximum velocity, of 5 x 10^5. Laufer provides the data in terms of k/u_τ^2 vs. y/R and $\mu_{eff}/(u_\tau R)$ vs. y/R,

where, u_τ = friction velocity

R = radius of the pipe

y = distance from pipe wall

When applying this data to channel flow, it is necessary to replace the radius R by h, the half - width of the channel. Also for the sake of simplicity, u_τ at inlet is obtained from the expression derived from the 1/7 - power law, i.e. equation (6.2.14) with b = 1/7. The inlet values of ε are obtained by rearranging the expression for μ_{eff} to $\varepsilon = C_\mu \rho k^2/\mu_{eff}$ and using the measured values of k and μ_{eff}.

(c) Outlet

$$\frac{d\omega}{dx_1} = \frac{d\psi}{dx_1} = \frac{dk}{dx_1} = \frac{d\varepsilon}{dx_1} = \frac{dT^*}{dx_1} = 0$$

where, $T^* = \dfrac{T - T_c}{T_s - T_c}$

T_c = temperature on the centre - line

T_s = temperature at the wall

(d) Wall

$\psi = 0$; $\dot{q}''_s$ = constant

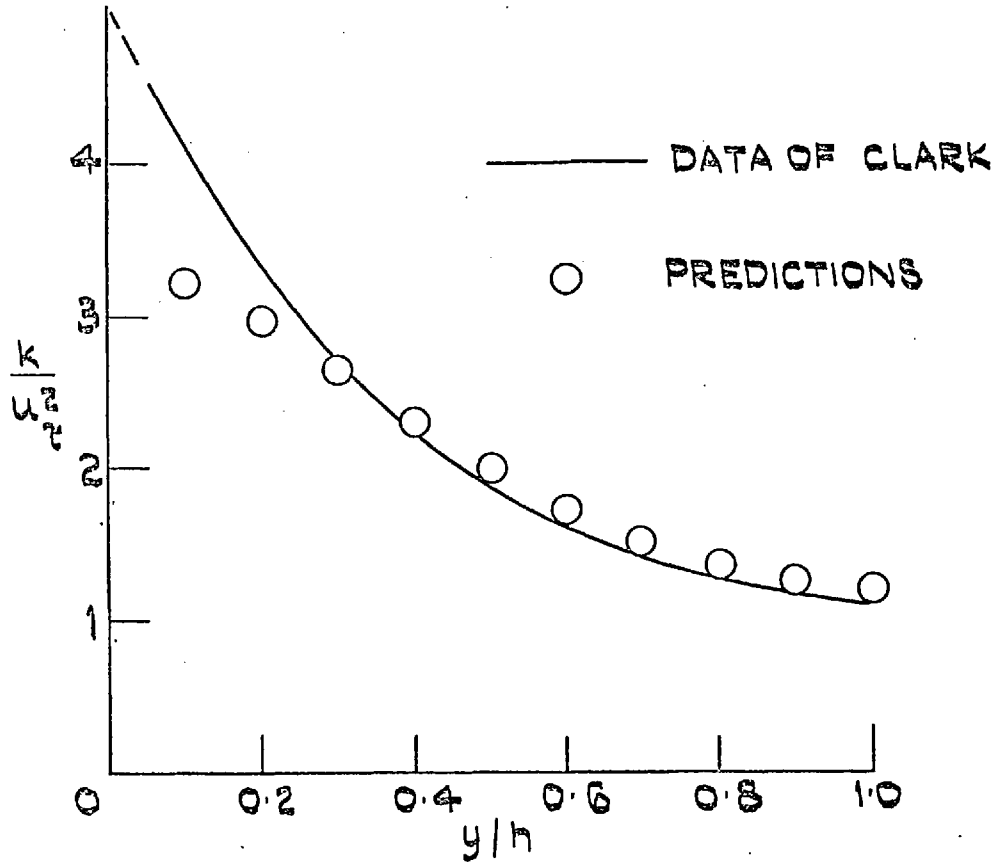


FIG. 6.3.2: COMPARISON BETWEEN THE PREDICTED AND MEASURED PROFILES OF k/u_τ^2 AT $(Re)_{de} = 1.6 \times 10^5$

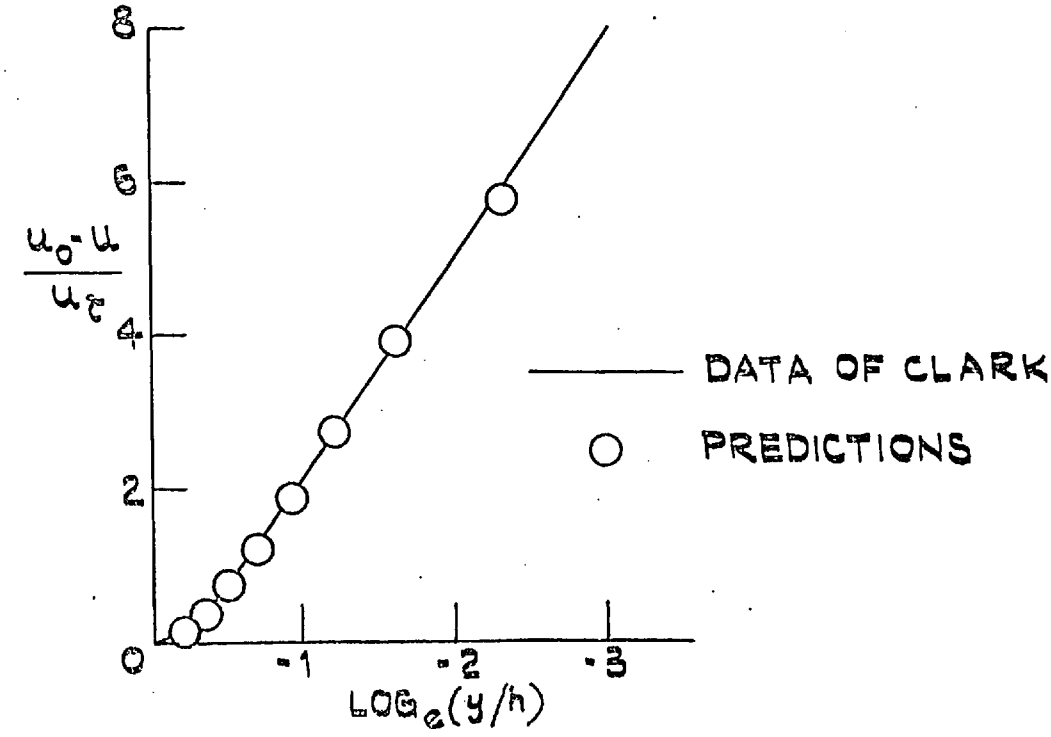


FIG. 6.3.3: COMPARISON BETWEEN THE PREDICTED AND MEASURED PROFILES OF VELOCITY DEFECT AT $(Re)_{de} = 1.6 \times 10^5$

(e) Centre - line

$$\omega = 0; \qquad \psi = -\rho \bar{U} h;$$

$$\frac{dk}{dx_2} = \frac{d\varepsilon}{dx_2} = \frac{dT}{dx_2} = 0$$

6.3.3 The predictions

(a) Fully - developed flow data

In Figs. 6.3.2 and 6.3.3, the predictions of k/u_τ^2 vs. y/h and $\frac{u_o - u}{u_\tau}$ vs. $\log_e\left(\frac{y}{h}\right)$ (where u_o = velocity on the centre - line of channel) for fully - developed flow in a parallel channel at $(Re)_{d_e} = 1.6 \times 10^5$ are compared with the measurements of Clark (1968). Fig. 6.3.2 shows that good agreement between the predictions and measurements of k/u_τ^2 is obtained only for $y/h \geq 0.3$. The difference between the predictions and measurements for $y/h < 0.3$ is mainly due to the choice of the constant C_μ. Fig. 6.3.3 shows that the measurements and predictions of velocity defect are in good agreement.

In Table 6.3.1, the predicted values of friction factor, $2\tau_s/(\rho \bar{u}^2)$, and Stanton number, St, at two values of $(Re)_{d_e}$ are compared with experimental values obtained from Knudsen and Katz (1958). The friction factor data was obtained from:

$$\frac{1}{\sqrt{f}} = 4.0 \log_e\left[(Re)_{d_e}\sqrt{f}\right] - 0.4$$

where, $f = 2\tau_s/(\rho \bar{u}^2)$

$(Re)_{d_e}$	$2\tau_s/(\rho \bar{U}^2)$		St	
	Predicted	Measured	Predicted	Measured
4×10^4	5.40×10^{-3}	5.30×10^{-3}	3.22×10^{-3}	3.20×10^{-3}
4×10^5	3.30×10^{-3}	3.40×10^{-3}	2.03×10^{-3}	2.02×10^{-3}

Table 6.3.1

The Stanton number data was obtained from:

$$St = 0.021 \, (Re)_{d_e}^{-0.2} \, (Pr)^{-2/3}$$

The agreement between the predictions and measurements for both friction factor and Stanton number are shown to be very close. This means that both the predicted trends and magnitudes with respect to $(Re)_{d_e}$ are correct.

(b) Developing flow data

Fig. 6.3.4 illustrates the comparison between Stanton number predictions and the measurements of Byrne et al (1969) for developing flow in a channel. Before discussing this comparison, we should first of all discuss the experimental rig of Byrne et al and establish the validity of the experimental data by comparison with flat plate data.

In their paper, Byrne et al state that the entry region of their apparatus consisted of a converging mouthpiece which led to 1" wide sandpaper strips placed on the top and bottom walls at the entrance of a parallel channel, Fig. 6.3.5. The purpose of these strips was to ensure the immediate onset of turbulent boundary layer flow. The sandpaper

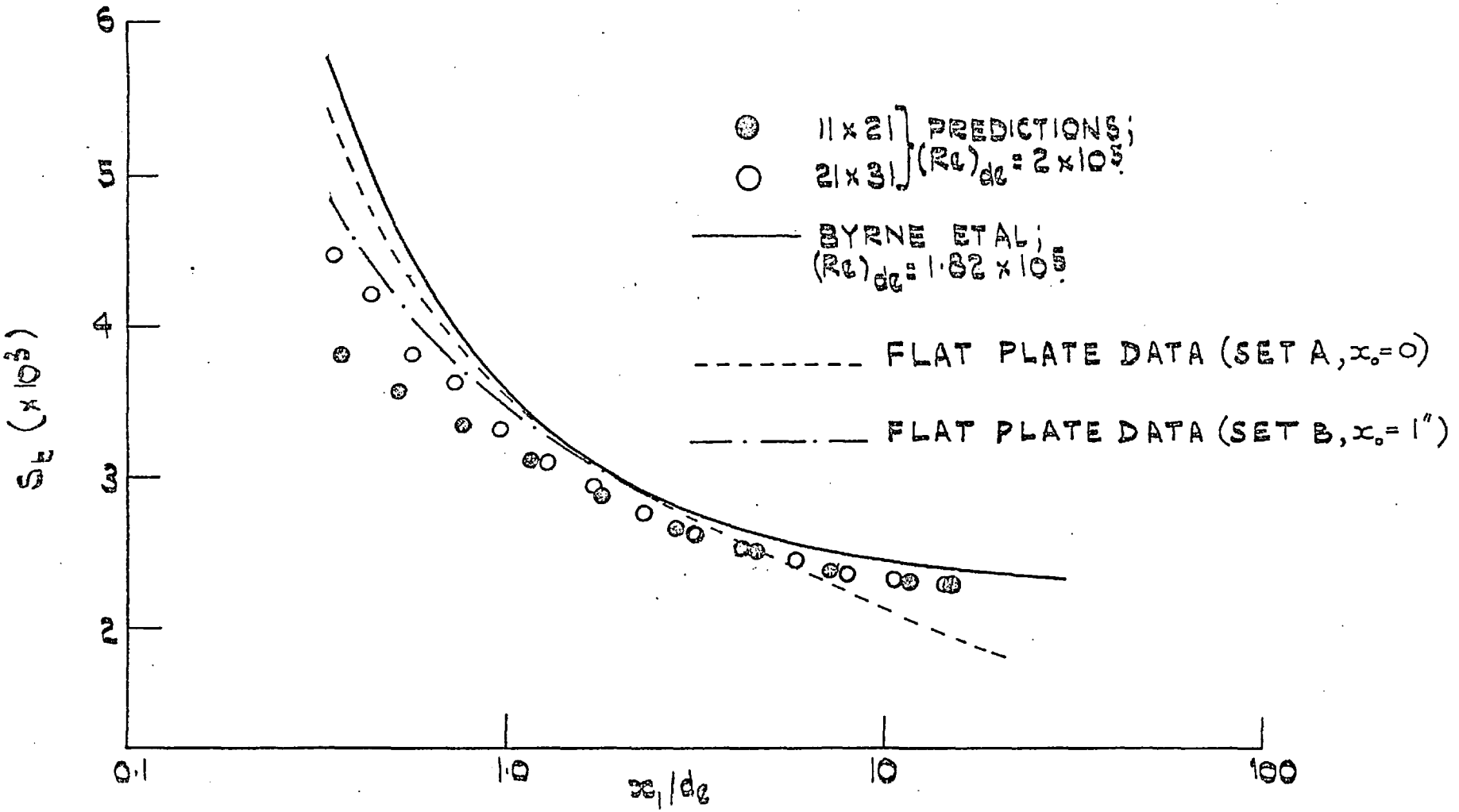


FIG. 6.3.4 : COMPARISON BETWEEN THE PREDICTIONS AND MEASUREMENTS OF STANTON NUMBER FOR DEVELOPING FLOW IN A CHANNEL.

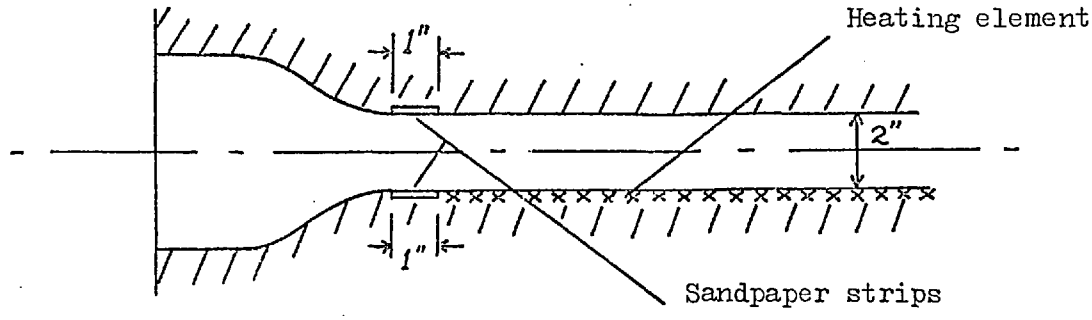


Fig. 6.3.5

strip on the lower wall was followed immediately by the heating element. There is in fact some inconsistency in their paper because the diagram of the heating element in their Fig. 2 shows a 2" wide strip of sandpaper followed by the heating element. But assuming that the layout of the heating element and the thermocouple positions (given in their Fig. 2) is correct, one can deduce that the results in the form of St vs. x_1/d_e are plotted in their Fig. 13 with respect to the leading edge of a 1" wide sandpaper strip. However Byrne et al do not establish the point at which transition to a turbulent boundary layer flow occurs.

For the sake of comparison with the flat plate data, we shall assume that transition occurs between the leading edge of the 1" sandpaper strip and the leading edge of the heating element. The flat plate results are plotted from the correlation, as given by Hartnett, Eckert and Birkebak (1959), which is as follows:

$$St = 0.0296\,(Re)_x^{-0.2}\,(Pr)^{-2/3}\left[1 - \left(\frac{x_0}{x}\right)^{9/10}\right]^{-1/9}$$

where,

$$(Re)_x = Ux/\nu$$

U = free - stream velocity

x = axial distance from start of turbulent boundary layer

x_0 = length of unheated section

The plotted flat plate data in Fig. 6.3.4 represents two extreme values of x_o:

(i) x_o = 0, Set A results

x = distance from leading edge of heating element

(ii) x_o = 1", Set B results

x = distance from leading edge of 1" sandpaper strip

Both these sets of results are compared with the results of Byrne et al by putting $(Re)_{x=d_e} = 1.82 \times 10^5$. The results in Fig. 6.3.4 of St $vs.$ x_1/d_e are plotted on the basis that x_1 = distance from the leading edge of the 1" sandpaper strip. In the region $x_1/d_e \leq 3.0$, the Set A results are in closer agreement with the results of Byrne et al than the Set B results. However in the region $x_1/d_e > 4$, neither Set A nor B compare very closely with the channel data. This is because (due to the influence of both channel walls) the channel boundary layers are approaching the fully - developed condition but the flat plate boundary layers continue to develop indefinitely. Nevertheless the close agreement with the Set A results for $x_1/d_e \leq 3.0$ indicates that the results of Byrne et al are valid and also that the turbulent boundary layer probably starts at or near the leading edge of the heating element.

Assuming the latter to be true, it is particularly appropriate to compare the data of Byrne et al with the present predictions, where the velocity and thermal boundary layers start at the same point. Fig. 6.3.4 illustrates predictions corresponding to two grid distributions *. The

---

* The grid spacing in the x_2 - direction is uniform, and that in the x_1 - direction is caused to progressively increase with x_1 up to $\left(\frac{x_1}{h}\right)_{max} = 60.0$. The value of $\left(\frac{x_1}{h}\right)_{max}$, where $\left(\frac{x_1}{h}\right)_{max} \geq 60.0$, does not influence the predictions.

two sets of predictions agree well for $x_1/d_e > 1.5$ but indicate some discrepancy in the entrance region. This is due to differences in the calculated inlet values of u_τ^2 and the coefficients $C_\mu\left(\frac{y_P}{h}\right) = k_P/u_\tau^2$ for the two grids (where subscript P indicates the near - wall node). Both of these factors control the inlet value of near - wall k_P . Now at inlet, we assume that the velocity profile is uniform, i.e. u_P = constant. Therefore for a given value of laminar viscosity μ , u_τ^2 from equation (6.2.14) is a function only of y_P , that is u_τ^2 is proportional to $\left[1/y_P\right]^{\frac{2}{1+n}}$. Thus when the uniform grid distribution in the cross - stream direction is refined by a factor of 2, i.e. from 11 to 21 grid nodes, u_τ^2 increases by 1.19 and also it happens that $C_\mu\left(\frac{y_P}{h}\right) = k_P/u_\tau^2$ increases by 1.19. As a result the near - wall value of $k_P^{1/2}$ increases by about 20%. It can be shown with reference to equation (6.2.23) that the latter accounts for most of the difference in the predicted inlet values of Stanton number.

For values of $x_1/d_e \geq 1.5$, the trends of both sets of predictions are in good agreement with the data of Byrne et al, but the predictions underestimate the data by about 10%. The discrepancies between the predictions and the experimental data in the inlet region, $x_1/d_e < 1.5$, are large but these can be corrected by:

(a) moving the inlet boundary to a position a little way downstream of the start of the turbulent boundary layer, so that u_τ^2 at inlet can be specified from the flat plate equation, $\frac{\tau_s}{\rho U^2} = \frac{u_\tau^2}{U^2} = 0.0296\left(Re\right)_x^{-0.2}$

(b) moving the inlet near - wall node to the edge of the velocity boundary layer, where the thickness, δ, of the latter can be given by the appropriate flat plate equation: $\delta/x = 0.383/\left(Re\right)_x^{0.2}$

(c) putting $k_P = \frac{u_\tau^2}{\sqrt{C_\mu}}$, where k_P is the inlet near - wall value of k.

It can be shown with reference to equations (6.2.20) and (6.2.23) that

the above changes would produce Stanton numbers (at the inlet boundary) in close agreement with the flat plate values for $\alpha_o = 0$ and thus with the measurements of Byrne et al.

6.4 In - line tube banks

6.4.1 Limitations of present turbulence model

Before reviewing the relevant data on tube banks it is appropriate at this stage to discuss the important limitations of the turbulence models described in section 6.2. Perhaps the most important limitation concerns the assumption that the flow within any domain is fully turbulent. For high Reynolds numbers, the above assumption may be true for the main bulk of the fluid but it is not necessarily true for the near - wall region. Thus the assumption (implicit in the chosen wall functions) that the wall boundary layers are always turbulent does not take into account the many flow situations which contain both laminar and turbulent boundary layers. The latter also means that the present models cannot deal with the phenomenon of transition from a laminar to a turbulent boundary layer. Thus it follows that the types of recirculating flow situations which we are able to predict correctly are limited by the present choice of turbulence models.

As an illustration of the latter limitation we shall consider the possibility of predicting transverse turbulent flow over a single cylinder; and we shall refer to the evidence of a number of investigators which is summarised in the Engineering Sciences Data Item No. 70013. The latter indicates that, for a smooth cylinder in a low - turbulence - level free - stream with $Re \leq 3 \times 10^6$, the boundary layer on the front face of the cylinder is laminar and transition to turbulence occurs on the back face of the cylinder. For $Re > 5 \times 10^6$, the transition point moves onto the upstream face of the cylinder, and it is stated (but no reference is given) that for $Re > 10^7$ the flow round the cylinder becomes

almost entirely turbulent. It is clear from the above, that the present turbulence models cannot be used to predict the flow over a single cylinder for $Re \leq 10^7$.

Another limitation of the present turbulence models is the use of wall functions which are derived from characteristics for zero - pressure - gradient conditions. The latter can be used satisfactorily to predict flow in situations where the pressure gradient is small, e.g. as in developing flow in a parallel channel. However for situations where the pressure gradients are large these wall functions cannot produce accurate predictions. Such a situation is given by the flow near the upstream face of a circular cylinder. Thus although the flow round a cylinder for $Re \geq 10^7$ may be entirely turbulent, the wall functions will not produce accurate predictions of the flow because of the high pressure gradient on the front face.

Therefore the main limitations of the present turbulence models are as follows:

(a) The practical situation, where both laminar and turbulent boundary layers occur, cannot be predicted.

(b) The wall functions only give correct predictions of turbulent boundary layers with small pressure gradients.

6.4.2 Review of appropriate data

We shall now consider the possibility of using the present turbulence models to predict turbulent flow through in - line and/or staggered tube banks. We shall do this by discussing the results of relevant data. As mentioned earlier, there is very little experimental data on the local characteristics of flow through tube banks. However a review by Zhukauskas et al (1968) of a wide range of mean tube bank data does provide some guidance in understanding the nature of the different flow regimes. Of the range of data reviewed by Zhukauskas, perhaps the most useful set

is that of Stasyulyavichyus and Samoska (1964), (1968), which are discussed below. For the sake of brevity only, we shall refer below to Stasyulyavichyus and Samoska by the abbreviation S and S.

In our discussion below, parts (a) and (b) are devoted to the consideration of pressure drop and heat transfer data respectively. Then from (a) and (b), some conclusions are drawn in (c) concerning the possibility of using the present turbulence models to predict turbulent flows through tube banks. Finally in part (d) we discuss briefly the influence of vortex shedding on the characteristics of flow through tube banks. The phenomenon of vortex shedding cannot be taken into account in our present prediction procedure and turbulence models, so it is important to estimate its influence on the experimental flow.

(a) Pressure drop data

First of all, we shall consider S and S's pressure drop data. Their staggered tube bank results illustrate the influence of the number of rows on the mean pressure drop per row for the range $2 \times 10^4 \leq Re \leq 2 \times 10^6$. These results show that for $Re > 2 \times 10^5$ and $N \geq 7$ (where N = total number of rows) the mean pressure drop per row achieves constant values for both 1.19×0.94 and 1.47×1.04 banks.

The flow mechanism, which causes this phenomenon is not well understood but one influential factor is almost certainly the variation in the level of turbulence as the flow passes through the bank. Each tube acts as a generator of turbulence, which influences the flow characteristics on the following tube; and so the turbulence level increases until equilibrium conditions are achieved. This type of variation of turbulence level*,

---

* In this case, k is defined by $\frac{1}{2}\left(\overline{u'^2} + \overline{v'^2}\right)$, where, u' and v' = the fluctuating components of velocity in the x_1 and x_2 directions respectively.

$\frac{k}{\bar{U}^2}$, has been measured by Pearce (1972), where,

k = kinetic energy of turbulence

$\bar{U}$ = mean velocity through the minimum cross - section between the tubes

His results for an in - line bank, 1.89 x 1.89, at $Re = 3.4 \times 10^4$ show that $k/\bar{U}^2$ rises from 8.55×10^{-6} at the first row to 1.38×10^{-2} at the fifth row and then remains almost constant. Now for high - Reynolds - number flow, the pressure drop is primarily a function of the turbulence level and the flow pattern in the bank. Thus the above results for the 1.19 x 0.94 and 1.47 x 1.04 banks with $Re > 2 \times 10^5$ suggest that the pressure drop per row must be constant in the region where the flow is fully-developed and $k/\bar{U}^2$ is constant.

The pressure drop characteristics for a larger bank, 2.48 x 1.28, do not however agree exactly with the trend for the small banks. For N = 7, the characteristic decreases to a minimum value in the range $2 \times 10^5 \leq Re \leq 4 \times 10^5$, and then a gradual increase to a constant value for $Re \geq 8 \times 10^5$ is indicated. The latter trend is confirmed by the measurements of Hammeke et al (1967) for a 2.06 x 1.38 staggered bank with N = 10. S and S concluded from their results with $N \geq 7$ that for $S_T/S_L \leq 1.7$ equilibrium conditions indicated by a constant pressure dropoccur at about $Re = 2 \times 10^5$, and that for $S_T/S_L > 1.7$ equilibrium conditions occur at about $Re = 8 \times 10^5$ after passing through a transition region in the range $2 \times 10^5 \leq Re \leq 8 \times 10^5$.

It is interesting to note that the pressure drop characteristics for staggered banks ($S_T/S_L > 1.7$) are similar to the coefficient of drag (C_D) characteristic for a smooth cylinder in a low - turbulence - level free - stream. Both characteristics pass through transition regions, but equilibrium occurs at $Re \approx 8 \times 10^5$ for the staggered banks and at $Re \approx 10^7$ for the single cylinder.

From the above similarity, one may deduce the nature of the flow on a tube in the n^{th} row of a staggered bank, where $n \geq 7$. For such a tube, one might suppose that the transition point between the laminar and turbulent boundary layers may move onto the front face of the tube at about $Re = 2 \times 10^5$ and that the boundary layer may become almost entirely turbulent by $Re = 8 \times 10^5$. This phenomenon may be promoted by a combination of the high level of turbulence in the bank for $N \geq 7$ and by the influence of the natural tube - wall roughness elements on the thin laminar boundary layers.

The behaviour of the pressure drop characteristics for in - line tube banks, S and S (1968), are apparently not so consistent as the above. In the range $10^5 \leq Re \leq 10^6$, some of the banks display a constant pressure-drop characteristic whereas other banks display a gradual decrease. In this case, S and S only provide data for N = 7, so the influence of the number of rows is not demonstrated. However Hammeke et al's measurements for a 2.06 x 1.38 in - line bank with N = 10 may provide some clue of the influence of the number of rows. In this case, the pressure drop characteristic displays a slight waviness but it is essentially independent of Reynolds number in the range $2 \times 10^4 \leq Re \leq 10^6$. Thus this finding may indicate a trend, which one might expect to find in at least a restricted range of in - line bank geometries for $N \geq 10$. Nevertheless the above results do not give us much guidance concerning the nature of the boundary layers on tubes within an in - line arrangement. For further information we must now refer to the heat transfer results, and then try to draw some conclusions from the available pressure drop and heat transfer data for both staggered and in - line banks.

(b) Heat transfer data

First we should consider the variation of heat transfer as a function of the tube position in a bank. Data from McAdams (1954) and that of

Welch and Fairchild (1964) indicate that the heat transfer in both staggered and in - line arrangements rises steadily from the first row to about the third or fourth row and then becomes almost constant. This data agrees very closely with the variation of the turbulence level, $\frac{k}{\overline{U}^2}$ through an in - line bank as measured by Pearce (1972). Details of the latter variation were given in (a). Now, from data such as that of Seban (1960) and Geidt (1951), we know that there is a direct relationship between the heat transfer from a single cylinder and the free stream turbulence. Therefore it is not surprising that there is also a direct relationship between the variations of heat transfer and turbulence level through a tube bank.

However, as for the pressure drop data, we are mainly concerned with the results in the fully - developed flow situation, that is with the heat transfer results for the n^{th} row, where $n \geq 5$. Therefore the results of S and S (1964), (1968) for tubes in the 5th row are of particular interest and are discussed below.

For the sake of clarity, the results are considered in the form of $Nu \propto Re^m$ where m is a constant exponent. The results for all staggered tube banks in terms of the exponent m are as follows:

$Re < 2 \times 10^5$; $m \approx 0.6$

$Re > 8 \times 10^5$; $0.78 \leq m \leq 0.93$

The staggered bank characteristics are subjected to a transition region in the range $2 \times 10^5 \leq Re \leq 8 \times 10^5$.

The results for in - line tube banks, S and S (1968), are similar to the above and may be summarised as follows:

$$Re < 10^5; \quad 0.60 \leq m \leq 0.69$$

$$Re > 4 \times 10^5; \quad 0.76 \leq m \leq 0.92$$

Most of the in-line bank results display a change in slope in the range $10^5 \leq Re \leq 2 \times 10^5$, but the more tightly packed banks (such as the

1.68 x 1.13 bank) display a change in slope at $Re = 4 \times 10^5$. The average measurements of Hammeke et al (1967) for both staggered and in - line banks with 10 rows are in broad agreement with the above results.

(c) Conclusions for the reviews in (a) and (b)

What can one conclude from the above collection of both pressure drop and heat transfer data? The latter suggest that the laminar to turbulent transition processes on tubes in both staggered and in - line banks occur within the same Reynolds number range. The results also suggest that the transition processes for the in - line tubes may be completed at lower values of Re than for the staggered tubes.

However these results do not answer the question, 'What relative proportions of the tubes are covered by laminar and turbulent boundary layers for $Re > 2 \times 10^5$?' Only the comparison of the C_D characteristic for a smooth cylinder with the pressure drop characteristic for a staggered tube bank ($S_T/S_L > 1.7$) gives us some guidance in answering that question. In our earlier discussion in (a), we noted that the two characteristics are similar, but that after transition the former reaches a constant value of C_D for $Re > 10^7$ whereas the pressure drop characteristic of the latter reaches a constant value at about $Re = 8 \times 10^5$. Experimental evidence suggests that the flow on the front side of a single cylinder in a free stream is almost fully turbulent for $Re > 10^7$. Similarly we might suppose that, because of the influence of the enhanced turbulence, the flow over a tube in the n^{th} row of a staggered bank, where $n \geq 5$, is almost fully turbulent for $Re \geq 8 \times 10^5$. However the heat transfer characteristics for in - line tube banks are similar to the above, and so we might also suppose that the flow over a tube within an in - line bank must also be fully turbulent for at least $Re \geq 10^6$, if not for $Re \geq 2 \times 10^5$.

On the basis of the above supposition we shall, in the following sub - sections, go on to consider the predictions of fully - developed flow over in - line banks. However we shall not consider the prediction of flow over staggered banks, because the pressure variations round tubes in a staggered bank are much higher than the corresponding values in an in - line bank. It will be recalled that, as discussed in 6.4.1, the present wall functions are not designed to predict flows with a high variation of wall static pressure. Thus in choosing to predict flow through in - line banks rather than through staggered banks, we are assuming that the limitations of the turbulence model and wall functions (as discussed in 6.4.1) will not be so apparent for the former flow as for the latter.

(d) The matter of vortex shedding

The phenomenon of vortex shedding in tube banks should be discussed at this point before passing onto the following sub - sections, which are concerned with the predictions. Although this phenomenon, resulting from flow over single cylinders and other blunt bodies, has been studied in some detail, not much is known of its behaviour and effects in tube banks. However a major contribution in the latter direction has resulted from the work of Bauly (1971). His results and those of others suggest that vortex shedding does not always occur within tube banks, but its occurrence is dependent on the Reynolds number, the number of tube rows, and perhaps more so on the values of S_T and S_L . From the results of various data, Bauly puts forward a hypothesis concerning the occurrence of vortex shedding in terms of S_T and S_L . This hypothesis is summarised by the plots in Fig. 6.4.1. No exact values of S_T and S_L are put on this diagram because the lines demarking one region from another are probably dependent on Reynolds number and the number of rows.

If Bauly's hypothesis is correct, it would appear that, for a wide range of S_T and S_L, vortex shedding after the first row (and at least after the fifth row) has little influence on the flow characteristics. However if vortex shedding is significant and if the present models for random turbulence are correct, then the difference between the predictions and the measurements will show up the influence of vortex shedding on such characteristics as local and bulk values of heat transfer.

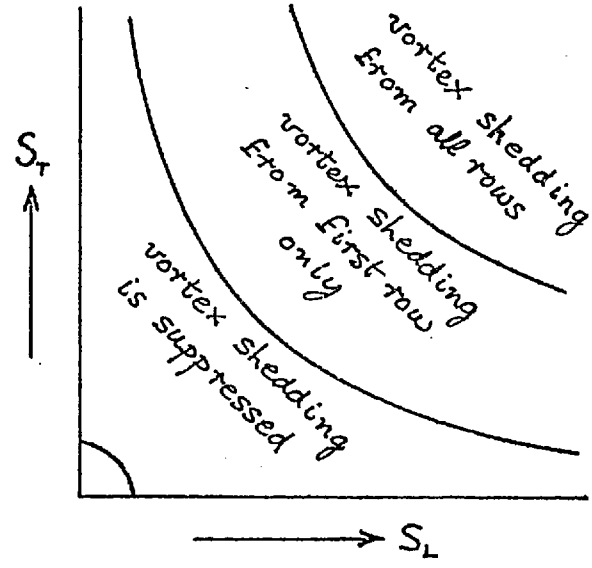


Fig. 6.4.1

6.4.3 The boundary conditions

With reference to Fig. 6.4.2, the boundary conditions for the problem of fully - developed flow through in - line tube banks are as follows:

(a) Reynolds and Prandtl numbers

The Reynolds number is given by:

$$Re = \frac{\rho \bar{U} D_t}{\mu} = \frac{2 \rho \bar{U} R}{\mu}$$

where, $\rho = \bar{U} = R = 1 \therefore Re = 2/\mu$

$\bar{U}$ = mean velocity through minimum cross - section between the tubes

D_t = diameter of tube

The Prandtl number, appropriate to air, is:

Pr = 0.7

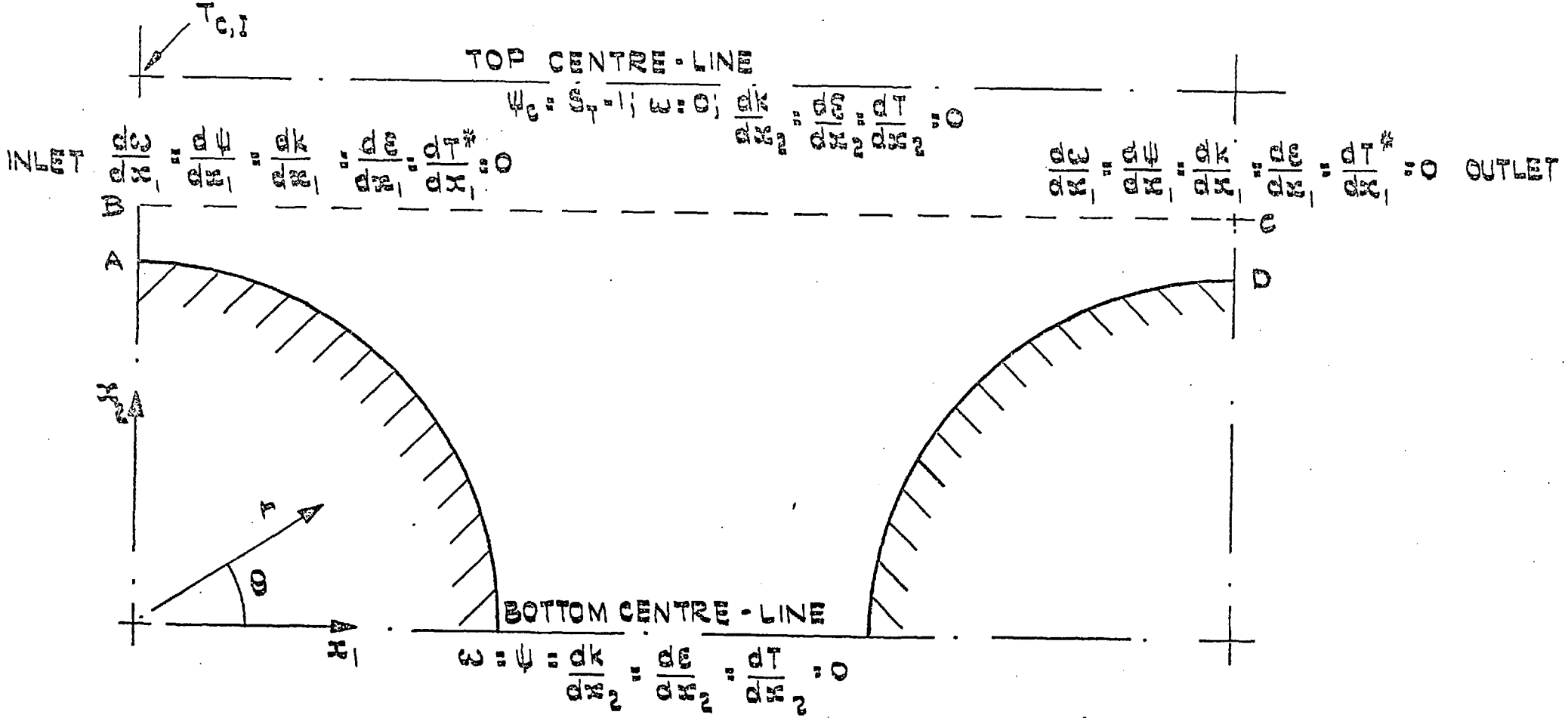


FIG. 6.4.2: BOUNDARY CONDITIONS FOR TURBULENT FLOW THROUGH IN-LINE TUBE BANKS.

(b) Inlet and outlet

$$\frac{d\omega}{dx_1} = \frac{d\psi}{dx_1} = \frac{dk}{dx_1} = \frac{d\varepsilon}{dx_1} = \frac{dT^*}{dx_1} = 0$$

where, $T^* = \dfrac{T - T_S}{T_{c,I} - T_S}$

$T_{c,I}$ = temperature on the centre - line at inlet

T_S = wall temperature

(c) Top centre - line

$$\omega = 0; \quad \psi_c = S_T - 1; \quad T_{c,I} = 1$$

$$\frac{dk}{dx_2} = \frac{d\varepsilon}{dx_2} = \frac{dT}{dx_2} = 0$$

(d) Bottom centre - line

$$\omega = \psi = 0;$$

$$\frac{dk}{dx_2} = \frac{d\varepsilon}{dx_2} = \frac{dT}{dx_2} = 0$$

(e) Wall

$$\psi = T_S = 0$$

(f) Pressure drop parameter, or Euler number

Referring to Fig. 6.4.2, the Euler number is defined by $\dfrac{p_A - p_D}{\rho \cdot \bar{u}^2}$

Now the pressure drop, $p_A - p_D$ can be determined via the path A B C D as follows:

$$p_A - p_D = (p_A - p_B) + (p_B - p_C) + (p_C - p_D)$$

But because of the fully - developed flow situation:

$$p_A - p_B = -(p_c - p_D)$$

$$\therefore \; p_A - p_D = p_B - p_c$$

The pressure drop, $p_B - p_c$, and therefore the Euler number, is determined from the numerical integration of the x_1 - momentum equation, as described by Gosman et al (1969).

(g) Stanton and Nusselt numbers

The local Stanton number is defined as:

$$St = \frac{\dot{q}''_s / c_p}{\rho \bar{u} (T_{AB} - T_s)}$$

where, $\dot{q}''_s / c_p$ is obtained from equation (6.2.23)

T_{AB} = average of bulk temperatures at inlet and outlet

The average Stanton number is obtained from:

$$\overline{St} = \frac{1}{\pi} \int_0^{\pi} St \, d\theta$$

The average Nusselt number is obtained from:

$$\overline{Nu} = \overline{St} \; Re \; Pr$$

6.4.4 The predictions

(a) Influence of grid distribution on local and bulk quantities

The F.N.P. grid distribution in a typical in - line tube bank section may be altered using two methods, which are independent of each other. The first method involves the alteration of the non - dimensional distance between the tube walls and near - wall nodes, $\frac{y_p}{R}$, and the second involves the alteration of the grid spacing in the main field of flow. The influences of these two methods

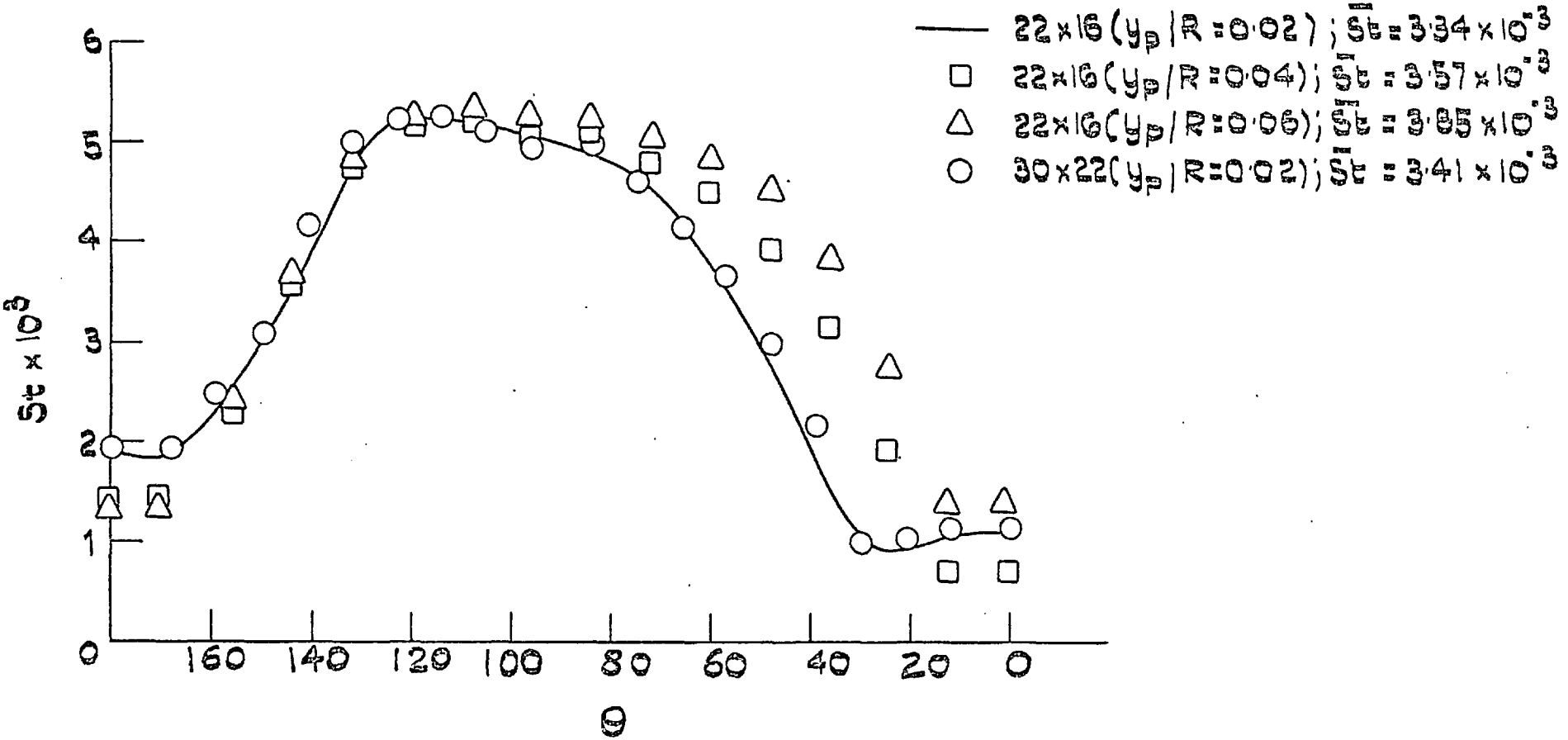
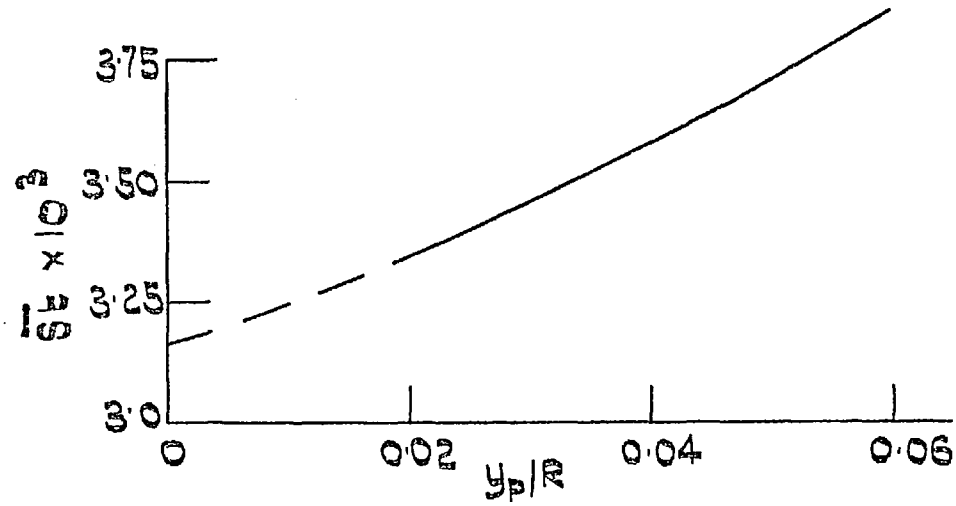
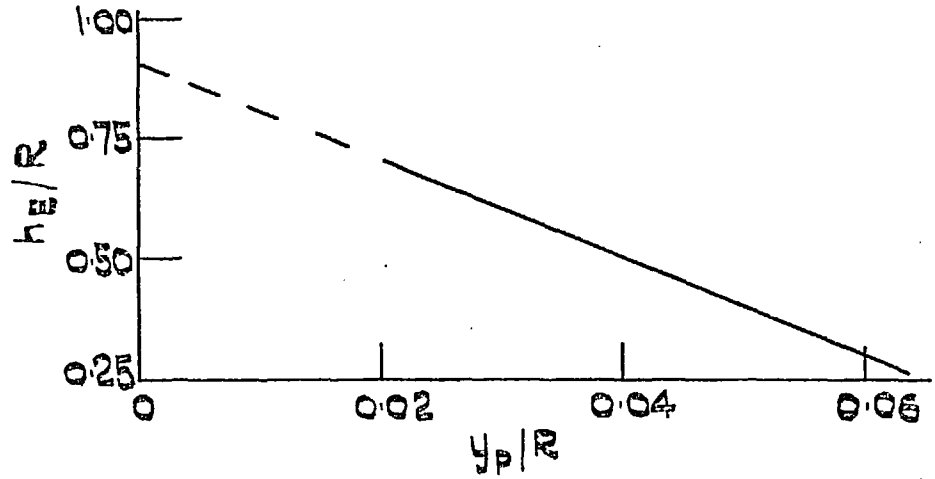


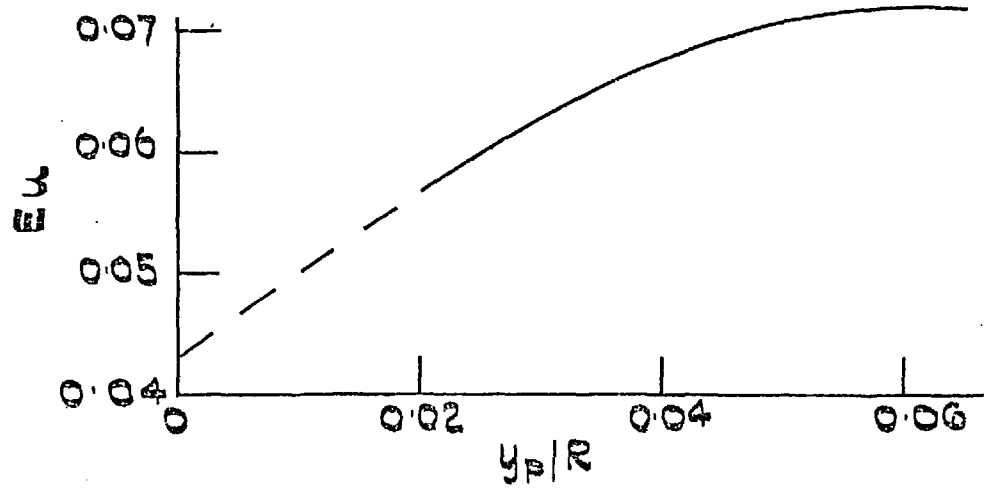
FIG. 6.4.3: INFLUENCE OF GRID DISTRIBUTION ON THE PREDICTIONS OF LOCAL STANTON NUMBER $S_T = 2{\cdot}06$, $S_L = 1{\cdot}38$, $Re = 10^5$, $Pr = 0{\cdot}7$, T_s = CONSTANT.



(a). MEAN STANTON NUMBER, $\bar{St}$



(b) NON-DIMENSIONAL EDDY HEIGHT, h_E/R



(c) EULER NUMBER, Eu

FIG. 6.44: INFLUENCE OF NON-DIMENSIONAL DISTANCE BETWEEN THE WALL AND THE NEAR-WALL NODE ON THE MEAN FLOW PARAMETERS, $\bar{St}$, h_E/R AND Eu FOR $S_T = 2{\cdot}06$, $S_L = 1{\cdot}38$, $Re = 10^5$, $Pr = 0{\cdot}7$, T_s = CONSTANT AND A GRID 22 × 16.

on the predictions of local Stanton number are shown in Fig. 6.4.3. In the latter the results for the grids 22 x 16 (y_P/R = 0.02) and 30 x 22 (y_P/R = 0.02) are in close agreement. This means that a change in the grid spacings in the main field has a negligible influence on the accuracy of the predictions.

However when the distance y_P/R (for a constant grid distribution of 22 x 16) is varied from 0.02 to 0.06, there is a significant variation in the local Stanton number for $180 \geq \theta \geq 150$ and $90 \geq \theta \geq 0$. Fig. 6.4.4 also illustrates the effect of varying y_P/R in terms of the mean Stanton number, the Euler number and the non - dimensional recirculation eddy height, h_E/R, where,

h_E = maximum value of x_2 for the reattachment streamline.

In order to understand the factors which are responsible for the influence of y_P/R we should concentrate our attention on the results in Fig. 6.4.4 (b). The reason for giving primary consideration to the latter is that the eddy height and thus the flow pattern round the tubes is shown to be a strong function of y_P/R. Now we know that the flow pattern controls the magnitude of the convection terms in the finite - difference equations for ϕ, and hence in the equations for k and T. Therefore it seems reasonable to deduce that the apparent influence of y_P/R on the values of local and mean Stanton numbers (which are functions of k and T at the near - wall nodes) and on Euler number (which is a function of k, ε and ψ in the main field) is primarily due to the influence of y_P/R on the flow pattern.

We also know that the flow pattern in any flow field is a function of the stream function and vorticity distributions. Now it can be shown that the near - wall values of local and space - average vorticity are strong functions of y_P/R. For instance, referring to equation (6.2.12), the local near - wall vorticity is given by:

$$\omega_p = - \frac{b\, u_p}{y_p}$$

In this equation ω_p is proportional to u_p and inversely proportional to y_p . But, from the power law, we know that u in the near - wall region is a weak function of y . Thus ω_p is approximately inversely proportional to y_p . Similarly, the space - average vorticity, $\bar{\omega}_p$, is also approximately inversely proportional to y_p or y_p/R . This means that the influence of $\bar{\omega}_p$ in the equation for near - wall ψ_p decreases with increasing y_p/R . The above influence is correct only in flows where the near - wall velocity profile is at least approximately described by the power law. However in flows, where reattachment and separation points occur, the above influence is far from correct. Thus for flow over in - line tube banks, this influence leads to the characteristic in Fig. 6.4.4 (b).

How can the undesirable influence of y_p/R be removed? The answer lies mainly in the generation of wall functions which will produce accurate predictions of flows with and without separation and reattachment points. One of the weaknesses of the present wall functions is the assumption that the shear stress, τ, is constant in the near - wall Couette flow region. However for the sake of generality and of removing the influence of y_p/R , future sets of wall functions should satisfy the full Couette flow equation, $\tau = \tau_s + \frac{dp}{dx}\, y$,

where, τ_s = wall shear stress

dp/dx = pressure gradient parallel to the wall

y = normal distance from the wall

Nevertheless it is possible that the use of wall functions based on the assumption of one - dimensional flow in the near - wall region is not in general satisfactory. Therefore to achieve complete generality it may be necessary to generate special two - dimensional flow wall functions to deal with separated and reattachment flow regions.

The above elaborations have not been attempted here, so we should now consider the value of the present set of predictions. As mentioned above, the wall functions based on the one - dimensional flow assumption should satisfy the full Couette flow equation; and indeed the present wall functions can be made to satisfy the latter (at least approximately) by making y_P/R very small. However, because of the use of the new - upwind method, converged solutions for $y_P/R < 0.02$ are not obtainable. So the best we can do is to extrapolate plots, such as those in Fig. 6.4.4, to a value of $y_P/R = 0$. Referring to Fig. 6.4.4, all the plots against y_P/R produce sensible results at $y_P/R = 0$. However our only measure of accuracy is obtained by comparing the predictions with available experimental results. For example, the results of Hammeke et al (1967) for $Re = 10^5$ are:

$$\overline{St} = 0.00478$$

$$Eu = 0.070$$

The corresponding predicted values for $y_P/R = 0.02$ are:

$$\overline{St} = 0.00334$$

$$Eu = 0.057$$

In this case, the Stanton number is under - predicted by about 29% and Euler number by about 19%. Better agreement with the experimental values is obtained as y_P/R increases. However as y_P/R increases, h_E/R decreases to values much smaller than one would expect in practice. Therefore for this reason the predictions for $y_P/R = 0.02$ are taken to be the most reliable. All the predictions discussed below have been

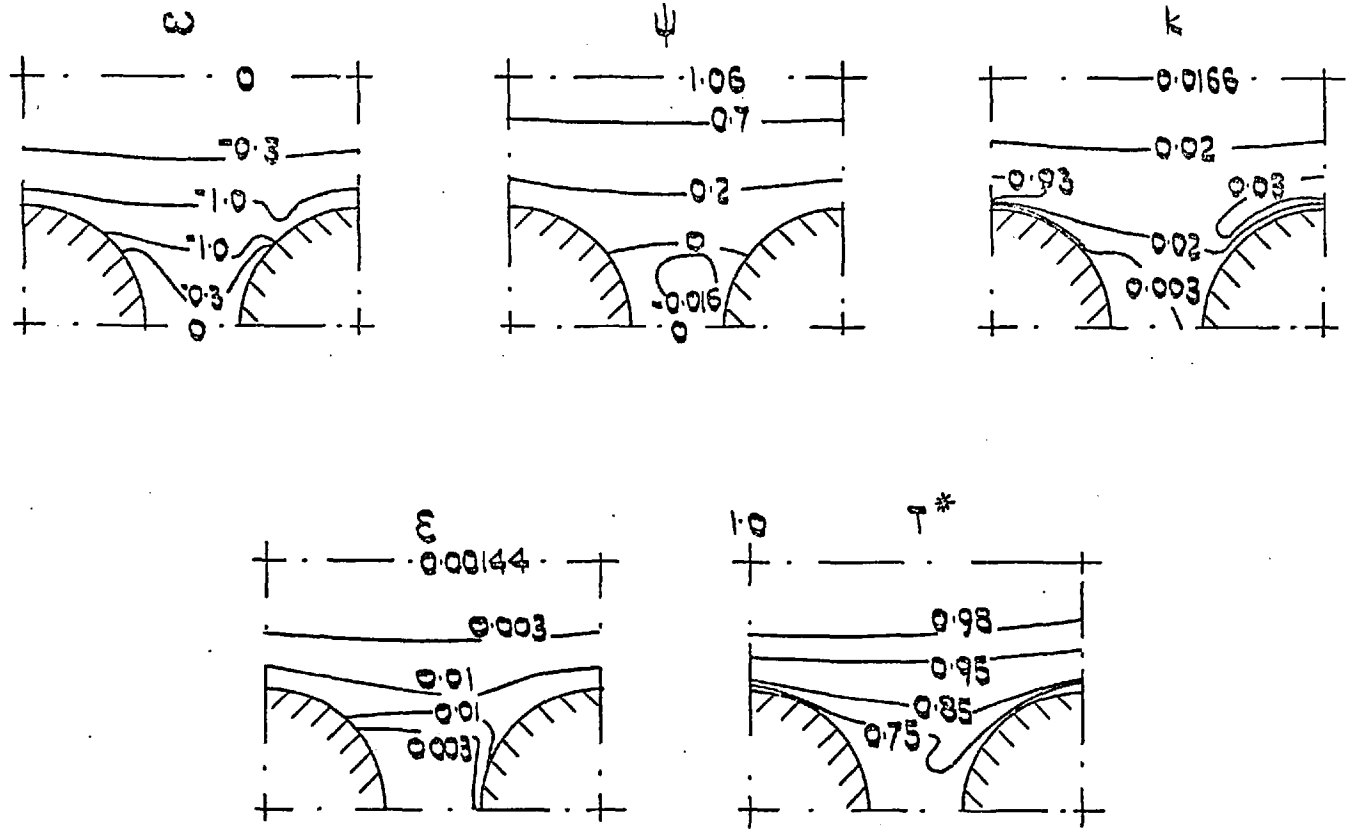


FIG.6.4.5: CONTOURS OF ω, ψ, k, ε AND T^* FOR TURBULENT FLOW THROUGH AN IN-LINE BANK WITH $S_T = 2{\cdot}06$, $S_L = 1{\cdot}38$, $Re = 10^5$, $Pr = 0{\cdot}7$ AND T_s = CONSTANT

produced with a $y_p/R = 0.02$.

(b) Contours of the dependent variables

Contour plots of $\omega, \psi, k, \varepsilon$ and T^* for fully - developed flow through an in - line tube bank with $S_T = 2.06$, $S_L = 1.38$, $Re = 10^5$, $Pr = 0.7$ and T_s = constant are shown in Fig. 6.4.5. One of the main features of these contours is that the maximum near - wall gradients of k and T^* (or T) occur near the reattachment point and the top of the tubes. Now the reattachment point for these results (with $y_p/R = 0.02$) occurs at $\theta = 145.6$, but from Fig. 6.4.3 the maximum value of Stanton number occurs at $\theta = 120$. It is however well known that maximum rates of heat transfer in turbulent flow usually occur at reattachment points, and one would expect the latter to be also true of flow through in - line tube banks. In the case of the present predictions, the large difference between the positions of reattachment and maximum Stanton number is largely due to the fact that the wall functions are not satisfactory for this particular flow.

(c) Comparison of measured and predicted values of kinetic energy of turbulence

Very few measurements of turbulence quantities have been performed in tube banks. This is because of the difficulties of probing between bundles of tubes and the difficulty of interpreting the measurements. However the recent results of Pearce (1972) do give some guide concerning the magnitude of the kinetic energy of turbulence for fully - developed flow through in - line tube banks. Pearce's results are in terms of $\frac{\overline{u'^2} + \overline{v'^2}}{2\,\overline{U}^2}$, where,

u', v' = the fluctuating components of velocity in the x_1 and x_2 directions respectively

$\overline{U}$ = mean velocity in the minimum section between the tubes

and, $\frac{\overline{u'^2} + \overline{v'^2}}{2\,\overline{U}^2}$ can be regarded as approximately equal to $k/\overline{U}^2$.

As mentioned earlier in 6.4.2 (a), Pearce's results for an in - line bank, 1.89 x 1.89, show that for a constant value of Re the value of $k/\bar{U}^2$ rises from the first tube row up to the fifth row and then remains constant. This shows that the flow after the fifth row is fully developed. Also his measurements at the eighth row of a ten row in - line bank with $S_T = S_L = 1.89$ show that $k/\bar{U}^2 \simeq 1.96 \times 10^{-2}$ at $Re = 1.38 \times 10^4$, and that $k/\bar{U}^2$ gradually decreases with increasing Re to $k/\bar{U}^2 \simeq 0.81 \times 10^{-2}$ at $Re = 8.07 \times 10^4$. The latter result is somewhat surprising when compared with the turbulence measurements of Clark (1968) in fully - developed channel flow. In the latter case, which is similar to fully - developed flow through in - line tube banks when S_L is small, measurements of $k/\bar{U}^2$ do not show much variation with Re in the range $1.5 \times 10^4 \leq Re \leq 4.5 \times 10^4$, where, $Re = \bar{U}h/\nu$

$\bar{U}$ = mean velocity

h = channel half - width

The fact that S_L for the bank $S_T = S_L = 1.89$ is large may be a governing factor in the variation of $k/\bar{U}^2$ with Re.

Assuming that the measurements are reliable, we now compare the measurements of Pearce (1972) with the present predictions for an in - line tube bank with $S_T = S_L = 1.89$. The comparison is illustrated in Table 6.4.1. The predictions are of the same order as the measurements, but are independent of Re. This is because at high Re, μ_{eff} is assumed to be much greater than the molecular viscosity μ, and thus the latter does not enter the equations for the present model of turbulence.

$S_T \times S_L$	Re	Fully - developed values of $k/\bar{U}^2$	
		Measured *	Predicted
1.89 x 1.89	1.38×10^4	1.96×10^{-2}	2.68×10^{-2}
	3.88×10^4	1.20×10^{-2}	2.68×10^{-2}
	8.07×10^4	0.81×10^{-2}	2.68×10^{-2}

Table 6.4.1

(d) Comparison of the predicted and measured bulk data

Some comparisons with the bulk data of Hammeke et al for an in - line bank with $S_T = 2.06$ and $S_L = 1.38$ have already been discussed in 6.4.4 (a). It was shown in 6.4.4 (a) that for $Re = 10^5$ the predicted values of Eu for a grid of 22 x 16 ($y_p/R = 0.02$) is 0.057 and that the corresponding measured value is 0.070. Indeed both the predicted and measured values of Eu are independent of Re. However it was shown in 6.4.4 (a) that the predicted Eu results are strongly dependent on y_p/R, so that although the above comparison is encouraging further research will be required to produce predictions which are independent of y_p/R.

---

* The values of $k/\bar{U}^2$ were measured on the centre - line between the longitudinal rows of tubes at the 8th row in a 10 - row bank

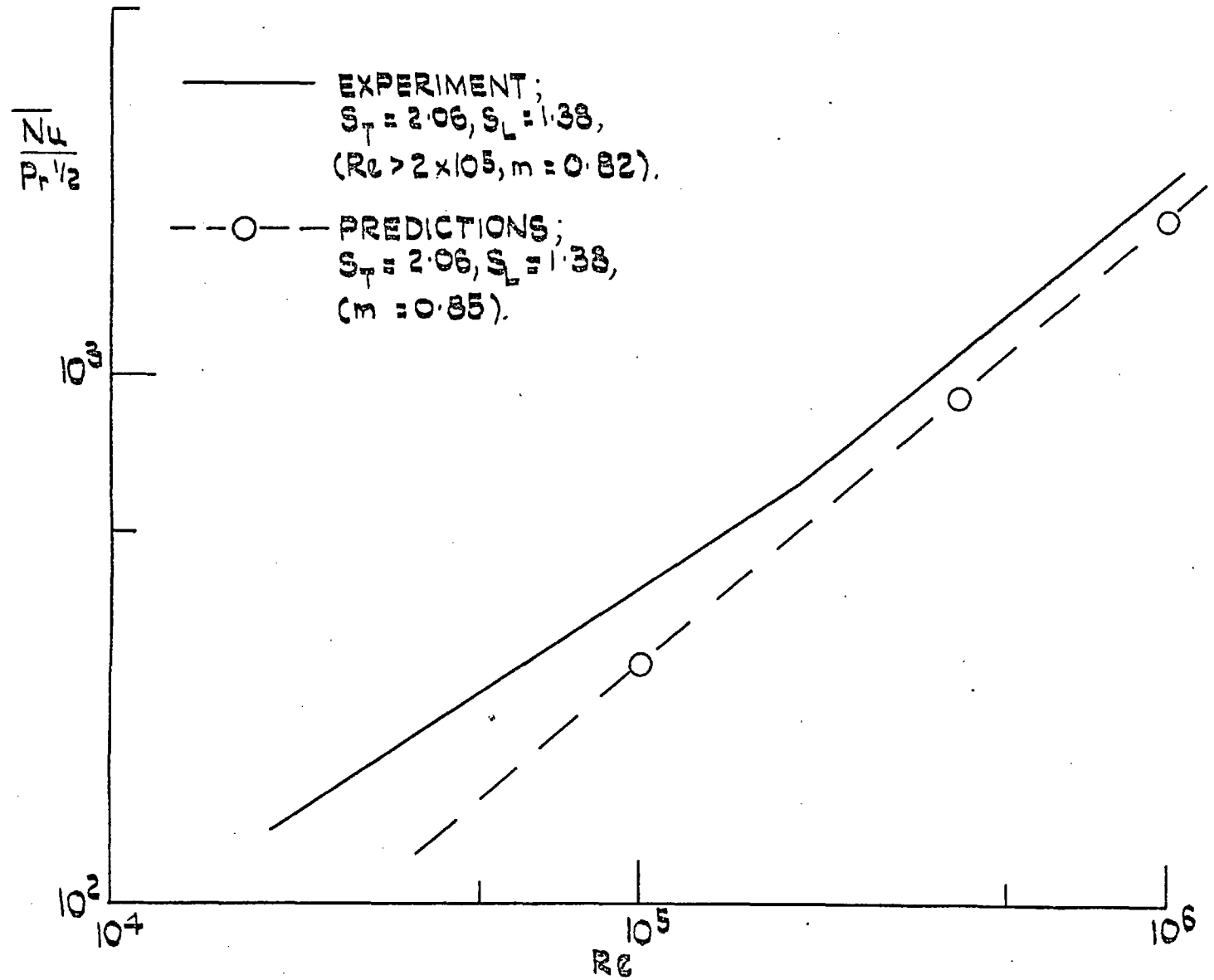


FIG.6.4.6: PREDICTIONS OF NUSSELT NUMBER COMPARED WITH THE MEASUREMENTS OF HAMMEKE ET AL.

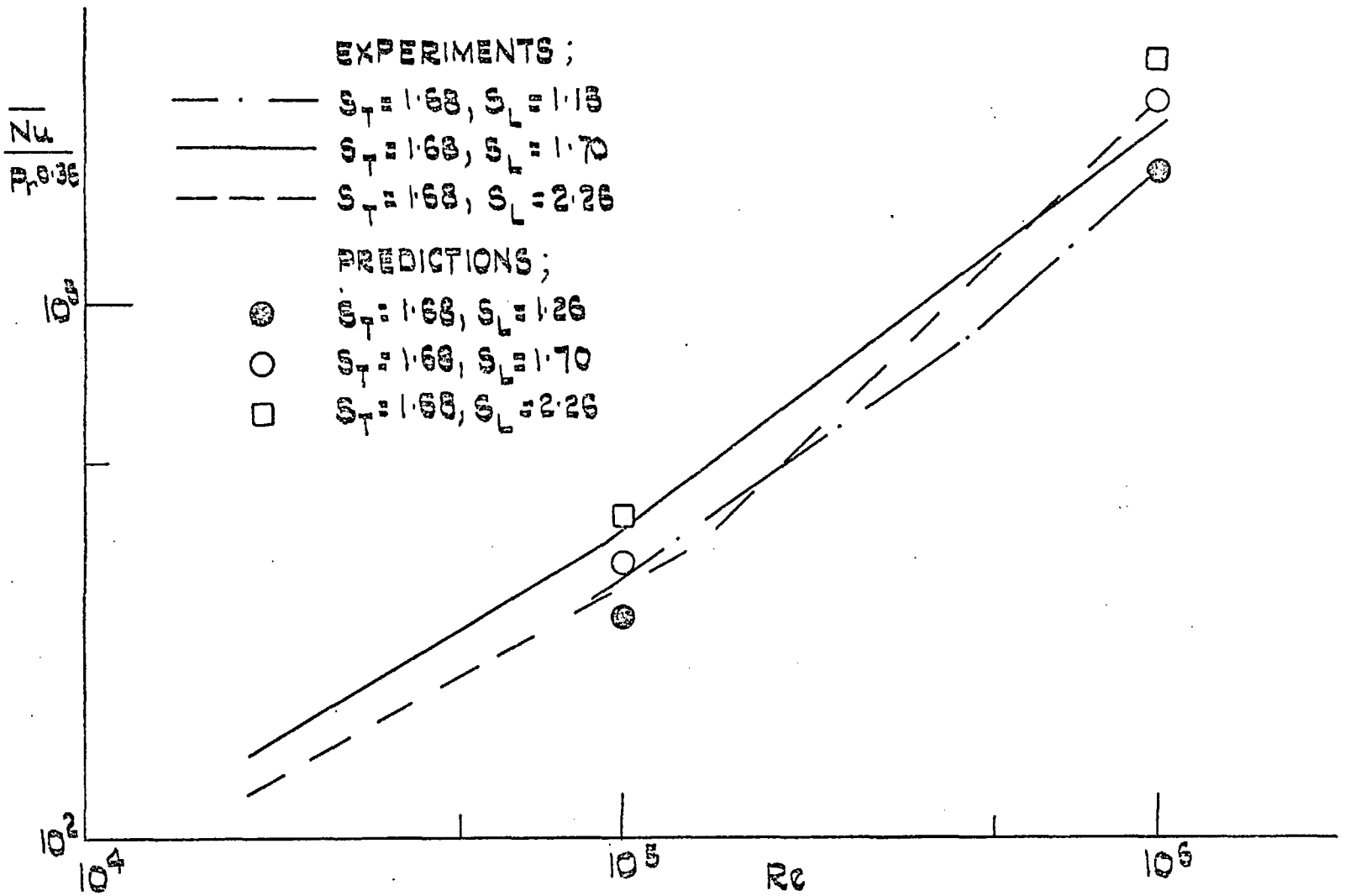
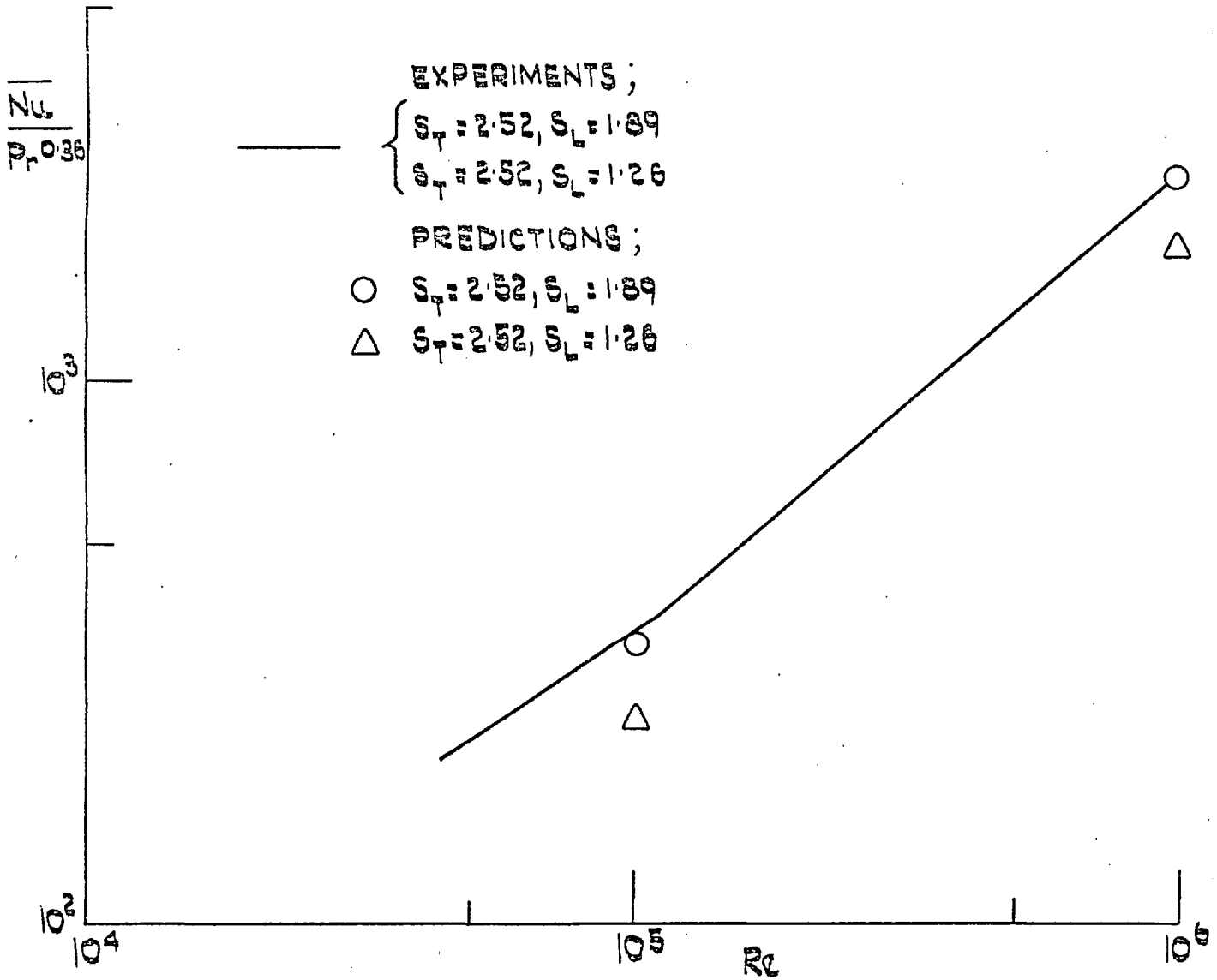


FIG.6.4.7: PREDICTIONS OF NUSSELT NUMBER COMPARED WITH THE MEASUREMENTS OF STASYULYAVICHYUS AND SAMOSHKA.



6.48: PREDICTIONS OF NUSSELT NUMBER COMPARED WITH THE MEASUREMENTS OF STASYULYAVICHYUS AND SAMOSHKA.

It was also shown in 6.4.4 (a) that the predictions of $\overline{St}$ are much less dependent on y_p/R than the predictions of the Eu and h_E/R parameters. It is therefore worth pursuing the comparisons of the predictions and measurements of bulk heat transfer characteristics. The comparisons with the measurements of Hammeke et al are illustrated in Fig. 6.4.6. This plot shows that for $Re > 2 \times 10^5$ the measurements are under - predicted by only about 20% and that the measurements and predictions have approximately the same Reynolds number exponent m.

Further comparisons of predicted and measured heat transfer data are shown in Figs. 6.4.7 and 6.4.8. In these figures, the appropriate predictions at $Re = 10^5$ and 10^6 are compared with the measured characteristics of Stasyulyavichyus and Samoshka (1968). In Fig. 6.4.7, the predicted results for the banks, 1.68 x 1.70 and 1.68 x 1.26, compare quite closely with the measurements for the banks, 1.68 x 1.70 and 1.68 x 1.13 respectively. However the slopes of the respective measured and predicted characteristics are not exactly the same. For the 1.68 x 2.26 bank, the discrepancies between the measurements and predictions are much larger than for the other two banks. Indeed the measured characteristic slope for the bank 1.68 x 2.26 is very different from those for the 1.68 x 1.70 and 1.68 x 1.13 banks. This difference may well be connected with the influence of vortex shedding as discussed in section 6.4.2 (d). Thus the results for the larger bank, 1.68 x 2.26, may be strongly influenced by vortex shedding, whereas the influence of the latter may be suppressed in the smaller banks, 1.68 x 1.70 and 1.68 x 1.13.

In Fig. 6.4.8, it is encouraging to note that there is close comparison between the predictions and measurements for the bank, 2.52 x 1.89. But the predictions for the bank, 2.52 x 1.26, fall well

below the corresponding measurements, which coincide with those of the 2.52 x 1.89 bank. These measurements suggest that if S_T is large enough the heat transfer results are independent of S_L in the range $1.26 \leq S_L \leq 1.89$. The reasons for this are probably very complex, but it is obvious that the present turbulence model and wall functions cannot predict this characteristic.

The predictions and mean measurements (for the range $10^5 \leq Re \leq 10^6$) of pressure drop, which correspond to the heat transfer data in Figs. 6.4.7 and 6.4.8, are shown in Table 6.4.2. Except for the 1.68 x 2.26 bank

S_T	S_L	Euler Number	
		Measured	Predicted
1.68	1.26	0.086	0.061
1.68	1.70	0.100	0.092
1.68	2.26	0.113	0.160
2.52	1.26	0.050	0.043
2.52	1.89	0.071	0.084

Table 6.4.2

results, the predictions compare reasonably well with the measurements. This suggests that the hydrodynamics of the main flow region above the recirculation eddy (which has some similarities to flow through a channel) are predicted correctly using grids with $y_P/R = 0.02$. The latter may be inferred because the pressure drop is calculated from the numerical integration of the momentum equation in the main flow region. However

as the results are dependent on y_P/R, these comparisons can only be regarded as encouraging and not as yet successful.

6.5 Discussion of results

It is now appropriate to summarise the results given in sections 6.3 and 6.4. In section 6.3, the predictions of fully - developed channel flow compare closely with the measurements. This means that the present turbulence model and wall functions are satisfactory for this particular flow situation. However in the prediction of developing flow in a channel the predictions for $x_1/d_e > 1.5$ are satisfactory but large discrepancies between the predicted and measured values of Stanton number occur for $x_1/d_e < 1.5$. These discrepancies are mainly due to the fact that the inlet near - wall boundary conditions are not satisfactory. Corrections to the latter, which would reduce the above discrepancies considerably, are suggested.

In section 6.4, the limitations of the present turbulence model and wall functions are outlined, and in the light of these limitations the review of appropriate tube bank data is concerned mainly with data for $Re \geq 10^5$. Also due to the above limitations we restrict ourselves to the prediction of fully - developed flow through in - line tube banks for $Re \geq 10^5$.

The initial results of flow through in - line tube banks indicate that the predictions are dependent on the grid parameter, y_P/R. The reason for the influence of y_P/R is due to the inadequacy of the present wall functions, which are applicable only to fully - developed zero - pressure - gradient turbulent boundary layers. However the trends and magnitudes of the mean Stanton number predictions compare reasonably well with most of the measurements of Hammeke et al and Stasyulyavichyus and Samoshka. It is also encouraging to note that the predicted values of

pressure drop, corresponding to the above predictions of heat transfer, compare quite closely with the mean measured values in the range $10^5 \leq Re \leq 10^6$. But all the above predictions are dependent on the chosen grid condition, $y_p/R = 0.02$. The latter dependency can only be removed by the use of more general wall functions which can produce accurate predictions of both reattachment and separation points.

7. DISCUSSION AND CONCLUSIONS

The previous chapters 4 to 6, which are concerned with predictions and comparisons with other data, each contain a discussion of results; but in order to obtain an eagle's view of the territory covered we need a concluding chapter in which the main findings of this thesis are drawn together. Section 7.1 seeks to summarise the results of this work; and section 7.2 makes a number of recommendations concerning avenues for future research.

7.1 Summary of the main results

7.1.1 Introduction to summary

The results of this thesis can best be considered in two distinct parts. The first part, which concerns the development of the numerical method, is described in 7.1.2; and the second part, which considers the application of the turbulence models, is considered in 7.1.3.

7.1.2 The development of the numerical method

Most research work seeks to build on the progress make by other workers, and the present work is no exception. Much of the work of this thesis is based, at least initially, on the work described by Gosman et al (1969). The latter authors describe a numerical procedure for solving the conservation of mass, momentum and energy equations for two-dimensional flow situations, which may include recirculation. The procedure is a general one as it can theoretically solve problems of flow in domains of arbitrary shape. However in general before the solution procedure can be put into effect it is necessary to calculate an orthogonal grid to map the domain of interest. This requirement brings to light one drawback of the procedure because the available methods for calculating all the required orthogonal grid components are complicated and laborious. It is true that many domains can be mapped orthogonally using rectangular, cylindrical and spherical co-ordinates, but there are many other domains of engineering interest which do not fall into this category.

The present work makes some contribution towards overcoming the above limitation. This is done by the introduction of the RAND grid arrangements and the corresponding numerical equations. The main advantage of the RAND grids is that they may be quickly calculated for domains of any shape. But depending on the shape of the domain and the flow pattern, numerical errors due to false diffusion may limit the validity of the predictions. This work suggests a means of reducing the effects of false diffusion by the introduction of the new - upwind scheme for approximating the convection terms in the conservation equations. This scheme does not however adequately fulfil Scarborough's convergence criteria and thus the numerical procedure can only be applied under restricted conditions, which nevertheless include some turbulent flows. The predictions summarised below demonstrate the properties of the numerical procedure using the RAND grid arrangements.

(a) Flows with analytical solutions

As with all new tools, the procedure requires testing to establish its advantages and weaknesses. This is achieved by applying the procedure to two flows with analytical solutions, and to laminar flow over a single cylinder for which there are many other numerical predictions and experimental measurements. The predictions of the flows with analytical solutions demonstrate the accuracy of the new - upwind scheme used in association with the RAND grid arrangement. However due to the non - satisfaction of Scarborough's convergence criteria at high Reynolds numbers, these predictions also demonstrate the restricted use of the new - upwind scheme.

(b) Laminar flow over a single cylinder

Predictions of the hydrodynamic and heat transfer properties of laminar flow over a single cylinder at $Re = 40$ are shown to be in close agreement with a wide range of measurements and other predictions. However the applicability of the procedure to this problem is limited to low Reynolds numbers, i.e. $Re < 100$, for two reasons.

The first reason concerns the boundary layer thickness near the front

stagnation point of the cylinder. This is known to be inversely proportional to the square root of the Reynolds number. Thus the boundary layer thickness decreases with increasing Reynolds number. This means that if we are to obtain correct predictions of this flow (at least on the front face) at high Re , the RAND grid must be refined in the region adjacent to the front face. However the RAND grid cannot be economically refined in one region of a domain without producing extra grid nodes in other less important parts of the field. One solution to this problem is the use of a hybrid grid system, where the grid in the near-wall region is orthogonal (i.e. a cylindrical co-ordinate grid in the case of the cylinder) and the grid away from the wall is rectangular. Thoman and Szewczyk (1969) describe the application of a version of such a grid arrangement.

The second reason concerns the new-upwind scheme which causes the divergence of the numerical procedure for $Re > 100$. This means that if a hybrid grid arrangement were applied to the problem of flow over a single cylinder at high Reynolds numbers, convergence could only be achieved by using the standard-upwind scheme.

(c) Laminar flow over in-line tube banks

The usefulness of the RAND grid solution procedure is demonstrated by the predictions of laminar flow over in-line tube banks. As no other predictions are known for this problem, the accuracy of the predictions is checked by comparing solutions which differ only by the fineness of the grid. The latter comparisons indicate that the predictions are independent of the grid mesh and therefore are reliable. Further proof of accuracy is given by the close comparison between the predictions and available measurements of Euler number for $Re \leq 100$. The heat transfer predictions correspond to fully-developed thermal conditions for which there are no experimental results, but by comparison with available experimental trends the fully developed values are shown to be of the correct order.

7.1.3 The application of the turbulence models

We now consider the results of incorporating a turbulence model into the solution procedure. The validity of the model is tested initially by applying the solution procedure to the relatively simple problem of developing turbulent flow in a parallel channel. The predictions for $x_1/d_e \geq 1.5$ are in good agreement with the measurements, but significant discrepancies are evident for $x_1/d_e < 1.5$. It is indicated that the latter can be removed by the use of more accurate inlet boundary conditions.

Although developing flow in a channel can be predicted satisfactorily by using the present turbulence models, the latter are not designed as yet to produce accurate predictions of the following flow situations:

(a) situations where transition from laminar to turbulent boundary layers occur

(b) situations where there are large pressure gradients along wall boundaries

(c) situations where vortex shedding is a controlling factor in the flow pattern

However there are some flow situations exhibiting recirculation where the influences of the above may not be important. The results of a careful examination of data for flow over single cylinders and tube banks indicate that fully - developed flow over in - line tube banks for $Re > 10^5$ may not be greatly affected by the above flow phenomena. Thus one might expect that the predictions should be reasonably accurate. Indeed the results show that the predicted Stanton and Euler numbers display the correct trends and the correct orders of magnitude, but unfortunately the predictions are somewhat dependent on the grid parameter y_p/R. This dependency is mainly due to the inadequacy of the present wall functions, which are based on the simple assumption that zero - pressure - gradient conditions exist at all points on wall boundaries. The predictions

are obviously sensitive to the inadequacy of the above assumption.

7.2 Recommendations for future research

The discussion in this section focuses on some of the points raised in the previous section. When considering future research it is useful to continue thinking in terms of the distinct categories of numerical procedures and turbulence models. We shall consider the former first of all.

(a) Numerical procedures

As pointed out in 7.1.1, the RAND grid arrangement and its solution procedure suffer from one main limitation, that of being applicable to laminar flows with low Reynolds numbers. This is because the grid cannot be refined economically along non - rectangular boundaries and also because the new - upwind scheme causes the solution procedure to diverge at high values of Reynolds number. In order to achieve economic distributions of fine grids along non - rectangular boundaries it would appear that the most promising alternative to the RAND grid is the hybrid grid system. Thus a thorough investigation should be directed at the optimisation of numerical schemes associated with a given hybrid grid layout. Also further research on means of procuring unconditional convergence using the new - upwind scheme should be carried out. Alternatively, a search for other methods of reducing the influence of false diffusion at high Reynolds numbers may be more profitable.

(b) Turbulence models

As regards the turbulence models, the present work indicates the need for wall functions which can produce accurate predictions of both separation and reattachment regions, i.e. where wall pressure gradients are not zero. Most of the previous turbulent recirculating flow problems, e.g. Runchal (1969) and Roberts (1972), involved separation points due to

the geometry of the confined flow. The present problem of flow over in - line tube banks involves flow separation due to adverse pressure gradients round the upstream tube. Such problems require wall functions which are strongly sensitive to wall pressure gradients and are largely independent of the grid node distribution in the near - wall region.

One possible 'short - term' method of overcoming the limitations of the present wall functions is to use the low Reynolds number model of turbulence of Jones and Launder (1972) as a replacement for the high Reynolds number model and the wall functions. As the low Reynolds number model describes the variation of k, ε and μ_{eff} down to the wall, very fine near - wall grid distributions must be used but this means that the wall functions are no longer required. Research into the application of the low Reynolds number model to recirculating flow problems may not only provide solutions which are independent of grid distribution and reasonably accurate, but may also give pointers concerning the generation of appropriate wall functions.

However the generation of such wall functions should not be divorced from what might be called the 'long - term' objective of producing satisfactory turbulence models for recirculating flows. The work of Jones and Launder (1972) shows that two - equation models of turbulence can be used to give accurate predictions of a wide range of two - dimensional boundary layer flows with and without large pressure gradients. The reasons for these good results are that the flow near the wall boundary is correctly modelled, and also that the flow consists of a single dominant velocity gradient. For the latter the scalar effective viscosity model is known to give good predictions. However the accuracy of applying such models to two - dimensional recirculating flows is known to have some weaknesses. For instance, Roberts (1972) shows that incorrect predictions of swirling flows are obtained if one assumes that the effective viscosity is a scalar quantity. Perhaps the latter is an extreme example of the

weakness of the two - equation model, but on the other hand further evidence is required to show that a scalar effective viscosity model gives accurate modelling of two - dimensional non - swirling recirculating flows. Another problem concerns the constants in the turbulence model equations. It is likely that these so - called constants are not in general constants but are in fact functions of parameters such as the local Reynolds number of turbulence. The above matters require further investigation in conjunction with the development of satisfactory wall functions.

The progress of the numerical analyst in this field will depend largely on the supply of accurate and comprehensive data obtained from relatively simple two - dimensional flows, such as the free jet impinging on a plane. Therefore to meet this need much further research should be devoted to the task of supplying accurate measurements of time - averaged turbulence and mean flow parameters in such flows.

Appendix A.1: The error due to the standard – upwind scheme for the convection terms

In this appendix, more details of the truncation error due to the standard – upwind difference scheme are provided. The purpose of providing these details, which are abstracted from the work of Wolfshtein (1967), is to indicate which parameters are the most influential in controlling the magnitude of the error.

In his investigation, Wolfshtein considered the very simple problem of a source of property ϕ in a zero – viscosity uniform – velocity stream, which is inclined at an angle β to the mesh lines. The exact solution to this problem is that no diffusion occurs and ϕ remains constant along any streamline. Fig. A.1.1 illustrates the comparison between the exact and predicted solutions at some distance downstream from the point source. The predictions obviously cause a smearing of the exact ϕ profile and this smearing suggests that 'false' diffusion of the property ϕ occurs in the direction normal to the stream.

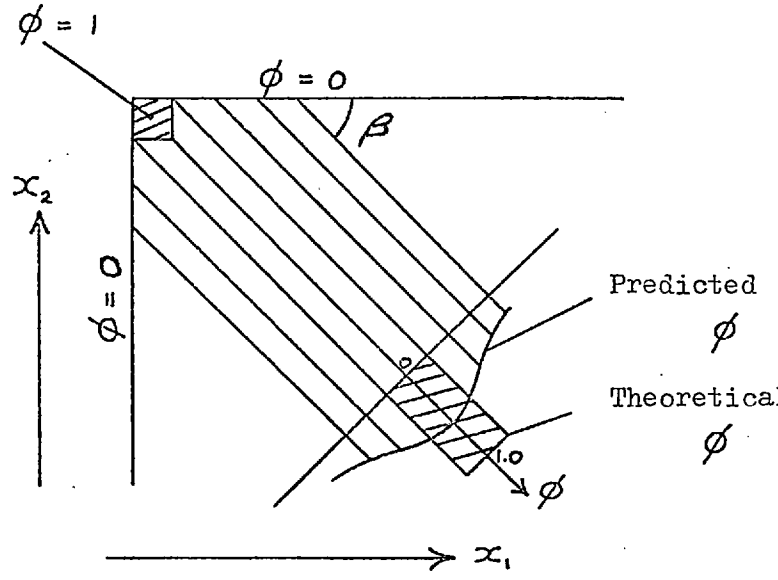


Fig. A.1.1

Wolfshtein showed that the appropriate expression for the false diffusion coefficient, Γ_{false}, which is responsible for the false diffusion effect is:

$$\Gamma_{false} = 0.36 \rho V h \sin 2\beta$$

where, V = uniform stream velocity

h = uniform mesh size

β = angle of inclination of the streamlines to the mesh

For the purpose of estimating the effect of this coefficient in the calculation of flows with non - zero viscosity, Wolfshtein expressed the equation for Γ_{false} in the following form:

$$\frac{\Gamma_{false}}{\Gamma_{eff}} = 0.36\, R_{eff}\, \sigma_{eff}\, \frac{h}{L} \sin 2\beta \qquad \text{(A.1.1)}$$

where, $R_{eff} = \frac{VL}{\nu_{eff}}$ = local effective Reynolds number

$\sigma_{eff} = \frac{\mu_{eff}}{\Gamma_{eff}}$ = effective Prandtl number

L = appropriate dimension of flow

It can be concluded from equation (A.1.1) that the false diffusion error in terms of the false diffusion coefficient is a function of the effective Reynolds and Prandtl numbers, the relative grid size and, most important of all, the angle β . So when the standard - upwind scheme is applied to the prediction of uniform viscosity laminar flows, it is obvious from equation (A.1.1) that the false diffusion coefficient can become much larger than the real diffusion coefficient where $\beta \neq 0$, $\sigma_{eff} \geq 1$ and the local Reynolds number is very large. Nevertheless it is encouraging to note that for a given Reynolds number based on laminar viscosity, the ratio of the false diffusion coefficient with respect to the real diffusion coefficient for a turbulent flow is always much smaller than for the equivalent laminar flow situation with $\sigma \geq 1$. This is because the turbulent effective viscosity is always much larger than the laminar viscosity and the turbulent effective Prandtl number is of the order unity. However in both laminar and turbulent flow situations false diffusion is never entirely eliminated unless either $h \to 0$ or $\beta = 0$. The former is not a practical proposition from the point of view of

computer storage and time, and the latter usually occurs only in limited regions of a recirculating flow.

Appendix A.2: The calculation of parameters associated with the new - upwind method of approximating the convection terms in equation (3.2.1)

In this appendix, we illustrate the method of calculating the G's in equation (3.2.17), where the latter is the expression for the new - upwind approximation of the convection terms. To illustrate the method, we shall focus our attention on the G's relevant to the expression for the east boundary of a typical cell, equation (3.2.15). For ease of reference, equation (3.2.15) is repeated here as follows:

$$
\begin{aligned}
I_c = {} & \mathcal{P}_{PE}\left\{A_{E2}\left[\phi_P(1-G_{EP}) + \phi_{SE}\,G_{EP}\right]\right. \\
& \left. - A_{E1}\left[\phi_E(1-G_{EE}) + \phi_N\,G_{EE}\right]\right\} \\
& + \mathcal{P}_{ME}\left\{A_{E2}\left[\phi_P(1-G_{EP}) + \phi_{NE}\,G_{EP}\right]\right. \\
& \left. - A_{E1}\left[\phi_E(1-G_{EE}) + \phi_S\,G_{EE}\right]\right\}
\end{aligned}
\qquad (3.2.15)
$$

Referring to Fig. A.2.1, which shows the east boundary of a typical cell $\mathcal{P}$, we define $(u_1)_e$, $(u_2)_e$ and α as follows:

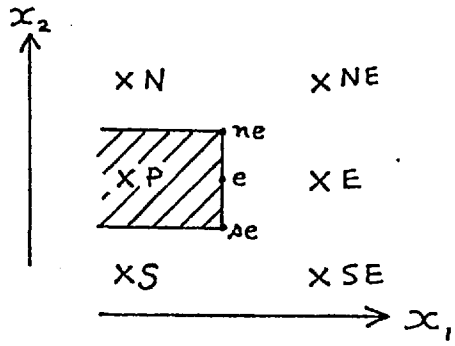


Fig. A.2.1

$$
(u_1)_e = \left(\frac{1}{\rho}\frac{\partial\psi}{\partial x_2}\right)_e \approx \frac{2}{\rho}\left(\frac{\psi_{ne}-\psi_{se}}{x_{2,N}-x_{2,S}}\right)
$$

$$
\approx \frac{1}{2\rho}\left(\frac{\psi_{NE}+\psi_N-\psi_{SE}-\psi_S}{x_{2,N}-x_{2,S}}\right) \qquad (A.2.1)
$$

$$
(u_2)_e = -\left(\frac{1}{\rho}\frac{\partial\psi}{\partial x_1}\right)_e \approx -\frac{1}{\rho}\left(\frac{\psi_E-\psi_P}{x_{1,E}-x_{1,P}}\right) \qquad (A.2.2)
$$

$$\alpha = (u_2)_e / (u_1)_e \qquad \text{(A.2.3)}$$

where, $(u_1)_e$ and $(u_2)_e$ are the velocity components through point e in the x_1 and x_2 directions respectively.

We now consider the special situation in Fig. A.2.2, where the velocity vector for the case $(u_1)_e > 0$ and $(u_2)_e > 0$ is at an angle $\beta_e = \tan^{-1}\alpha$ to the vector for $(u_2)_e = 0$ and $(u_1)_e > 0$. An extension of the vector $(u_1)_e > 0$ and $(u_2)_e > 0$ intersects the line between nodes P and SE at a point F.

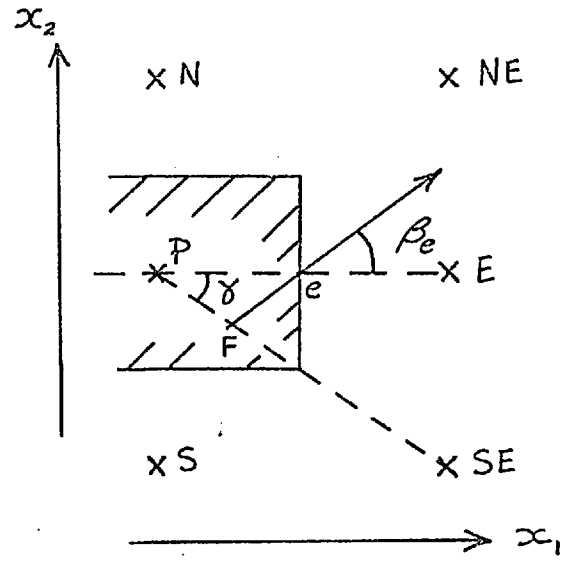


Fig. A.2.2

It can be easily shown that, for this case, equation (3.2.15) reduces to:

$$I_c = A_{E2}\left[\phi_P(1 - G_{EP}) + \phi_{SE}\, G_{EP}\right] \qquad \text{(A.2.4)}$$

From our knowledge of the node co - ordinates and the parameter α, G_{EP} can be determined as follows:

$$G_{EP} = \ell_1 / \ell_2$$

where, ℓ_1 = distance between node P and point F

ℓ_2 = " " " P and node SE

From the triangle PFe:

$$\ell_1 = \frac{(x_{1,E} - x_{1,P}) \sin\beta_e}{2 \sin(\beta_e + \gamma)}$$

$$\therefore\ G_{EP} = \frac{(x_{1,E} - x_{1,P})\sin\beta_e}{2\ell_2 \sin(\beta_e + \gamma)}$$

$$= \frac{(x_{1,E} - x_{1,P})\sin\beta_e}{2\ell_2(\sin\beta_e\cos\gamma + \cos\beta_e\sin\gamma)}$$

$$\therefore\ G_{EP} = \frac{(x_{1,E} - x_{1,P})}{2\left[(x_{1,E} - x_{1,P}) + (x_{2,P} - x_{2,S})/\alpha\right]} \qquad \text{(A.2.5)}$$

Therefore the relevant parameters for the flow situation in Fig. A.2.2 may be summarised as follows:

(a) $(u_1)_e > 0,\ (u_2)_e > 0, \qquad 0 < \beta_e < \pi/2$

$$P_{PE} = 1.0,\ P_{ME} = 0.0,\ G_{EP} = \frac{(x_{1,E} - x_{1,P})}{2\left[(x_{1,E} - x_{1,P}) + (x_{2,P} - x_{2,S})/\alpha\right]}$$

similarly for,

(b) $(u_1)_e < 0,\ (u_2)_e < 0, \qquad \pi < \beta_e < 3\pi/2$

$$P_{PE} = 1.0,\ P_{ME} = 0.0,\ G_{EE} = \frac{(x_{1,E} - x_{1,P})}{2\left[(x_{1,E} - x_{1,P}) + (x_{2,N} - x_{2,P})/\alpha\right]}$$

(c) $(u_1)_e > 0,\ (u_2)_e < 0, \qquad 3\pi/2 < \beta_e < 2\pi$

$$P_{PE} = 0.0,\ P_{ME} = 1.0,\ G_{EP} = \frac{(x_{1,E} - x_{1,P})}{2\left[(x_{1,E} - x_{1,P}) + (x_{2,N} - x_{2,P})/\alpha\right]}$$

(d) $(u_1)_e < 0,\ (u_2)_e > 0, \qquad \pi/2 < \beta_e < \pi$

$$P_{PE} = 0.0,\ P_{ME} = 1.0,\ G_{EE} = \frac{(x_{1,E} - x_{1,P})}{2\left[(x_{1,E} - x_{1,P}) + (x_{2,P} - x_{2,S})/\alpha\right]}$$

Similar formulae for the other G's can easily be derived.

REFERENCES

ACRIVOS, A., SNOWDEN, D.D., GROVE, A.S. and PETERSEN, E.E. (1965). 'The steady separated flow past a circular cylinder at large Reynolds numbers'. J.Fluid Mech., 21, pp 737-760.

ACRIVOS, A., LEAL, L.G., SNOWDEN, D.D. and PAN, F. (1968). 'Further experiments on steady separated flows past bluff objects'. J. Fluid Mech., 34, pp 25-48.

APELT, C.J. (1958). 'The steady flow of a viscous fluid past a circular cylinder at Reynolds numbers 40 and 44'. A.R.C. 20, 502.

BARFIELD, W.D. (1970). 'Numerical method for generating orthogonal curvilinear meshes'. J.Comp.Phys., 5, pp 23-33.

BAULY, J.A. (1971). 'Vortex shedding in tube banks'. Symposium on Internal Flows, University of Salford, 20-22 April, 1971, Paper 25, pp D1-D9.

BERGELIN, O.P., DAVIS, E.S. and HULL, H.L. (1949). 'A study of three tube arrangements in unbaffled tubular heat exchangers'. Trans. ASME, 71, pp 369-374.

BERGELIN, O.P., BROWN, G.A., HULL, H.L. and SULLIVAN, F.W. (1950). 'Heat transfer and fluid friction during viscous flow across banks of tubes - III; a study of tube spacing and tube size'. Trans. ASME, 72, pp 881-888.

BERGELIN, O.P., BROWN, G.A. and DOBERSTEIN, S.C. (1952). 'Heat transfer and fluid friction during flow across banks of tubes - IV; a study of the transition zone between viscous and turbulent flow'. Trans. ASME, 74, pp 953-960.

BIRD, R.B., STEWART, W.E. and LIGHTFOOT, E.N. (1960). Transport Phenomena. John Wiley, New York.

BOUSSINESQ, T.V. (1877). Mem.pres.Acad.Sci. Third Edition, Paris XXIII, 46.

BYRNE, J., HATTON, A.P. and MARRIOTT, P.G. (1969). 'Turbulent flow and heat transfer in the entrance region of a parallel wall passage'. Proc.Instn.Mech.Engrs., 184, Pt.1, No.39, pp 697-712.

CLARK, J.A. (1968). 'A study of incompressible turbulent boundary layers in channel flow'. Trans. ASME, J. of Basic Eng., 90, pp 455-468.

COLLIS, D.C. and WILLIAMS, M.J. (1959). 'Two-dimensional convection from heated wires at low Reynolds numbers'. J. Fluid Mech., 6, pp 357-384.

COMTE-BELLOT, G. (1965). 'Écoulement turbulent entre deus parois parallèles'. Pub.Sci. et Tech. du Min de l'Air, No. 419.

DENNIS, S.C.R., HUDSON, J.D. and SMITH, N. (1968). 'Steady laminar forced convection from a circular cylinder at low Reynolds numbers'. The Physics of Fluids, 11, pp 933-940.

DENNIS, S.C.R. and CHANG, G-Z. (1970). 'Numerical solutions for steady flow past a circular cylinder at Reynolds numbers up to 100'. J.Fluid Mech., 42, pp 471-489.

ECKERT, E.R.G. and SOEHNGEN, E. (1952). 'Distribution of heat transfer coefficients around circular cylinders in crossflow at Reynolds numbers from 20 to 500'. Trans. ASME, 74, pp 343-347.

GIEDT, W.H. (1951). 'Effect of turbulence level of incident air stream on local heat transfer and skin friction on a cylinder'. J.Aero. Sci., 18, pp 725-730 and p 766.

GOSMAN, A.D., PUN, W.M., RUNCHAL, A.K., SPALDING, D.B. and WOLFSHTEIN, M. (1969). Heat and Mass Transfer in Recirculating Flows. Academic Press, London.

GOSMAN, A.D., LOCKWOOD, F.C. and TATCHELL, D.G. (1970). 'A numerical study of the heat transfer performance of the open thermosyphon'. Imperial College, Mech.Eng.Dept. Rep. EF/TN/A/27.

GROVE, A.S. (1963). Ph.D. Thesis, University of California, Berkeley.

GROVE, A.S., SHAIR, F.H., PETERSEN, E.E. and ACRIVOS, A. (1964). 'An experimental investigation of the steady separated flow past a circular cylinder'. J.Fluid Mech., 19, pp 60-68.

HAMIELEC, A.E. and RAAL, J.D. (1969). 'Numerical studies of viscous flow around circular cylinders'. The Physics of Fluids, 12, pp 11 - 17.

HAMMEKE, K., HEINECKE, E. and SCHOLZ, F. (1967). 'Heat transfer and pressure drop measurements in smooth tube bundles with transverse flow, especially at high Reynolds numbers.' Int. J. of Heat and Mass Transfer, 10, No.4, pp 427-446.

HANJALIC, K. and LAUNDER, B.E. (1971). 'A Reynolds stress model of turbulence and its application to asymmetric boundary layers'. Imperial College, Mech.Eng. Dept. Rep. TM/TN/A/8.

HARLOW, F.H. and NAKAYAMA, P.I. (1968). 'Transport of turbulence energy decay rate'. Los Alamos Sci. Lab. Univ. California Rep. LA-3854.

HARTNETT, J.P., ECKERT, E.R.G. and BIRKEBAK, R. (1959). 'Determination of convective heat transfer to non-isothermal surfaces including the effect of pressure gradient'. Proceedings of the Sixth Midwestern Conference on Fluid Mechanics, pp 47-70. Austin University Press, Texas.

HILBERT, R. (1933). Forsch. Gebiete Ingenieurw., 4, pp 215-224.

HINZE, J.O. (1959). Turbulence. McGraw-Hill, New York.

HOMANN, F. (1936). 'Einfloss grösser Zähigkeit bei Strömung um Zylinden'. Forsch. Ing. Wes., 7, p 1.

JONES, W.P. and LAUNDER, B.E. (1970). 'The prediction of laminarisation with a 2-equation model of turbulence'. Imperial College, Mech.Eng.Dept. Rep. BL/TN/A/40.

JONES, W.P. and LAUNDER, B.E. (1972). 'The calculation of low-Reynolds-number phenomena with a two-equation model of turbulence'. Imperial College, Mech.Eng. Dept. Rep. TM/TN/A/17.

KAWAGUTI, M. (1953). 'Numerical solution of the Navier-Stokes equations for the flow around a circular cylinder at Reynolds number 40'. J. Phys. Soc. Japan, 8, No.6, pp 747-757.

KNUDSEN, J.G. and KATZ, D.L. (1958). Fluid Dynamics and Heat Transfer. McGraw Hill, New York.

KOLMOGOROV, A.N. (1942). 'Equations of turbulent motion of an incompressible fluid'. (In Russian) Izv. Akad. Nauk SSR ser. Phys. No. 1-2.

LAUFER, J. (1951). 'Investigation of turbulent flow in a two-dimensional channel'. NACA Report 1053.

LAUNDER, B.E. (1971). 'Improved modelling of the Reynolds stresses'. Imperial College, Mech. Eng. Dept. Rep. TM/TN/A/9.

LAUNDER, B.E. and YING, W.M. (1971). 'Numerical solutions of flow between rotating eccentric cylinders'. Imperial College, Mech. Eng. Dept. Rep. EF/TN/A/42.

LAUNDER, B.E. and SPALDING, D.B. (1972). 'Turbulence models and their application to the prediction of internal flows'. Imperial College, Mech. Eng. Dept. Rep. TM/TN/A/18.

LE FEUVRE, R.F. (1970). 'The application of a semi-orthogonal finite-integral technique to predict inclined-plane and cylindrical Couette flows'. Imperial College, Mech. Eng. Dept. Rep. EF/TN/A/33.

McADAMS, W.H. (1954). Heat Transmission. McGraw-Hill, New York.

MUELLER, T.J. and O'LEARY, R.A. (1970). 'Physical and numerical experiments in laminar incompressible separating and reattaching flows'. AIAA Paper No. 70-763.

NG, K.H. and SPALDING, D.B. (1969). 'Some applications of a model of turbulence for boundary layers near walls'. Imperial College, Mech. Eng. Dept. Rep. BL/TN/14.

OMOHUNDRO, G.A., BERGELIN, O.P. and COLBURN, A.P. (1949). 'Heat transfer and fluid friction during viscous flow across banks of tubes'. Trans. ASME, 71, pp 27-34.

PEARCE, H.R. (1972). Private communication.

PRANDTL, L. (1945). 'Uber ein neues Formelsystem für die ausgebildete Turbulenz'. Nachr. Akad. Wiss., Göttingen, IIA, 6-19.

RELF, E.F. (1913). Tech. Rep. and Memo, Adv. Comm. Aero (ARC) London, No. 102.

ROBERTS, L.W. (1972). 'Turbulent swirling flows with recirculation'. Imperial College, Mech. Eng. Dept. Rep. EF/TN/R/45.

RODI, W. and SPALDING, D.B. (1970). 'A two-parameter model of turbulence and its application to free jets'. Warme-und-Stoffubertragung, Bd.3, p 85.

RUNCHALL, A.K. (1969). 'Transfer processes in steady two-dimensional separated flows'. Imperial College, Mech. Eng. Dept. Rep. EF/R/G/1.

SAMOSHKA, P.S. and STASYULYAVICHYUS, Yu.K. (1968). 'A study of the thermal physics of an in-line array of tubes in a transverse flow of air at high Reynolds numbers'. Trudy Akedemii Nauk, Litovskoi SSR, Series B, 4, Pt. 55, pp 133-143.

SCHLICHTING, H. (1968). Boundary-Layer Theory. McGraw-Hill, New York.

SEBAN, R.A. (1960). 'The influence of free stream turbulence on the local heat transfer from cylinders'. Trans ASME, J. of Heat Transfer, pp 101-107.

SPALDING, D.B. and JAYATILLAKA, C.L.V. (1965). 'A survey of the theoretical and experimental information on the resistance of the laminar sub-layer to heat and mass transfer.' Proc. 2nd All-Union Conf. on Heat and Mass Transfer, Minsk, USSR, 1964, 2, pp 234-264 (In Russian) (English Trans. Rand Corp. California 1966).

SPALDING, D.B. (1970). Private communication.

SPALDING, D.B. (1971). Private communication.

STASYULYAVICHYUS, Yu.K. and SAMOSHKA, P.S. (1964). 'Heat transfer and aerodynamics of staggered tube bundles with a transverse flow of air in the Reynolds number region $Re > 10^5$.' Inzhenerno - fizicheskii zhurnal, 7, pp 10-15.

TAKAISI, Y. (1969). 'Numerical studies of a viscous liquid past a circular cylinder'. The Physics of Fluids, 12, Supplement II, pp 86-87.

TAKAMI, H. and KELLER, H.B. (1969). 'Steady two-dimensional viscous flow of an incompressible fluid past a circular cylinder'. The Physics of Fluids, 12, Supplement II, pp 51-56.

TANEDA, S. (1956). 'Experimental investigation of the wakes behind cylinders and plates at low Reynolds numbers'. J. Phys. Soc. Japan, 11, No.3, pp 302-307.

THOM, A. (1933). 'The flow past circular cylinders at low speeds.' Proc. Roy. Soc. London, A141, pp 651-669.

THOM, A. and APELT, C.J. (1961). Field Computations in Engineering and Physics. D. van Nostrand Co., London.

THOMAN, D.C. and SZEWCZYK, A.A. (1969). 'Time-dependent viscous flow over a circular cylinder'. The Physics of Fluids, 12, Supplement II, pp 76-85.

TRITTON, D.J. (1959). 'Experiments on the flow past a circular cylinder at low Reynolds numbers'. J.Fluid Mech., 6, pp 547-567.

VAN DER HEGGE ZIJNEN, B.G. (1957). 'Modified correlation formulae for the heat transfers by natural and by forced convection from horizontal cylinders'. App.Sci.Res., Section A, 6, pp 129–140.

WELCH, C.P. and FAIRCHILD, H.N. (1964). 'Individual heat transfer in a crossflow in-line tube bank'. Trans.ASME, J. of Heat Transfer, pp 143–148.

WOLFSHTEIN, M. (1967). 'Convection processes in turbulent impinging jets'. Imperial College, Mech. Eng. Dept. Rep. SF/R/2.

ZHUKAUSKAS, A., MAKARIAICHIUS, V. and SHANCHIAUSKAS, A. (1968). Heat Transfer in Banks of Tubes in Crossflow of Fluid. Mintis, Vilnius.

NOMENCLATURE*

Chapter 2

Symbol	Meaning	Equation, section, etc., of first mention**
a_ϕ	a coefficient in the general elliptic equation	(2.4.1)
A	a coefficient in the one - dimensional equation for vorticity	(2.5.2)
b_ϕ	a coefficient in the general elliptic equation	(2.4.1)
B	a coefficient in the one - dimensional equation for vorticity	(2.5.2)
c_ϕ, d_ϕ	coefficients in the general elliptic equation	(2.4.1)
$J_{\phi,j}$	component of the diffusional - flux of ϕ in direction j	(2.1.3)
p	static pressure	(2.1.2)
S_ϕ	source term in equation for ϕ	(2.1.3)
S_ω	source term in equation for ω	(2.3.4)
T	temperature	Table 2.4.1
u_i	component of velocity in direction i	(2.1.1)
x_i	a general Cartesian co - ordinate (i may take values 1, 2, 3)	(2.1.1)
x_j	a general Cartesian co - ordinate (j may take values 1, 2, 3)	(2.1.2)
x_n	normal distance from a wall boundary	(2.5.1)
$\Gamma_{T,eff}$	effective thermal diffusivity	Table 2.4.1

---

* This nomenclature includes the important symbols in Chapters 2 to 6. Symbols are set out in sections which correspond to each chapter. If a symbol is used consistently throughout, it is only mentioned for the chapter of first mention.

** Numbers in brackets, i.e. (5.3.1), correspond to equations; and numbers without brackets, i.e. 5.3.1, correspond to sections.

Symbol	Meaning	Equation, section, etc., of first mention
$\Gamma_{\phi,eff}$	effective diffusivity for ϕ	(2.2.2)
μ_{eff}	effective viscosity	(2.2.1)
ρ	fluid density	(2.1.2)
$\sigma_{\phi,eff}$	effective Prandtl number for ϕ	(2.2.3)
τ_{ij}	component of shear stress tensor which operates on the i - plane in the direction j	(2.1.2)
τ_s	wall shear stress	2.5(d)
ϕ	any dependent variable or conserved property	(2.1.3)
ψ	stream function	(2.3.1)
ω	vorticity	(2.3.2)

Subscripts

C	at a point a short distance from wall
eff	effective, i.e. including laminar and turbulent contributions
i	in the direction i
j	in the direction j
n	in the direction normal to a wall boundary
S	at the wall
ϕ	pertaining to variable ϕ
ω	pertaining to vorticity

Chapter 3

Symbol	Meaning	Equation, section, etc., of first mention
A_{E1}, A_{E2}	coefficients in the east convection term of the difference equation	(3.2.8)
A_{N1}, A_{N2} A_{S1}, A_{S2} A_{W1}, A_{W2}	coefficients in the convection terms of the difference equation	(3.2.10)

Symbol	Meaning	Equation, section, etc., of first mention
A_P, A_N, A_S A_E, A_W A_{NE}, A_{NW} A_{SE}, A_{SW}	main coefficients in the convection terms of the difference equation	(3.2.22)
B_N, B_S B_E, B_W	coefficient in the diffusion terms of the difference equation	(3.2.18)
c_p	specific heat of fluid	(3.3.24)
G_{EP}, G_{EE}	coefficients in the east convection term of the difference equation	(3.2.15)
G_{NP}, G_{NN} G_{SP}, G_{SS} G_{WP}, G_{WW}	coefficients in the convection terms of the difference equation	(3.2.17)
P_{ME}, P_{PE}	coefficients in the east convection term of the difference equation	(3.2.15)
P_{MN}, P_{PN} P_{MS}, P_{PS} P_{MW}, P_{PW}	coefficients in the convection terms of the difference equation	(3.2.17)
$\dot{q}''_{wall}$	wall heat flux	(3.3.24)
r	radius or distance from axis of symmetry	Fig. 3.3.3
V_P	volume per unit depth of a cell represented by a node P	(3.2.19)
x_t	tangential distance along a wall boundary	(3.3.6)
β	angle of inclination of streamline to grid line	3.2.1(a)
θ	angle of radial arm with respect to the positive x_1 – axis	Fig. 3.3.3
$\overline{\phi_e}$	average value of ϕ_e	(3.2.3)
$\overline{\omega_p}$	space – average vorticity for cell containing node P	(3.3.9)

Subscripts

n,s e,w	at points on the sides of the cell walls containing node P
N, S E, W	at neighbouring nodes which lie respectively north, south, east and west of node P
ne, se nw, sw	at the corners of the cell walls containing node P
NE, SE NW, SW	at nodes which lie near to nodes N, S, E and W
P	at node P
slip	indicating wall slip value
south	pertaining to the south wall of cell containing node P
t	in the tangential direction to a wall boundary
wall	pertaining to the wall
west	pertaining to the west wall of cell containing node P

Chapter 4

Symbol	Meaning	Equation, section, etc., of first mention
A, B	functions in the ω and ψ equations for a cylindrical Couette flow	(4.3.1)
C	function in ψ equation for a cylindrical Couette flow	(4.3.2)
h	half the normal distance between the walls of a plane Couette flow	(4.2.1)
Re	Reynolds number: $(\psi_{2R} - \psi_o)/\mu$ $(\psi_{R_I} - \psi_{R_o})/\mu$	4.2.2(b) 4.3.2(b)
R_I	radius of inner cylinder of a cylindrical Couette flow	(4.3.2)
R_o	radius of outer cylinder of a cylindrical Couette flow	4.3.2(a)
U	velocity of the moving wall of a plane Couette flow	(4.2.1)
x_R	R_I / R_o	4.3.2(a)

Symbol	Meaning	Equation, section, etc., of first mention
X	distance along the stationary wall of a plane Couette flow	(4.2.1)
Y	normal distance from the stationary wall of a plane Couette flow	(4.2.1)
μ	laminar viscosity	(4.2.1)
ψ_{R_I}	stream function value at the inner cylinder of a cylindrical Couette flow	(4.3.2)
ψ_{R_o}	stream function value at the outer cylinder of a cylindrical Couette flow	4.3.2(a)
ψ_{2h}	stream function value at the moving wall of a plane Couette flow	4.2.2(a)
ψ_o	stream function value at the stationary wall of a plane Couette flow	(4.2.2)
Ω	angular velocity of outer cylinder of a cylindrical Couette flow	4.3.2(a)

Chapter 5

Symbol	Meaning	Equation, section, etc., of first mention
C_D	drag coefficient	5.2.2(d)
C_{DF}	friction drag coefficient	5.2.2(d)
C_{DP}	pressure drag coefficient	5.2.2(d)
d	diameter of cylinder	5.2.2(b)
D_e	equivalent diameter	5.3.4(c)
D_t	diameter of tube	5.3.2(a)
D_v	hydraulic diameter: $\frac{2 D_t (2 S_T S_L - \pi/2)}{\pi}$	5.3.3(c)

Symbol	Meaning	Equation, section, etc., of first mention
Eu	Euler number:	
	$(p_A - p_D)/(\rho \bar{U}^2)$	5.3.2(a)
h	half - width of channel test section	Fig. 5.2.3
k	thermal conductivity	5.2.3(c)
L	length	5.3.4(c)
Nu	local Nusselt number	Fig. 5.2.12
$(Nu)_{B,I}$, $(Nu)_{B,E}$	Nusselt numbers	Table 5.3.1
$(Nu)_{AB}$, $(Nu)_{LM}$		
$\overline{Nu}$	mean Nusselt number	Table 5.2.6
p_A, p_B p_C, p_D	static pressures at wall points A, B, C and D. (Fig. 5.3.1)	5.3.2(a)
p_S	static pressure on the channel wall below the cylinder	5.2.2(c)
p_θ	static pressure on the cylinder wall at an angular position of θ	5.2.2(b)
p_∞	reference static pressure far upstream of the cylinder	5.2.2(b)
Pr	Prandtl number	5.2.3(a)
$\dot{q}''_s$	wall heat flux	5.2.3(a)
R	radius of cylinder	5.2.2(b)
Re	Reynolds number:	
	$U d/\nu$	5.2.2(b)
	$U_c d/\nu$	5.2.2(c)
	$\bar{U} D_t/\nu$	5.3.2(a)
S_L	non - dimensional longitudinal spacing of tubes: S'_L/D_t	5.3.3(a)
S'_L	longitudinal spacing of tubes	——
S_T	non - dimensional transverse spacing of tubes: S'_T/D_t	5.3.2(a)

Symbol	Meaning	Equation, section, etc., of first mention
S_T'	transverse spacing of tubes	Table 5.3.1
T_m	mean temperature: $\frac{1}{2}(T_s + T_\infty)$	Table 5.2.6
T_s	wall temperature	5.2.3(a)
T_∞	reference temperature	Table 5.2.6
u_θ	velocity in the circumferential direction	5.2.2(b)
U	free - stream velocity	5.2.2(b)
U_c	velocity at the cylinder position in the test channel in the absence of the cylinder	5.2.2(c)
$\bar{U}$	mean velocity through minimum cross - section between the tubes	5.3.2(a)
x_E	length of recirculating eddy with respect to centre of cylinder	Fig. 5.2.7
x_{VC}	distance of centre of eddy from centre of cylinder	Fig. 5.2.7
y_E	maximum value of positive x_2 denoting edge of recirculating eddy	Fig. 5.2.7
ν	kinematic viscosity: μ/ρ	5.2.2(b)
ψ_c	stream function value on the centre - line between longitudinal rows of tubes	5.3.2(a)
ψ_s	stream function value at tube walls	5.3.2(a)
ω_s	wall vorticity	Fig. 5.2.8

Subscripts

AB	average bulk value
B	bulk value
C	at the centre - line
E	at the exit (or referring to recirculating eddy)
I	at the inlet
LM	log mean value

NP	at near – wall node
Θ	at an angle Θ
∞	reference value

Chapter 6

Symbol	Meaning	Equation, section, etc., of first mention
a	constant; constant in the power law equation	6.2.1(b); (6.2.10)
A_P	area of near – wall cell	(6.2.28)
A_R	an area	(6.2.31)
b	constant; constant in the power law equation	(6.2.1(b); (6.2.10)
B_N, B_W, B_{NE}, B_{SW}	coefficients in the equation for near – wall node	(6.2.31)
C_1, C_2	coefficients in the differential equation for ε	(6.2.4)
C_{ps}	a coefficient	(6.2.33)
C_μ	coefficient in equation for effective viscosity	(6.2.2)
C'_μ	coefficient in equation for effective viscosity	(6.2.1)
d_e	equivalent diameter	6.3.2(a)
E	constant in log – law equation	(6.2.9)
f	friction factor	6.3.3(a)
h	channel half – width	6.3.2(a)
h_E	maximum value of x_2 co – ordinate for the reattachment streamline	6.4.4(a)
k	kinetic energy of turbulence	(6.2.1)
l	a length scale of turbulence	(6.2.1)
l_{nm}	distance along curve or straight line joining points n and m	6.2.2(d)
m	constant exponent	6.4.2(d)

Symbol	Meaning	Equation, section, etc., of first mention
N	number of tube rows	6.4.2(a)
P_A, P_B, P_C, P_D,	static pressures at points A, B, C and D (Fig. 6.4.2)	6.4.3(f)
P	P – function	(6.2.19)
P_k	production term in the differential equation for k	(6.2.5)
$(Re)_{d_e}$	Reynolds number based on equivalent diameter	6.3.2(a)
R_{P1}, R_{P2}, R_{PS}	ratios of areas	(6.2.32)
St	local Stanton number	Table 6.3.1
$\overline{St}$	mean Stanton number	6.4.3(g)
u	velocity parallel to a wall	6.2.2(b)
u_o	velocity on centre – line of channel	6.3.3(a)
u_τ	friction velocity: $\sqrt{\tau/\rho}$	(6.2.13)
u_+	u/u_τ	(6.2.8)
u'	the fluctuating component of velocity in the x_1 direction	6.4.2(a)
v'	the fluctuating component of velocity in the x_2 direction	6.4.2(a)
$\overline{v}_{nm}$	mean velocity between points n and m in the direction from n to m	6.2.2(d)
y	normal distance from wall	6.2.2(b)
y_+	$y\sqrt{\tau\rho}/\mu$	(6.2.8)
ε	dissipation rate of turbulence energy	(6.2.2)
K	constant in the log – law equation	(6.2.9)
σ	laminar Prandtl number	(6.2.19)

Symbol	Meaning	Equation, section, etc., of first mention
σ_k	a coefficient in the differential equation for k	(6.2.3)
σ_o	turbulent Prandtl number	(6.2.19)
σ_ε	a coefficient in the differential equation for ε	(6.2.4)
μ_+	μ_{eff}/μ	(6.2.8)
$\dot{\phi}''$	flux of ϕ	(6.2.17)